NOAA Technical Memorandum ERL PMEL-18

OCEAN REMOTE SENSING USING LASERS

Howard R. Gordon, Editor

Pacific Marine Environmental Laboratory
Seattle, Washington
May 1980

DISCLAIMER

Foreword

The papers presented here summarize the results of a one-day conference on the use of lasers and lidars in ocean remote sensing, held at Patricia Bay, B.C., on June 22, 1978. The purpose of the conference was to assess and document the present state of application of lasers to oceanography. This small but promising field is currently seeing advances which, while not as rapid as one might wish, are probably more limited by funds than by talent. If the promises are all realized, it would be possible to measure remotely profiles of upper ocean temperature, salinity, waves, sediment and chlorophyll to interesting accuracies; the use of the sensors on low-flying aircraft would greatly extend the rate of data-gathering over present methods. While we are not yet there, the results presented in this report clearly point the way.

John R. Apel,   Environmental Research Laboratories
Director, PMEL   National Oceanic and Atmospheric Administration
                        3711 15th Avenue N.E.
                        Seattle, Washington 98105

Preface

Over the past several years there has been a considerable effort in the remote sensing of ocean properties using visible, infrared, and microwave radiation in both the active and passive modes. This has led to the development of the collection of sensors flown aboard the SEASAT-1 and NIMBUS-7 satellite systems for measuring sea surface temperature and roughness, surface wind speed and direction, sea surface topography, significant wave height, and surface chlorophyll. All of these ocean sensors are capable of measuring only surface properties, and cannot provide information concerning the distribution of properties with depth because of the negligible penetration of infrared and microwave radiation into the water, and the passive nature of the visible sensors. The most viable method now known of obtaining vertical profiles of properties is through the use of radar-like range-gated systems with lasers as the radiation source. Such laser systems, usually referred to as lidar, operating near the wavelength of maximum transmittance of the water, would have sufficient penetration power to provide information over depths of the order of tens of meters in favorable cases.

Because of the potential of such systems, operating from aircraft or spacecraft, for providing information useful in both oceanographic and climatic studies, Dr. John R. Apel suggested to the Editor that a one-day symposium be organized for the purpose of bringing together investigators actively studying problems associated with the applications and limitations of lasers to the remote sensing of ocean properties. The relevant applications were considered to be: temperature and salinity profiles, using time-resolved (range-gated) Rayleigh, Raman, and Brillouin scattering; sediment load, using Tyndall scattering; chlorophyll a concentration, using laser-induced in vivo fluorescence; and bathymetry. The meeting was held on June 22, 1978, at the Institute of Ocean Sciences, Patricia Bay, near Victoria, British Columbia, Canada, immediately following the IUCRM Colloquium on "Passive Radiometry Of The Ocean" (June 14-21). It consisted of eight invited papers, all of which are presented in this report, and an open session devoted to a general discussion of the various sensing techniques and their prognosis. This session is summarized at the end of the report.

The Editor wishes to thank Dr. J.F.R. Gower of the Institute of Ocean Sciences, Patricia Bay, for his hospitality in hosting the meeting, and Dr. John R. Apel for suggesting the meeting and supporting the preparation of this report.

Howard R. Gordon, Editor

Contents

OCEAN REMOTE SENSING USING LASERS[1]

Summary of the Open Session

Reported By

Howard R. Gordon[2]
NOAA/PMEL

The purpose of this section is to report the results of the general discussion session of the meeting, not to editorialize or present personal opinions. The session consisted of a general discussion of each of the three main topics addressed at the meeting: temperature and salinity sensing, bathymetry, and fluorosensing chlorophyll a. Of these, only the bathymetric applications appear to have reached the point of being truly operational. It is now possible to measure depth D to a precision of 4 to 10 cm (depending on the surface wave structure) to a depth of 6 to 10 beam attenuation lengths (i.e., $\alpha D = 6$ to 10 where α is the beam attenuation coefficient). At night present systems have achieved measurements to depths of 15 attenuation lengths.

The fluorosensing of chlorophyll a has yet to reach the operational level. At the present stage of development, the emphasis has been on measuring only the surface concentration from aircraft using the pulse height of the fluorescent return. This yields an accuracy of ±50% when compared to surface measurements which were known to be imprecise due to patchiness. Although most measurements have been in the 2 to 20 $\mu g/l$ range, the minimum sensitivity is believed to be about 0.5 $\mu g/l$.

Some problems plaguing this technique are (1) the fact that the quantum efficiency of phytoplankton fluorescence depends on the ambient light level (photoinhibition) as well as the width of the exciting pulse, and (2) the fact that the total fluorescence seems to be dependent on the beam transmittance coefficient, which is usually ignored in models of the fluorescent return. A proposed solution of the latter problem is to normalize the signal to the Raman return, while the former problem can at present be handled only by operating the system at night, and may in fact define the limit of precision of the technique.

The problem of sensing temperature and salinity profiles consumed the largest portion of the discussion session. These applications are clearly the farthest from operational of the three. In fact, of the proposed methods for sensing temperature (Rayleigh, Raman, and Brillouin

---

scattering) the Rayleigh method has yet to be attempted in water, the Brillouin method has been tested only in a turbid harbor where temperature profiling would be impossible, and the Raman method has undergone only one field test in clear ocean water. It appears to be too early to decide which of these techniques is likely to lead to an operational system for providing the oceanographic community with temperature profiles; however, the proponents of each of the methods were asked to present the present state-of-the-art of their technique and their opinions of the ultimate temperature accuracy achievable. The result of this survey is summarized in the following table.

Method	Present ΔT (°C) In Field Tests	Ultimate ΔT (°C) Achievable
Rayleigh	1.5 - 2.0*	0.1
Raman	1.2 - 1.5**	0.1**
Brillouin	4	0.1

*In atmosphere at a range of 5km.
**per diffuse attenuation length.

Note that the advocates of each method envision an ultimate accuracy of 0.1 °C.

There was very little discussion concerning the measurement of salinity. Such a measurement seems possible only with the Raman system using a dual polarization technique. The projected accuracy of 1°/oo, however, would be useful only in coastal areas with very large salinity gradients.

ATMOSPHERIC EFFECTS ON OCEANOGRAPHIC LIDAR

R. L. Schwiesow and V. E. Derr
National Oceanic and Atmospheric Administration
Environmental Research Laboratories
Wave Propagation Laboratory
Boulder, Colorado 80302

Researchers must consider the effects of atmosphere between the lidar and the water surface when interpreting lidar (light detection and ranging) returns from the sea. This report reviews such atmospheric effects and directs the reader to source documents.

1. INTRODUCTION

This brief review reminds users of oceanographic lidar that they must consider the effect of the atmosphere on laser-transmitted and scattered-received signals to analyze properly oceanographic lidar returns. Readers can obtain detailed descriptions of atmospheric effects from the references cited in this report and those in more extensive bibliographies, such as that of Derr et al. (1974).

We divide atmospheric effects into the broad categories of attenuation, scattering, and refraction.

2. ATTENUATION

Attenuation is characterized by an attenuation coefficient α in the well-known form

$$T = \exp(-\alpha x), \tag{1}$$

which we cite only to establish common terminology. T is the atmospheric transmission and x the path length in the atmosphere.

The components of the attenuation coefficient can be written

$$\alpha = \sigma + k, \tag{2}$$

where σ is scattering and k is absorption coefficient. The total attenuation and each component can be divided into aerosol and molecular terms, respectively, in the form

$$\alpha = \alpha_a + \alpha_m. \tag{3}$$

2.1 Broadband Attenuation

Broadband attenuation in the visible region (the most useful spectral range for ocean lidar) results from aerosol absorption, aerosol scattering, amd molecular scattering. Useful studies are provided by Selby and McClatchey (1975) and McClatchey et al. (1971). For example, McClatchey et al. (1971) give the attenuation coefficients shown in Table 1 for atmospheric models characterized by visual range.

Aerosol effects on attenuation far outweigh molecular contributions. Aerosol attenuation varies greatly between atmospheres with different characteristics. Broadband attenuation for a particular atmospheric type changes by approximately 50% over the visible wavelength region.

The effect of broadband attenuation is especially important for spectroscopic techniques that cover a significant spectral range (e.g., Raman scattering). In Raman analysis, differences in atmospheric attenuation at two different wavelengths affect the apparent ocean scattering intensities at those wavelengths. Broadband attenuation also reduces the actual signal-to-noise ratio relative to that expected if atmospheric effects are neglected.

Table 1. Attenuation at 0.5145 μm Wavelength

Visibility (km)	α_a (km^{-1})	α_m (km^{-1})
5	0.858	0.015
23	0.176	0.015

2.2 Line Absorption

Significant narrowline attenuation, which is purely molecular absorption, exists in the visible region. Figure 1 includes part of the spectral data from Curcio et al. (1964) and emphasizes the existence
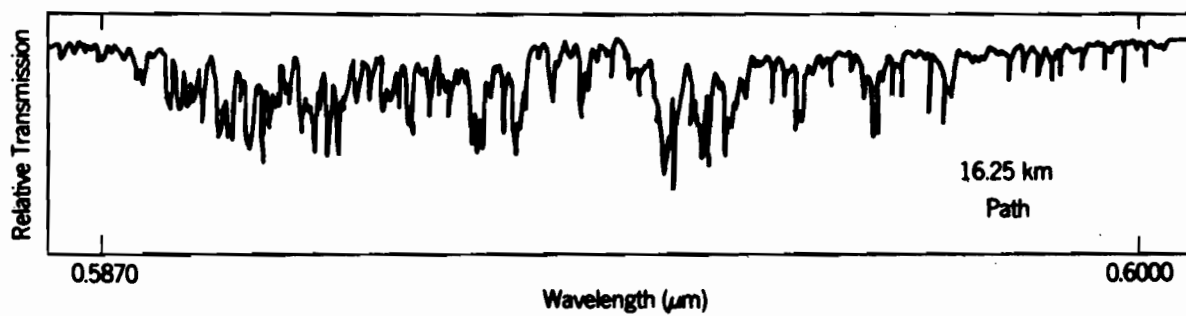
Figure 1. Absorption spectrum in the boundary layer by Curcio et al. (1964).

5

of spectral features. The line absorption features can have an effect on signal-to-noise ratio when laser and/or scattered wavelengths coincide with absorption lines.

The 0.540 to 0.852 μm region is discussed in Curcio et al. (1964), and the 0.440 to 0.550 μm interval in Curcio et al. (1955). At wavelengths shorter than 0.440 μm, the visible absorption spectrum is generally structureless down to 0.35 μm. McClatchey and O'Agati (1978) explain a technique for calculating high-resolution absorption spectra at selected (laser-line) locations.

3. SCATTERING

Sources of noise that affect the performance of oceanographic lidar can arise from the backscatter produced by the intervening atmosphere.

3.1 Laser Scattering

First-order laser (lidar pulse) backscatter from the atmosphere can be time-gated to prevent interference with the ocean signal. At most, the lidar return from the atmospheric surface layer within one range-resolution element of the water surface can contaminate the ocean-return signal. Analysis must allow for this slight mixing of atmosphere and ocean signal.

Pulse time stretching by multiple backscattering in the atmosphere can cause an atmospheric signal that overlaps in time the main return from the water. Multiple backscatter effects should be negligible except in the presence of fog or low cloud. If the line-of-sight from the lidar to the ocean is not clear of cloud, the analysis becomes extremely difficult.

Another special interference comes from multiple, forward scattering of sea-surface reflections. Although specular reflection from the sea surface is not an atmospheric problem, the strong reflected signal can be scattered into the receiver beam by a two-step, forward-scattering process. Forward scattering is much stronger than backscatter if the size parameter of the scatterer is greater than one. We do not attempt to calculate the multiple-scattered reflectance in this review, but we point out that it must be considered in many oceanographic lidar experiments.

Atmospheric backscatter of the laser afterpulse fluorescence is a problem common to oceanographic and atmospheric lidars. Standard techniques, such as increasing the range to the target so that it is greater than the afterpulse time, shuttering the receiver, and reducing the transmitter-receiver beam overlap, can be applied to the afterpulse problem.

3.2 Solar Scattering

Solar radiation is scattered into the lidar receiver during daytime operation. An example of the radiance spectrum is given in Figure 2, taken from Hovis (1977). This spectrum shows a peak in the blue region and an increase in total scattered intensity as the depth of the scattering region is increased from 0.91 to 14.9 km.

Gating techniques cannot be used to reduce solar radiance because the solar input is continuous during a lidar measurement. However, total received solar radiance can be reduced by restricting the spectral bandpass of the receiver to the minimum consistent with the spectrometric technique used in the lidar analysis.

Solar scattering interference depends greatly on lidar-sun relative geometry. McClatchey et al. (1971) present scattering patterns for various sun-receiver geometries at selected wavelengths for model atmospheres.

3.3 Depolarization

The effects of the ocean on a polarized signal are important for Raman analysis of temperature profiling and for other applications. The atmosphere also depolarizes a lidar signal.

Höhn (1969) has observed a maximum depolarization angle in the forward direction of 5×10^{-5} rad for a 0.63-μm laser beam over a 4.5-km atmospheric path. This depolarization is attributed to scattering rather than refractive mechanisms. Ice-crystal clouds strongly depolarize a lidar signal but are not present in most ocean-sensing experiments.

4. REFRACTION

Any lidar system that relies on phase coherence of propagating beams is sensitive to refractive index inhomogeneities in the atmosphere. Examples of such phase-sensitive systems are those relying on heterodyne detection or on near-diffraction-limited performance.

Fried and Mevers (1974) analyzed the effect of refractive turbulence on light propagating from a point source to derive the following expression for the effective aperture:

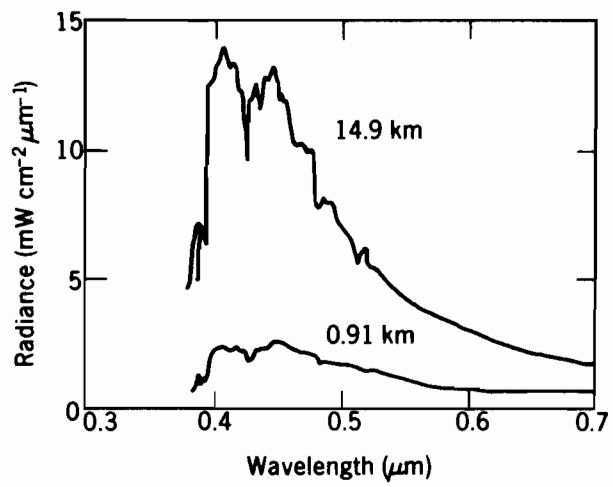$$d_o = 0.190 \ (C_N^2 \times \lambda^{-2})^{-3/5}. \tag{4}$$

Figure 2. Spectrum of solar backscattered radiance (Hovis, 1977) taken from 0.91-km and 14.9-km altitude.

Effective aperture d_0 depends on the propagation distance x, wavelength λ, and structure parameter for refractive index fluctuations C_N. The structure parameter, usually appearing as C_N^2, is discussed in detail by Lawrence and Strohbehn (1970). The effective aperture is that diameter over which the received wavefront is approximately plane, within limits discussed in Fried and Mevers (1974).

Measurements of d_0 are within the range

$$1 \text{ cm} \leq d_0 \leq 12 \text{ cm} \tag{5}$$

for a 4-km path a few meters above the terrain in an experiment reported by Goldstein et al. (1965). Averaging day and night measurements, these authors obtain the approximate value of $4 \times 10^{-16} \text{ cm}^{-2/3}$ for C_N^2. Although these measurements give useful approximation for refractive effects in the atmosphere, the vertical path in the marine climate should be analyzed appropriately for a particular experiment.

The performance of lidar using either interferometric and heterodyne spectral processing is severely limited by atmospheric turbulence.

5. SUMMARY

The atmosphere between an oceanographic lidar system and the ocean volume being probed has an effect on the received lidar signal when the system is space or airborne. The mechanisms that can modify the atmospheric signal include attenuation, scattering, and refraction.

Attenuation is caused by absorption and scattering of the beam by aerosols and molecules. Aerosol and molecular scattering and aerosol absorption vary only slowly over the visible spectral range. Molecular absorption exhibits sharp, distinctive spectral features in the visible region. In most lower-atmospheric situations, aerosol effects outweigh molecular effects.

The atmosphere backscatters laser pulse and afterpulse fluorescence into the receiver. Laser light specularly reflected by the sea is near-forward scattered into the receiver by a multiple scattering process. Solar radiation is scattered into the receiver beam. The intensity of the received solar scatter increases with height of the lidar.

Index of refraction inhomogeneities distort the optical wavefronts of both transmitted and received signals. The atmosphere limits the beam aperture over which spatially-coherent operation can occur.

9

6. REFERENCES

Curcio, J. A., L. F. Drummeter, and T. H. Cosden (1955). The absorption spectrum of the atmosphere from 4400 to 5500 Å, *NRL Report*, 4669.

Curcio, J. A., L. F. Drummeter, and G. L. Knestrick (1964). An atlas of the absorption spectrum of the lower atmosphere from 5400 Å to 8520 Å, *Applied Optics* 3(12): 1401-1409.

Derr, V. E., M. J. Post, R. L. Schwiesow, R. F. Calfee, and G. T. McNice (1974). A theoretical analysis of the information content of lidar atmospheric returns, NOAA Technical Report ERL 296-WPL 29 (U.S. Department of Commerce).

Fried, D. L. and G. E. Mevers (1974). Evaluation of r_0 for propagation down through the atmosphere, *Applied Optics* 13(11): 2620-2622.

Goldstein, I., P. A. Miles, and A. Chabot (1965). Heterodyne measurements of light propagation through atmospheric turbulence, *Proceedings of the IEEE*, 53(9): 1172-1180.

Höhn, D. H. (1969). Depolarization of a laser beam at 6328 Å due to atmospheric transmission, *Applied Optics* 8(2): 367.

Hovis, W. A. (1977). Remote sensing of water quality, *Proceedings, Application of Remote Sensing to the Chesapeake Bay Region*, NASA Conference Publication 6, 141-148.

Lawrence, R. S. and J. W. Strohbehn (1970). A survey of clear-air propagation effects relevant to optical communications, *Proceedings of the IEEE*, 58(10): 1523-1545.

McClatchey, R. A., R. W. Fenn, J. E. A. Selby, F. E. Volz, and J. S. Garing (1971). Optical properties of the atmosphere, Air Force Cambridge Research Laboratories report AFCRL-71-0279.

McClatchey, R. A., and A. P. O'Agati (1978). Atmospheric transmission of laser radiation: computer code LASER, Air Force Geophysics Laboratory report AFGL-TR-78-0029.

Selby, J. E. A. and R. A. McClatchey (1975). Atmospheric transmittance from 0.25 to 28.5 μm: computer code LOWTRAN 3, Air Force Cambridge Research Laboratories report AFCRL-TR-75-0255.

LIDAR HIGH-RESOLUTION SPECTROSCOPY FOR
OCEANOGRAPHIC MEASUREMENTS

R. L. Schwiesow
National Oceanic and Atmospheric Administration
Environmental Research Laboratories
Wave Propagation Laboratory
Boulder, Colorado 80302

A review of high-resolution spectroscopic measurements for
temperature and wind profiles in the atmosphere shows promise of
subsurface measurements of temperature and current in the ocean.
The mechanism of Doppler-shifted scattering offers different advantages
and technical difficulties that are characteristic of Brillouin and
Raman scattering.

1. OVERVIEW

This report presents the principles of high-resolution lidar
applied to oceanic measurements of subsurface temperature, current and
turbidity. High resolution means here the ability to determine the
Doppler shifts from scattering centers in motion. Comparing this spectro-
scopic technique with other optical methods of measuring oceanographic
parameters helps clarify the high-resolution approach.

1.1 Comparison With Other Techniques

At least three types of temperature-dependent spectroscopy are
useful or potentially useful for remote measurement of temperature pro-
files in the ocean. These types are Raman, Brillouin, and Rayleigh.
Each scattering mechanism relies on different properties of the ocean to
infer temperature (Table 1).

Table 1.   Temperature-Dependent Scattering Mechanisms

Type	Basis
Raman	Environmental perturbation of molecular energy levels
Brillouin	Bulk (collective) properties of the liquid
Rayleigh	Molecular kinetics

Raman scattering measures the difference between energy levels in the H_2O molecule, which arise from intramolecular motions. These energy levels are perturbed by the environment (principally temperature and salinity), probably by the effect of these variables on the formation of a weakly-bound water dimer. Temperature is determined from the slope of the Raman spectrum (Walrafen, 1967), which is modified by the environment of the molecule.

Brillouin scattering depends on the periodic (lattice-like) density variations in water resulting from acoustic waves. The lidar beam in backscatter selects from the field of random thermally-generated acoustic waves, those waves propagating along the optical axis that have a wavelength equal to one-half the optical wavelength. These selected acoustic waves propagate toward and away from the lidar, giving Doppler shifts (equally up and down in frequency from the incident laser frequency) that depend on the acoustic propagation velocity. The speed of sound is in turn dependent on temperature, salinity, and pressure.

Rayleigh scattering is scattering directly from water molecules. These molecules are in random thermal motion and will Doppler shift the scattered light. Thermally induced molecular velocities are directly proportional to temperature, and in fact are used as one definition of (kinetic) temperature. Suspended particulates also scatter the incident lidar light and Doppler shift the scattered radiation by an amount depending on their velocity (which follows the current). Particulate or hydrosol scattering is termed Tyndall or Mie scattering.

We shall discuss four categories that allow further description of the Rayleigh (molecular kinetics) temperature profiling method in terms of high-resolution spectroscopy, an atmospheric analog, oceanographic applications, and laboratory research.

2.1 Doppler Shifts

Doppler shifts arise from the line-of-sight (lidar axis) component V_L of the total velocity V of a scattering center, as illustrated in Figure 1. This shift in frequency is

$$\Delta\nu = 2\nu_0 \, V_L/c$$

$$= 4 \text{ MHz/m s}^{-1} \text{ at } \lambda = 0.5 \text{ }\mu\text{m} \tag{1}$$

for a laser frequency ν_0. At a wavelength of 0.5 μm, which is near the wavelength of maximum transmission of seawater (frequency $\nu_0 = 6 \times 10^{14}$ H_2), the Doppler shift is 4 MHz for a scatterer with component $V_L = 1$ m s^{-1}.

To put this spectral resolution in perspective, we can compare the characteristic spectral width of various types of scattering. The peak separation of the multi-component Raman line is approximately 200 cm^{-1}, easily measurable with a small grating spectrometer and wider than the bandpass of a good interference filter. The separation of the Brillouin peak from the central Tyndall line is approximately 0.384 cm^{-1} (11.5 GHz) at 273 K. Resolution of the Brillouin wing from the main peak requires use of an optical interferometer. The 1/e half-width of the Rayleigh peak is approximately 1.75 GHz (0.058 cm^{-1}) at 273 K. This resolution is associated with a good Fabry-Perot interferometer and with coherent (heterodyne) optical processing.

Comparative resolutions of temperature-dependent scattering are given in Table 2.

Table 2. Spectral Resolution for Various Scattering Mechanisms

Type	Resolution
Raman	200 cm^{-1}
Brillouin	0.384 cm^{-1} (11.5 GHz)
Rayleigh	1.74 GHz (0.058 cm^{-1})

Noise from background light decreases as the spectral resolution of the receiver increases (optical bandwidth decreases). High resolution spectroscopy requires sophisticated, but not necessarily complicated, techniques.
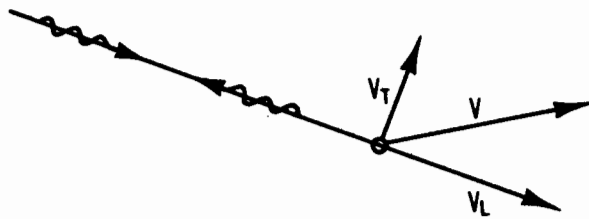
13

Figure 1. Doppler shift from the line-of-sight component of velocity, V_L. Velocity V is resolved into components transverse (V_T) and longitudinal (V_L) with respect to lidar axis.

2.2 Depth Resolution

Depth resolution in an oceanographic lidar is most easily achieved by pulsing the transmitter. A pulse τ long for a backscatter lidar gives a depth resolution

$$\Delta Z = c\tau/2.66 \tag{2}$$

where c is the vacuum speed of light, and where we take the refractive index of water to be 1.33. A pulse τ long is frequency broadened by an amount

$$\Delta\nu = 1/\tau \tag{3}$$

simply by the additional Fourier components introduced by modulating the carrier.

Equations (2) and (3) together with spectral resolutions required for parameter measurement restrict the depth resolution available in a Rayleigh-scattering system. Table 3 shows depth resolution, where we have assumed the need for approximately 50 intensity samples across a 1/e Rayleigh linewidth and the need for 0.5 m s^{-1} resolution in current measured at a 45° angle of incidence.

Table 3. Available Depth Resolution for Rayleigh-Doppler Scattering

Parameter	Frequency Resolution	Depth Resolution
T(Z)	30 MHz	3.7 m
Current	2 MHz	40 m

Adequate depth resolution is available for many temperature profiling purposes. It is possible to improve the resolution in Table 3 by processing fewer samples across the Rayleigh linewidth. There is essentially no useful depth resolution for current measurements. A Doppler-based lidar would measure the current averaged through the first one or two optical depths, weighted by the two-way transmission to each incremental depth element. An optical depth is here the depth at which incident light is attenuated to 1/e of the intensity at the surface. A continuous wave laser would be as applicable as a pulsed laser to current measurements from the point of view of useful depth resolution.

2.3 Laser Requirements

Frequency resolution for pulses discussed in the previous section applies to the linewidth of the laser transmitter for the lidar as well. To obtain meaningful measurements of the Rayleigh linewidth requires a laser frequency stable to better than 30 MHz during a pulse. Laser requirements for current measurements are even more stringent.

At present, only gas lasers are satisfactory for the molecular kinetics approach to oceanographic temperature profiling. The best commercially available liquid (dye) and solid-state lasers have line-widths of 1 to 5 GHz because of refractive index changes in the lasing medium during a pulse.

3. ATMOSPHERIC ANALOG

Molecular kinetic temperature profile measurements have been reported for the atmosphere. Direct wind measurements using the Doppler shift from aerosols have also been made. These atmospheric results give promise of the feasibility of high-resolution oceanographic lidar sensing, which has not yet been demonstrated.

3.1 High-Resolution Line Shape

The spectrum of laser light backscattered from the atmosphere exhibits the features shown in Figure 2. Mie scattering from aerosols exhibits an intensity B and spectral width S determined by instrumental linewidths. The integrated area under the aerosol spike is proportional to the backscatter coefficient of the altitude resolution element selected by the time gate on the receiver.

The aerosol peak is superimposed on a broader return that is the sum of Doppler-shifted, molecular scattering for all thermally-induced kinetic velocities. The molecular return has some peak intensity L and full-width-at-half-maximum W. Both the molecular density and molecular backscatter coefficient at any altitude are known to a good approximation and can be compared with the observed integrated-over-frequency signal.

If the atmosphere is moving with some bulk drift velocity, the entire aerosol-plus-molecular spectrum will be shifted in frequency from the transmitter frequency at ν_0. Equation (1) gives the magnitude of the wind-induced shift of the spectrum center.
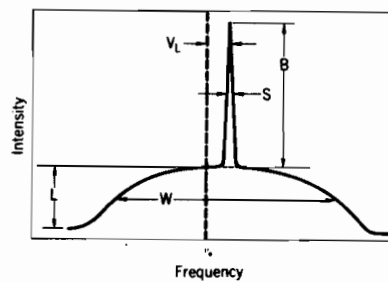
Figure 2. Schematic high-resolution spectrum of lidar backscatter showing molecular scattering intensity L, Doppler width W from molecular kinetics, hydrosol scattering intensity B, receiver resolution S, and Doppler shift V_L from collective motion (current).

17

The lidar lineshape from atmospheric scattering is exactly analogous to the ocean scattering case. For oceanographic work, the Mie scattering is from hydrosols, V_L is a measure of current, and W measures temperature-dependent, molecular kinetics velocities in water.

3.2 Temperature Measurements

Fiocco et al. (1971) have reported on temperature measurements in the atmosphere using a Rayleigh linewidth method. In this early work Fiocco estimated temperature accuracies of a few degrees. Measurements were made (at night) at ranges of a few hundred meters and over a 3- to 5-km interval.

A balloon sounding 30 km from the lidar site provided a check on the molecular kinetics results and was the basis for estimated temperature accuracies. In the atmosphere, Brillouin doublet separations are smaller than in water and interfere with the Rayleigh spectrum. Although Brillouin contributions are not obvious in Figure 3, corrections for interference were made when temperatures were inferred from the observed linewidth.

Fiocco's experiment used a chopped CW argon laser and a piezoelectrically scanned Fabry-Perot interferometer. Data for approximately 1 h were collected to produce Figure 3. Figure 3 exhibits most of the elements schematically indicated in Figure 2. The apparatus used in this experiment is applicable to oceanographic measurements. Technique and results from the atmosphere suggest the feasibility of high-resolution oceanographic lidar.

3.3 Wind Measurements

Benedetti-Michelangeli et al. (1972) used a modified form of the temperature-profiling lidar of Fiocco et al. to measure wind. Figure 4 reproduces a typical wind-measurement spectrum from their experiment. A single spectrum required data for 384 s. Data were taken from a range gate several hundred meters long centered at 1.5-km range.

Although the instrumental resolution was 47 MHz, the correlation data processing scheme used in the experiment provided a wind component uncertainty of $\pm$ 0.27 m s^{-1}. Rawinsonde comparisons with the lidar data show good agreement within the uncertainties of each measurement method and the 35-km horizontal separation between the two measurements.

Results and techniques of the wind measurement experiment are directly applicable to oceanographic research, as was the case for temperature profiling.
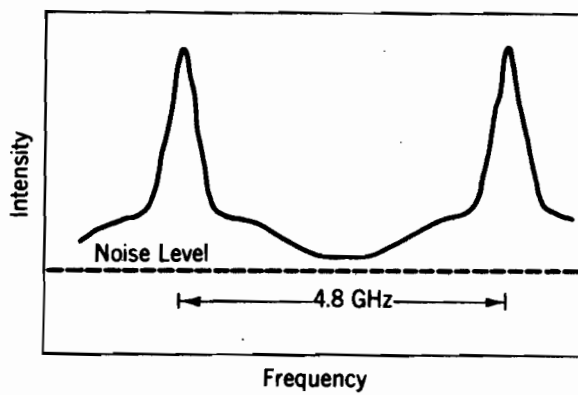
18

Figure 3.   High-resolution spectrum of atmospheric lidar backscatter taken by Fiocco et al. (1971) showing molecular scattering linewidth corresponding to 303 K.
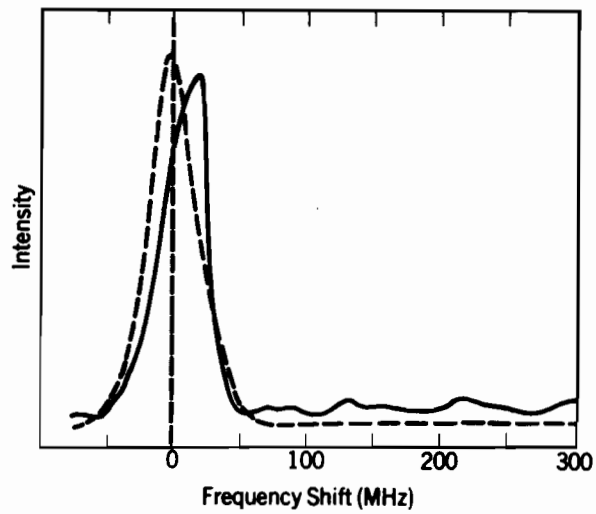
Figure 4. High-resolution aerosol scattering spectrum (solid curve) measured by Benedetti-Michelangeli et al. (1972) showing a radial velocity component $V_L = 3.18$ m s^{-1}. Laser reference spectrum is dashed.

3.4 Airborne High-Resolution Lidar

Many oceanic applications of temperature profiling and current mapping require that measurements be made over large areas. For example, one application provides input to climate dynamics studies. Wide-area coverage implies measurements from an airborne platform.

Although the resolutions involved in the lidar measurement of molecular and aerosol velocities are quite high (1 part in 2×10^7 for temperature, 1 in 5×10^8 for current and wind), we have shown that high-resolution lidar from a light aircraft is practical (Schwiesow et al., 1977b). Experiments on determining the velocity structure of waterspouts used a Doppler lidar based on a CO_2 laser operating in the infrared at 10.6 μm wavelength and an optical homodyne detection method with a resolution of 1 in 10^9). The infrared is not suited for subsurface measurements, of course.

At least three experiments on high-resolution atmospheric lidar determination of temperature and wind suggest the practicality of high-resolution measurements of oceanographic temperature profiles and currents. Methods must be refined for atmospheric measurements and must be developed for oceanographic purposes.

4. OCEANOGRAPHIC APPLICATIONS

4.1 Temperature Profiles

For an assembly of molecules in random, equilibrium motion, kinetic theory predicts a Maxwell-Boltzmann velocity distribution. Doppler lidar senses one component of the velocity. The spectrum of backscattered intensity is given by

$$I(\nu) = L \exp(-\nu^2/K), \tag{4}$$

which is a Gaussian function. Frequency ν is measured from the center (axis of symmetry) of the spectrum, which will not be ν_0, the laser frequency, if there is relative motion between the lidar and center of mass of the scatterers in the sample volume. Intensity scaling factor L is seen from Figure 2 to be the molecular scattering intensity at the Gaussian peak.

Variable K determines (or is determined by) the width of the spectrum. From kinetic theory and the Doppler equation (1) it follows that

$$K = 8kT/m\lambda_0^2 \tag{5}$$

where k is Boltzmann's constant, T the absolute temperature, and λ_0 the incident laser wavelength. The molecular mass m is at least the mass of an H_2O molecule. Weak intermolecular couplings in the liquid may produce an effective m larger than the single-molecule mass. I am not aware of any kinetic study of m in the liquid, although Raman studies demonstrate some degree of intermolecular coupling. If coupling does affect m through temperature, salinity, and/or pressure, K will deviate slightly from the simple linear dependence on temperature shown in equation (5).

Batchelor (1970) verifies that Maxwell-Boltzmann statistics apply to the liquid as well as the gas phase.

The width W of the molecular spectrum (full width at half maximum) is

$$W = 2(K \ln 2)^{1/2}. \tag{6}$$

It is indicated schematically in Figure 2. (At 296 K, for example, W is 3.48 GHz for a monomolecular mass.) The Rayleigh linewidth varies with the square root of temperature. A measurement of T to 1°C (1 part in 300) requires a determination of W to 1 part in 600. Data processing must be more sophisticated than simply scaling width from a spectral plot. Research on data analysis is discussed in Section 5.

4.2 Turbidity

The ability of the high-resolution lidar to separate aerosol and molecular contributions to the lidar backscatter intensity allows one to measure turbidity without recourse to assumptions about absorption/ scatter ratios. In the simple case of no multiple scatter and a constant Rayleigh backscatter coefficient, the measured molecular scatter intensity L(z) determines the integrated attenuation in the form

$$L(z) = L_0 \int_0^z \exp[-2\alpha(z)z] \, dz. \tag{7}$$

Questions of multiple scatter and other refinements of analysis are discussed by Sizgoric and Carswell (1975). If the molecular backscatter changes with temperature of other environmental variables, L_0 must be converted to a function $L_0(z)$, which is known if the environment is specified by other measurements. Intensity L, one of the spectrally-determined parameters in Figure 2, is used directly for attenuation. Spectral parameters B and S then give the profile of hydrosol backscatter coefficient $\beta(z)$ in the form

$$(1/2) \, B(z)S(z) = \beta(z) \int_0^z \exp[-2\alpha(z)z] \, dz, \tag{8}$$

where the integral is available from equation (7) and the BS product approximates the area under the hydrosol spike in Figure 2.

One can infer both the hydrosol loading and something about its composition from $\alpha(z)$ and $\beta(z)$. One application of $\alpha(z)$ data is to determine the depth to which a laser fluorosensor of chlorophyll penetrates. A measure of fluorescence profile includes both chlorophyll backscatter and total attenuation terms in the manner of equation (8).

4.3 Current

The relevant spectral parameter for current measurements is the shift V_L between the laser frequency ν_0 and the symmetry axis of the spectrum. Equation (1) gives the conversion between frequency shift and longitudinal (line-of-sight) component of scatterer velocity with respect to the lidar.

Section 2.2 establishes that current measurements are a weighted average of the current existing in the first 40 m or a few optical depths, whichever is smaller. Figure 5 presents schematically two approaches to determining magnitude and direction of the current. A conical scan gives a sinusoidal velocity vs. time variation (Figure 6) from which the magnitude of the velocity (amplitude of the sinusoid) and azimuth (phase) are available. A differential Doppler technique (Schwiesow et al., 1977a) measures the transverse V_T component by an intersecting, 2-beam geometry (Figure 5). It does not require an assumption of horizontal homogeneity in the flow. Current is found from C $V_L/\sin\theta$, where θ is the cone half-angle, or from $C = V_T$ with the differential scheme.

Doppler lidar information from hydrosol scattering contains more than the average current over the sensed layer. A complete velocity spectrum is available. The velocity spectrum (intensity vs. velocity) indicates shears, reversed flow, and other features of the flow on scales smaller than the lidar resolution volume (Schiesow et al., 1977b).

5. LABORATORY RESEARCH

A working, high-spectral-resolution, oceanographic lidar does not exist. Preparatory research is underway on temperature extraction, spectral processing, and other topics.

5.1 Temperature Extraction

Measurement of temperature from high-resolution spectra such as that in Figure 2 requires accurate determination of W. One method that uses
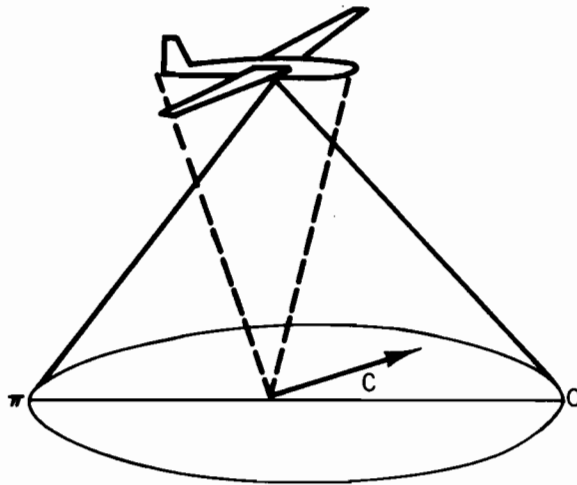
Figure 5. An approach to current measurement using a conical scan and an assumption of horizontal homogeneity to determine current $\vec{C}$. Alternative approach (dashed) using differential Doppler.
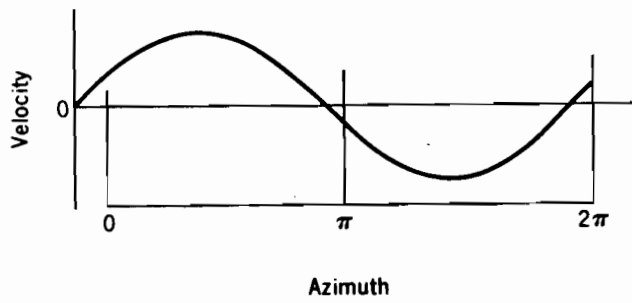
Figure 6. Schematic of velocity sensed by conical scan with aircraft velocity removed showing current from an azimuth slightly less than $\pi/2$.

all available data fits a parameterized equation to the observed spectrum. An example of such an expression is

$$I'(\nu) = B[1 + C \sin^2(\pi\nu/F)2^{-1}$$
$$+ L\{\exp[-\nu^2/K] + \exp[-(F-\nu)^2/K]$$
$$+ \exp[-(F+\nu)^2/K]\}, \quad 0 \le \nu \le F/2 \qquad (9)$$

where we have included a Fabry-Perot response to the hydrosol spike, the Fabry-Perot free spectral range F (given), and the periodic nature of the interferometer bandpass. This intensity expression includes only four parameters because we assume $V_L \ll S$. Parameter C is a function of S and F.

Methods exist to adjust parameters B, L, C, and K numerically to achieve the best fit in a least squares sense between the observed $I(\nu)$ and calculated $I'(\nu)$. With four parameters and 1024 spectral data points, for example, the fit is firmly overconstrained. We take advantage of the fact that the expected spectrum is known to reduce the effect of noise on determining K that would result if a direct width measurement were made.

With an analytical expression for $I'(\nu)$, noise can be added to a theoretically-generated data set and the controlled signal-plus-noise input used to exercise the fitting routine. Such data simulations test the sensitivity of the K-fitting to signal-to-noise ratio and give an estimate of random-error-induced uncertainties in inferred temperature.

5.2 Technique Development

High-resolution atmospheric lidar results previously reported for the visible wavelength range have used a Fabry-Perot interferometer for spectral analysis. This technique is incoherent in the sense that it measures optical intensity as a function of interferometer geometry. Infrared Doppler lidar systems generally use a coherent (homodyne or heterodyne) spectral analysis technique where the optical heat from the photodetector is scanned by an electronic analyzer.

Both coherent and incoherent processing schemes are affected by atmospheric refractive index inhomogeneities, but in different ways. Inhomogeneities in the refractive index of the ocean will have even stronger effects. Existing propagation theories are applicable to an analysis of refractive effects on high-resolution ocean lidar. Propagation analysis provides one input to the coherent-incoherent spectral processing choice for the field system.

26

Present laboratory results have demonstrated the sensitivity of high-resolution visible spectrometric techniques to stray light in the interferometer. This sensitivity dictates the need for research on instrumental filtering.

The Rayleigh backscatter intensity as a function of temperature for both pure and ocean water is a highly important, but not well-known, quantity for further development of high-spectral-resolution oceanographic lidar. Preisendorfer (1976) gives some data on backward scattering coefficient at a single temperature, but much additional work is needed.

6. CONCLUSIONS

Remote sensing of ocean temperature profiles, current, and turbidity using the spectral shape of Rayleigh and Mie backscatter from the ocean appears feasible on the basis of the foregoing analysis. The analysis does not completely specify the sensitivity, accuracy and precision expected, but we are encouraged to perform a more thorough system analysis, taking into account all significant factors found in environmental use. We are encouraged by the success of the atmospheric measurements of temperature and wind, from Rayleigh linewidth and Mie frequency shift respectively, to anticipate a useful role for high-spectral-resolution oceanographic lidar measurements.

Some aspects of the Rayleigh linewidth technique, such as interferometric measurements and parameterized spectral curve fitting to determine linewidth, are developed satisfactorily. On the other hand, we must determine the effect of temperature and salinity on the intensity of Rayleigh backscatter from ocean water, whether heterodyne methods may overcome present inadequacies in the spectral processing technique for temperature and current applications.

7. REFERENCES

Batchelor, G. K. (1970). *Fluid Dynamics,* Cambridge University Press, 55.

Benedetti-Michelangeli, G., F. Congeduti, and G. Fiocco (1972). Measurement of aerosol motion and wind velocity in the lower troposphere by Doppler optical radar, *J. Atmos. Sci.,* 29(7): 906-910.

Fiocco, G., G. Benedetti-Michelangeli, K. Maischberger and E. Madonna (1971). Measurement of temperature and aerosol to molecule ratio in the troposphere by optical radar, *Nature Physical Science,* 229(3): 78-79.

Preisendorfer, R. W. (1976). *Hydrologic Optics,* U. S. Department of Commerce/NOAA, 126-127.

Schwiesow, R. L., R. E. Cupp, M. J. Post, and R. F. Calfee (1977a). Coherent differential Doppler measurements of transverse velocity at a remote point, *Applied Optics* 16(5): 1145-1150.

Schwiesow, R. L., R. E. Cupp, M. J. Post, R. F. Abbey, Jr., and P. C. Sinclair (1977b). Velocity structures of waterspouts and dust devils as revealed by Doppler lidar measurements, *Preprints, 10th Conference on Severe Local Storms,* American Meteorological Society, 116-119.

Sizgoric, S. and A. I. Carswell (1975). Underwater probing with laser radar, *Water Quality Parameters,* ASTM STP 573, American Society for Testing and Materials, 398-413.

Walrafen, G. E. (1967). Raman spectral studies of the effects of temperature on water structure, *J. Chemical Physics* 47(1): 114-126.

OCEAN PARAMETERS USING THE BRILLOUIN EFFECT

Joseph C. Hirschberg, Alain W. Wouters and James D. Byrne[*]
University of Miami
Department of Physics
Coral Gables, Florida
33124

The Brillouin effect is used for measuring temperature and turbidity in seawater. A laser beam is projected into the sea and back-scattered light is measured interferometrically. Experimental work is described together with plans for future experiments.

1. INTRODUCTION

Certain parameters of the ocean are very important to measure rapidly. Among these are temperature and turbidity in the upper 10-50 meters. Existing remote sensing methods are approximate.

Temperature is measured by infrared either from an aircraft or satellite. In theory this is fine, but there are difficulties. The measurements are done in the 10 μm region. This is where the radiation at 300° K is a maximum and it outweighs the reflected sunlight. It also corresponds to a relatively transparent atmospheric window. A minor difficulty is that the window is only partly transparent. Water vapor interferes with infrared measurements. The effect of water vapor can be taken into account by using two wavelengths of I.R., both near 10 microns.

A major difficulty is the extremely small transparency of the water at 10 μm. This means that only the temperature of the top 1/100 mm or so of the ocean is being measured. Since this is also the layer that loses heat to the air by condensation, evaporation and radiation, it is often cooler by 1°-3°C than the bulk layers just below. This depends on mixing and is not easy to correct for.

We therefore proposed the use of visible, blue-green laser light of about 480 nm. This propagates beneath the sea better under most conditions than any other wavelength of light. It turns out that Raman and Brillouin scattering can provide information about conditions in the sea. We chose to investigate Brillouin scattering in detail.

2. BRILLOUIN SCATTERING

This results from the interaction of light and sound waves in liquid and solids. We will consider the case for liquid water (Fig. 1).

Because of thermal energy, sound waves in all directions and of all wavelengths are present in any liquid above 2-10°K. Of these, the light interacts with those which satisfy the Bragg law. Unless the angle θ is zero (forward scattering) there will be two Doppler shifted scattered returns. The wavelength shift follows the law

$$\Delta\lambda = \pm\lambda\frac{nv}{c} \sin \frac{\theta}{2} ;$$

c/n is the light velocity in the liquid, and v is the sound velocity. The angle θ can be measured (for backward scattering it is π and the shift is a maximum). Thus a measurement of $\Delta\lambda$ can be used to determine the sound velocity. This is a known function (Fig. 2) of the temperature, depth and salinity.

Using a pulsed or modulated laser, the depth can be found and used in the formula. The salinity is often known in fresh water and the open ocean to a sufficiently high accuracy. However, in estuarine waters, evaporation and fresh water runoff make the salinity highly variable. Under such circumstances, often very important from an oceanographic or environmental point of view, a measurement of salinity is necessary. This will be described later; for now we will assume that it has been done.

3. MEASUREMENT OF THE BRILLOUIN EFFECT IN THE LABORATORY

The Brillouin shift is very small, which has the great advantage of not being affected by water coloration ("gelbstoff", for example). However, its measurement involves the use of an interferometer. Since we had several in our laboratory, we chose to use a Fabry-Perot. Typical Brillouin shifts are about 1/10 Angstrom, which requires a resolving power of about 50,000. A Fabry-Perot consists of a pair of partially "silvered" flat mirrors and produces, in the focus of a lens, a circular interference pattern characterized by sharp fringes. The shapes of the fringes are shown (Fig. 3). Here R is the power reflection coefficient, T is transmission and L the absorption. For example, if T = L, I = $I_0/4$, a depends on the reflectance R, and is very small for high values of R. Using multilayer coatings the finesse or ratio of S to a can easily be as high as 100.

Using a Fabry-Perot we measured the Brillouin scattering in a sample of seawater brought to the laboratory. An argon-ion laser beam was directed through a tank of water (Fig. 4) and light at a known angle
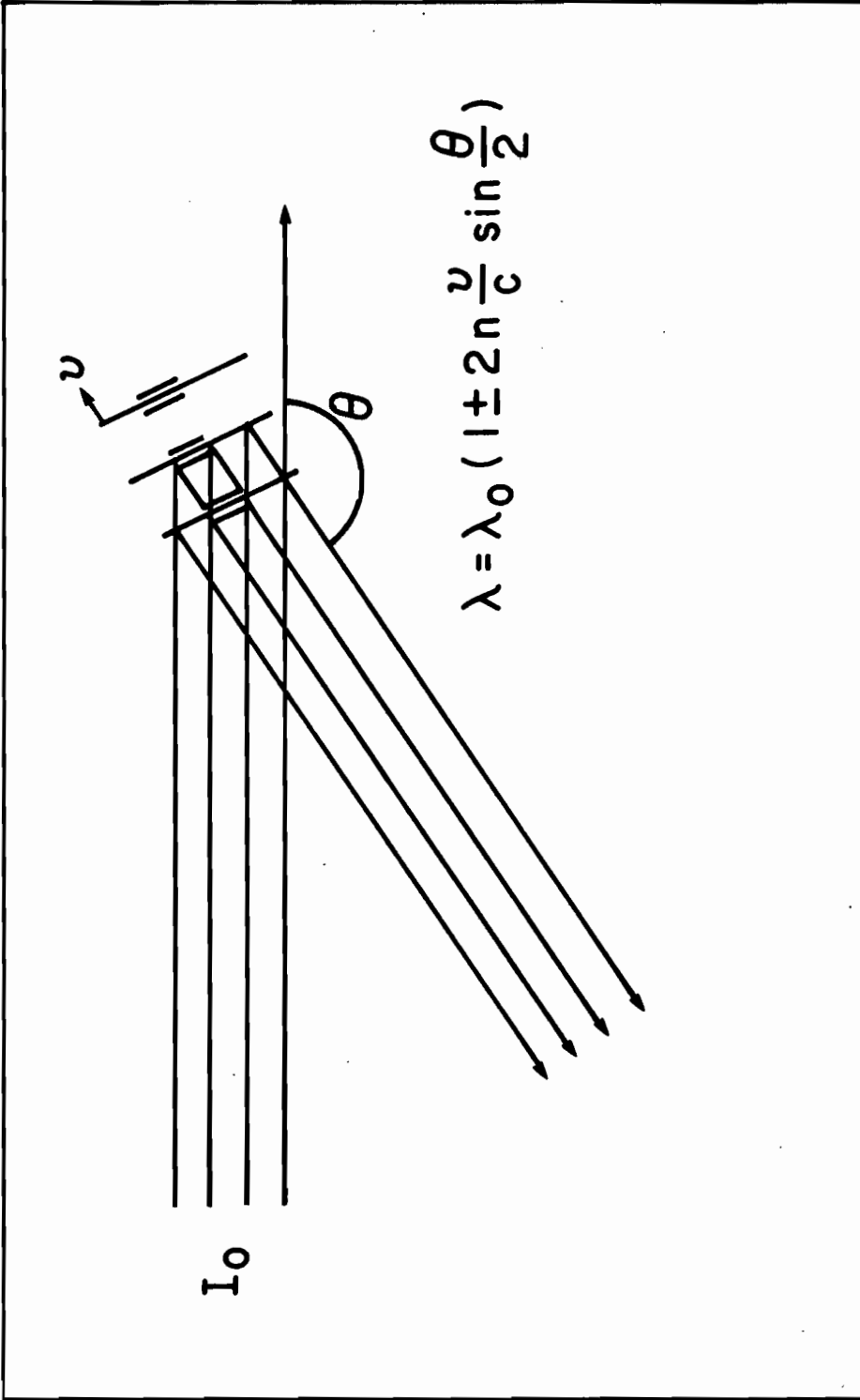
Figure 1. Brillouin Effect.

$$\lambda = \lambda_0 \left(1 \pm 2n \frac{\upsilon}{c} \sin \frac{\theta}{2} \right)$$
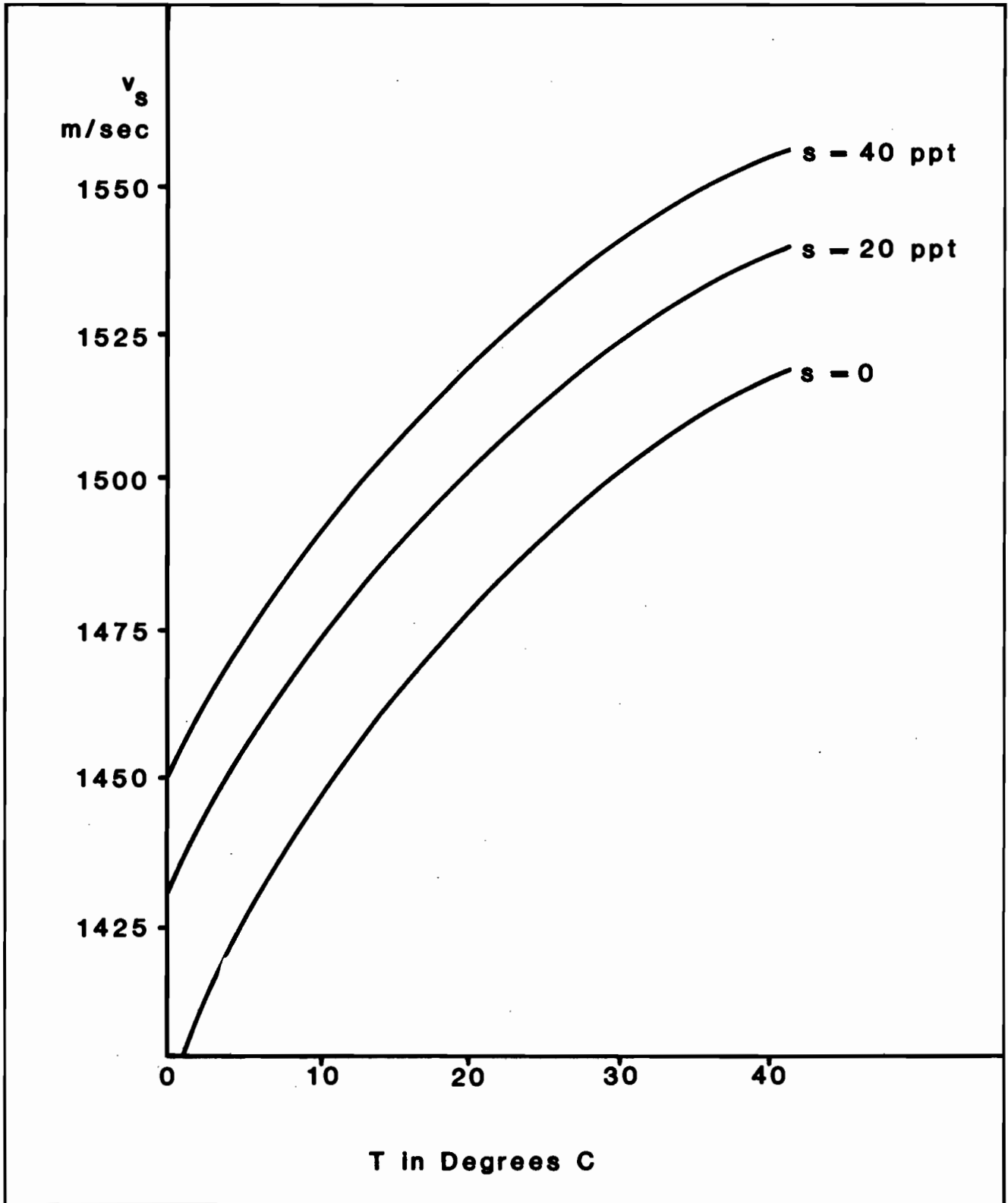
Figure 2.   Sound velocity of v_s plotted against temperature T for various values of salinity (redrawn from R. J. Urick, Principles of Underwater Sound for Engineers).
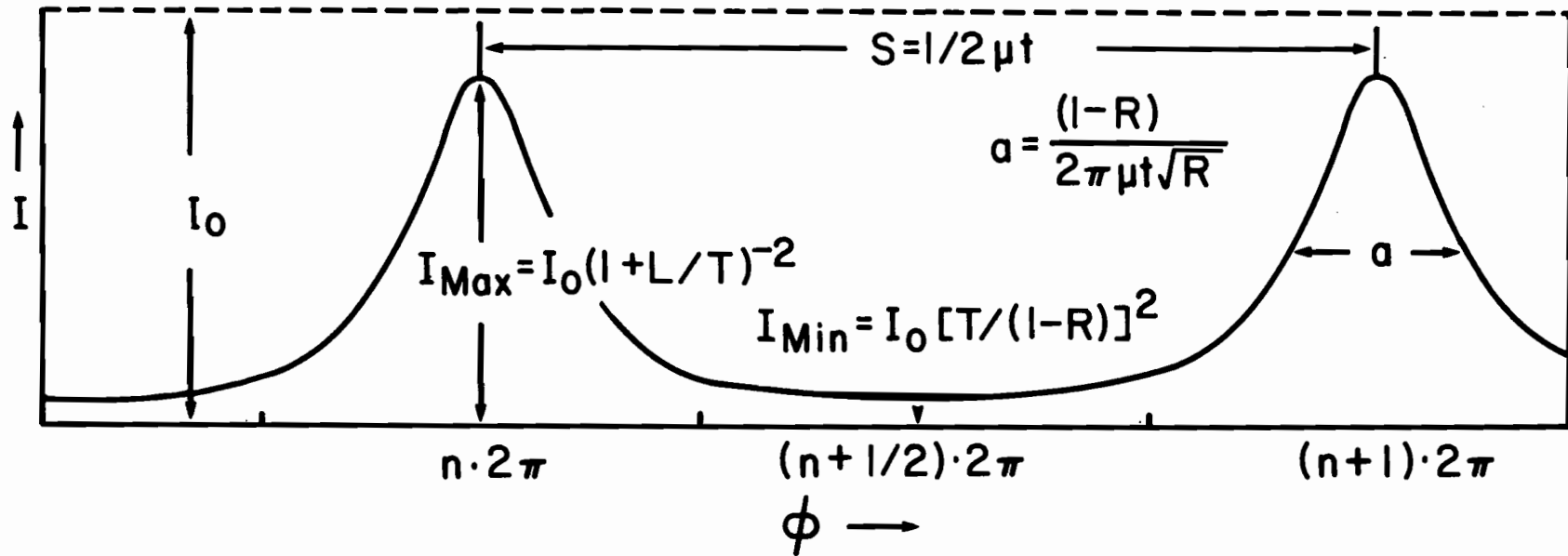
Figure 3. The Airy function for about two orders. This shows the appearance of the fringes produced as ϕ is varied. A number of pertinent parameters are shown.
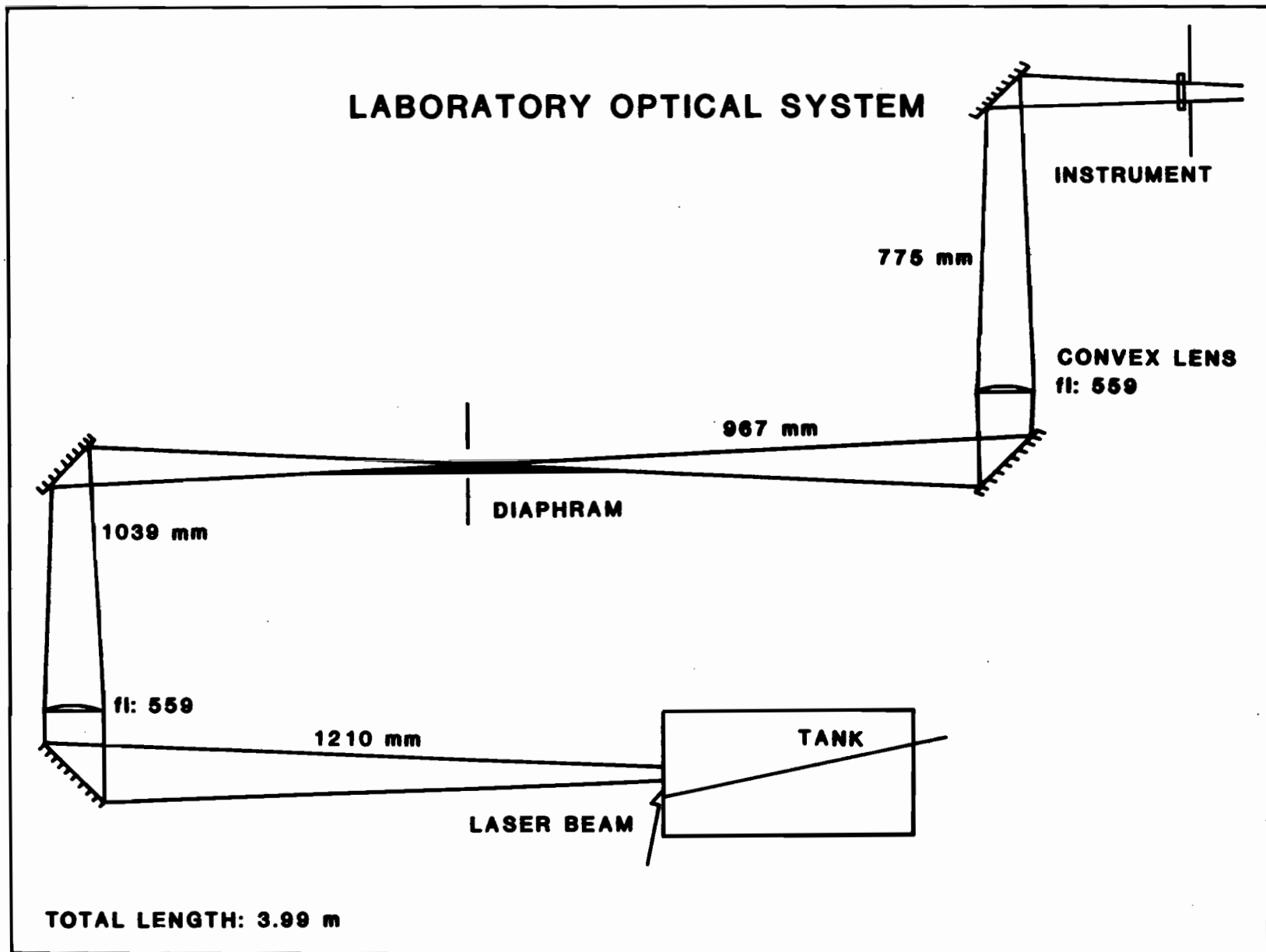
Figure 4. Laboratory Optical System.
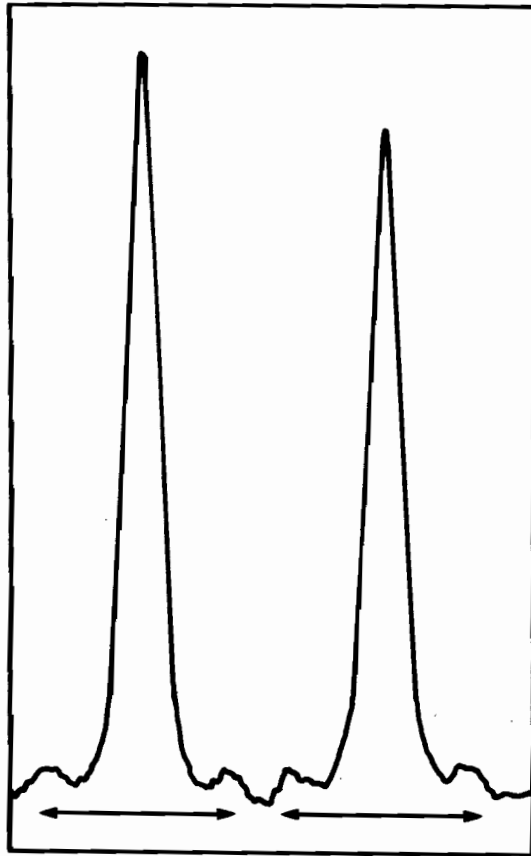
$\theta = 135°$

$2\triangle\lambda = 0.74$ FSR
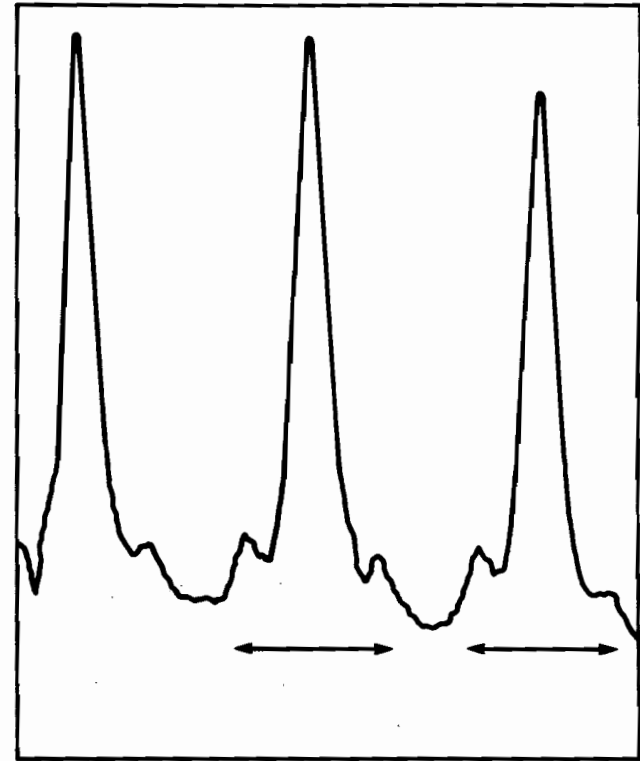
$\theta = 90°$

$2\triangle\lambda = 0.55$ FSR

$$\frac{\triangle\lambda_{135}}{\triangle\lambda_{90}} = 1.34 \text{ instead of } \frac{\text{Sin } 67°5}{\text{Sin } 45°} = 1.31$$

Figure 5.   Brillouin Effect in Tap Water.

was measured with the interferometer. The resulting fringes were measured with a microdensitometer and the results compared with theory. The results were favorable so we decided to test the method in the field.

4. FIELD TESTS

A site was chosen in the Miami (Fig. 6) ship canal. On incoming tides, dirt from dredging in the outer part of the channel came in; on outgoing tides the usual harbor trash appeared. This meant that conditions of water clarity were not favorable and a good test of practicability was provided. We moved the laser to an empty room at a Florida Power and Light Company test facility beside the ship canal. Mirrors were set up beside the sea wall (depth 20 ft.) and the experiment set up as shown (Fig. 7). This time a photomultiplier was used directly without using the photographic plate. The advantage here is that the photomultiplier is linear, which the photographic process is not.

The turbid water made the central (undeviated) peak very large, but when several fringes were averaged (Fig. 8) the results were very good, and quite consistent.

We are now preparing a shipboard trial using a Michelson interferometer working into two Fabry-Perots (Fig. 9). The Michelson has sine-shaped interference fringes, and will be arranged to cancel the central peak. It has a second channel through which the central peak will be measured to obtain the water turbidity. The two Fabry-Perots will be tuned to obtain a discriminator type response (Fig. 10). The result is that small displacements in the position of the Brillouin peaks due to changes in sound velocity will give an almost linear change in the ratio of the two channels B and C (Fig. 11).

4.1 Salinity Correction

In those cases where it is important to determine the salinity, a combination of Brillouin and Raman returns may be used. The reason is that the functional behavior of the salinity in the two measurements is different.

The behavior of sound velocity salinity and temperature is shown (Fig. 2) as well as Raman depolarization (Fig. 12) (Chang and Young, 1974). Both measurements can be used, the salinity determined, and the temperature deduced from the sound velocity.

We are also building a coaxial laser and detecting optical system. This corrects for corrugations in the sea and is the only configuration suited for airborne operation.

36
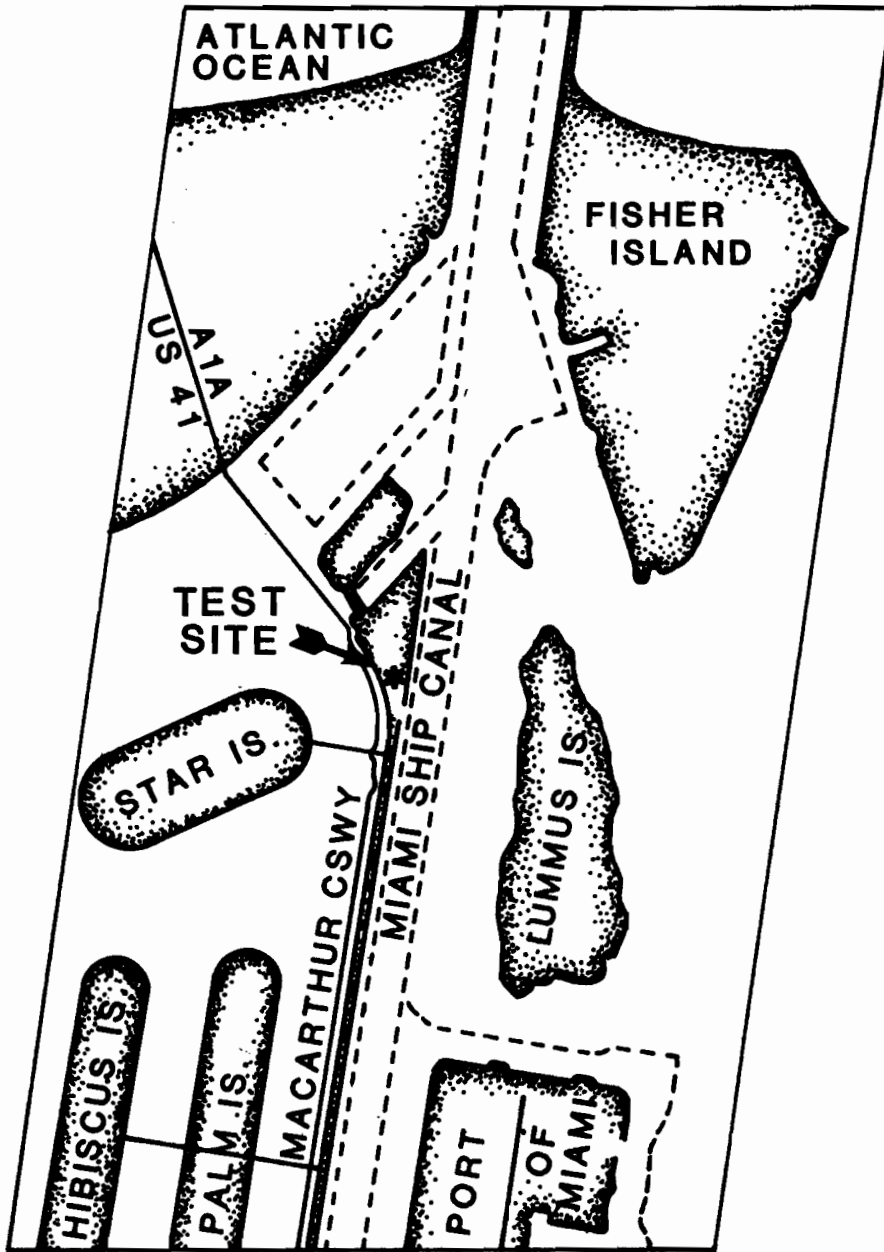
Figure 6. Field Experimental Site.
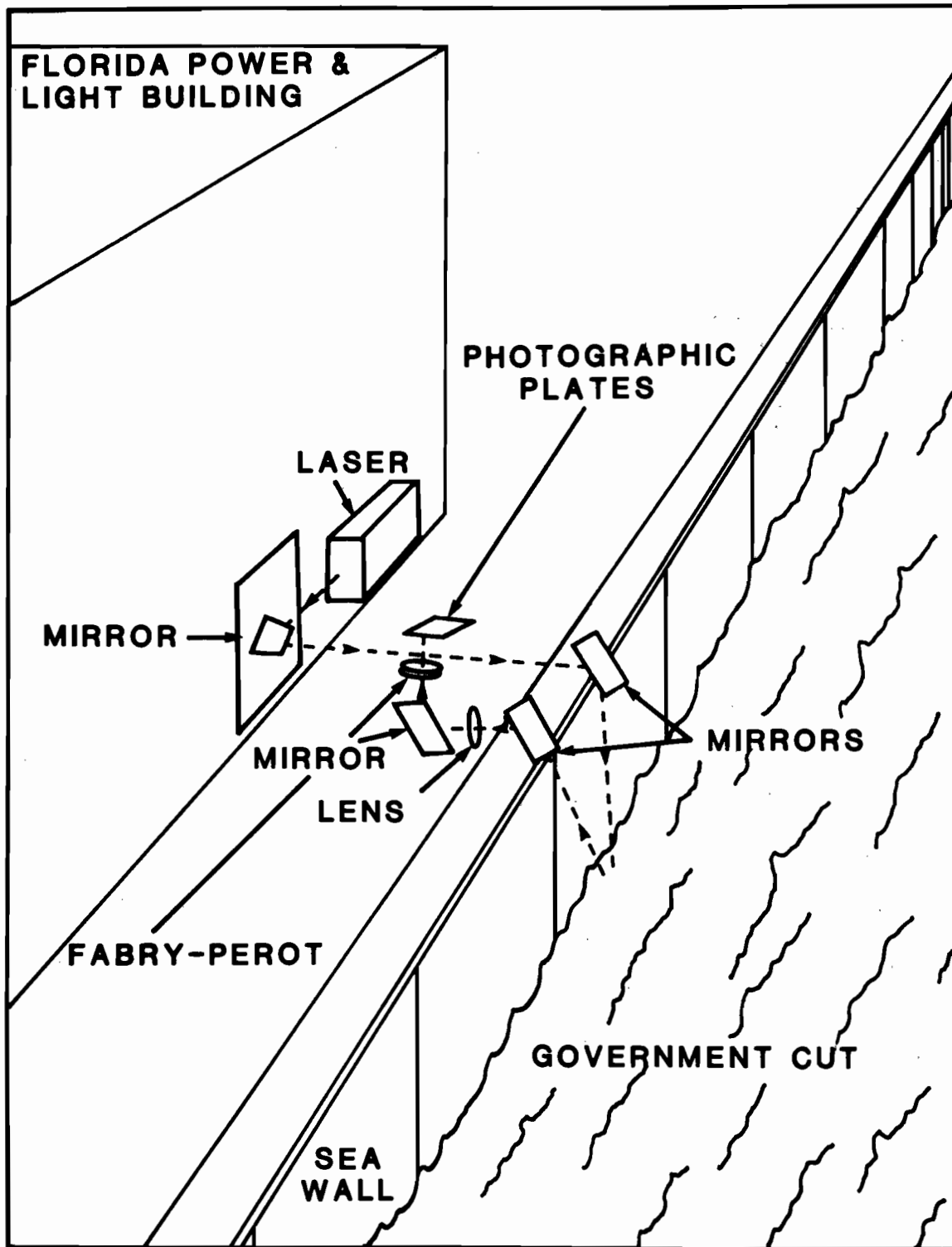
Figure 7. Field Experiment Optical System.
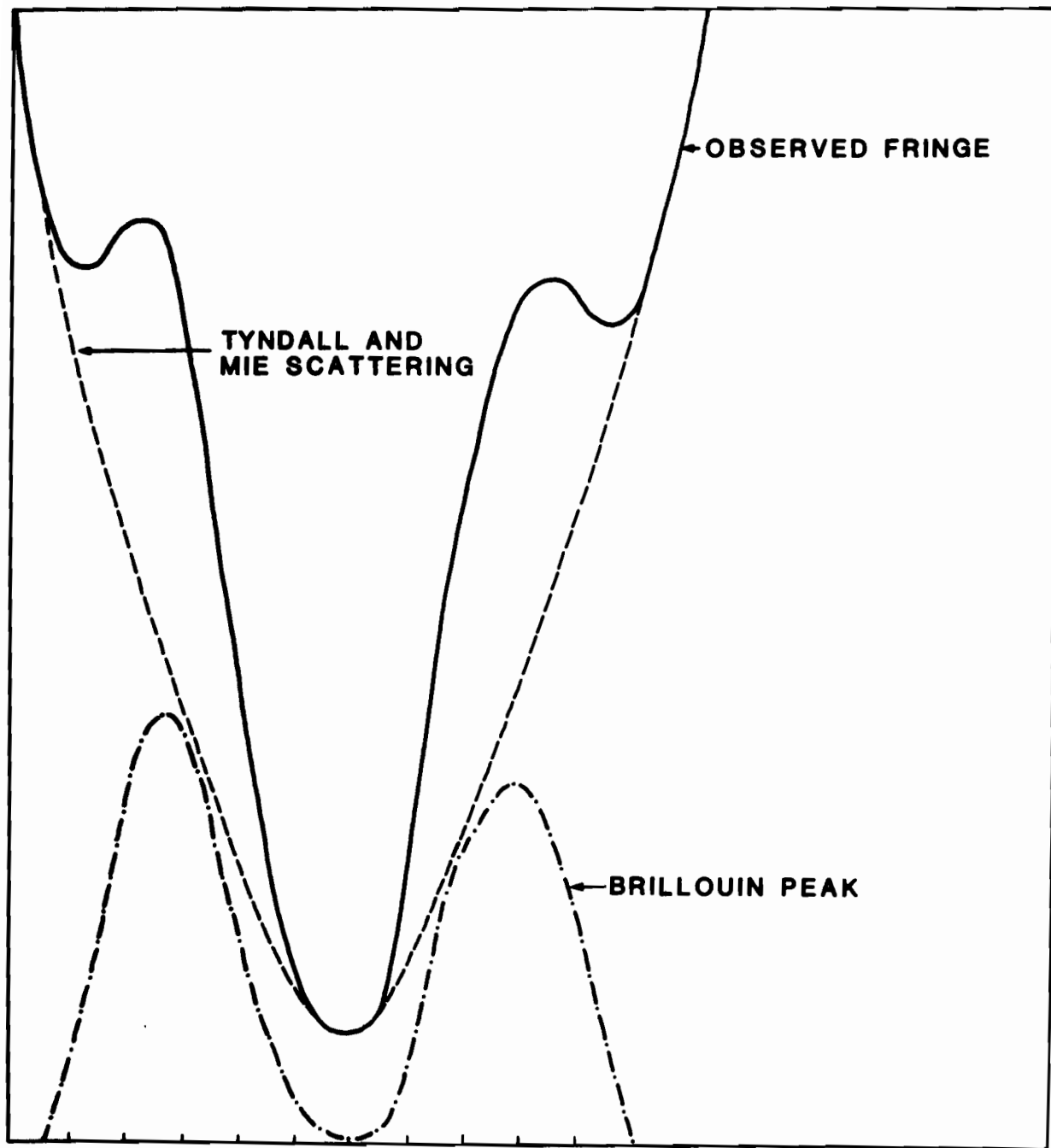
Figure 8. Fabry-Perot Fringes showing Brillouin Effect (average of 17 orders).
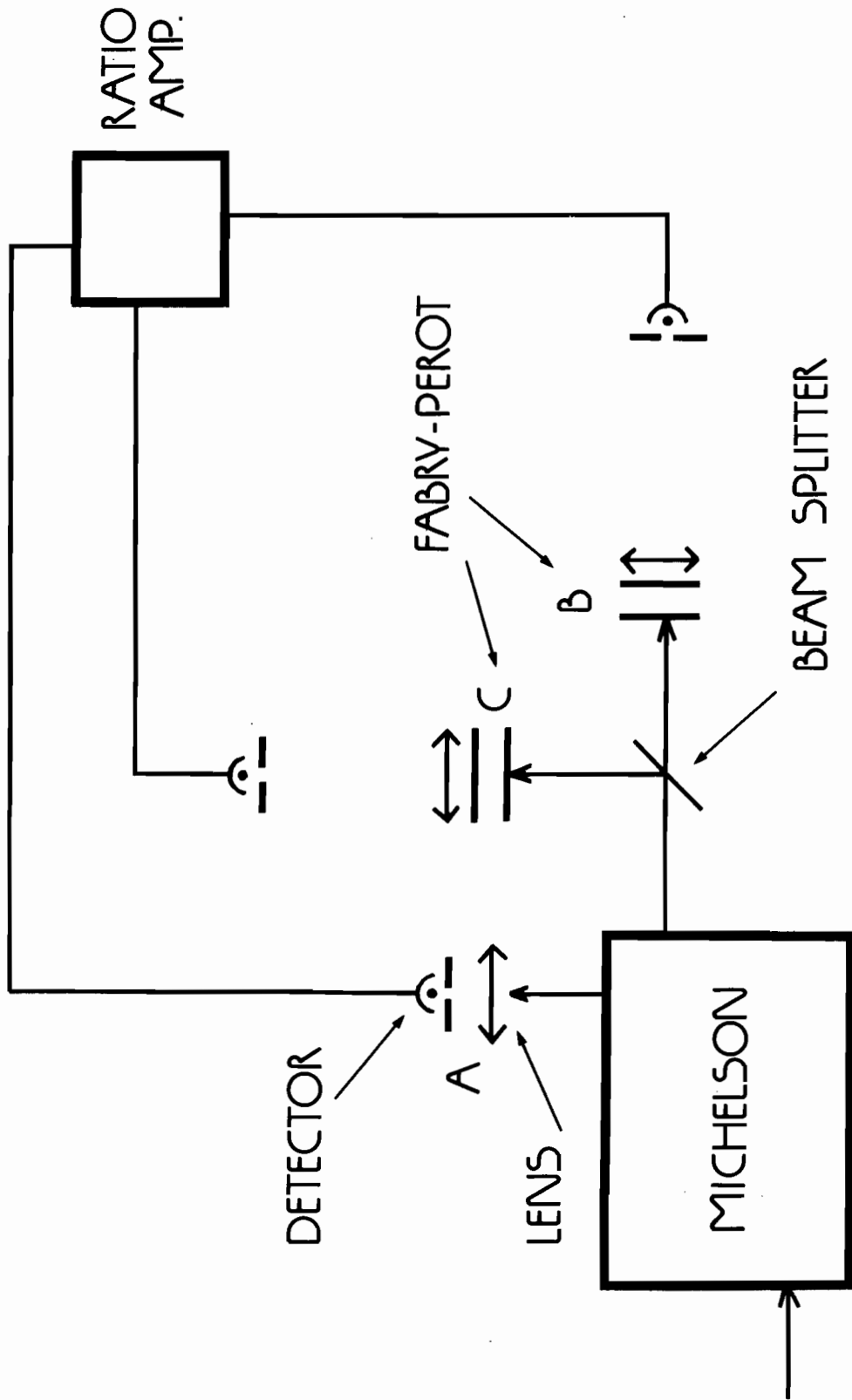
Figure 9. This shows the light leaving the Michelson passing through a beam splitter and falling on two Fabry-Perot Interferometers. The Fabry-Perots are adjusted with their pass-bonds on either side of the Brillouin peaks, as shown in Figure 10.
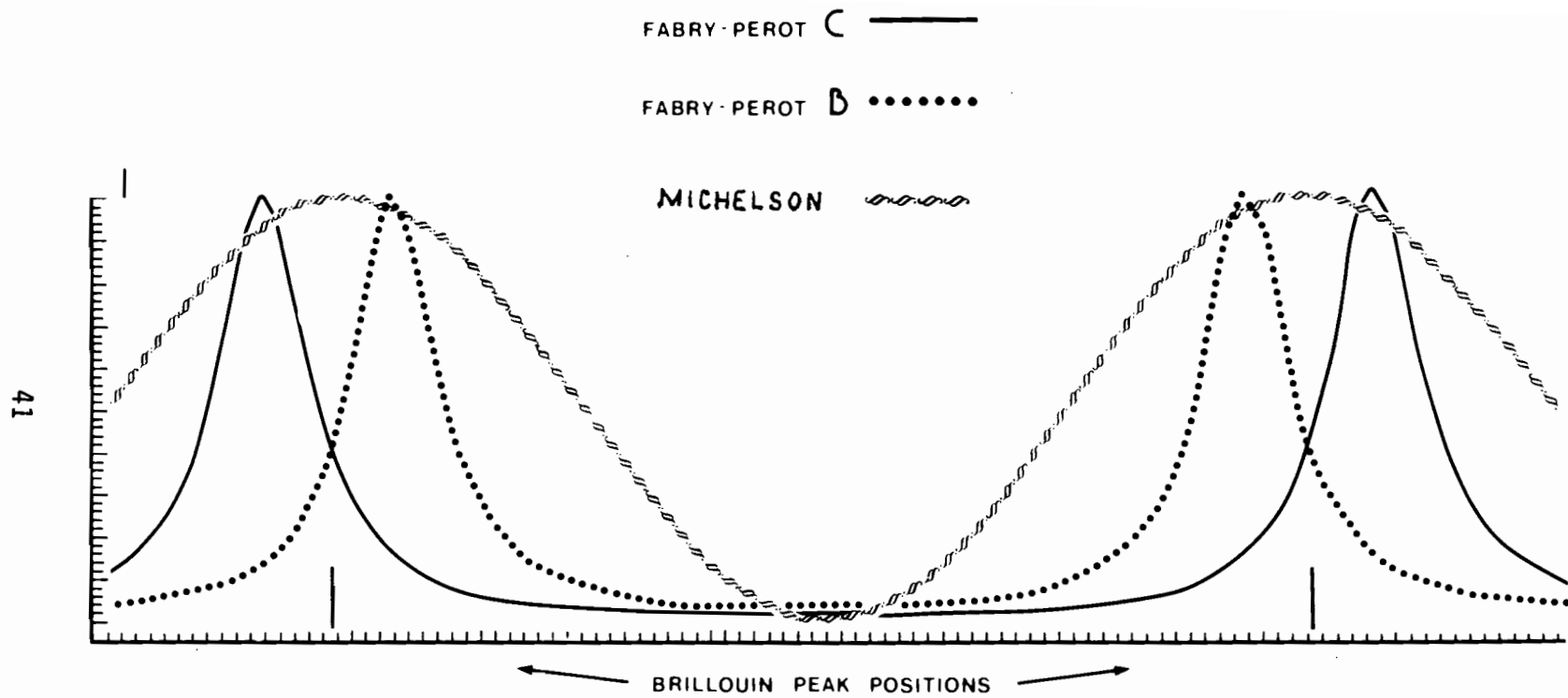
Figure 10. This shows the pass-bands of the two Fabry-Perot Interferometers. They are arranged so that a small change in the wavelength of the Brillouin peaks will be measured as a change in the ratio of the intensities from Fabry-Perots B and C.
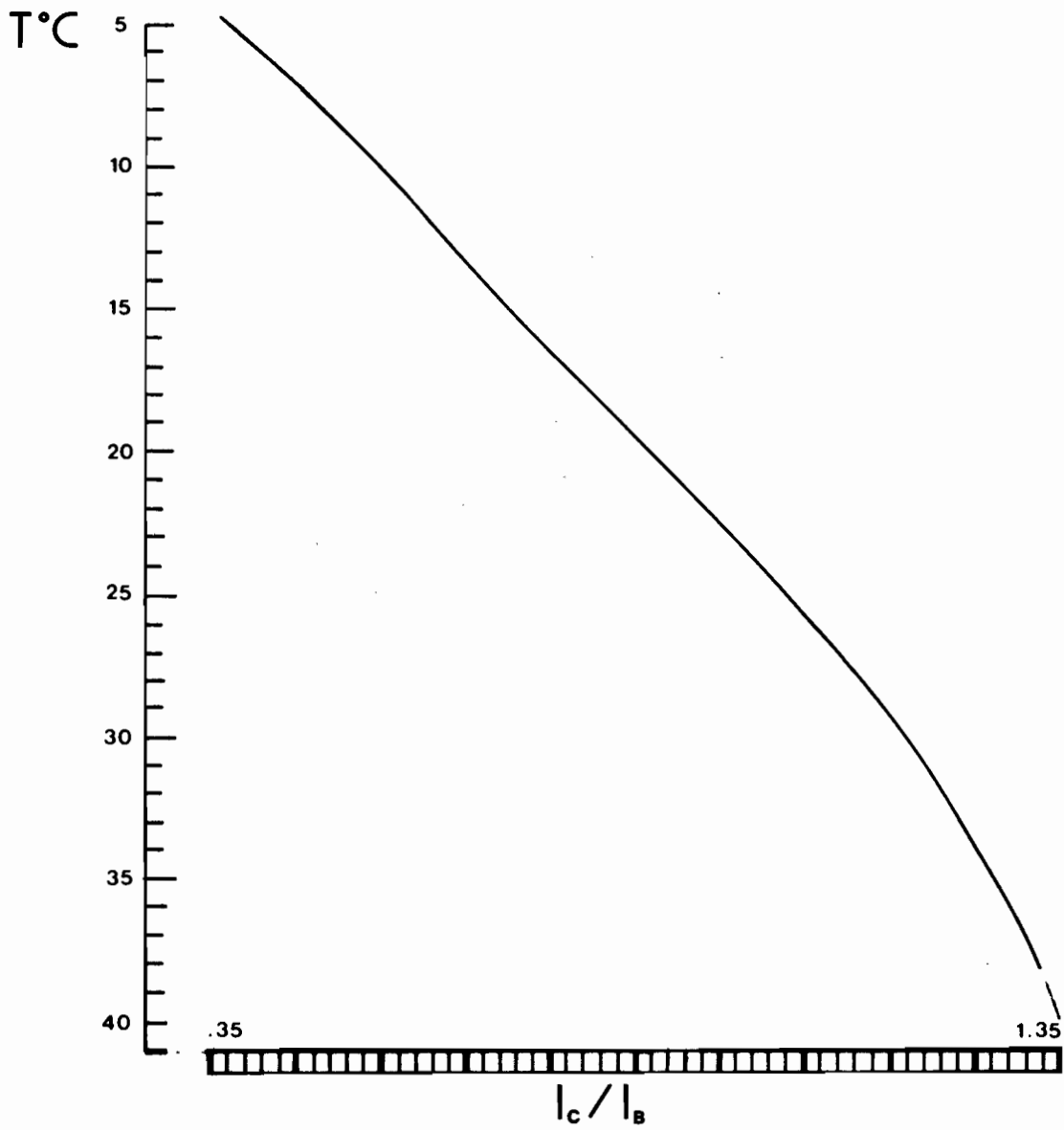
Figure 11. The ratio of Fabry-Perot channel C to channel B as a function of temperature in degrees celsius.

42
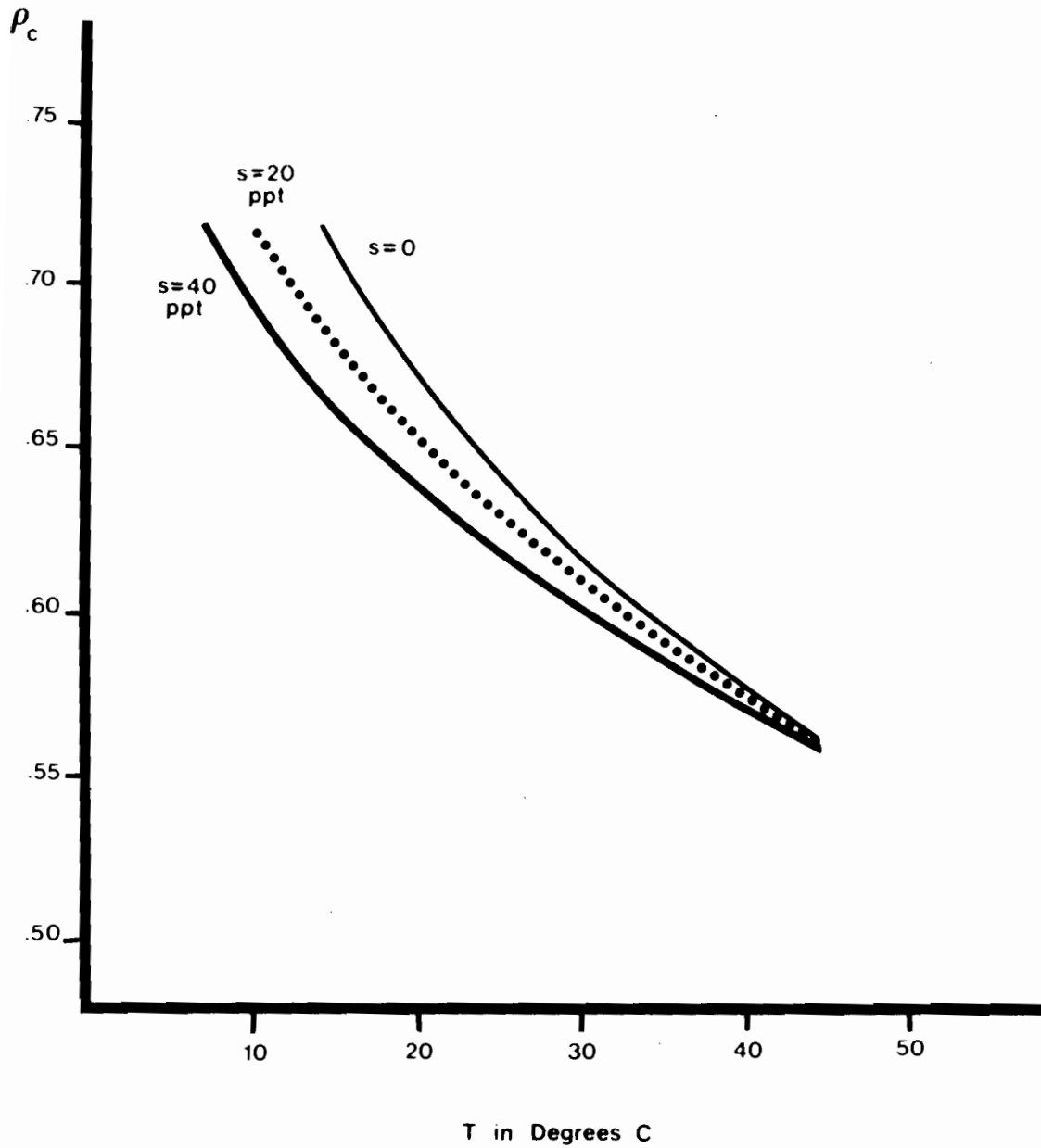
Figure 12. Circular depolarization ratio, ρ_c, plotted versus temperature, T, and with salinity, s.

5. REFERENCES

Benedek, G. and T. Greytak (1965). *Proceedings of IEEE* 53: 1623.

Chang, C.H. and L.A. Young (1974). AVCO Everett Research Lab Note 960, Everett, Massachusetts.

Del Grosso, V.A. (1974). *J. Acoust. Soc. Am.* 56: 1084.

Hirschberg, J.G. (1977). The use of Brillouin and Raman scattering to measure temperature and salinity below the water surface. Waste Heat Management and Utilization Conference, Miami Beach FL, May 11, 1977.

Hirschberg, J., A. Wouters and J. Byrne (1975). Laser measure of salinity, temperature and turbidity in depth, *Remote Sensing Energy Related Studies*, ed. N. Veziroglu, Wiley & Sons, New York.

Hirschberg, J., A. Wouters, F. Cooke, K. Simon and J. Byrne (1975). Laser application to measure vertical sea temperature and turbidity, NASA Report NASA CR-139184, January.

Hirschberg, J., A. Wouters, K. Simon, J. Byrne and C. Deverdun (1976). Laser application to measure vertical sea temperature and turbidity: design phase, NASA Report NASA CR-144854, January.

Kim, H.H. (1977). *Applied Optics* 16: 46.

Kullenberg, G. (1974). *Optical Aspects of Oceanography*, Chapter 2, eds. N.G. Jerlov and E.S. Nielsen, Academic Press, New York.

Leonard, D.A. and B. Caputo (1976). NOAA Seminar, Boulder, Colorado.

McCluney, W.R. (1975). Radiometry of water turbidity measurements, *J. Water Pollut. Control Fed.* 47(2): 252-266, February.

Stommel Report. The role of the oceans in climate production, Ocean Science Committee of the National Academy of Sciences, 1975.

White, M.B. (1976). *Optical Engineering* 16: 145.

Wouters, A. (1976). The double mach Zehnder 'perfect' interferometer, Florida Section of the OSA, Miami FL, January 26.

Wyrtki, K., et al. (1976). Predicting and observing El Nino, *Science* 191: 343.

Zimmerman, A.V., III (1976). *Final Report*, NASA CR-145149.

EXPERIMENTAL FIELD MEASUREMENTS
OF SUBSURFACE WATER BY RAMAN SPECTROSCOPY

Donald A. Leonard
Computer Genetics Corporation
Wakefield, Massachusetts

Using a pulsed laser and range gating detection techniques, Raman scattering can be analyzed as a function of depth in a radar-like echo mode, and thus subsurface temperature and salinity profiles can be obtained. Experiments are described in which Raman data has been obtained as a function of depth in open waters of the Atlantic and the Mediterranean and also from subsurface coastal zone waters.

Temperature accuracy of 1°C was obtained in the first optical attenuation length. Extrapolations from the available data indicate that accuracies of 0.1°C temperature and 1 part per thousand salinity may be achievable with a well-engineered, dual polarization instrument. With an airborne platform such a subsurface measurement system could be used to obtain real time data with wide area coverage of great utility in the areas of earth and ocean physics and weather and climate prediction.

1. INTRODUCTION

There currently exists no known capability to remotely measure subsurface ocean temperature profiles. A remote, wide area coverage, airborne or satellite measuring device capable of surface penetration and temperature measurement to ocean depths the order of 100 meters would provide for weather and climate prediction, valuable and complementary information to the ocean surface temperature data that is now currently available. Such a remote subsurface temperature measurement capability would also benefit other research and technology areas such as, for example, sea-air interaction modeling, the physics of oceanic mesoscale systems, behavior of ocean fronts and other mixed layer ocean dynamics, the synoptic behavior of acoustic propagation in the ocean and the monitoring and validation of models for thermal discharges into water bodies relevant to the operation of conventional fossil fuel and nuclear power plants and for ocean thermal energy conversion (OTEC) power plants.

In this paper we report experimental remote sensing of subsurface water temperature using the Raman technique. The physical basis of the measurement can be described by the following: (a) liquid water exists

45

in at least two forms, monomer and polymer; (b) the two forms are in chemical equilibrium as a function of temperature; (c) the O-H Raman stretching frequency is significantly different for the monomer and polymer forms; (d) the relative concentration of monomer vs. polymer can be determined from the Raman spectrum and thus, the temperature can be inferred.

This model is shown in a heuristic manner by means of the Raman spectrum in Figure 1. Liquid water is considered as being composed of two species, polymers which are hydrogen bonded and monomers which are not, both in rapid equilibrium with each other as a function of temperature. Each species has its individual Raman spectrum proportional to its concentration as shown in the schematic; the total observed Raman spectrum being composed of the sum. Simultaneous measurement of the Raman spectra at the two wavelengths λ_1 and λ_2 provides a measure of the concentration ratio, and through an equilibrium constant, the temperature. Such a two-species mixture model of liquid water has previously been successfully used in interpreting sound absorption measurements (Lieberman, 1956) and in infrared (Thomson et al., 1966; Worley and Klotz, 1966) and Raman spectroscopic studies (Murphy and Bernstein, 1972).

Our investigations were aimed at bringing the Raman technique from the theoretical and laboratory stages to the point where field experiments could be used to validate the concept for practical remote sensing utilization. We have obtained highly resolved experimental Raman spectra of subsurface ocean water from two research vessels in both coastal and open ocean waters. These experimental results strongly support our design calculations which showed that Raman spectra can be used for remote sensing of subsurface ocean temperature profiles.

2. PREVIOUS LABORATORY EXPERIMENTS

Walrafen (1967) at Bell Telephone Laboratories was one of the first to experimentally observe in the 1960's that the laser Raman spectrum of liquid water in the perturbed O-H stretch region (2800 to 3900 cm^{-1}) shifts toward longer wavelengths with increasing temperature. Walrafen's work showed that by monitoring the Raman spectra of liquid water in the O-H region, the variation of molecular structure due to the mobility of the hydrogen bonds may be observed and the shape of the Raman spectra, therefore, provides a means for measuring the temperature of liquid water.

Polarization spectroscopy may also be used to study the Raman spectrum of liquid water. Using this technique the water sample is illuminated with a polarized laser beam. Two Raman spectra are recorded, one in the same polarization as the laser beam, the other in the orthogonal
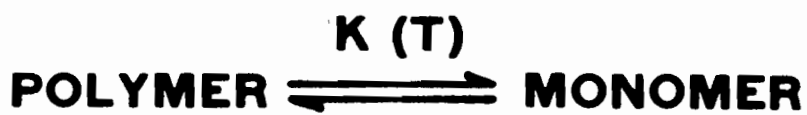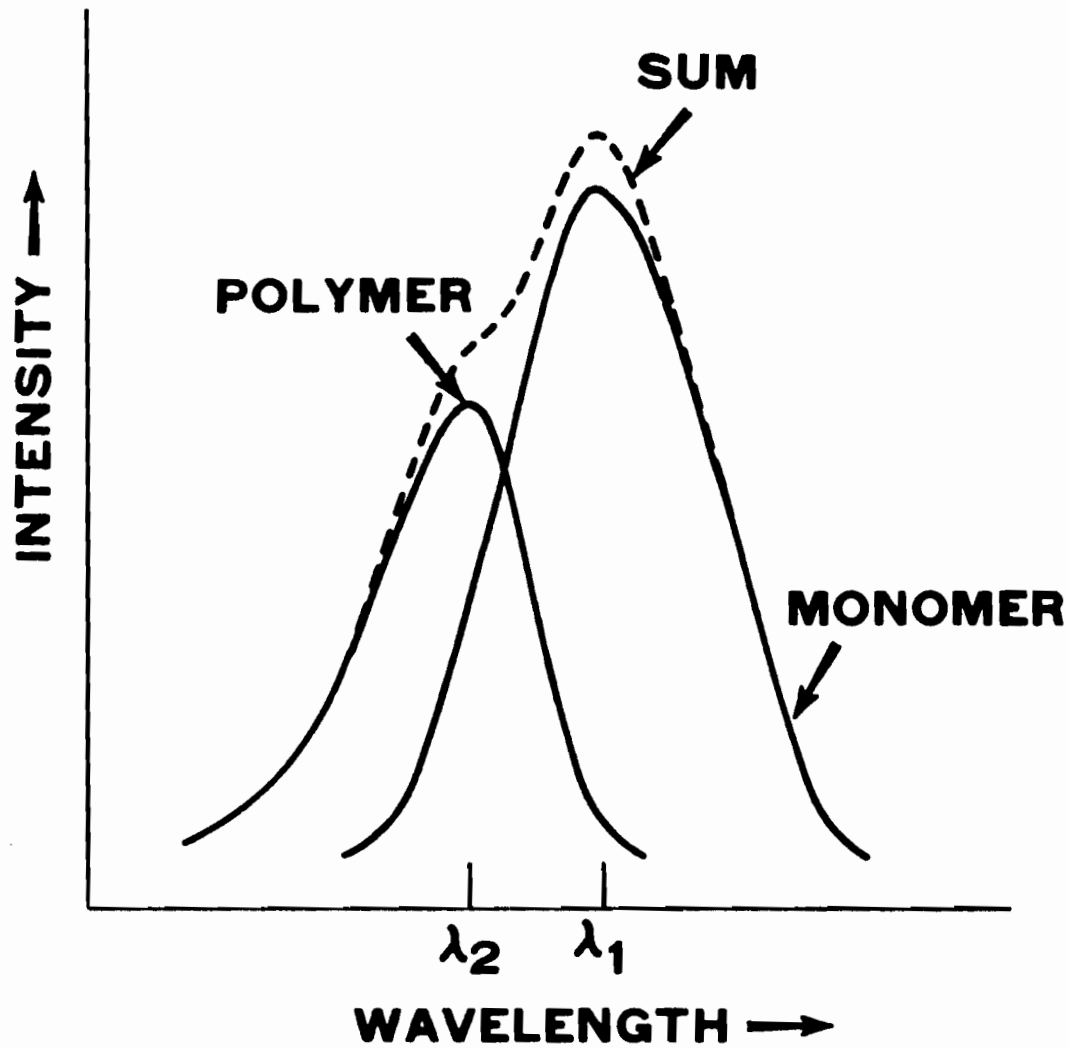
Figure 1. Raman Spectrum and Structure of Liquid Water.

polarization. The ratio of the two polarization spectra, when computed as a function of wavelength, is found also to be temperature dependent (Cunningham and Lyons, 1973). Polarization spectroscopy has unique advantages for deep penetration applications which will be discussed later in the paper.

Schwiesow (1971) first suggested and conducted experiments to show that the Raman techniques could be employed for remote water temperature measurements. More recently Chang et al. (1974) demonstrated the feasibility of the method as a remote temperature sensor in a series of laboratory experiments which investigated both a two-color technique and a depolarization technique. The basic sensitivity of the measurement was shown to be about 1% per C°, and it was estimated that the expected performance of an airborne system would be a temperature determination accuracy of 0.5°C at a depth of 4 diffuse attenuation lengths per joule of laser energy transmitted. The effect of salinity was also experimentally investigated and was shown to be separable from temperature using polarization techniques.

An experimentally measured value of 4.5×10^{-33} m^2/molecule-sr for the liquid water O-H stretching band Raman cross section has been reported by Slusher and Derr (1975). Table 1 shows a representative, but by no means complete, compilation of volume backscattering coefficients that have been measured by various investigators for distilled water and ocean and lake water of various types. Also included in Table 1 are Raman backscattering coefficients for distilled water and ice. The wavelength of light used for the measurements cited in Table 1 varies somewhat from investigator to investigator, but all use light in the blue-green near 500 nm so that order of magnitude comparisons may be considered valid.

From the data compiled in Table 1 it can be noted that the Slusher and Derr value for the Raman coefficient is essentially equal to the on-frequency backscatter coefficient of Tyler for distilled water. Far from being a "weak" effect the Raman return is comparable to the main on-frequency return from the water itself. This has implications when making comparisons between the Raman method and other laser scattering methods for remote subsurface measurements such as the Brillouin technique to determine sound speed (Hirschberg, 1976).

It should also be noted that the cross section for ice is comparable to that of liquid water. Slusher and Derr (1975) have obtained temperature measurements using Stokes to anti-Stokes line ratios in ice from 0° to -50°C. A Raman instrument capable of measuring liquid water temperature and salinity should therefore also be capable of not only detecting the spectral signature of ice but also of measuring ice temperatures.

TABLE 1. COMPARISON OF RAMAN AND VOLUME SCATTERING
COEFFICIENTS FOR WATER

<u>RAMAN SCATTERING COEFFICIENT, (λ = 488 NM) (METERS^{-1} STERADIAN^{-1})</u>

DISTILLED WATER	.00015	SLUSHER AND DERR (1975)[9]
ICE	.000093	SLUSHER AND DERR (1975)[9]

<u>VOLUME SCATTERING COEFFICIENT, $\sigma(180°)$ (METERS^{-1} STERADIAN^{-1})</u>

DISTILLED WATER	.00017-00020	TYLER (1961)[19]
OCEAN		
VARIOUS LOCATIONS, EASTERN NORTH ATLANTIC	.0005	JERLOV (1961)[17]
OFF BERMUDA (31°57'N, 65°11'W)	.002	MORRISON (1970)[20]
COASTAL		
BETWEEN WOODS HOLE AND THE 180M CONTOUR	.003-.004	SPILHAUS (1968)[21]
NEAR SANTA CATALINA ISLAND (33°32'N, 118°17'W)	.00020	TYLER (1961)[19]
LONG ISLAND SOUND (41°16'N, 70°08'W)	.02	MORRISON (1970)[20]
LAKE		
WINNIPESAUKEE, NEW HAMPSHIRE	.003	DUNTLEY (1963)[22]
PEND OREILLE, IDAHO	.0017-.0041	TYLER (1961)[19]

49

Laboratory experiments with natural waters were carried out by Zimmerman and Bandy (1975) who conducted laboratory laser induced scattering measurements with samples taken in estuarine waters near Norfolk, Virginia. While the purpose of their work was not to measure water temperature the Raman O-H stretch band is sufficiently resolved in the data that they published so that the ratio of monomer to polymer can be determined after subtraction of the fluorescence level to yield a water temperature value in the mid to upper 70's F°, which would be typical of a a laboratory situation. (The data of Walrafen (1967) was used as a calibration.)

3. PERFORMANCE ESTIMATES

The performance of a fully developed Raman lidar subsurface temperature measurement system, if not limited by interferences can be exactly calculated.

The number of Raman photoelectrons collected per second by an optical detector in a pulsed laser backscattering system can be expressed by the following equation:

$$N_{pe} = N_{LASER} N_{SCAT} \sigma_{RAMAN} \Delta R \frac{\Omega}{n^2} \, \varepsilon_{pe} \varepsilon_{op} \, T_{\lambda_1} T_{\lambda_2} \tag{1}$$

where

N_{PE}	= number of Raman photoelectrons detected
N_{LASER}	= number of laser photons transmitted
N_{SCAT}	= density of molecular scatters of a given species
σ_{RAMAN}	= Raman scattering cross section per particle per steradian
ΔR	= range resolution
Ω	= detection solid angle of collector
n	= refractive index of water
ε_{pe}	= photocathode photoelectric efficiency
ε_{op}	= optical system efficiency
$T_{\lambda_1} T_{\lambda_2}$	= two-way transmission, T_{λ_1} at laser wavelength T_{λ_2} at Raman wavelength

50

The subsurface water temperature measurement performance of a typical Raman lidar system was estimated using equation (1) with system parameters that assume modest but well-engineered components. The system parameters assumed are listed in Table 2 with a brief rationale for the particular choice of the value of each parameter.

The product of the system parameters shown in Table 2 yields a total Raman signal return of 3.5×10^5 photoelectrons per second with the assumption of unity two-way transmission loss, i.e. surface or near-surface measurements. As has been previously shown (Leonard,1974), in a well-engineered Raman system using a pulsed laser, the limiting noise can be reduced to the "shot noise" in the laser induced Raman signal itself. Therefore, the signal-to-noise (S/N) ratio can be given by the square root of the total number of photoelectrons collected in a given measurement time interval. This S/N assumption has been verified by data obtained in laser Raman field experiments (Leonard, 1974). If the signal in the above calculation is assumed to be equally divided between the two polarizations a basic S/N of $(1.75 \times 10^5)^{1/2}$ or 418 would be available. Based on a measurement sensitivity of 1% per C°, this would mean that a temperature precision of $(1/418) \times 100 \approx 0.2C°$ would have been achieved.

The ability to achieve depth penetration depends critically on the diffuse attenuation coefficient of the particular water being measured and is highly variable among open ocean, continental shelf and coastal waters. Table 3, which is based on data published by Ferguson (1975), lists the various types of ocean and coastal waters with values of diffuse attenuation coefficient, the range of the optimum transmission wavelength window and the rate of laser beam power loss in dB per meter of depth penetration.

The performance of a Raman lidar subsurface temperature measurement system as a function of depth, water quality and the other relevant operating parameters can be summarized by means of an "operating map" such as is shown in Figure 2. The operating map of Figure 2 has been calculated for a typical airborne open ocean measurement situation with a mixed layer depth of 100 meters. The basic parameters on the map are the number of Raman photoelectrons collected as the ordinate with the depth as measured in attenuation lengths displayed on the abscissa. The derived quantities of temperature precision in °C and the depth in meters as a function of water quality are also shown as alternate ordinate and abscissa quantities respectively. The operating lines on the map are drawn for various values of the parameter M where M is defined as

$$M = \left(\frac{P_L}{20}\right) \left(\frac{\Delta d}{10}\right) \left(\frac{1}{R}\right)^2 T \qquad (2)$$

51

TABLE 2. SYSTEM PARAMETER VALUES

SYSTEM PARAMETER	VALUE ASSUMED	RATIONALE
N_{LASER}	$2.3 \times 10^{17} \dfrac{PHOTONS}{SEC}$	THIS VALUE CORRESPONDS TO 0.1 WATT OF AVERAGE POWER AT 4600 Å. COMMERCIALLY AVAILABLE N_2 PUMPED DYE LASERS HAVE THIS CAPABILITY.
$N_{SCAT\ RAMAN}$	$1.5 \times 10^{-4} STER^{-1}M^{-1}$	THIS IS THE LATEST PUBLISHED VALUE FOR THE EXPERIMENTALLY MEASURED TOTAL RAMAN LIQUID WATER BACKSCATTER COEFFICIENT. (REFERENCE 9)
ΔR	1 METER	CORRESPONDS TO MINIMUM DEPTH RESOLUTION SET BY PULSE DURATION OF LASER.
$\dfrac{\Omega}{N^2}$	$2 \times 10^{-7} STER$	THIS COLLECTION SOLID ANGLE CORRESPONDS TO A 30 CM EFFECTIVE DIAMETER COLLECTOR ON A PLATFORM 500 METERS ABOVE THE SUBSURFACE SCATTERING VOLUME.
$\epsilon_{OP}\ \epsilon_{PE}$	5×10^{-2}	TYPICAL OVERALL OPTICAL AND PHOTOELECTRIC QUANTUM EFFICIENCY.

TABLE 3. UNDERWATER WINDOWS FOR VARIOUS OCEAN WATERS[*]

| WATER TYPE AND LOCATION	TRANSMISSION WINDOW		
	K (M-1)	LOSS (dβ/m)	(nm)
CLEAREST OCEAN, OPEN OCEAN; TROPICAL AND SUBTROPICAL, BELOW THERMOCLINE	0.02	0.087	430-470
CLEAREST OCEAN, OPEN OCEAN; TROPICAL AND SUBTROPICAL, ABOVE THERMOCLINE	0.03	0.130	440-480
WARM OCEAN, OPEN OCEAN; TROPICAL AND SUBTROPICAL, ABOVE THERMOCLINE	0.04	0.170	470-490
COOL OCEAN, OPEN OCEAN; TEMPERATE SUBARTIC AND ARTIC, ABOVE THERMOCLINE	0.07	0.300	475-495
SHELF, CONTINENTAL SHELF, SURFACE TO BOTTOM	0.10	0.430	490-510
COASTAL, COASTAL; RELATIVELY SHALLOW WATER, SURFACE TO BOTTOM	0.16	0.695	510-550
VERY TURBID, INSHORE COASTAL; HARBOR AND BAY WATER, SURFACE TO BOTTOM	0.40	1.737	550-570

53

[*]SEE REFERENCE 13.
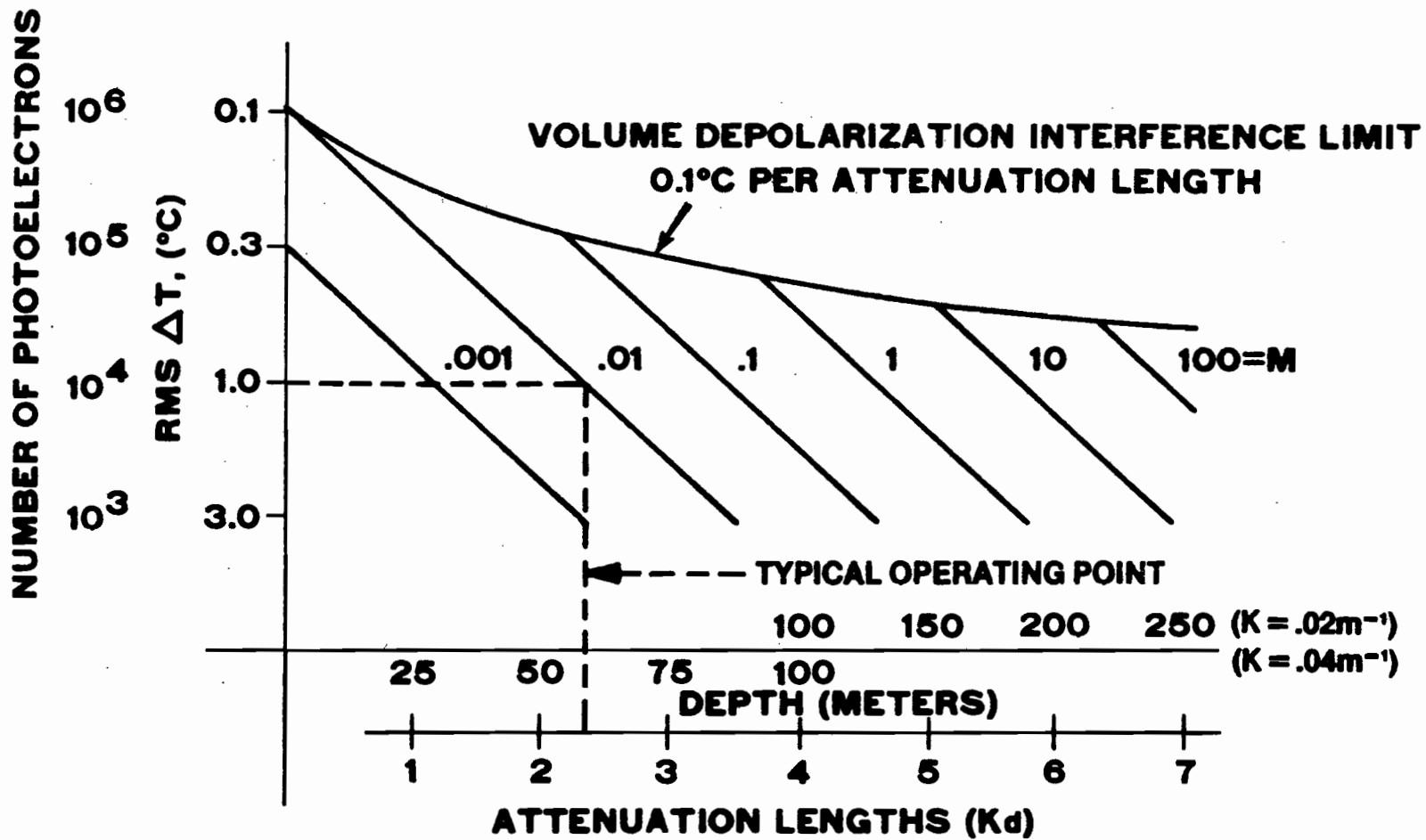
Figure 2. Typical System Operating Map (100 Meter Mixed Layer).

where P_L is the average laser power in watts, Δd is the depth resolution in meters, R is the altitude of the aircraft in kilometers, and T is the integration time of the measurement in seconds. Thus, for example, for a system with P_L = 0.2 watts, Δd = 10 meters, R = 1 kilometer and T = 1 second, the map parameter would be M = 0.01. This means that with such a system the allowed region of the operating map of Figure 2 is to the left of the line labeled M = 0.01. A typical operating point is shown corresponding to a temperature accuracy of 1°C and a depth penetration of 60 meters at the limit of a map function value of M = 0.01.

The map is constructed by using equation (1) to calculate the near surface (ordinate) values of the number of photoelectrons collected for each polarization for a given map parameter M. The overall optical and photoelectric efficiency, the effective diameter of the collector and the Raman scattering cross section are those given in Table 2. The slope of the lines is determined by the transmission loss as a function of depth given by exp[-2Kd], where K is the diffuse attenuation coefficient and d is the depth.

Also shown on the operating map is an upper boundary labeled "volume depolarization interference limit". This represents the most significant interference to the measurement and is caused by depolarization due to transmission through natural waters. Analysis of data published by Duntley (1971) has shown that the depolarization effect will produce an uncertainty in a Raman spectral temperature measurement the order of 0.1°C per attenuation length and in a Raman salinity measurement the order of 1 part per thousand per attenuation length.

4. EXPERIMENTAL RESULTS

4.1 Description of Raman Lidar Equipment

The subsurface water Raman spectra were obtained using a Raman lidar system originally designed and used by Leonard and Caputo (1974) as a single-ended transmissometer for airport glide slope visual range applications. This equipment was recently modified by CGC to include a capability to measure atmospheric profiles of water vapor and temperature in addition to atmospheric transmission profiles. As such the system was non-optimal for subsurface water measurements, but notwithstanding enabled useful new information to be obtained.

A block diagram of the equipment is shown in Figure 3. The laser source is a pulsed nitrogen laser operating at 337.1 nanometers and producing pulses of 100 kilowatts peak power with an effective pulse duration of 10 nanoseconds at a pulse repetition rate of 500 Hertz. The nitrogen laser uses an unstable resonator cavity and produces a beam
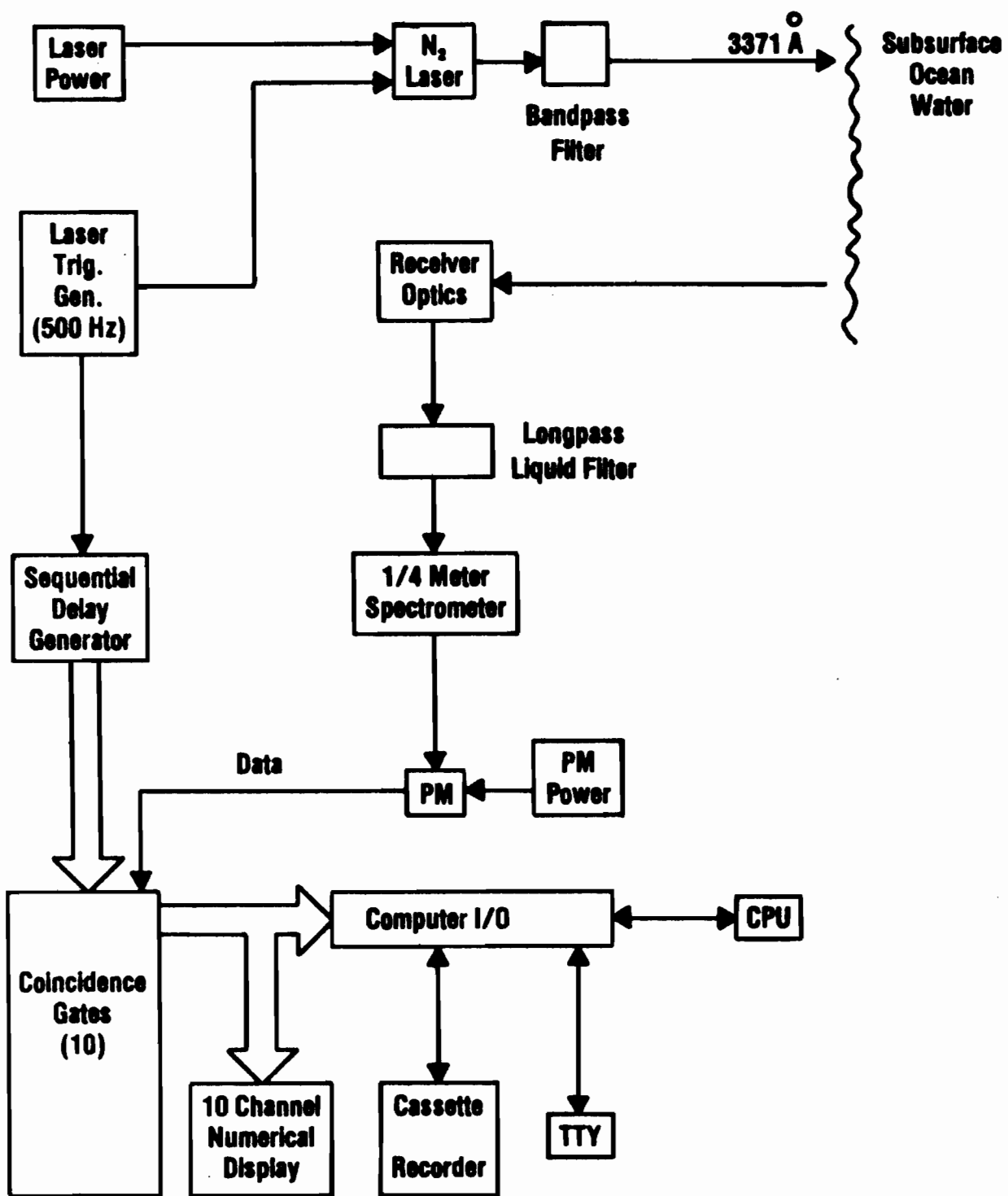
Figure 3. Block Diagram of Raman Lidar Equipment.

symmetric in the far field with a divergence of approximately 2 milliradians. The output from the laser is passed through an interference filter which passes the 337.1 nm laser line with a high efficiency but blocks spontaneous emission occurring in the laser gas discharge in the O-H Raman spectral region near 3800 Å .

The photons collected by the receiver optics are passed through a liquid filter and into a double 1/4 meter focal length scanning spectrometer having a 0.5 nanometer spectral resolution. The wavelength scanning of the spectrometer produces a spectral scan of the liquid water Raman O-H stretching band with sufficient resolution so that the monomer and polymer components can be resolved and a water temperature determined.

The liquid filter, a water solution of 2, 7-dimethyl-3, 6-diaza-cyclohepta-1, 6-diene perchlorate in a quartz walled cell, has the property of essentially complete isotropic volume bulk absorption of 337.1 nm but with nearly complete transparency at wavelengths of 350 nm and longer. This filter is used for blocking the strong on-frequency return at 337.1 nm which is reflected from the water surface and which the spectrometer alone is not able to adequately reject. It is far superior in this regard to the best interference filters commercially available, both in transmission characteristics and in angle requirements.

The Raman photon output from the spectrometer is detected by an RCA 8850 photomultiplier. The Raman photoelectron signal and a gate pulse suitably synchronized and delayed with respect to the laser firing are combined in ten (10) separate coincidence gates, the output from which are recorded using direct memory access (DMA) techniques with a Data General NOVA 1220 computer. The number of pulses occurring during the same data taking interval is also recorded. The ratio of the Raman photoelectrons to laser pulses recorded over a given time interval is the basic data obtained. The ten coincidence gates provide Raman data at ten separate range locations which can be varied both in width and spacing over the ranges 30 to 330 nanoseconds and 50 to 550 nanoseconds respectively.

The data taking is fully automated. The computer can be directed through the teletype (TTY) to specify the number of laser pulses over which to record data at each wavelength and the maximum and minimum wavelengths and the wavelength increments of each spectral scan. The data obtained are printed on the TTY in tabular form and also recorded on cassettes. A ten-channel numerical display of the data is also provided.

The plan and elevation views of the Raman lidar transceiver equipment are shown in Figure 4. The equipment is secured to a wheeled cart which was used on the afterdeck of the *Hayes*. The 45° mirror was

1.52 m

FOLDING
MIRROR

PLAN VIEW

LASER

.76 m

RECEIVER MIRROR
0.2 m DIA., 1.6 m F.L.

BAFFLE

FILTER/DETECTION ASSEMBLY
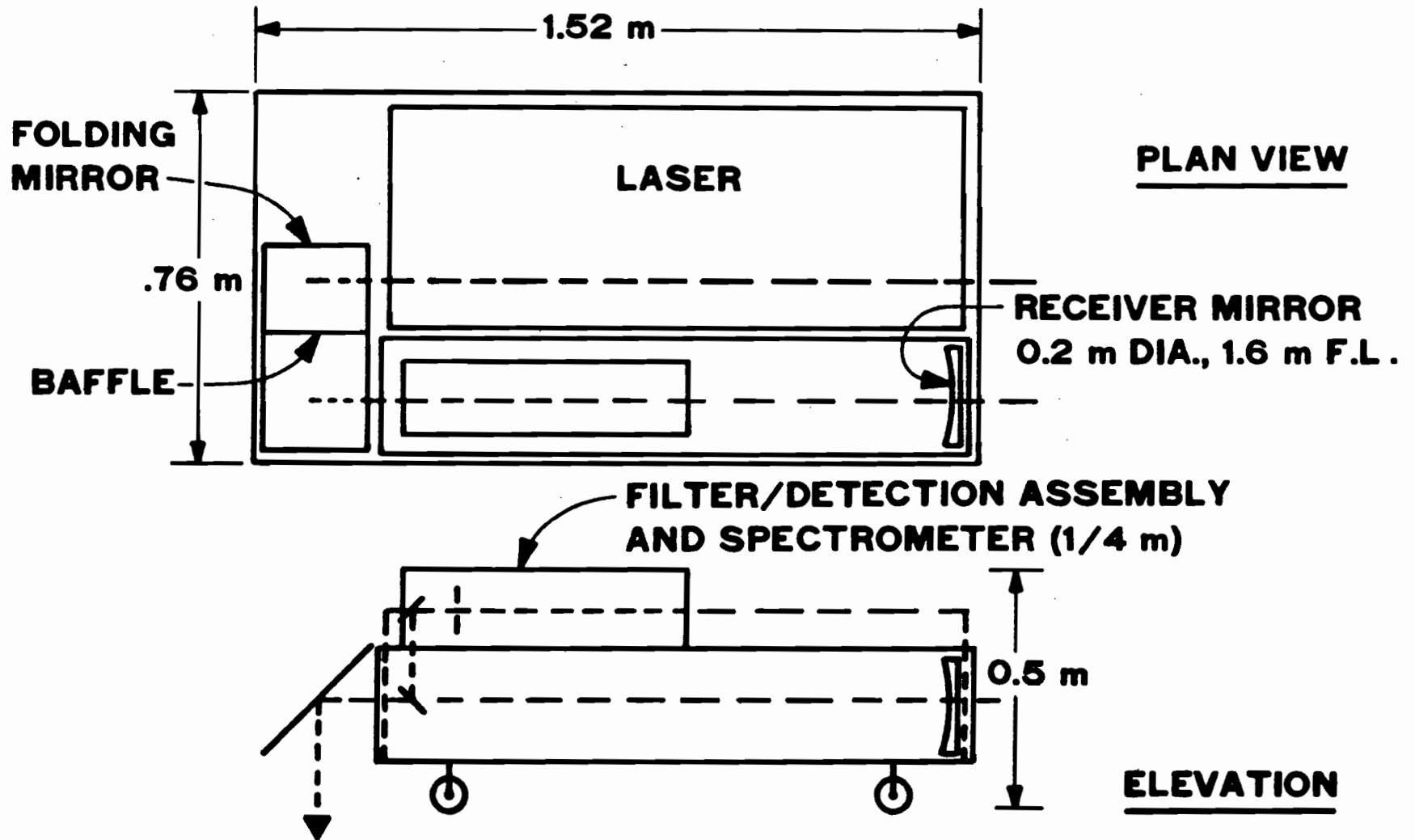AND SPECTROMETER (1/4 m)

0.5 m

ELEVATION

Figure 4. Plan View and Elevation of USNS Hayes Raman Lidar
Equipment.

rotated 180° to convert the system from an upward looking atmospheric lidar to a downward looking subsurface oceanographic lidar.

Figure 5 is a photograph of the USNS *Hayes,* which illustrates the unique twin-hull character of the research vessel. Figure 6 shows the Raman lidar transceiver in place on the afterdeck of the *Hayes* in a typical data-taking mode positioned to view the ocean water in the wake between the hulls. Subsurface Raman water spectra were obtained both with the ship stopped and as a function of speed while underway. The effects of foam and air bubbles in the wake were observed to cause increased signal attenuation as the ship speed increased but no measurable distortion of the Raman spectrum. The difference in Raman signal amplitude between a dead stop and full speed was about an order of magnitude.

4.2 Experimental Field Measurements -- *Hayes* Cruise

In this section the field measurements and the data obtained to date are described. The first preliminary field experiments were conducted aboard the Computer Genetics Corporation research vessel, the *Makai*, and Raman spectra were obtained from various depths in the Annisquam River, a tidal estuary in Massachusetts. The data were analyzed and a spectral temperature was obtained which agreed with laboratory calibrations. This work has been reported elsewhere (Leonard et al., 1977).

More recently (May-June 1977), resolvable Raman subsurface water temperature spectra were obtained in five open ocean locations from the decks of the Naval Research Vessel, USNS *Hayes*, during a North Atlantic/ Mediterranean research cruise. The locations shown in Table 4 ranged from the colder North Atlantic waters (sea surface temperature 4.7°C -- 15 May), 100 miles southeast of Cape Race, Newfoundland to the warmer Mediterranean Sea (19.7°C -- 2 June), 100 miles west of Sicily. Raman spectra were documented and recorded from depth regions of 0-10, 10-20, and 20-30 meters.

The significant new information and conclusions derived from these *Hayes* experiments are the following: (1) the Raman spectrum of the open ocean waters that were investigated for the first time were found to be essentially free of 337 nm laser induced interferences, (2) Raman spectral temperature measurements to a relative accuracy of $+ 1°C$ were made in natural ocean water from an ocean research vessel while underway, (3) Raman spectral measurements of the subsurface temperature gradient to a depth of 30 meters were obtained, and (4) the experimental results strongly support the previous concepts and system design calculations for the exploitation of induced Raman spectra for the remote sensing and quantitative measurement of subsurface ocean temperature.

59
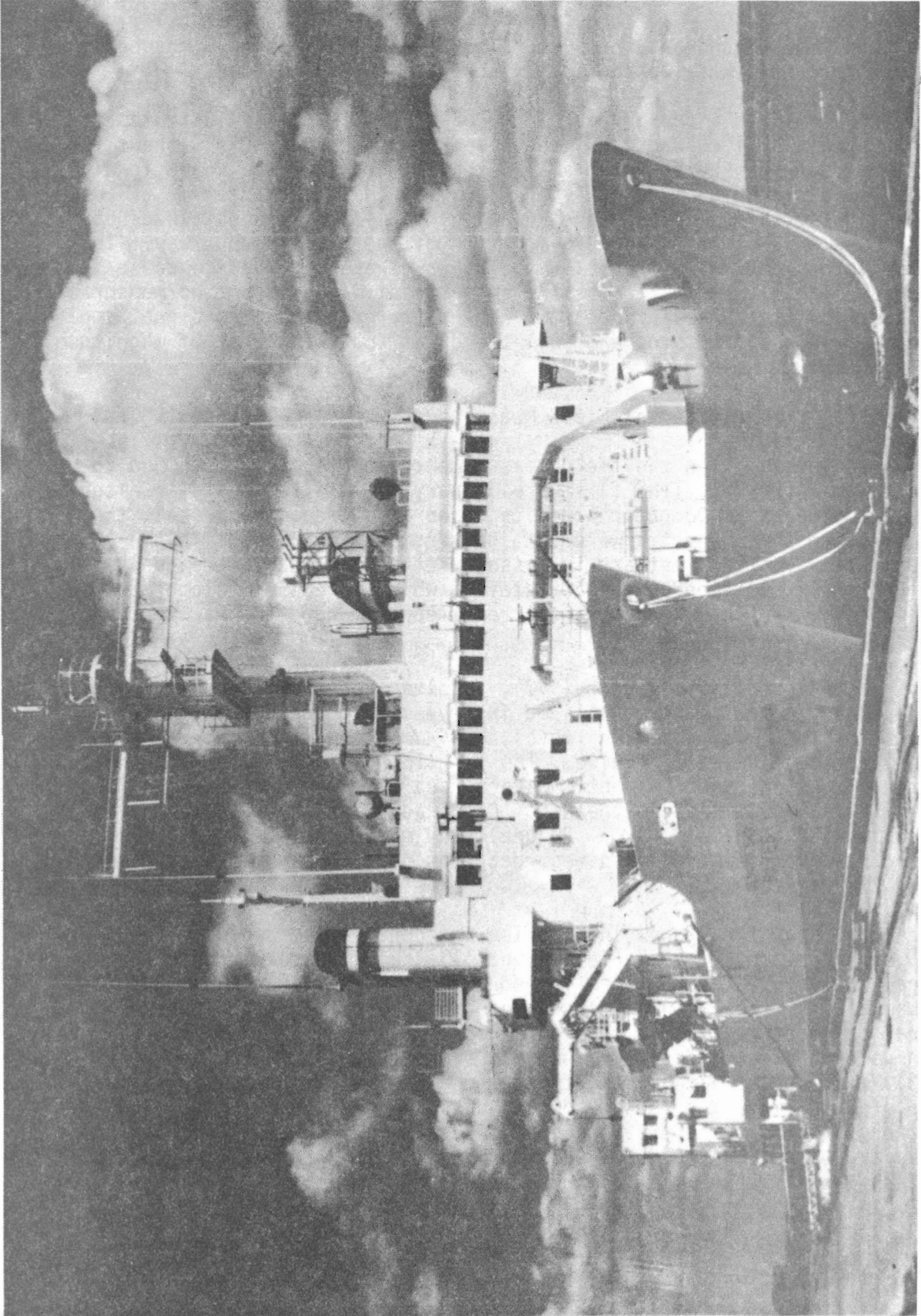
Figure 5. USNS Hayes.
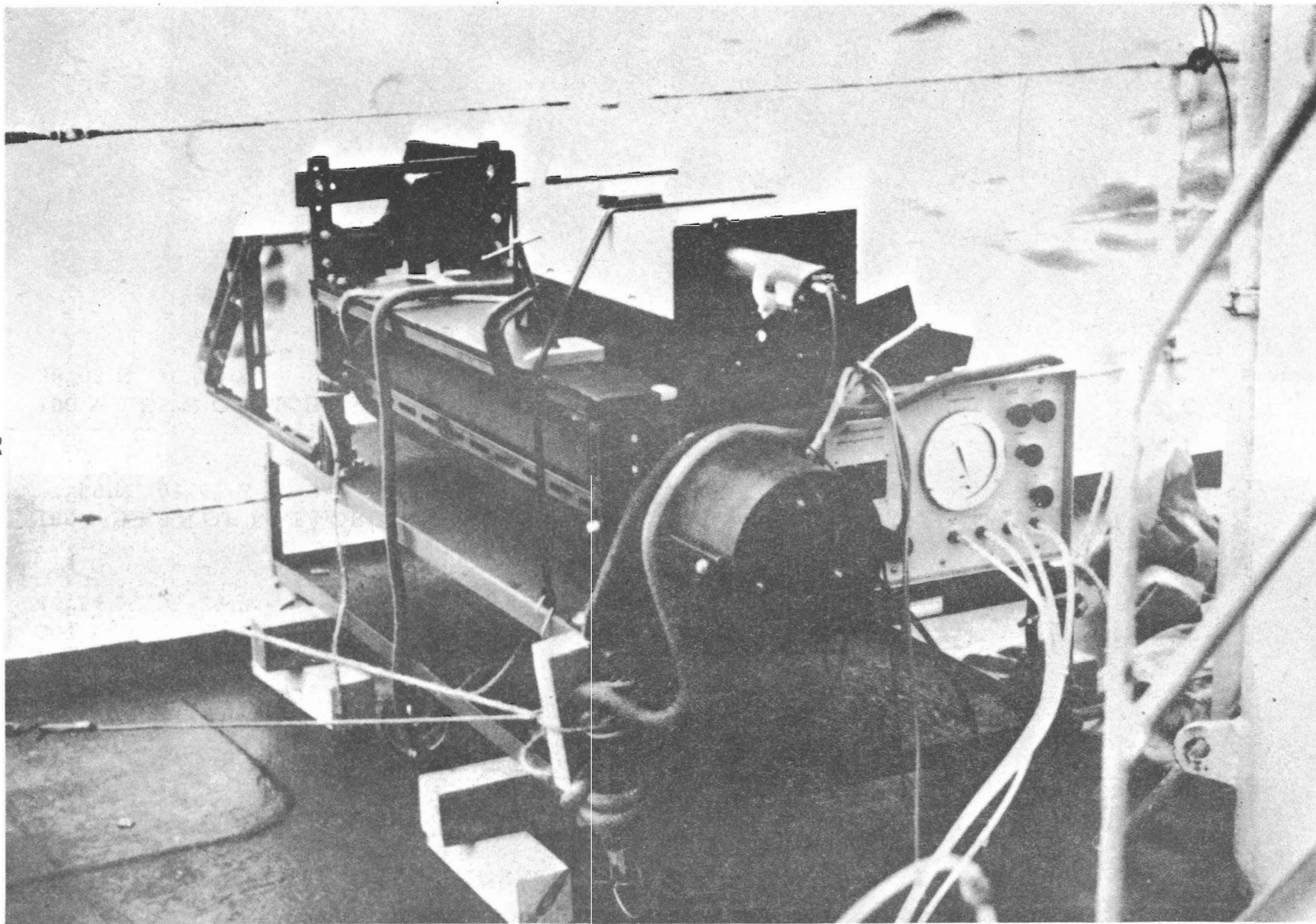
Figure 6. Raman Lidar Transceiver In Place on Hayes Afterdeck.

TABLE 4. SUBSURFACE RAMAN EXPERIMENTS AT SEA

LOCATION	DATE	SUBSURFACE TEMPERATURE
100 MILES SE OF CAPE RACE, NEWFOUNDLAND 45°54'N, 51°03'W	19 MAY 1977	4.7°C
300 MILES NW OF AZORES 43°54'N, 34°29'W	22 MAY 1977	15.7°C
100 MILES S OF MALLORCA 37°59'N, 03°47'E	1 JUNE 1977	19.2°C
100 MILES W OF SICILY 38°05'N, 10°33'E	2 JUNE 1977	19.8°C

4.2.1 Data Analysis

Several different experiments were performed and data obtained as follows: ·

4.2.2 Broad Spectral Scans

The purpose of the broad scans was to study the total 337.1 nm induced spectrum (i.e., fluorescence) in addition to the water Raman band itself. The fluorescence to Raman ratio is important for Raman system signal-to-noise considerations and measurements of this ratio in natural water are necessary for predicting system performance.

The spectra plotted on a logarithmic scale in Figure 7 shows typical raw laser induced data obtained at wavelengths between 360 and 500 nanometers. The background signal obtained with the laser blocked is also shown for comparison. The conclusion to be drawn is that the 3400 cm^{-1} liquid water Raman band is by far the most prominent feature of the spectrum and that the laser induced fluorescence is much less than a 1% effect. The response of the SPEX 1/4-meter spectrometer to a delta function wavelength impulse has not yet been calibrated and some significant portion of the residual induced signal may be an instrumental effect.

The data shown in Figure 7 was obtained in the Mediterranean 100 miles south of Mallorca at 37°50.5'N, 03°47.1'E on 1 June 1977. The character of the data with respect to fluorescence interference at the other Mediterranean location near Sicily and in the Atlantic locations southeast of Cape Race, Newfoundland and northwest of the Azores was basically the same.

4.2.3 Raman Band Shape Analysis for Temperature

The laser Raman spectra of the ocean waters clearly shows temperature dependent effects. The spectra of Figure 8 compares Labrador Current water with Gulf Stream water. The ground truth measurements of temperature were 4.7°C and 15.7°C as shown. Both spectra were for water in the first ten meters of depth. Analysis of the two band shapes with the standard two-color technique shows that the polymer component decreased by 13% between the Labrador Current and Gulf Stream with spectral temperature difference of 13°C compared with measured difference of 11°C.

4.2.4 Raman Spectra as a Function of Depth

Figure 9 shows raw Raman data obtained simultaneously at the three depths of 10, 20 and 30 meters at the Mediterranean location west of Sicily. The characteristic Raman band shape is clearly observable at
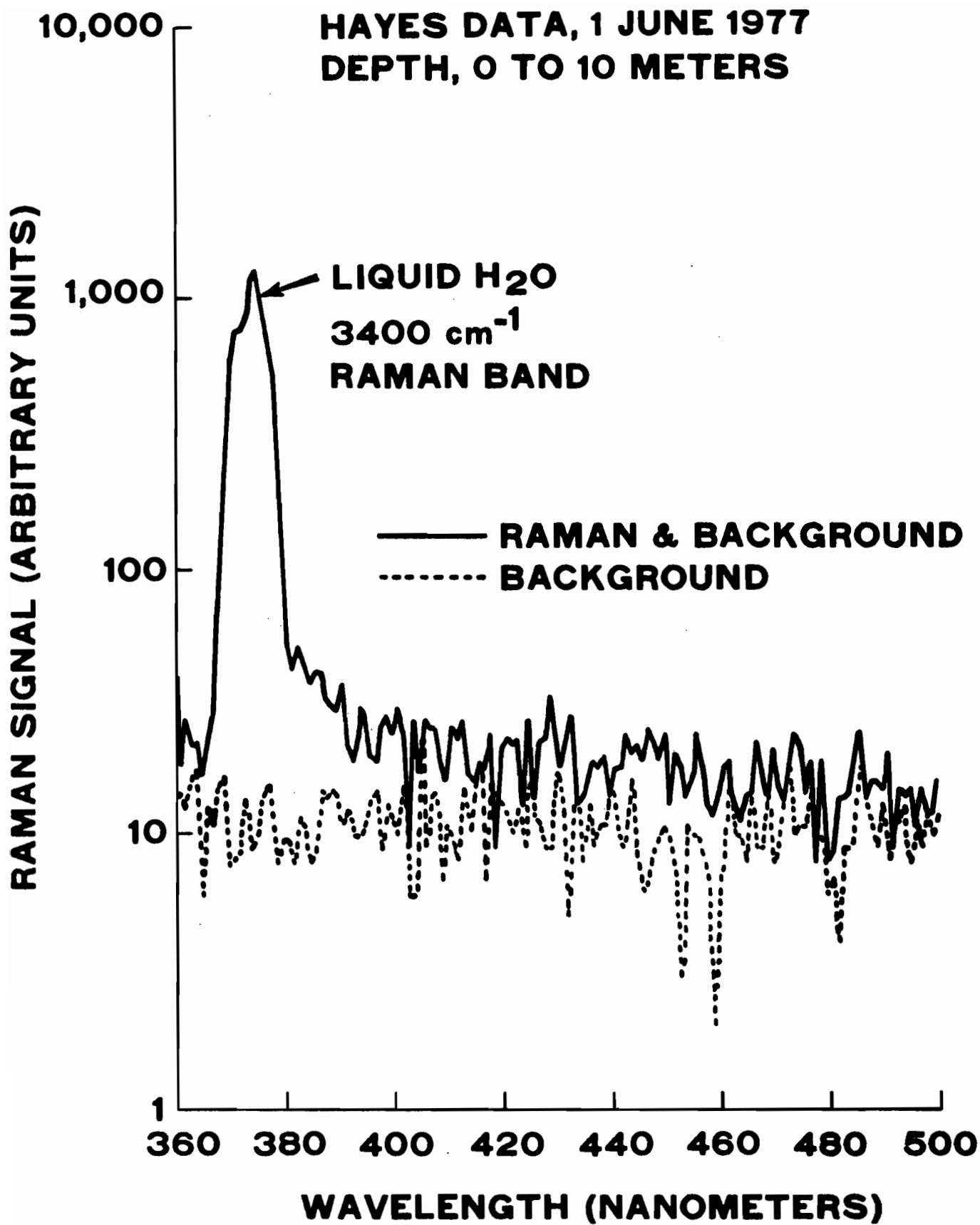
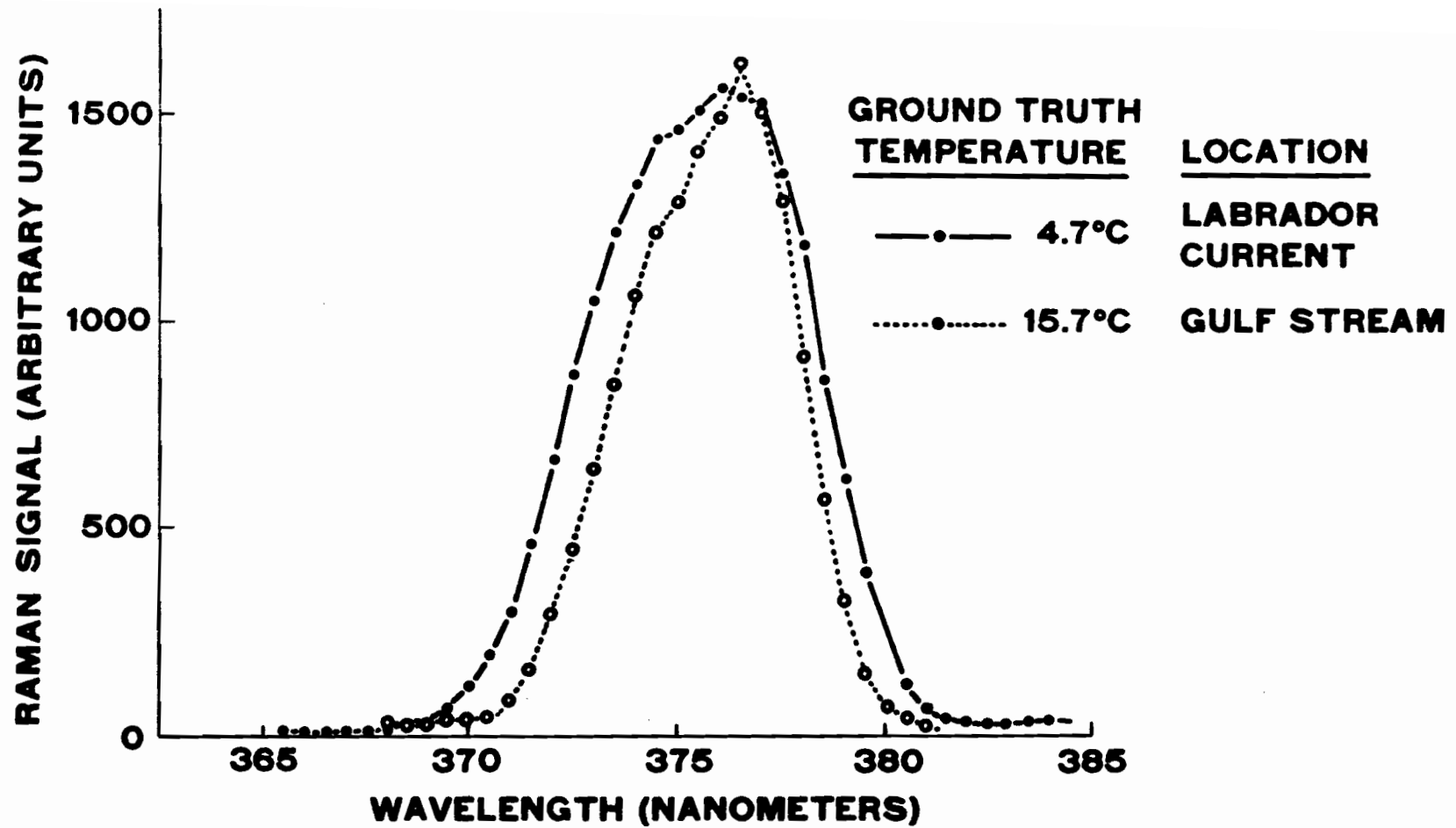Figure 7. Raman Water Band Plus Laser Induced Background.

64

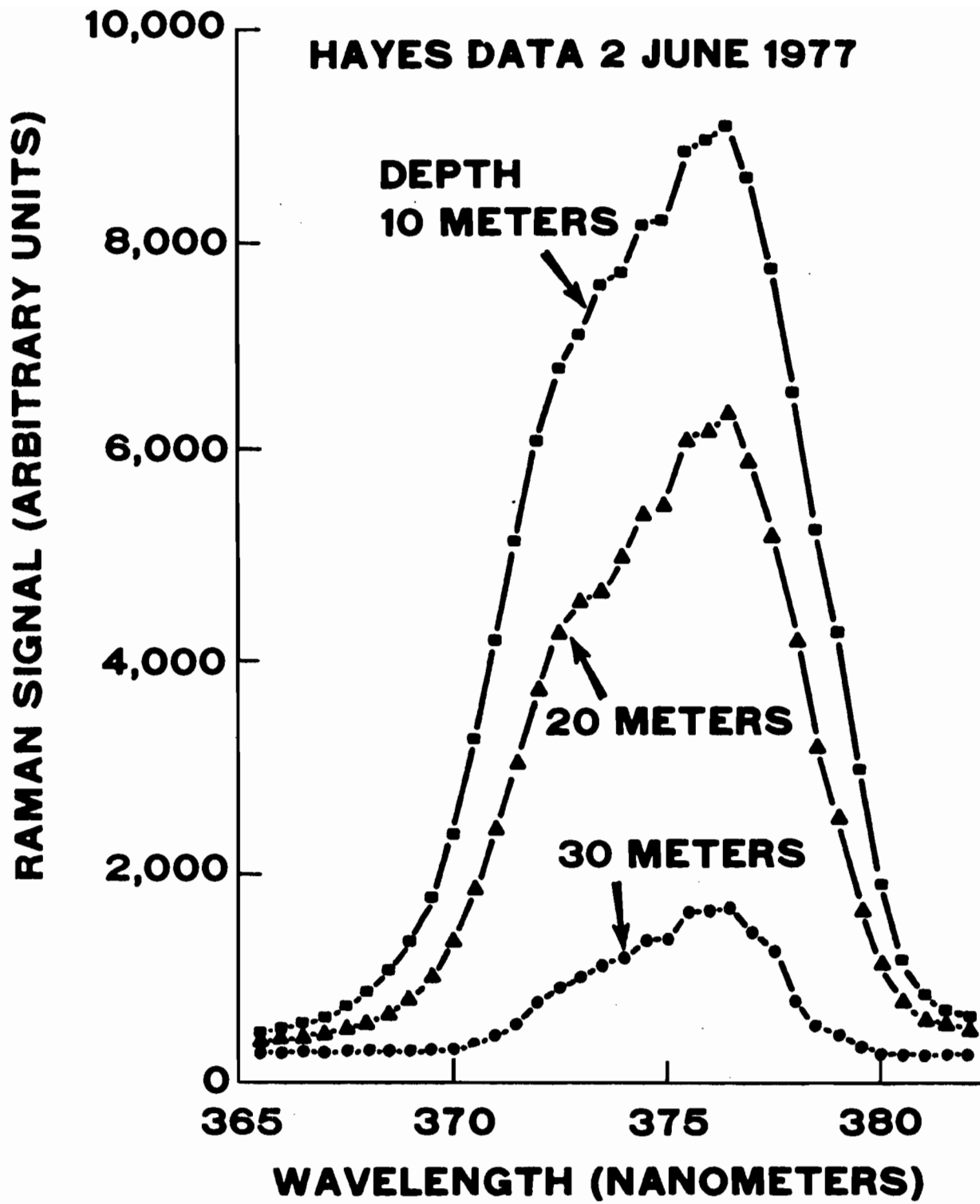Figure 8. Raman Spectra of Labrador Current and Gulf Stream.

Figure 9. Simultaneous Raman Spectra at Depths of
10, 20 and 30 Meters.

66

all three depths. The effect of differential attenuation with the 337 nm laser wavelength is apparent as seen by the apparent increase in spectral temperature as the depth increases, whereas simultaneous XBT records show that the temperature was decreasing in this range of depth. Analysis shows that a differential diffuse attenuation coefficient $dK/d\lambda$ of .003 m^{-1} per nm would account for the effect and can be used to derive the correct temperature as a function of depth from the data. This value of differential attenuation is consistent with published data (Jerlov, 1961) for ocean type water at the ultraviolet wavelength used although no independent ground truth measurements of the diffuse attenuation coefficient were available at the time the experiments were performed.

It should be noted that the use of a blue-green laser in the 450 to 500 nm wavelength region will enable penetration in the open ocean to about 100 meters with similar Raman spectral resolution as that already obtained at a depth of 30 meters. This is because based on published data (Saltzmann and Cooney, 1974), the diffuse attenuation coefficient is expected to be a factor of three smaller in the blue-green than at the 337 nm ultraviolet wavelength used in the experiments. It should also be noted that significant improvements in temperature measurement capability as a function of depth are expected with the use of polarization sensitive detection and that field experiments in open ocean waters using such techniques with blue-green tunable lasers are now being planned.

4.3 Experimental Field Measurements -- Coastal Results

A dye laser operating at 470 nm was added to the pulsed nitrogen laser lidar system and utilized in experiments conducted in Massachusetts coastal waters in November 1977 and in March and April 1978 using the CGC research vessel *Makai*.

The new results demonstrate that Raman temperature profiles are attainable in coastal waters, at least in the first optical attenuation length, using a simple two-color analysis procedure. As an example of such results, Figure 10 shows Raman spectra obtained at three depths in the Annisquam River between Babson Point and Wheeler Point on April 20, 1978. These Raman spectra were obtained at depths of 0.3 meters, 1.5 meters and 3.0 meters together with simultaneous thermocouple ground truth readings at the same depths. The spectra plotted in Figure 10 were normalized to have the same average peak value so that the relative shapes of the bands from the different depths could be analyzed to obtain temperature as a function of depth.

The two-color temperature analysis was carried out by taking for each band the ratio of the integral of the Raman signal in the 3100 to 3400 cm^{-1} wave number region to the integral in the 3400 to 3700 cm^{-1}

67
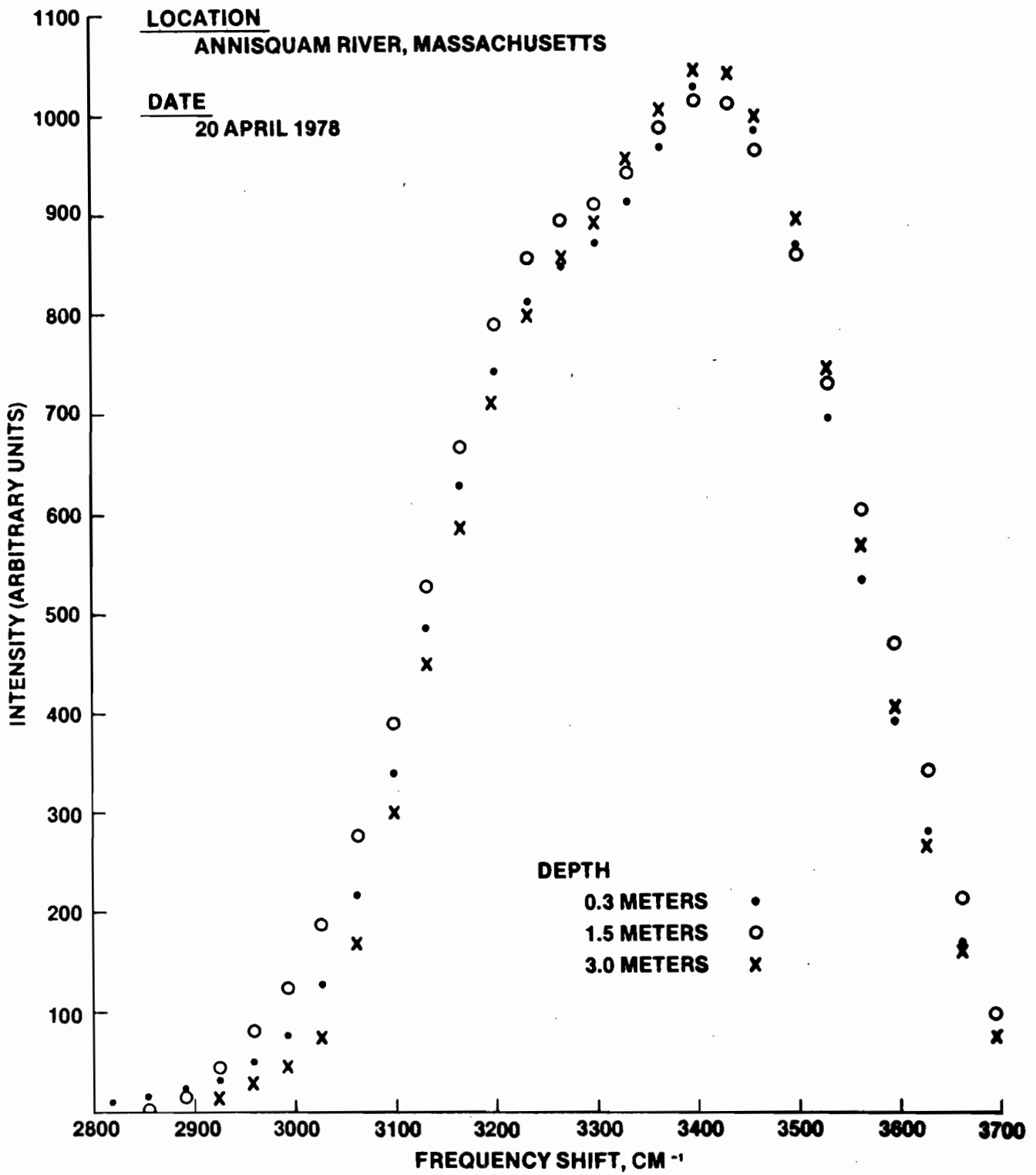
Figure 10. Raman Spectra From Three Depths in Annisquam River.

68

wave number region. Previous calibrations have shown that this integral ratio is temperature sensitive with a negative differential sensitivity of about 1% per C°. The results are shown in Table 5, which displays the Raman temperature profile and the ground truth temperatures as a function of depth.

The data in Table 5 is also displayed as a profile plot in Figure 11, where the Raman temperature and the ground truth temperatures are both shown as a function of depth. The $\pm$ 1.2°C RMS error bars on the Raman measurements were obtained by setting the mean of the Raman measurements and the mean of the ground truth measurements equal and then calculating the average RMS difference between the two measurements.

A diffuse attenuation coefficient (K) of 0.3 m^{-1} was obtained from the same data by analysis of the exponential decrease in the amplitude of the Raman signal as a function of depth, taking also into account the decrease in effective solid angle of the receiver as the depth increases. The value of K obtained is consistent with Jerlov's value for medium quality coastal water in the wavelength region near 500 nm. There is, thus, also reasonable validity to the assumption that the Raman data from the first three meters of depth falls within the first diffuse optical attenuation length. In future field work we plan to have diffuse attenuation ground truth in addition to temperature ground truth.

5. RESULTS AND CONCLUSIONS OF FIELD EXPERIMENTS

The following is a summary of the important results and conclusions that have been obtained from the field experiments discussed above.

1. Fluorescence interference does not prevent measurement of Raman spectral signature in coastal waters.

2. Raman spectral profiles have been obtained simultaneously from multiple depths in a variety of water quality conditions.

3. Detailed band shape analysis to date using actual field data agrees with published laboratory studies.

4. Spectral temperature has been obtained in first optical attenuation length ($\pm$ 1°C).

5. Attenuation coefficient ($dK/d\lambda$) has been obtained from spectral profile.

69

TABLE 5. SUMMARY OF COASTAL TEMPERATURE MEASUREMENTS

DEPTH	INTEGRAL RATIO	RAMAN TEMPERATURE	GROUND TRUTH TEMPERATURE
0.3 METER	2.08	8.1°C	6.7°C
1.5	2.01	4.6	6.1
3.0	2.03	5.7	5.6
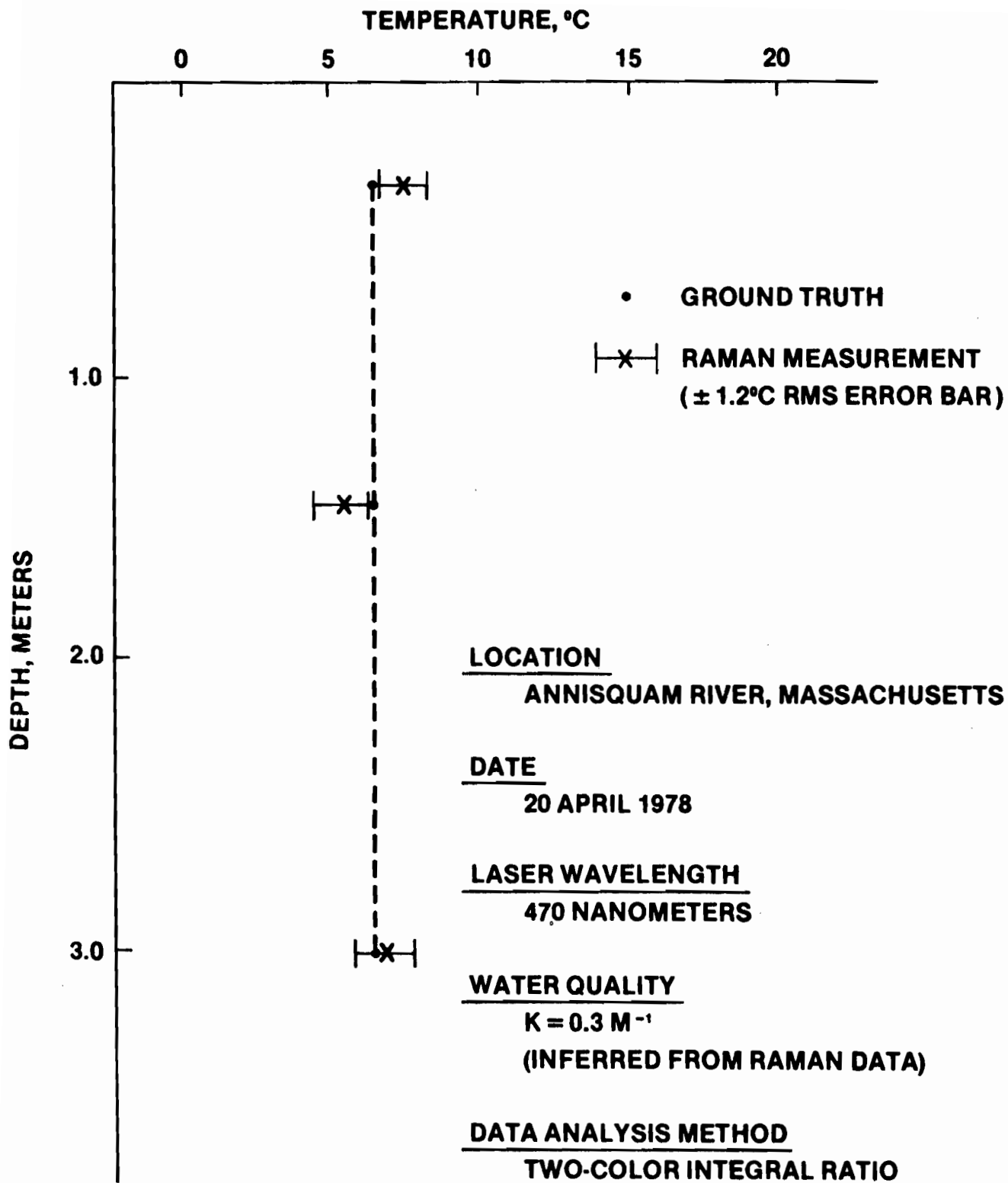
Figure 11. Raman Spectral Temperature and Ground Truth as Function of Depth in Coastal Water.

6. Raman temperature discrimination comparable to high
   resolution published laboratory data has been shown
   to be obtainable in natural water with simple instru-
   mentation under field conditions.

7. Dye laser/polarization studies are required for maximum
   depth penetration and salinity measurements.

6. ACKNOWLEDGEMENTS

72

7. REFERENCES

Chang, C.H., L.A. Young and D.A. Leonard (1974). Remote Measurement of fluid temperature by Raman scattered radiation, U.S. Patent 3, 986, 775 filed December 26, 1974.

Cunningham, K. and P.A. Lyons (1973). *J. Chem. Phys.* 59: 2132.

Duntley, S.Q. (1963). *J. Opt. Soc. Am.* 53: 214-233.

Duntley, S.Q. (1971). Underwater lighting by submerged lasers and incandescent sources, Scripps Report SIO-71-1, June.

Ferguson, G.D. (1975). Blue-green lasers for underwater applications, presented at the SPIE 19th Annual International Technical Symposium, San Diego, August 18-22.

Hirschberg, J.G. (1976). Technical Report NASA Contract NAS10-8795, March.

Jerlov, N.G. (1961). Optical measurements in the eastern North Atlantic, *Goteborg Kungl. Vetenskapsoch Vitterhets-Samhalles Handinger,* Sjatte, Foljden, Ser. B. 8: 11. (As described by Morrison. See Morrison reference below.)

Jerlov, N.G. (1968). *Optical Oceanography,* Elsevier.

Leonard, D.A. (1974). Technical Report AFAPL-TR-74-100, Air Force Aero Propulsion Laboratory, October.

Leonard, D.A. and B. Caputo (1974). *Optical Engineering* 13:10.

Leonard, D.A., B. Caputo, R.L. Johnson and F.E. Hoge (1977). *Geophysical Research Letters* 4: 279.

Lieberman, J. (1956). *Acoustic Soc. Am.* 28: 1253.

Morrison, R.E. (1970). *J. Geophys. Research* 75: 612.

Murphy, W.F. and J.J. Bernstein (1972). *J. Phys. Chem.* 76: 1147.

Salzman, J.A. and T.A. Cooney (1974). NASA Technical Note D-7669, June.

Schwiesow, R.L. (1971). AIAA Paper 7-1086, November.

Slusher, R.B. and V.E. Derr (1975). *Applied Optics* 14: 2116.

Spilhaus, A.F. (1968). *Limnol. Oceanog.* 13: 418-422.

Thomson et al. (1966). *Nature* 211: 1086.

Tyler, J.E. (1961). *Limol. Oceanog.* 6: 451

Walrafen, G.E. (1967). *J. Chem. Phys.* 47: 114.

Worley, J.D. and I.M. Klotz (1966). *J. Chem. Phys.* 45: 2868.

Zimmerman, A. and A.R. Bandy (1975). Final Technical Report, NASA
    Contract NAS1-11707, August.

AIRBORNE OCEANOGRAPHIC LIDAR (AOL) DATA ACQUISITION MODES AND RECENT RESULTS

Frank E. Hoge
National Aeronautics and Space Administration
Wallops Flight Center
Wallops Island, VA 23337

Robert N. Swift
EG&G Washington Analytical Services Center, Inc.
Riverdale, MD 20840

The unique instrument flexibility of the AOL for addressing a multitude of needed physical oceanographic and marine science measurements is discussed. In particular, the (1) bathymetry, (2) fluorosensing, (3) altimetry, (4) fluorescence decay spectrum (FDS), and (5) hybrid bathyfluorometry modes are briefly reviewed with respect to a variety of available hardware configurations. These system options include variation in transmitter wavelength, pulse repetition rates, and beam divergence as well as receiver field-of-view, charge digitizer gate width, scanning swath width, and spectrometer channel arrangement. The system has been operated in modes (1), (2) and (3) to date. Data presented includes the airborne measurements of plumes from fluorescent dye releases in tidal estuarine waters and the results of bathymetry and wave profiling investigations conducted in the vicinity of Wallops Flight Center. The possible extension of recent AOL tree height and foliage penetration results into the hydrosphere for submerged aquatic plant height and density measurement is proposed; however, AOL terrestrial applications, operation and results are not discussed.

1. INTRODUCTION

The Airborne Oceanographic Lidar (AOL) is a state-of-the-art scanning laser radar system having a multispectral time-gated receiving capability. The system is designed to allow adjustment in most transmitter and receiver settings. This built-in flexibility gives the AOL system potential application in many oceanographic areas. The hardware and software capabilities have been briefly discussed elsewhere (Bressel et al., 1977; Itzkan et al., 1978) but will be summarized as needed to portray the important aspects of the differing data acquisition modes being discussed below.

2. AOL EXPERIMENT MODES

The primary experiment modes: (1) bathymetry, (2) fluorosensing, (3) altimetry, (4) bathyfluorometry, (5) fluorescent decay will be briefly discussed and data presented when available.

2.1 Bathymetry Mode

Refer to Figure 1 during the following discussion. In this mode the AOL system laser (Avco Model C-5000) is filled with neon gas to yield an output wavelength of 540.1 nm. The 400 pulse per second (or less) output is folded into the adjustable beam divergence collimating lens, directed downward through the main receiver folding flat onto the scanner folding flat finally striking the angle adjustable (50 cm round) nutating scanner mirror which directs the beam to the earth's surface. The total surface, volume, and ocean bottom backscattered signals return through the same path but because of their uncollimated spatial extent are principally directed into the 30.5 cm Cassegrain receiving telescope. The horizontal and vertical fields of view of the receiving telescope are each separately controlled by a pair of remotely adjustable focal plane knife edges. The radiation is then collimated to eliminate undesirable skewing of the bandpass of the subsequent 0.33 nm narrow band interference filter. The radiation is then focused about 3 cm behind the face of the EMI D-279 PMT to avoid weak photocathode areas. The 45° folding flat and beam splitter between the collimating lens and the narrowband interference filter is used only in the fluorosensing mode to be discussed in the next section.

The PMT analog output waveform is routed through a multichannel 10X amplifier and is digitized according to the simplified system shown in Figure 2. Basically, the bathymetry waveform is fanned out or reproduced 40 times and sent to charge digitizers (CD). The 40 charge digitizers are gated "on" sequentially every 2.5 nanoseconds to obtain the proper segment of the waveform. Additionally, the CDs are held "on" for 2.5 nanoseconds. This so-called aperture time was later increased to 4 nanoseconds when the discriminator drivers were found to be amplitude unstable at 2.5 nanoseconds. The center of each 4 nanosecond gate remained spaced from its neighbor by 2.5 nanoseconds yielding a 0.75 nanosecond overlap with both adjacent CDs.

The CDs are fundamentally the analog-to-digital converters for the AOL waveform digitizing system. Their output is directed through CAMAC standard instrumentation to the Hewlett-Packard 21MX computer for recording. The peak of the surface return was delayed to fall in channel three as shown in Figure 2. The stability of the electronics was such that this was not a problem even during wide temperature excursions.

76

BAGGAGE HATCH

SCANNER MIRROR CENTER

SCANNER PLATFORM

TELESCOPE

ELECTRONICS RACKS

A/C

ACCESS HATCH

BATHYMETRY
DIRECTOR ASSY

PMT

SPECTROMETER

FLUOROSENSING DETECTOR ASSY

COLLIMATOR

SEC. A A

OPTICAL PLATFORM

BATHYMETRY
FOLDING MIRROR

LASER

LASER

A/C FWD

ADJ MIRROR
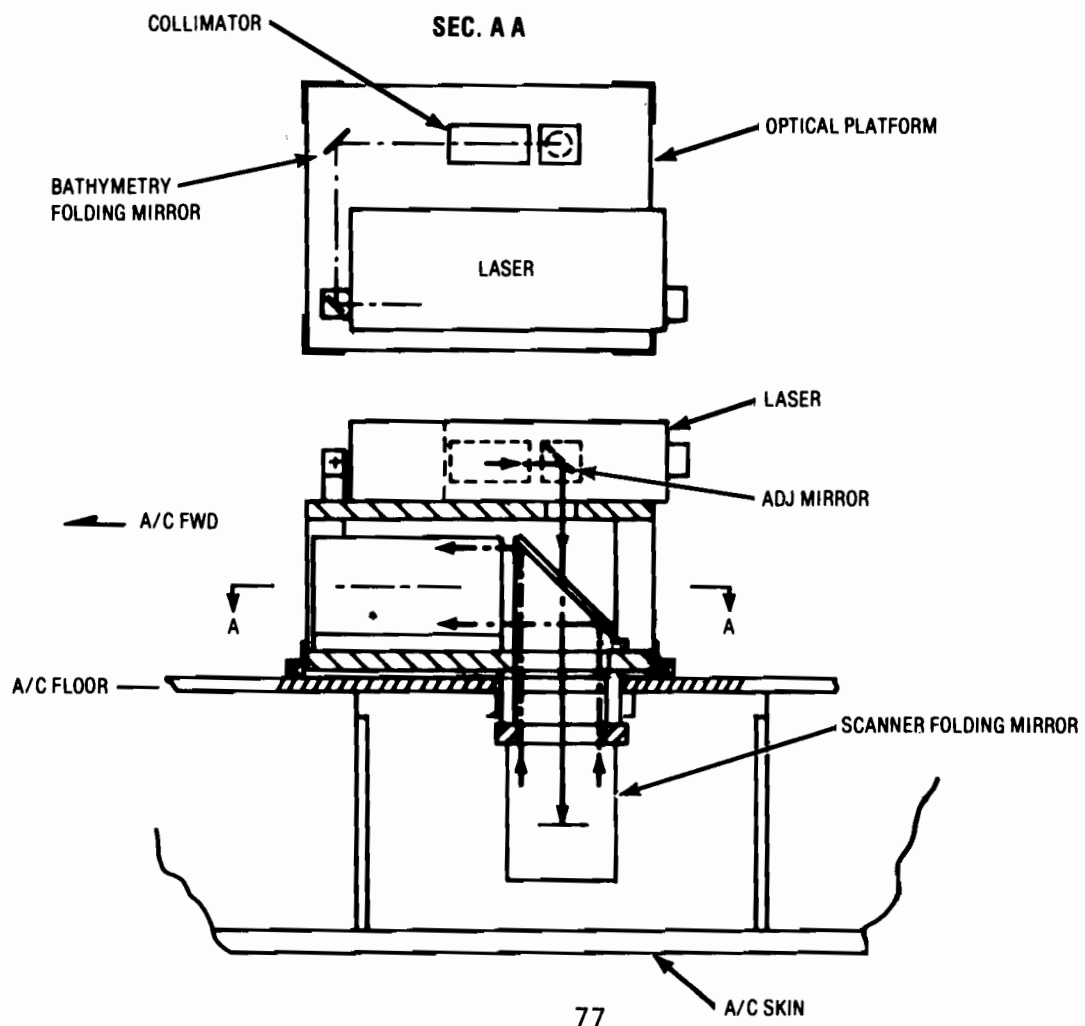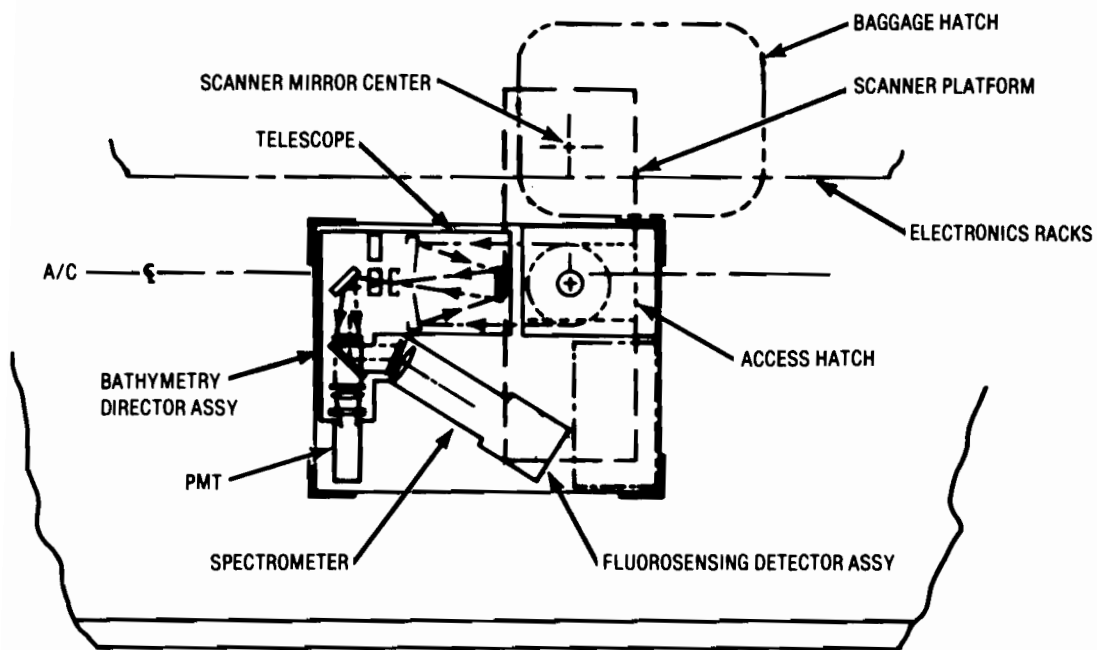
A/C FLOOR

SCANNER FOLDING MIRROR

A/C SKIN

77

Figure 1. Elevation and top-view of the Airborne Oceanographic Lidar major optical subsystems.
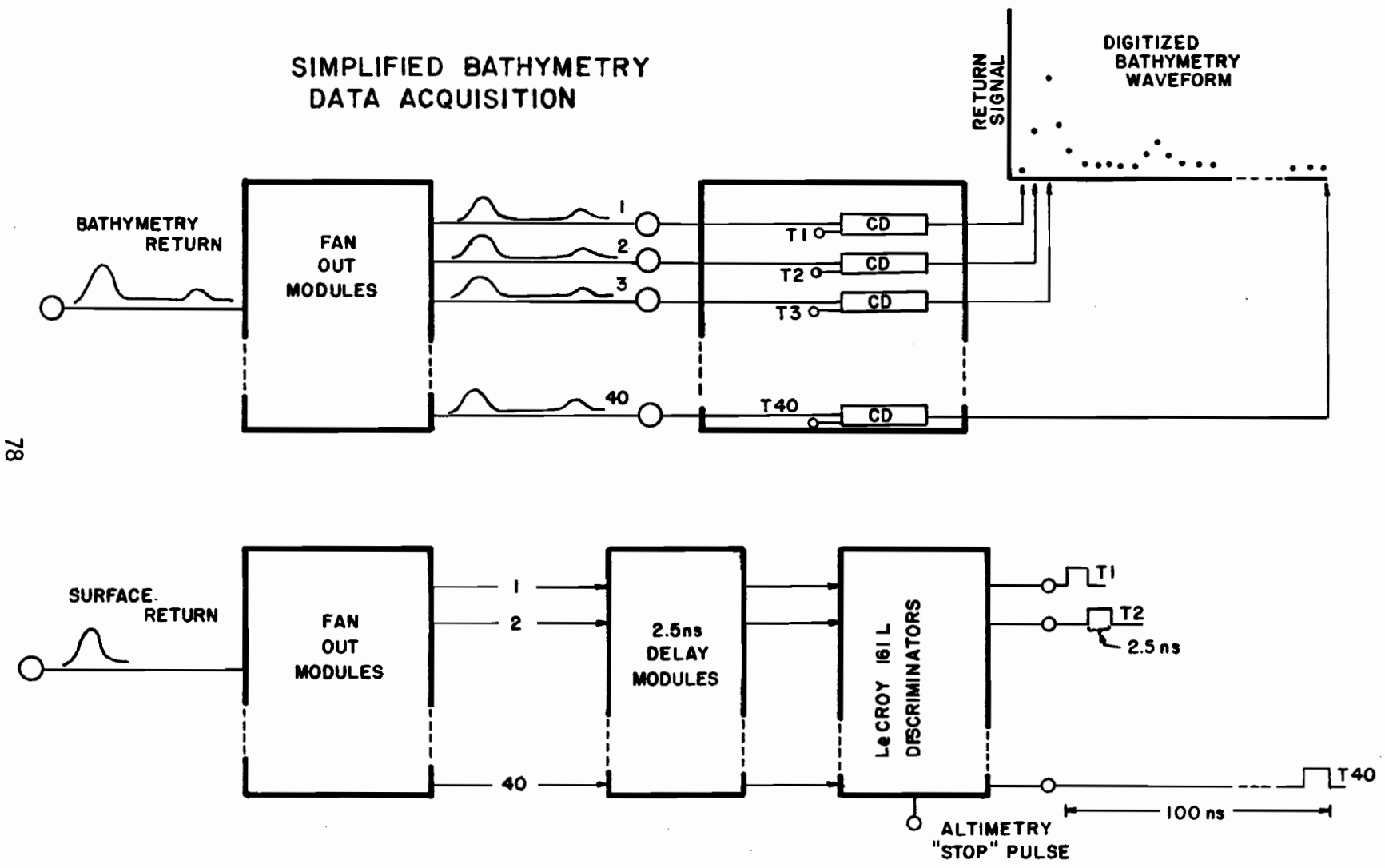
Figure 2. Simplified bathymetry mode data acquisition electronics.

However, a major problem was encountered in that the amount of systematic noise that appeared in succeeding channels was a function of the strength of the surface return into the channel three digitizer. This cross-channel coupling was found to be largely due to insufficient capacitive decoupling of the $\pm$ 6 volt and $\pm$ 12 volt busses in the CAMAC digitizers. Improvement was made by inserting individual decoupling capacitors for each channel. However, it was not possible to totally eliminate the problem with hardware. A software approach was then utilized since the effect was for the most part linear over about one-half of the digitizer range of 1024 bits. This technique has been briefly discussed elsewhere (Swift and Goodman, 1978). An actual wave-form containing a bottom return signal obscured by cross-channel coupling is shown in Figure 3(a). Shown in Figure 3(b) is a typical equivalent amplitude return pulse obtained from deeper water (> 100 nsec range). Upon subtraction the bottom signal is extracted as shown in Figure 3(c). A five-point centroid software tracker is used to extract the elapsed time from the surface to the bottom. Division by the index of refraction yields the depth measurement. A bottom profile obtained in the Chesapeake Bay using the AOL system and ground based software is shown in Figure 4. An Atlantic Ocean profile to much deeper depths is shown in Figure 5. Actual mapping missions have been performed with the scanner activated and experimental contour chart preparation is now in the final stages.

2.2 Fluorosensing Mode

In this configuration, the AOL system laser is generally filled with nitrogen gas and operated at 337.1 nm with a peak power of about 75 KW and a pulse width of 7 nsec. The nitrogen emission (UV) is used principally for surface phenomena for which it is best suited (Bristow, 1978). The neon (blue-green) is used when subsurface or thick, optically transparent surface layers or volumes are being probed. If a different wavelength is desired then the Avco dye module can be mounted in place of the bathymetry folding mirror (Figure 1). To date all of our experiments in fluorosensing have been performed using either nitrogen or neon. Use of the dye laser is anticipated when the neon and nitrogen laser applications are unsuitable.

The fluorosensing transmit path is obviously identical to the bathymetry transmit path. The fluorosensing return signal path is the same up to the beam splitting mirror which is used to direct a major portion of the excitation wavelength and the fluorescent return signals into the fluorosensing detector assembly. A small amount of the surface return signal is allowed to pass through a small opening in the beam splitter where it is sensed by the bathymetry photomultiplier and subsequently used to generate the CD gate pulses. Note that if nitrogen is being used in the laser, the narrowband interference filter is replaced by a Corning CS7-37 (Glass #5860) UV transmitting and visible absorbing

a)   ACTUAL DATA

CHANNEL

b)   DEEP WATER
             CALIBRATION DATA

CHANNEL

c)   BOTTOM RETURN

CHANNEL
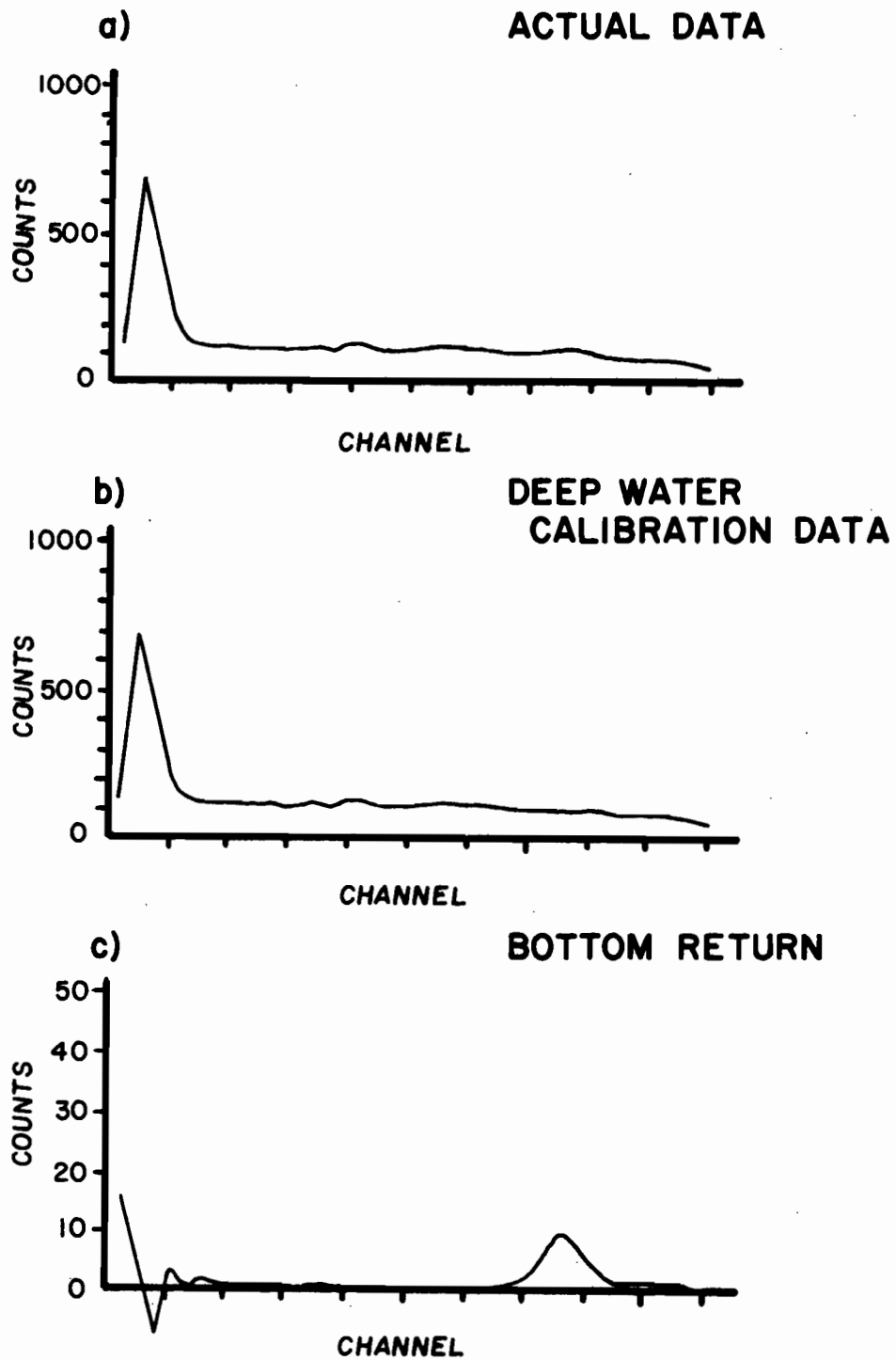
Figure 3. Removal of systematic electronic noise in the AOL charge digitiz-
ers by use of environmental subtraction calibration techniques.
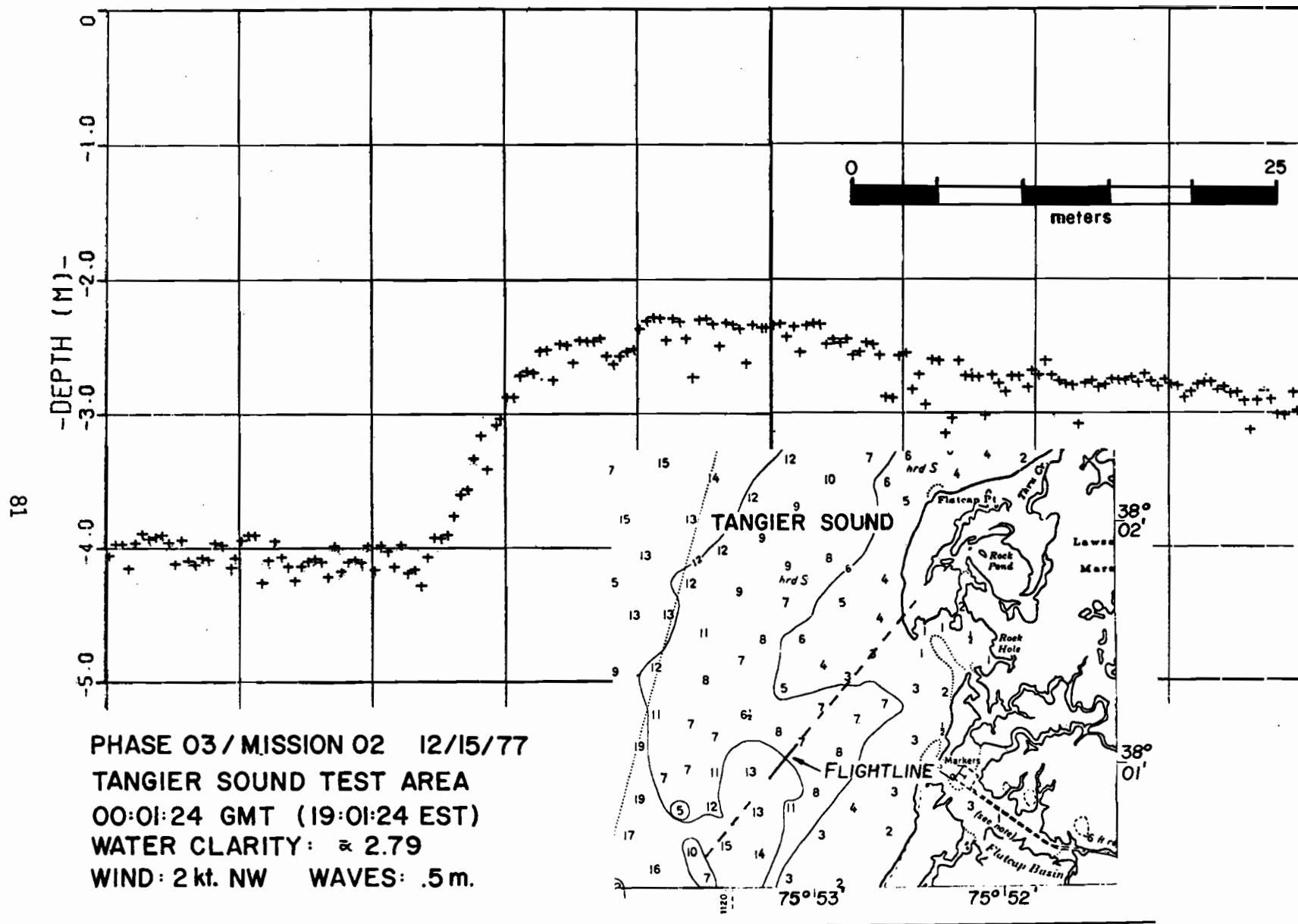
Figure 4. Sample of typical AOL bathymetry data taken in the Chesapeake Bay test site.

PHASE OI/MISSION O2   O9/OI/77
WINTER QUARTER SHOAL TEST AREA
16:18:25 GMT (12:18:25 EDT)
WATER CLARITY: ≈.60
WIND: I kt. E   WAVES: < .5 m.

SEA LEVEL

Philadelphia

Baltimore

Washington,
D.C.

OCEAN

Winter Quarter Shoal
Test Area

Wallops
Flight Center

ATLANTIC

DEPTH (M)

Figure 5.   Sample of typical AOL bathymetry data taken in Atlantic Ocean test site.

filter. Since no UV filter was supplied originally with the AOL, this one was added as part of a continuing AOL improvement program.

The fluorosensing detector assembly contains an 11 cm transmission diffraction grating blazed for 480.0 nm having 600 grooves per millimeter. An 11 cm diameter simple lens brings the dispersed radiation to the entrance surface of 40 quartz light guides. These guides are optically coupled to two separate banks of 20 RCA phototubes. The 40 light guides are physically located in the focal plane to receive the dispersed spectral components from 350 nm to 800 nm. This of course yields a single channel spectral bandwidth of 11.25 nm. The tubes are not shuttered or gated but are operated at all times. Ambient background radiation rejection is provided by the 0 to 20 milliradian adjustable field-of-view knife edge pairs located at the focal point of the receiving telescope. The pulsed analog outputs of the entire bank of phototubes are routed to buffer amplifiers that drive each of 40 CD input channels. All 40 CDs are gated on simultaneously at a temporal position determined by the surface return signal from the 41st or bathymetry photomultiplier tube. The fluorosensing data acquisition mode is shown in Figure 6. To avoid duplicate CD electronics actual physical cable routing is changed to effect a fluorosensing mode activation. About two hours is normally required to change from the fluorosensing to the bathymetry mode. The altimetry mode remains essentially unchanged.

The CD gate widths are switch selectable at 10, 50 or 150 nanoseconds using the LeCroy 161 discriminators or gate drivers. The 10 nsec gate width can be reduced to 4 nsec by potentiometer adjustment. Again, the leading edge of all the gates are set by the surface return pulse. In the present configuration the cable lengths are just sufficient to start the CDs about 3 nanoseconds above the surface.

2.2.1 Fluorosensing Mode Data

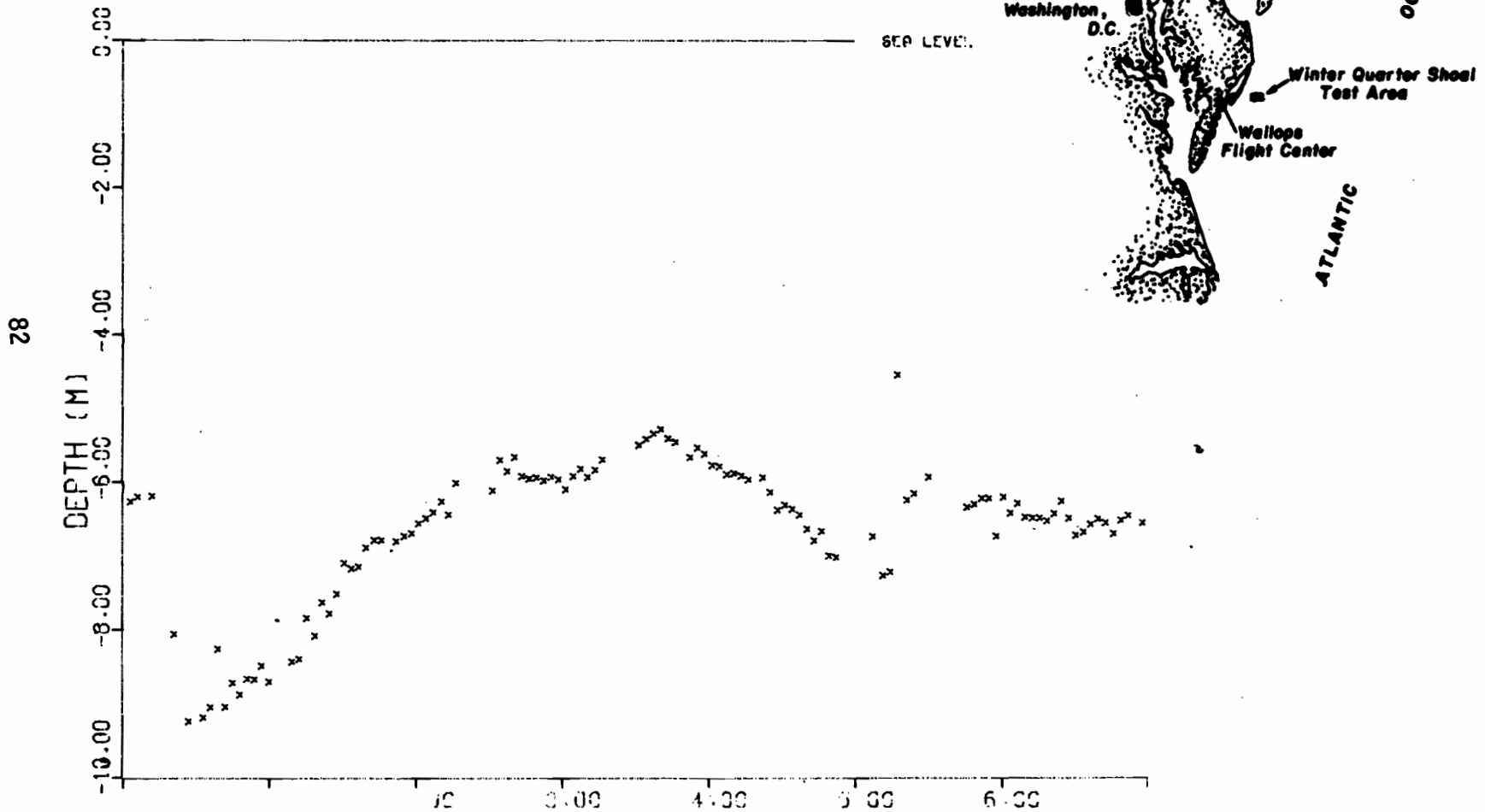In the fluorosensing mode the AOL has to date been flown on six User Flight Readiness Missions. To be described herein is the first such instrument evaluation mission. It concentrated on the mapping of dispersed fluorescein dye in a shallow tidal creek (Cockle Creek) in the immediate vicinity of Wallops Flight Center. The location of the test area of Cockle Creek is shown in Figure 7. This location was chosen for its (1) close proximity to NASA-WFC with regard to aircraft as well as boat dye-dispersal/truthing-team logistics, and (2) protection from high wind and wave conditions.

In order to (1) reduce the background to rather low levels but (2) still provide sufficient light for visual maneuvers by the aircraft and boat pilots, the experiments were performed immediately after sunset. This also allowed an altitude of 500 feet to be flown. In order to maximize the spatial extent of the laser stimulation the transmit beam divergence was set to its maximum value of 20 mr. Accordingly both the
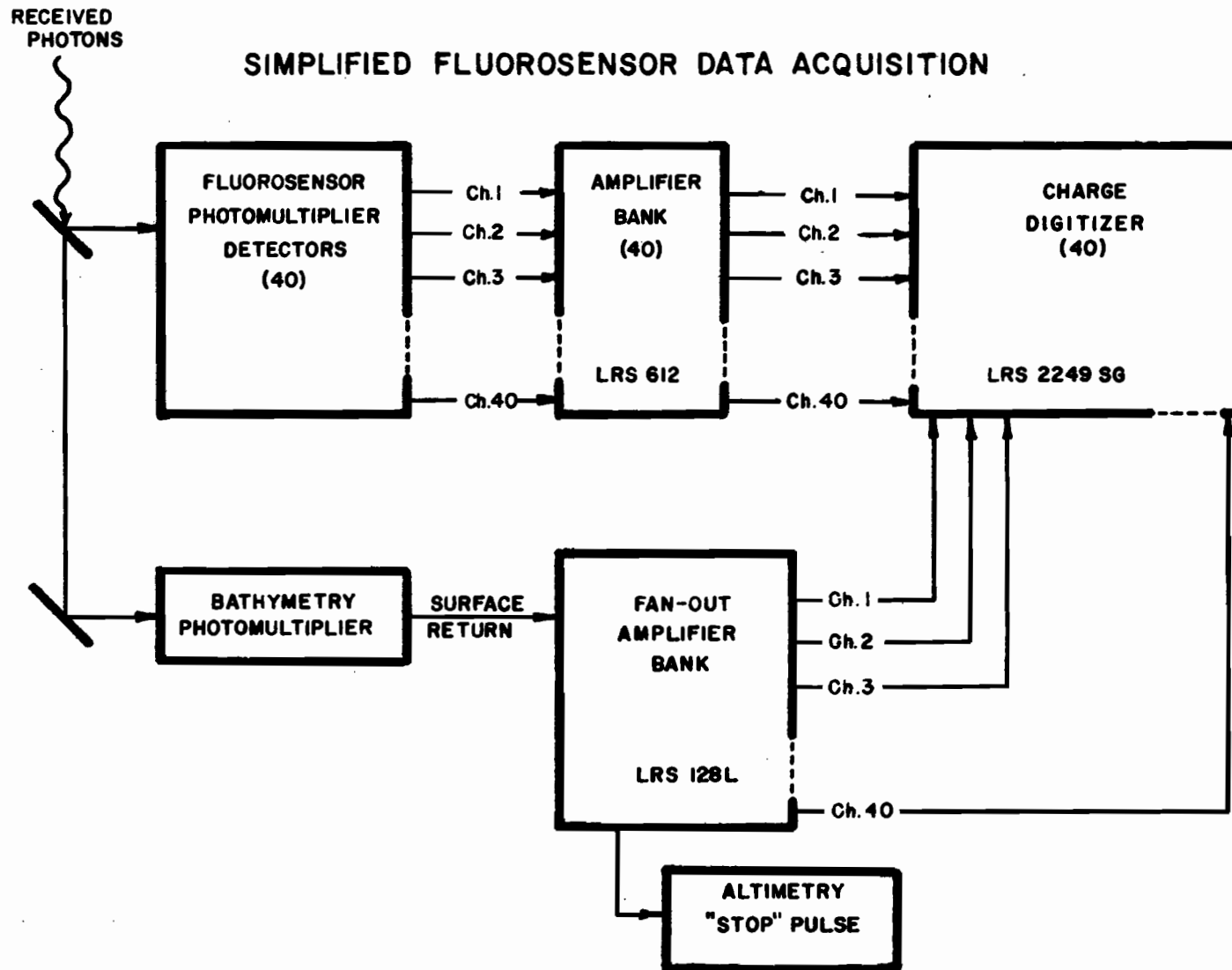
SIMPLIFIED FLUOROSENSOR DATA ACQUISITION

Figure 6. Simplified fluorosensing mode data acquisition electronics.
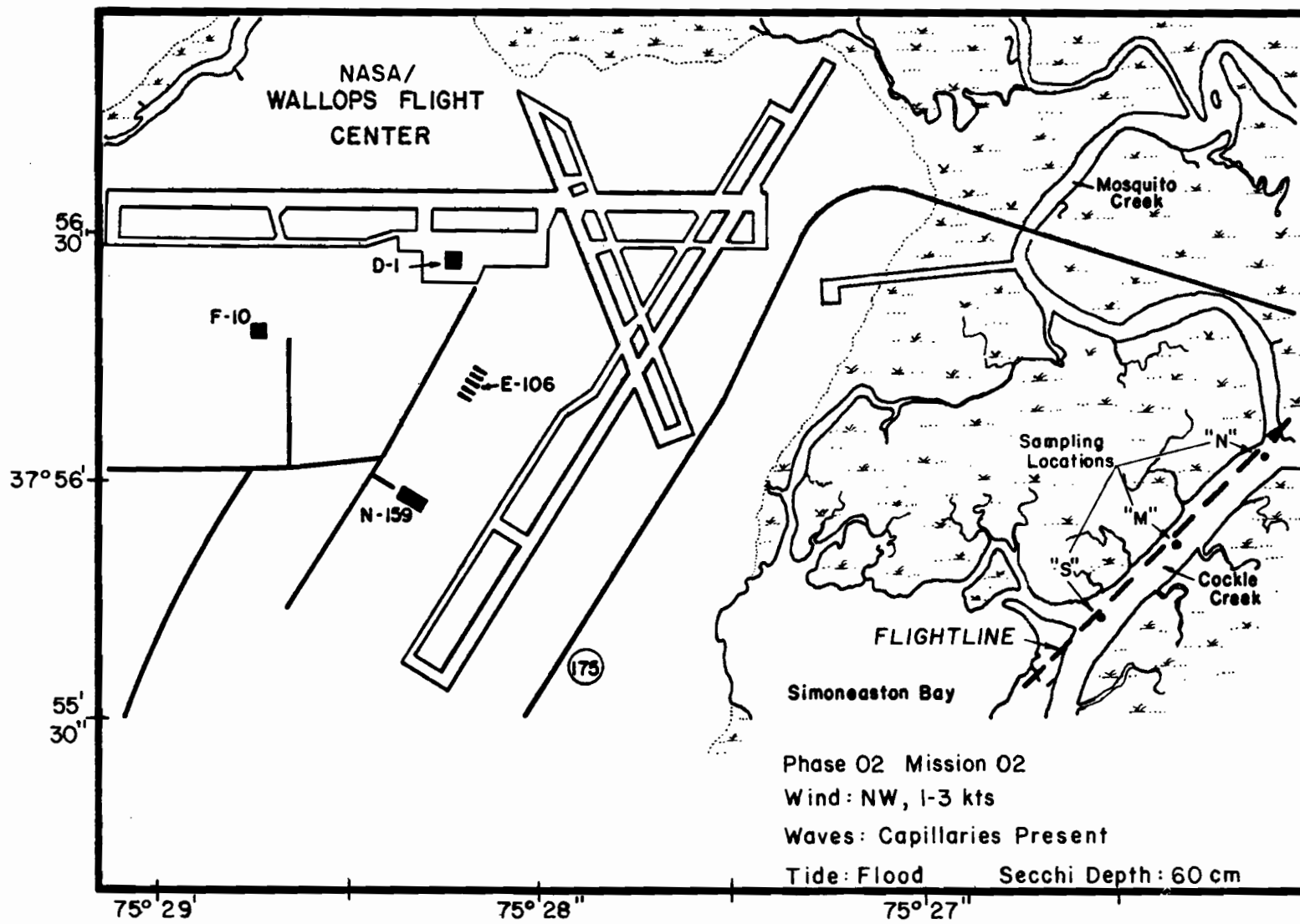
Figure 7. Location of initial fluorosensing dye tracer experiments in Cockle Creek test site.

horizontal and vertical receiver FOV knife-edge pairs were then set to 20 mr to match. The AOL was operated at a data acquisition rate of 200 pps. The dye was observed real-time in flight by noting the response of channel 15 (approximate peak fluorescein emission wavelength) during passage over the flight line. Pulse responses were observed corresponding to a two-way range time of approximately 1,000 nanoseconds on several passes made linearly along the dye plume. Interlaced active and passive spectral waveforms spanning 350 to 800 nm were recorded during all five passes over the linearly dispersed dye plume. In the Fluorosensing Mode the computer commands the laser to fire 100 pulses per second while sampling the CDs at 200 Hz. Thus, passive multispectral data is taken at 100 Hz between laser pulses and interlaced with the active laser induced fluorescence (LIF) data also gathered at 100 Hz. Accordingly, when the active data spectral waveform is recorded it contains LIF plus background upwelling irradiance. When passive data is recorded it contains only the background upwelling irradiance. Then, subtraction of the passive waveform from the active waveform yields the LIF. The assumption inherent in this process is that the background irradiance observed during the active spectral recording period is the same as observed during the passive recording period that occurred 0.01 sec before or after the active recording interval. Results from previous laboratory and ground tests of the AOL system suggest that this assumption is valid. It has proven to be reasonably good during these field tests as well. Our designated pass 2/1X is representative of this and similar missions performed during this time frame. A plot of the channel 15 response as a function of elapsed time over the flight line is shown in Figure 8 for pass 2/1X. The passive background has already been removed as noted therein. Space does not allow us to show all of the thousands of single shot laser induced fluorescence (LIF) spectral waveforms obtained during the mission. However, two sets have been selected from the 2/1X pass in the regions denoted as (a) and (b) on Figure 9. In Figure 9 the uppermost waveform denoted "active" is the LIF spectral waveform (including background radiation) obtained as a result of one transmitted laser pulse. The trace labeled passive is the next succeeding interlaced background radiation waveform. Clearly the LIF is thus obtained by removing the background by subtraction of the passive pulse waveform from the active pulse waveform. The residual LIF or active minus passive difference is given in Figure 9 by the lowermost spectral waveform on an expanded scale. Here, the local peaks and valleys (particularly evident in the vicinity of the dye fluorescence emission) are due to channel-to-channel gain differences. In Figure 9(a) neither the active nor passive waveforms have been corrected for gain or bias in any channel. Each channel is essentially independent from another. The most difficult problem of calibration is the proper balancing of the gain of the photomultiplier tubes. The apparent gain-mismatch between channels is caused by the present difficulty encountered in gain calibration balancing. The bias in each channel

PHASE 02 / MISSION 02
PASS 2/IX

CHANNEL 14, ACTIVE-PASSIVE
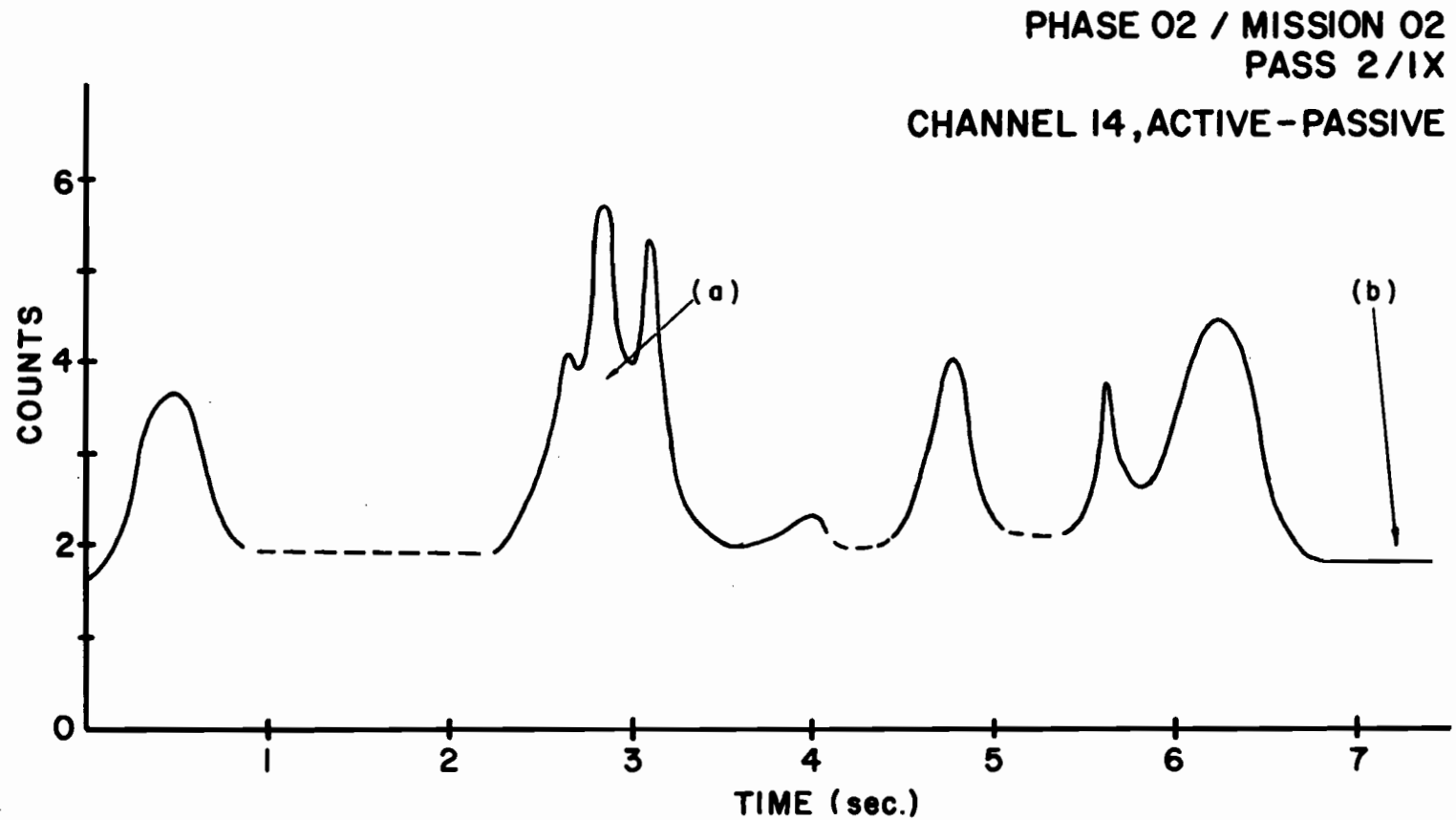
Figure 8. Amplitude response of Channel 14 during one pass over the dye plume. Complete spectral waveforms were selected for Figure 9 at the times denoted by (a) and (b).

(a) SPECTRAL WAVEFORMS DYE REGION

ACTIVE
PASSIVE
ACTIVE – PASSIVE
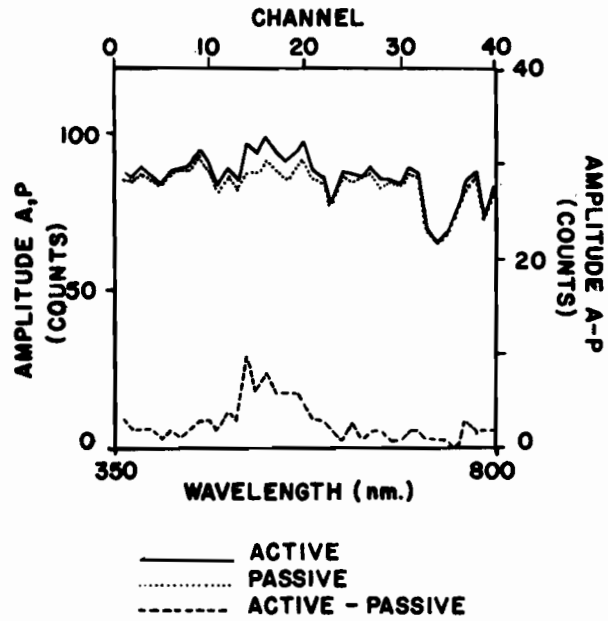
(b) SPECTRAL WAVEFORMS NO-DYE REGION
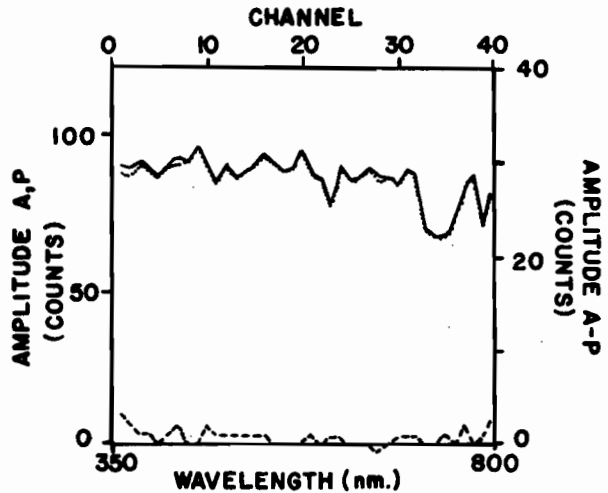
Figure 9. (a) AOL single pulse waveforms taken over the strongest por-
tion of the dye plume.
(b) AOL single pulse waveforms taken outside the dye plume.

is to some extent reduced by the passive or background subtraction. This is particularly evident in the A-P waveform of Figure 9(a). The A-P residual is non-zero for several reasons:

   a. There is known, broad spectral fluorescence from estuarine waters apparently due to dissolved organics. Further data analysis is now being performed to determine if, for example, the fluorescence seen in the laboratory samples is being observed in the AOL data. At this juncture it does not obviously appear in the uncalibrated single-shot AOL data as presented herein.

   b. The aircraft motion during the 0.01 seconds between active and passive data causes the receiving telescope to view a different spot on the water's surface. This new spot can, and does, frequently have a different (sometimes more and sometimes less) spatial, instantaneous upwelling. This can easily account for the fact that some residuals are largely negative -- indicating that the passive upwelling exceeded the LIF of the indigenous materials.

   c. A portion of the A-P residual is due to electronic noise generated by the discriminators that are used to gate the CDs "on". A gate pulse width of 10 nanoseconds gives rise to a nominal 0.1 GHz signal. This signal is very effectively broadcast throughout the charge digitizer module since microwave construction techniques cannot economically be used in these commercial modules. Twelve CD channels reside in each LeCroy 2249SG CD module.

The boat truth team obtained "no-dye" grab samples then dispersed approximately 3 kg of sodium fluorescein dye along the flight line prior to aircraft take-off. During the over flights additional surface grab samples were taken in three segmental areas plus one area determined visually to have the highest dye concentration. The grab sample locations and concentrations as keyed to Figure 7 are:

Position	Sample	Concentration (ppm)
N	1	0.0656
	2	0.0667
M	1	0.0377
	2	0.0328
S	1	0.280
	2	0.318
X	1	0.423

The "X" position, or fourth sample, was taken in a zone that appeared to have the highest visual concentration of the entire flight line.

2.2.2 Truth Data Analysis

The actual concentration of the field surface grab samples was determined by comparison with laboratory prepared standard samples having known concentrations of 0.05, 0.1, 0.5, 1, 10 ppm. The laboratory standards were prepared using the no-dye grab sample of creek water taken prior to the dye dispersal. Thus, comparison of the standard sample spectra with the field dye samples was facilitated. This is understandable by noting Figure 9. The fluorescence spectra of all estuarine field samples taken around land areas show a broad "blue water" or Gelbstoff fluorescence when excited in the ultraviolet (Zimmerman and Bandy, 1975; Hornig and Eastwood, 1973). All field samples were analyzed with an Aminco-Bowman SPF fluorometer using an excitation wavelength of 337 nm. To recheck the field dye concentration values, spectra were also taken using 450 nm excitation. These latter spectra generally possess less blue water fluorescence effects. No significant differences in concentration determinations were noted when using either excitation wavelength spectra. The "blue" water fluorescence observed in the truth samples was not seen in the AOL flight data (Figure 10). There are several possible reasons for this:

1. The Aminco-Bowman uses CW excitation of the sample whereas the AOL uses pulsed radiation source. Laboratory examination of the field truth samples under the same experimental conditions and parameters is necessary before any concrete conclusions can be made concerning the AOL determination of "blue" water fluorescence.

2. Similarly, the beam transmission of Cockle Creek was approximately 10.7 as derived from a Secchi disk reading of 66 cm (Rankin, 1975) giving rise to further strong attenuation at 337 nm. This is especially true since the blue water fluorescence is generally attributed to dissolved organics which therefore must be volumetrically stimulated.

3. The ultraviolet and near ultraviolet reflectivities of the AOL system scanner, scanner folding flat and the receiver folding flats had deteriorated by as much as 15 db. This was caused by the harsh aircraft environment to which they have been subjected.

2.3 Altimetry Mode

The so-called altimetry mode of the AOL is a required operation of each subsystem but produces highly useful data simultaneously. It is used to initiate the production of properly timed gates for the CDs in the bathymetry and fluorosensing modes. "Altimetry mode" is somewhat of a misnomer since altitude is the vertical distance from the aircraft to

90

PHASE 02 MISSION 02   MAY 10, 1978   1854 E.S.T.
COCKLE CREEK DYE SAMPLE
337 nm EXCITATION on AMINCO-BOWMAN SPF

"BLUE" WATER
FLUORESCENCE

SODIUM FLUORESCEIN
($\sim$.5 ppm)

AOL RAW DATA SENSITIVITY LEVEL

RELATIVE INTENSITY

350   450   550   650
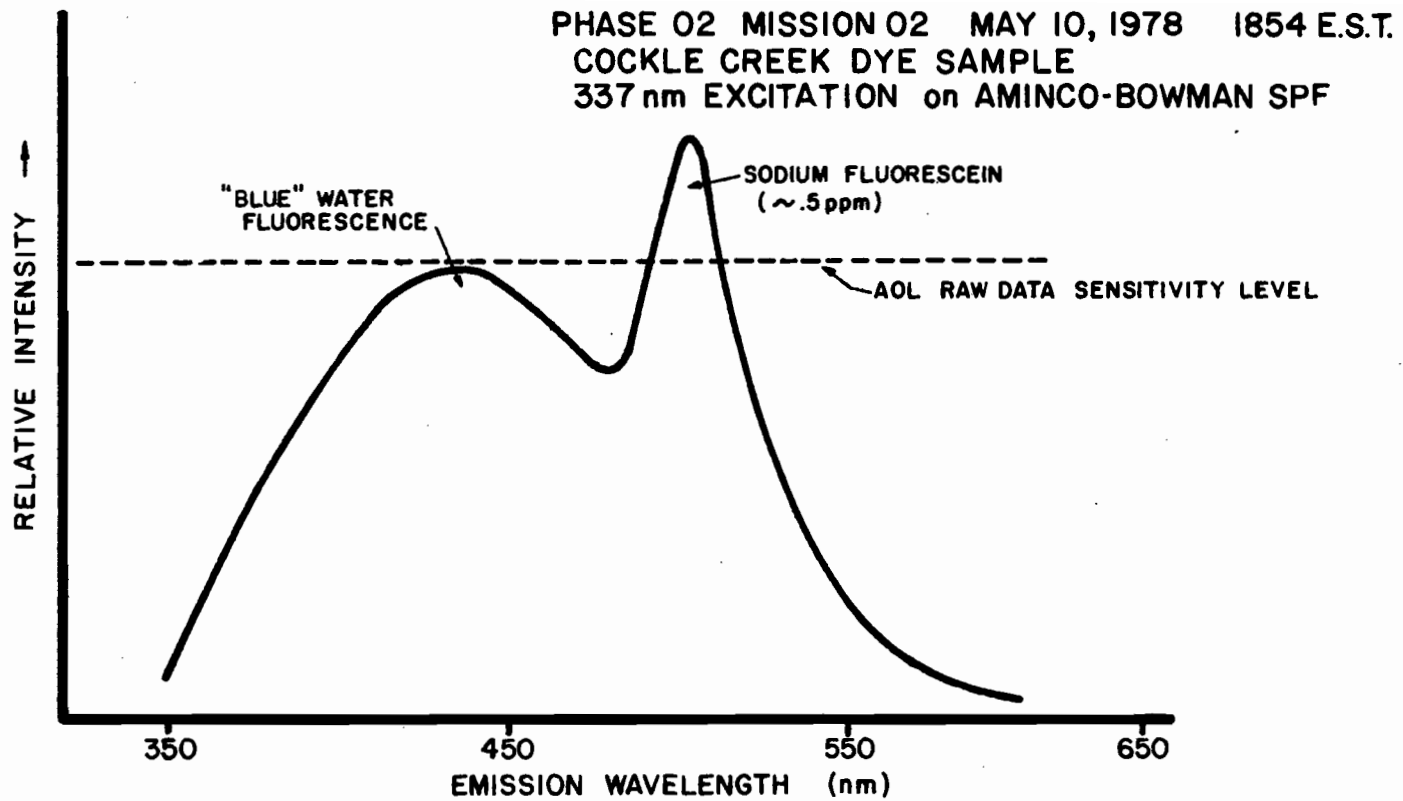
EMISSION WAVELENGTH   (nm)

Figure 10. Typical laboratory spectrum of a grab sample taken during the dye plume experiment.

the earth's surface and is only measured when the AOL scanner is set for 0° and the aircraft is in level flight. This mode could be more accurately called the "range finding mode."

The AOL altimetry mode operates in the conventional radar ranging manner. A counter is initiated and continues counting until the first arrival of a return pulse. The elapsed time is proportional to the two-way range between the AOL and the irradiated target.

A high speed photodiode is closely coupled to the C-5000 laser to supply a fast "start" pulse. The return pulse is generated in the bathymetry phototube, amplified and then buffered in the LeCroy Model 128L amplifiers. During the missions described herein, the LeCroy octal time digitizer OTD was used to generate all the range information. This OTD has since been replaced with a Hewlett-Packard 5360A computing counter equipped with a model 5379A time interval plug-in. This H-P counter eliminated the maximum range/granularity tradeoff which dictated that the aircraft be flown within a restricted altitude band. This time interval measurement is another in a series of hardware improvements continually being made to the AOL.

A sample of the AOL ranging data over the Atlantic Ocean is shown in Figure 11(a). The lowermost trace shows the unsmoothed AOL altimetry data as a function of time. This data was taken in support of NASA's Surface Contour Radar (SCR)(Kenney, et al., 1978). The SCR is a micro-wave oceanographic instrument permanently installed along with the AOL on the NASA Wallops Flight Center C-54 aircraft. The SCR obtained raster scanning range data of the surface during this ocean mission.

Post flight the SCR data was sampled at the near-nadir along-track position of the AOL laser spot. A comparison of the ocean surface elevations of the two instruments is shown in the uppermost portion of Figure 11(b). To facilitate comparison with the SCR, the AOL data was smoothed by using an 11-point running average. The SCR possesses a 1.2° beamwidth whereas the AOL beamwidth is adjustable to a maximum of 1.14°. The AOL was set for a beamwidth of 5 milliradians. The wider range of ocean surface elevation excursion is attributed to the lower spatial averaging of the AOL. Note that the long term motion of the aircraft is present in both data sets. The nominal ocean wave length observed was 41 meters.

2.4 Fluorescence Decay Spectrum Mode

Recall that the standard cable lengths (and thus the time delay) are adjusted to start the CDs about 3 nanoseconds above the surface. At this juncture it is important to point out that a digital delay is easily inserted in the surface return path so that a surface layer fluorescence spectrum can be obtained later in time. Then, by sequen-tially delaying the acquisition of a fluorescence spectrum the entire

April 14, 1978
Nadir Angle: 5°
Pulse Rate: 200 pps
Neon LASER

Aircraft Altitude: 238 m
Aircraft Groundspeed: 57 m/sec

—— SURFACE CONTOUR RADAR
------ AOL (11 point moving average)

—— AOL (per pulse plot)

63
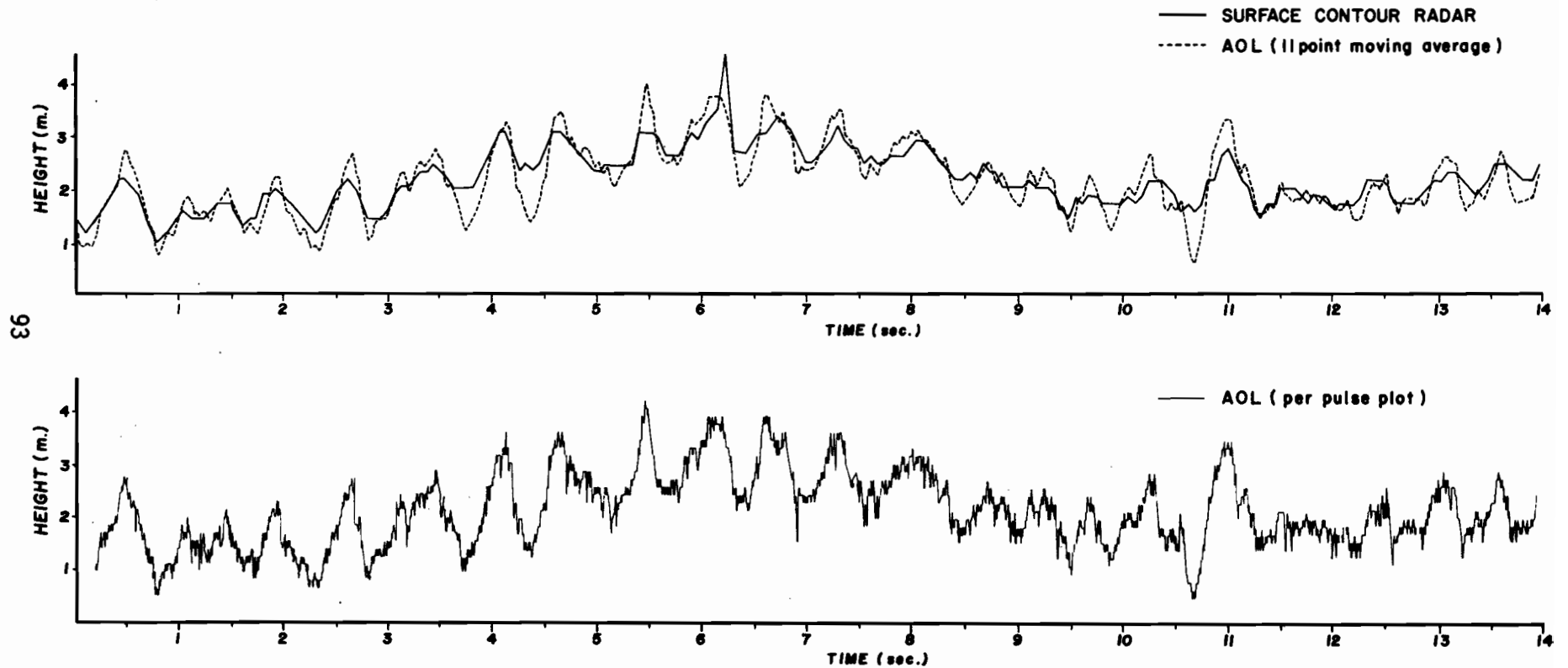
Figure 11. Slant range profile of the ocean surface taken with the AOL. Uppermost graph shows the same AOL data smoothed with an 11 point filter and compared with micro-wave Surface Contour Radar truth data.

Fluorescence Decay Spectrum (FDS) may be obtained. For very long time decay materials the 50 or 150 nanosecond sampling gate widths can be applied to each channel and commanded to digitally step later in time by increments of 1 nanosecond or more using a Berkeley Nucleonics Model 7030 digital decay generator which is interfaced to the HP 21MX computer. For shorter decay constant materials the 4 nsec gate width can be used. Of course the width of this latter gate sets the lowest time decay resolution capability of the AOL in this FDS mode. No FDS mode data has been obtained to date with the AOL.

2.5 Bathyfluorometry Mode

With the AOL configured for the bathymetry data acquisition mode it is possible to observe fluorescence-at-depth. This so-called bathy-fluorometry is achieved by digitizing the temporal analog output from any single chosen fluorosensor channel as if it were the usual bathymetry channel. To accomplish this, (1) the AOL system is placed into the standard bathymetry operational mode; (2) the fluorosensing folding flat and beam splitter is inserted into its normal position; (3) the analog output from any chosen fluorosensing channel is substituted in place of the usual bathymetry PMT output. To successfully resolve fluorescence-at-depth, the fluorescence decay time of the target material must be short compared to the required depth resolution. No data has been obtained in the bathyfluorometry mode to date.

2.5.1 <u>Other Ocean Remote Sensing Applications</u>

In addition to the applications reviewed herein, the AOL has the capability to provide important data in the study of:

1. Surface directional wave spectra using the conical scanner.

2. Depth resolved volumetric backscatter phenomenon
    -- Rayleigh backscatter
    -- Water Raman backscatter for subsurface ocean temperatures and dissolved material flourescence
    -- Subsurface ocean dye tracers for eddy viscosity determinations

3. Submerged aquatic plant height and spatial distribution.

It is in this latter area that marriage of the AOL tree height and terrestrial foliage penetration studies with the bathymetry efforts may lead to fruition.

3. ACKNOWLEDGEMENTS

The authors wish to thank all those members of the AOL Project Team and others who participated in the planning and execution of the aircraft missions and boat truth operations, the data acquisition, processing and analysis. In particular Bill Krabill, Earl Fredrick, Chris Blue, Marion Butler, Thomas Harmon, Wayne Barbely, John Kincaid, Robin Anderson as well as support by the Aeronautical Programs Branch personnel.

4. REFERENCES

Bressel, C., I. Itzkan, J.E. Nunes and F.E. Hoge (1977). Airborne oceanographic lidar system, *Proceedings of the 11th International Symposium on Remote Sensing of the Environment*, Environmental Research Institute of Michigan, Ann Arbor, Vol. 2, pp. 1259-1268.

Bristow, M.P.F. (1978). Airborne monitoring of surface water pollutants by fluorescence spectroscopy, *Remote Sensing of the Environment*, 7: 105-127.

Hornig, A.W. and D. Eastwood (1973). A study of marine luminescence signatures. NASA Ames Research Center Contract No. NAS2-6408, Baird Atomic, Inc., Bedford MA.

Itzkan, I., J.E. Nunes and F.E. Hoge (1978). Airborne oceanographic lidar system, *Digest of Technical Papers in IEEE/OSA Conference on Laser and Electro-Optical Systems*, San Diego CA, February 7-9, Paper THCC3, p. 84.

Kenney, J.E., Uliana, E.A., and Walsh, E.G., submitted for publication 1978: The Surface Contour Radar, *IEEE Transactions on Antennas and Propagation*.

Measures, R.M., W.R. Houston and D.G. Stephenson (1974). Laser induced fluorescence decay spectra -- a new form of environmental signatures, *Optical Engineering* 13: 494-501.

Rankin, M. (1975). In laser hydrography user requirements workshop minutes, NASA Report TMX-73274, ed. Lowell R. Goodman, NOAA, Rockville MD 20850, pp. 49-74.

Swift, R.N. and L.R. Goodman (1978). Using an environmental subtraction technique to enhance laser bathymetry, in *Digest of Technical Papers, IEEE/OSA Conference on Laser and Electro-Optical Systems*, San Diego, February 7-9, Paper THCC5, pp. 84-85.

Zimmerman, A. and A.R. Bandy (1975). The application of laser Raman scattering to remote sensing of salinity and turbidity, *Final Report*, NASA Langley Research Center Master Contract Agreement NAS1-11707, Task No. 33, Old Dominion University Research Foundation, Norfolk VA 23508, pp. 31.

AIRBORNE LASER-FLUOROSENSING OF
SURFACE-WATER CHLOROPHYLL <u>a</u>

by

M. Bristow, D. Nielsen and D. Bundy
U.S. Environmental Protection Agency
Environmental Monitoring and Support Laboratory
Las Vegas, Nevada 89114

R. Furtek and J. Baker
Department of Biological Sciences
University of Nevada, Las Vegas
4505 Maryland Parkway
Las Vegas, Nevada 89154

SUMMARY

In fresh-water environments, high concentrations of chlorophyll a indicate the presence of high levels of planktonic algae, suggesting, in turn, the existence of eutrophic conditions, that situation in which high concentrations of nutrients create algal bloom conditions. Such conditions can lead to malodorous and even toxic water conditions. Conversely, anomalously low chlorophyll a levels might indicate the presence or influence of a source of toxic pollutants. Chlorophyll a is also important in the marine environment. As phytoplankton are a primary food source, their distribution and productivity are of considerable interest to the fishing industry.

A program has therefore been conducted with the purpose of developing an airborne laser-fluorosensing device capable of directly mapping surface-water distributions of chlorophyll a without a requirement for empirical data-interpretation schemes derived from ground truth measurements.

A profiling airborne laser fluorosensor has demonstrated an ability to monitor general trends in relative surface water chlorophyll a distributions over the range from 2 µg/l to 20 µg/l at elevations from 200 m to 400 m under clear sky, daylight conditions. The laser fluorosensor in its present form is capable of monitoring chlorophyll a concentrations down to 0.4 µg/l with a minimum signal-to-RMS background noise ratio of 3. With the implementation of measures to increase the fluorescence signal and reduce the background noise, the detection of chlorophyll a levels should be possible down to 0.1 µg/l with a minimum signal-to-RMS background noise ratio of 20. Comparisons between chlorophyll a ground truth data and the airborne chlorophyll a fluorescence signal produced linear correlation coefficients in the range from 0.77 to 0.95.

It is anticipated that improvements in this degree of covariation can be accomplished by implementation of a number of measures. First, a need for more efficient and reproducible methods for making chlorophyll a ground truth determinations is indicated. Second, the laser-fluorosensor chlorophyll a fluorescence signal has been shown to be sensitive to changes in the water optical attenuation coefficient. A means for correcting for this effect by concurrently monitoring the water Raman emission signal has been proposed. Finally, it is suggested that tests be conducted to determine the optimum wavelength for exciting fluorescence from in vivo chlorophyll a contained in mixtures of algae from the different color groups.

Attempts to monitor changes in the surface water distribution of blue-green algae using the single wavelength excitation laser-fluoro-sensor technique were not successful.

CONTENTS

101

TABLES

LIST OF ABBREVIATIONS AND SYMBOLS

ABBREVIATIONS

CRT	-- Cathode Ray Tube
EMI	-- Electromagnetic interference
f/number	-- Ratio of focal length to diameter of optical system aperture
FLD	-- Fraunhofer line discriminator
FWHM	-- Full width at half maximum height
{OH}	-- Notation for hydroxyl radical, as in water molecule
ppb	-- Parts per billion
pps	-- Pulses per second
r	-- Pearsons product moment linear correlation coefficient
RFI	-- Radio frequency interference
RMS	-- Root mean square value
SBNR	-- Signal to background noise ratio
s	-- Sample standard deviation
UV	-- Ultraviolet
$\bar{x}$	-- Sample mean
θ	-- Laser beam divergence

SUBSCRIPTS

b	-- Backward scatter
c	-- Chlorophyll a
f	-- Forward scatter
F	-- Fluorescence
L	-- Laser
N	-- Non-chlorophyllous material
pp	-- Peak to peak
P	-- Peak
R	-- Raman
Rec	-- Receiver
RMS	-- Root mean square
Tr	-- Transmitter
W	-- Water
λ	-- Wavelength

LIST OF ABBREVIATIONS AND SYMBOLS (continued)

SYMBOLS

a	--	Absorption coefficient
A	--	Intercept constant in Equation 9
b	--	Scattering coefficient
B	--	Slope constant in Equation 9
d	--	Terms defined by Equations 16 and 18
D	--	Dimensionless radiance distribution factor
H	--	Target range
k	--	Water diffuse attenuation coefficient
n	--	Concentration
P	--	Peak power
R	--	Reflectivity
T	--	Effective area of telescope aperture
v	--	Noise signal voltage
V	--	Peak signal voltage
x	--	Optical path length
X	--	Optical attenuation terms, defined by Equations 13 and 14
α	--	Water beam attenuation coefficient
β	--	Atmospheric attenuation coefficient
δ	--	Constant in Equation 20
Δ	--	Fraction of emission band seen by detector
η	--	System optical efficiency
μ	--	Refractive index
σ	--	Excitation cross section

SECTION 1

INTRODUCTION

In fresh-water environments a high concentration of chlorophyll a
indicates high levels of planktonic algae, suggesting, in turn, the
existence of eutrophic conditions, that situation in which high con-
centration of nutrients create algal bloom conditions. Such conditions
can lead to malodorous and even toxic water conditions. Conversely,
anomalously low chlorophyll a levels might indicate the presence or
influence of toxic pollutants. Chlorophyll a is also of importance in
the marine environment. Phytoplankton are the principle producers
and suppliers of energy in the marine ecosystem. They are the prin-
cipal food source for the herbivores such as zooplankton, which in
turn are an important food source of the carnivores characterized by
the fish population. As a consequence, information relating to
phytoplankton productivity is of considerable interest to the fisheries
industries.

Chlorophyll a determinations are routinely accomplished by lab-
oratory analysis on grab samples. This approach is both time-consuming
and costly in terms of manpower and facilities. In addition, because
of the finite time required to take grab samples from launches or heli-
copters, it is not always possible to obtain a synoptic record for a
given water surface due to water movement and diurnal effects. Also,
delays in transporting water samples to the laboratory for analysis
or the practice of freezing algae samples collected on filters are known
to produce large errors due to irreversible degradation of the chloro-
phyll a. In contrast, both airborne and satellite remote-monitoring
techniques are capable of rapidly and cost effectively providing data
for certain water quality parameters from large areas of water surface
without influencing the nature of the sample. The principal limitation
of remote sensing is its inability to provide information from below the
photic zone, commonly defined as that region from the surface to the
depth at which 99% of the surface light has disappeared. For active
as well as passive sensors operating in the optical region, this depth
is generally on the order of 0.5 to 10 meters and is conveniently
characterized by the reciprocal of the attenuation coefficient measured
at a given wavelength.

The purpose of the present program is to develop a compact, inte-
grated airborne system capable of mapping trends, gradients and anoma-
lies in the distribution of surface water chlorophyll a present as
planktonic algae.

106

SECTION 2

REVIEW

Two passive remote-sensing methods are presently under development for monitoring distributions of surface water fluorescent tracer dyes and chlorophyll a.

In the first approach, photographic cameras or multichannel radio-metric scanners are used to monitor the backscattered solar radiation in the visible and near infrared regions. These techniques generally provide imagery of high resolution with excellent spatial coverage, which can be used to obtain qualitative information on the location and extent of algae blooms, suspended sediment concentrations such as efflu-ent plumes, oil spills, pollution-dumping sites and tracing dye dis-persions. However, this approach has achieved only limited success in predicting the concentration of water quality parameters, in particular, chlorophyll a and suspended sediment. Much effort has been expended on formulating interpretation procedures for extracting information on chlorophyll a, e.g., references 1, 2 and 3, and suspended sediment con-tent of surface waters, e.g., references 4, 5 and 6. With the aid of ground truth data, empirical interpretation schemes have been devised which are able to predict these parameters for waters containing particulates and algal distributions of a specific color, generally for a limited geographical region, but are seen to break down when applied to different water conditions. As yet, no universal model exists which can provide either absolute or relative chlorophyll a concentrations from passive radiometric data. These problems arise in part from the spectral overlap of the radiation backscattered by algae and particulate matter, in part from the differing nature of the spectral and scattering properties of different types of algae and suspended sediments, and in part from the presence of dissolved materials that impart a character-istic color to the water. In addition, the limited optical transmission of water, particularly in the near infrared, atmospheric backscatter and surface water specular reflection of sky radiation further complicate the interpretation of the photographic or radiometric data. Finally, for successful operation of these devices, clear sky conditions in the absence of solar glitter are generally required. For passive airborne measurements made under cloud cover, signal-to-noise ratios are con-siderably reduced.

In the second approach, two airborne sensing techniques are worth mentioning with regard to their ability to remotely monitor surface water chlorophyll a.. Both methods are passive but, rather than record changes in the backscattered solar spectrum, they detect variations in

107

the solar-induced chlorophyll a fluorescence emission band at 685 nm
that, ideally, can be directly related to the chlorophyll a concen-
tration. Neville & Gower (7) used a multichannel spectrometer to
monitor the ratio of the solar-induced fluorescence emission from the
chlorophyll a band at 685 nm to the incident irradiance. Variations
in airborne fluorescence measurements and the corresponding chlorophyll
a ground truth data were found to be highly correlated.

The other passive fluorosensing approach presently under develop-
ment employs a Fraunhofer Line Discriminator (FLD) to monitor the solar-
induced target fluorescence observed in the region of the minimum of a
solar Fraunhofer line (8). This device has been flown in a helicopter
to map the surface water concentration of Rhodamine WT fluorescent
tracing dye in the parts per billion (ppb) range (8) and more recently
has been used to map the areal extent of marshland contaminated by an
oil well blowout (9). When operated in the scanning mode, spatial
coverage can be achieved by making a single pass over a target with
navigation data provided by conveniently located ground-based trans-
ponder units. Surface water chlorophyll monitoring has not yet been
attempted with this device, although it has been used to monitor the
changes in chlorophyll a fluorescence of tree vegetation induced by
geochemical soil anomalies (10). As with all passive remote-sensing
devices operating in the optical region, it is dependent on bright
daylight conditions for a usable signal-to-noise ratio. In addition,
the specificity of the FLD technique is reduced both by the limited
number and distribution of usable Fraunhofer lines and by the broad
spectral nature of the solar source.

Recently, active remote monitoring systems employing lasers have
been used to excite, detect and record the fluorescence of surface
water targets. These airborne laser-fluorosensor systems operate by
exciting fluorescence in a surface water volume, using a pulsed laser,
and by collecting a small fraction of the multidirectional fluorescence
emission, using a large-aperture telescope sighted on the excitation
spot. The backscattered fluorescence pulse is then passed through a
spectral analyser onto a photodetector, and the resultant electronic
signal is displayed, digitized and recorded. The schematic shown in
Figure 1 illustrates the general optical principle involved in which
the laser spot size might be on the order of 1 m to 2 m in diameter
from a platform elevation of 200 m. Laser beams are highly directional,
can have high average or peak power and low beam divergence, and can be
chosen or tuned to operate at any desired visible or ultraviolet (UV)
excitation wavelength. Using laser excitation sources, acceptable
signal-to-solar background-noise ratios can be obtained so that laser
fluorosensors can be operated on a 24-hour basis. Three fluorescence
parameters can be measured using this technique. Firstly, either the
amplitude of the fluorescence signal, generally at the wavelength of
peak emission, can be related to the concentration of a particular
target of known fluorescence quantum efficiency or, alternatively for
an opaque or optically thick target, the quantum efficiency can be
measured and used as an identifying feature. Secondly, the fluo-
rescence emission spectra can be monitored and recorded at a number of

Laser transmitter

Telescope receiver

Receiver field of view

Blue or UV laser beam

Fluorescence emission from target

Surface water fluorescent target

Laser excited target area
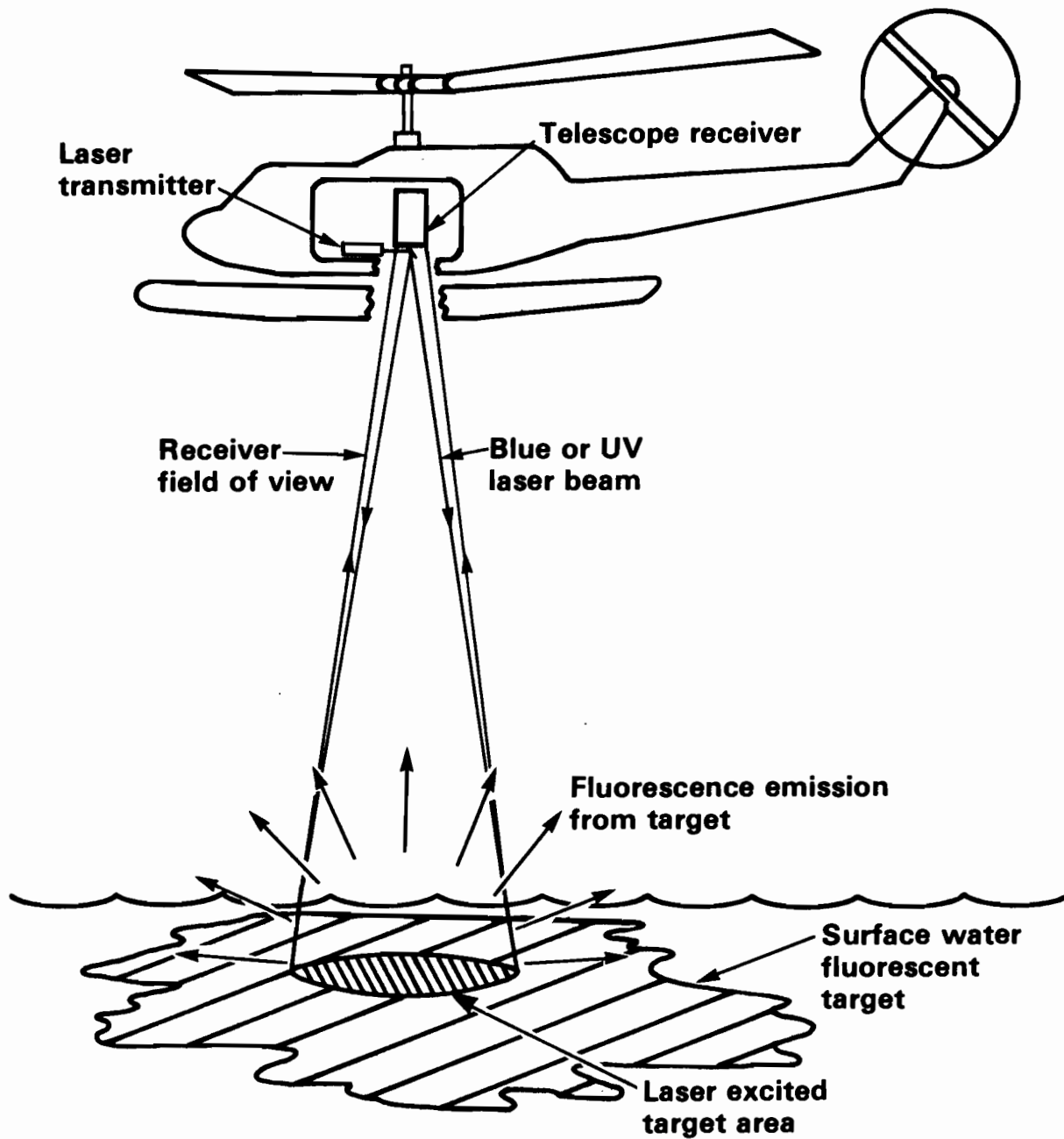
Figure 1. Principle of operation of airborne laser fluorosensor.

discrete wavelengths. In addition, the fluorescence absorption or excitation spectrum can, in principle, be determined using a dynamically scanned tunable laser source, although such systems are not yet commercially available. Finally, the fluorescence decay time spectrum can be measured as a function of wavelength. All of these parameters are unique for a given fluorescence target and in combination constitute an unambiguous signature with which to identify or characterize the target in relation to the fluorescent background or to competing fluorescent targets.

Airborne laser fluorosensors have been used to detect surface water oil spills (11, 12, 13) and in one case to obtain the fluorescence emission spectra from a number of oil slicks (14). They have been successfully used to remotely profile surface water chlorophyll a present in phytoplankton (15, 16) and finally they have demonstrated a potential for remotely monitoring the highly fluorescent lignin materials in pulp and paper mill effluents (12, 13). The feasibility of remotely monitoring algae and phytoplankton with laser-induced fluorescence was first proposed by Hickman and Moore (17). They demonstrated that an acceptable signal-to-noise ratio could be obtained for the 685-nm chlorophyll a fluorescence emission in relation to the solar background using existing laser technology. Mumola and Kim (18) were the first to operate a laser fluorosensor from an airborne platform in which a flashlamp-pumped dye laser operating at 590 nm was used to excite chlorophyll a fluorescence at 685 nm. Comparison of the airborne in vivo chlorophyll a fluorescence measurements with corresponding ground truth chlorophyll a data produced a linear correlation coefficient of 0.43* for a sample size of 19 for which the average laser-fluorosensor measurement was 11% greater than that for the ground truth data.

In many situations the ratio of in vivo fluorescence to extractable chlorophyll a has been observed to vary over as much as a tenfold range (19). The reason for this variability can be explained in terms of the fluorescence cross section (or the excitation coefficient) for a given substance, which is a measure of the quantity of incident excitation radiation converted to a fluorescence emission. The fluorescence cross section for chlorophyll a when measured in vivo is known to be dependent on a number of factors including water temperature, stress induced by toxic substances or lack of nutrients, the presence of photopigment degradation products, the intensity of the solar background, the intensity and the wavelength of the excitation radiation, the duration of the excitation radiation, and the relative concentrations of the different algae color groups present (16, 19, 20, 21, 22, 23, and 24).

In vivo flurometry performed on algae has generally employed an excitation wavelength of about 436 nm located close to the center of the blue-violet (Soret) absorption band of chlorophyll a. However, data presented by Friedman and Hickman (25) and by Mumola et al. (16)

---

*The linear correlation coefficient was calculated by the present authors from graphical data presented by Mumola & Kim (18).

showed not only that the absolute value of the fluorescence cross section varies considerably between algal divisions or color groups but also that these cross sections exhibit considerable variability with wavelength. This problem arises because of the presence of different light-absorbing photosynthetic pigments among the different algal color groups. For example, blue-green algae or cyanophyta, often employed as indicators of eutrophic conditions in fresh water, contain, in addition to significant amounts of chlorophyll a and β-carotene, the blue pigment c-phycocyanin. This substance effectively blocks light absorption by the various chlorophyll and carotene pigments in the blue-green region and has a strong absorption band centered at 622 nm. This red radiation is then internally coupled directly into the chlorophyll a photosynthetic system. It therefore becomes clear that large changes in relative concentration of the different algal color groups on either a spatial or a temporal basis can be expected to have a significant effect on the accuracy of the predicted chlorophyll a concentration when only a single excitation wavelength is used. This will be true regardless of whether the in vivo measurements are made with a field fluorometer or an airborne laser fluorosensor. Attempts to circumvent this problem have been made by employing an airborne laser fluorosensor which sequentially operates at several excitation wavelengths (16, 21). The number of laser wavelengths required is dictated by the number of algal color groups anticipated to be present in the surface water sample, with the wavelength of each laser tuned to lie close to the peak absorption wavelength for the given algal pigment. With a knowledge of the laser power, the water attenuation coefficients, and the fluorescence cross sections for each algal color group at each laser wavelength, together with the fluorescence power levels at 685 nm excited by each laser, it is, in principle, possible to solve a series of laser-fluorosensor equations to obtain the equivalent chlorophyll a concentration for each algal color group. On a test flight over the tidal flow region of the James River in Virginia, the four-wavelength laser fluorosensor was used to measure chlorophyll a concentrations for each of the golden, brown green and blue-green algal color groups (16). Comparison of the total laser fluorosensor chlorophyll a values with corresponding ground truth produced a linear correlation coefficient of 0.90* for a sample size of 7. In this case the average laser fluorosensor chlorophyll a value was approximately 28% below that for the ground truth data. A review of this multiwavelength approach by Browell (20) demonstrated that relatively small uncertainties in the values for the water attenuation coefficients and the algal color group fluorescence cross sections undergo considerable amplification when used to calculate the total in vivo chlorophyll a values. More recently, laboratory studies performed on known mixtures of four carefully controlled algal monocultures (each from a different color group) using the four-wavelength laser fluorosensor have obtained a linear correlation

---

*The linear correlation coefficient was calculated by present authors from graphical data presented by Mumola et al. (16).

coefficient of 0.99 for covariation between the in vivo laser fluorosensor chlorophyll a measurements and the corresponding extractable chlorophyll a data (21). However, the stable laboratory conditions employed for these measurements are neither typical nor representative of the true field environment. A number of unpredictable factors not present in these measurements are known to have a significant influence on the algal color group fluorescence cross sections. These are stress induced by nutrient limitations, the effect of toxic substances, changes in water temperature, age of the algal communities, the intensity of the solar background radiation and the wavelength, intensity and duration of the fluorescence excitation light source (19, 20, 22). In the absence of either in situ or remotely sensed data relating to the water attenuation coefficient and algal fluorescence cross sections, Browell (20) has suggested that both single and multi-wavelength laser fluorosensors are, at best, capable of providing only a qualitative or relative measure of surface water chlorophyll a concentration.

In light of these observations and with a view to reducing system complexity, a program has been initiated to design, build and test a single excitation wavelength airborne-laser fluorosensor. The remotely sensed fluorescence signature will then be used to produce surface water maps showing isopleths of surface water chlorophyll a concentration as illustrated in Figure 2. Whereas field fluorometers almost universally employ a wavelength of about 440 nm to excite fluorescence in planktonic algae (24), other studies, based on laboratory investigations performed on water samples and algal monocultures suggest that wavelengths in the 600-nm region are more suitable for monitoring the overall chlorophyll a level for disparate mixtures of algae (15, 16, 25). In particular, from the measurements made on specific algal color groups presented in Reference 16, it is apparent that at 620 nm the fluorescence excitation cross sections for the green, blue-green, red and golden brown algal color groups are all approximately equal. With these observations in mind, a flexible approach was adopted allowing different excitation wavelengths to be evaluated with a view to optimizing both the degree of correlation attainable between the airborne and ground truth data and also system sensitivity. In particular it was planned to employ a wavelength of 440 nm to facilitate comparison between the airborne data and the fluorometrically determined ground truth data and also a wavelength of 620 nm for the reasons stated above.

The principal advantage of the fluorometric approach, whether active or passive, over the reflectance spectroscopy approach is its provision of raw data directly proportional to chlorophyll a concentration. The data can then be analyzed without the need for empirical interpretation models established beforehand with ground truth data. In this respect the airborne laser-fluorosensor is similar in principle and operation to field fluorometers that are widely used for in situ monitoring of both surface and subsurface in vivo chlorophyll a (19, 24, 26). The principal difference between these two fluorometric techniques is that the in situ system employs a constant pathlength cell, whereas, with the remote sensing approach, the effective sample

112
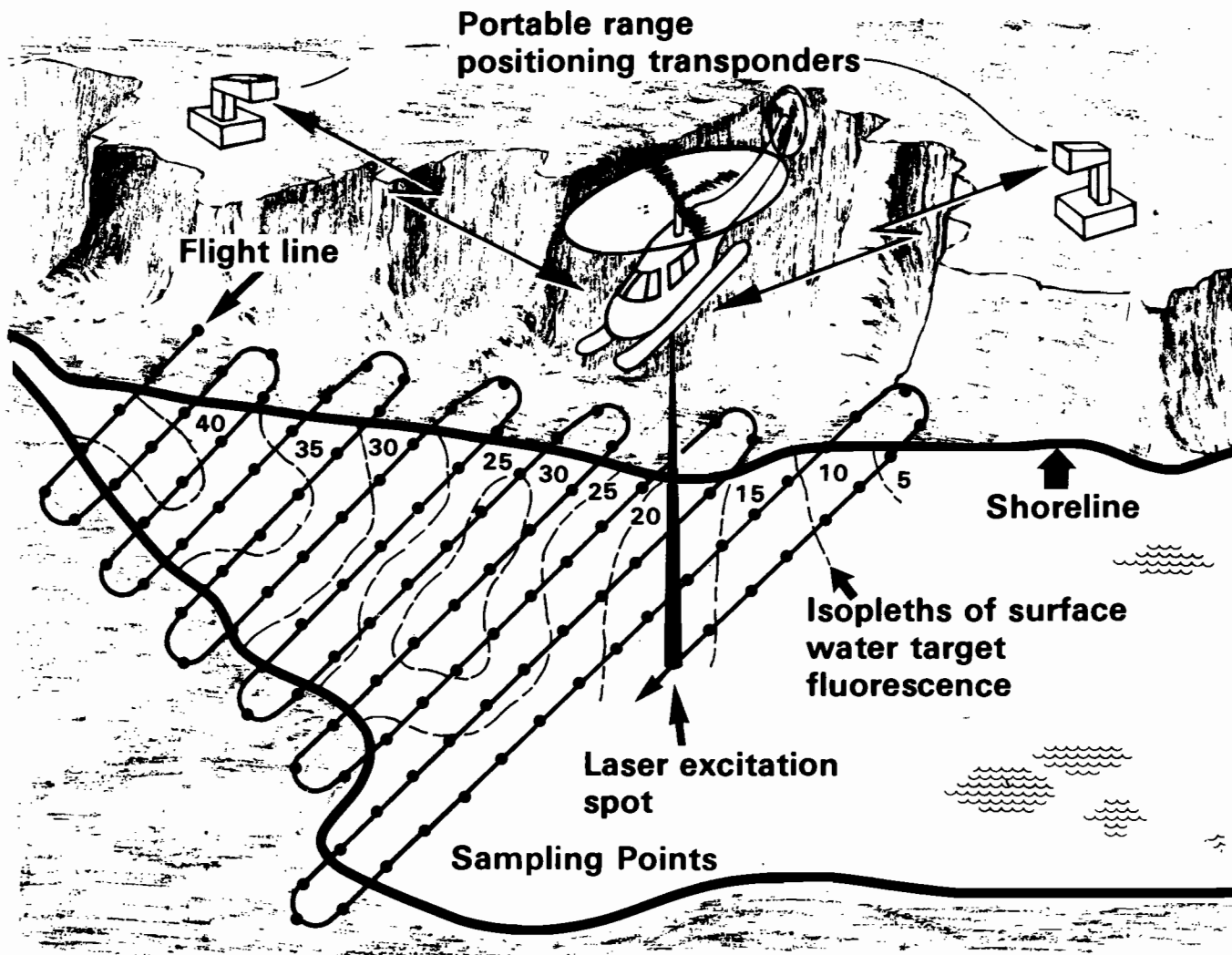
Figure 2. Schematic illustrating possible mode of operation of an airborne laser fluorosensor for mapping surface water chlorophyll _a_ distributions.

pathlength and resultant fluorescence signal are dependent on the variable optical attenuation lengths for the laser and fluorescence wavelengths. A method for compensating for this variable sample length by concurrently measuring the water Raman band emission is discussed in Section 6.

SECTION 3

CHLOROPHYLL a MONITORING WITH AIRBORNE-LASER FLUOROSENSORS

The laser fluorosensor equation for remote monitoring of in vivo chlorophyll a at normal incidence has been derived by Browell [20] and is presented below as Equation 1. The chlorophyll a concentration, n_c, which is assumed to remain constant with depth, is given as a function of either known or measurable parameters:

$$n_c = \left[\frac{P_F H^2}{P_L}\right]\left[\frac{4\pi\Delta F}{T^\eta Tr^\eta Rec}\right]\left[\frac{\mu_w^2 \exp\{H(\beta_L + \beta_F)\}}{(1-R_w)^2}\right]\left[\frac{k_L + k_F}{\sigma_c}\right] \quad \mu g/l$$

where P_F = Peak detected fluorescence power at fluorescence wavelength F, watts.

P_L = Peak detected laser output power at laser wavelength L, watts.

H = Aircraft elevation or range above fluorescent target, m.

T = Effective area of telescope receiver, m^2.

ΔF = Fraction of fluorescence band seen by detector.

$^\eta T_r$ = Laser (transmitter) efficiency.

$^\eta Rec$ = Telescope (receiver) efficiency.

R_w = Specular reflectance for air-water interface at normal incidence for visible spectrum.

μ_w = Refractive index for water over visible spectrum.

β_L = atmospheric beam attenuation coefficient at laser wavelength L, m^{-1}.

β_F = atmospheric beam attenuation coefficient at fluorescence wavelength F, m^{-1}.

n_c = concentration of total in vivo chlorophyll a from algae in irradiated sample, $\mu g/l$.

k_L = diffuse attenuation coefficient for water at laser wavelength L, m^{-1}.

k_F = diffuse attenuation coefficient for water at fluorescence wavelength F, m^{-1}.

σ_c = in vivo cross section for chlorophyll a fluorescence over complete fluorescence band centered at 685 nm when excited at laser wavelength L, m^2/mg.

Factors within the first set of square brackets in Equation 1 are measured directly from each digital or analog laser fluorosensor record obtained for a given sampling station. Those within the second set of square brackets are known or measurable laser fluorosensor system constants, whereas those within the third set of brackets relate to known environmental factors. However, it is the difficulty in anticipating the behavior of the environmental factors within the fourth set of square brackets, specifically σ_c, k_L and k_F, that constitutes the major limitation to the implementation of this remote-sensing technique. The assumptions made during the derivation of Equation 1, in particular those regarding the parameters σ_c, k_F and k_L, are discussed below:

(1) It is assumed that the combined reflected and backscattered sky and backscattered solar background levels have been subtracted from the detector signal to obtain P_F. In addition, it is assumed that the laser-induced background signal at 685 nm due to dissolved organics is negligible in relation to the chlorophyll a fluorescence signal.

(2) The surface water excitation volume is assumed to lie completely within the telescope field of view.

(3) By integrating the fluorescence signal to infinite depth it is necessary to assume that the total water depth is at least an order of magnitude greater than the characteristic attenuation lengths given by $(k_F)^{-1}$ and $(k_L)^{-1}$. It should be noted that light penetration is characterized by the diffuse attenuation coefficient k rather than by the related beam attenuation coefficient α, as both singly and multiply scattered excitation and fluorescence radiation contribute to the measured fluorescence signal (20, 27). In addition, values for k are generally smaller than those for α at a given wavelength because multiple scattering effects result in an increased level of illumination at a given depth, whereas α, which is measured with a narrow collimated beam, accounts only for single scattering losses. Specifically, k accounts for absorption and both forward and backward-scattering losses. Further discussion of the relationship between k and α is provided in Section 4 (e).

(4) Inherent in the integration of the fluorescence signal to infinite depth is the assumption that n_c, k_L, k_F and σ_c all remain

constant with depth. It is generally considered that, if k_L and k_F remain constant to depths at least double those defined by the attenuation lengths $(k_L)^{-1}$ and $(k_F)^{-1}$, then errors induced in n_c as calculated from Equation 1, can be kept below 10%. Concurrent vertical profiles of the beam attenuation coefficient α and the in vivo chlorophyll a fluorescence obtained in a marine environment by Kiefer and Austin (28) have shown that the transmissometer and the fluorometer signals remain constant down to 10 meters with $\alpha \approx 1$ m^{-1}. Similar measurements made in a fresh-water environment by Baker and Baker (29) have shown that both n_c and α remained constant down to about 3 meters for $\alpha > 4$m^{-1}. Although no infallible rule exists which guarantees that n_c, σ_c, k_L and k_F will remain constant to depths characterized by $2(k^{-1})$ or $2(\alpha^{-1})$, most coastal, estuarine and inland waters have α values greater than 1m^{-1}, such that wind-induced mixing should ensure that this surface layer will remain homogeneous with regard to both particulate and algal matter.

(5) The assumption is made that the fluorescence lifetime for in vivo chlorophyll a is less than or equal to the laser pulse width. In the present case, with a laser pulse width of about 200 nsec, and a chlorophyll a fluorescence lifetime of less than 1 nsec (30), this condition is clearly met. However, in situations where the laser pulse width is less than or equal to the fluorescence lifetime, the value of P_F would be reduced in relation to P_L due to the effect of pulse spreading induced by the fluorescence decay phenomenon. This problem can be avoided by either applying a suitable correction to the peak power measurements or measuring pulse energy rather than peak power for both the laser and fluorescence signals.

(6) For clear atmospheric conditions over limited ranges of the order of 300 m, the atmospheric attenuation term exp $\{H(\beta_L + \beta_F)\}$ remains essentially constant with a value close to unity, so that the effect of the terms within the third set of square brackets can be considered to be constant.

(7) Several assumptions are made with regard to the fluorescence emission cross section σ_c. Firstly, it is assumed to remain constant with both depth and horizontal location. Secondly, since σ_c is defined purely in terms of chlorophyll a, it is assumed that the fluorescence emission at 685 nm is due solely to the excitation of chlorophyll a pigment. Finally, it is assumed that the percentage proportions of the different algal divisions (color groups) remain constant with depth and horizontal location. It is necessary to make this latter assumption because, as mentioned in Section 2, the magnitude of the cross section for in vivo chlorophyll a fluorescence varies considerably between algal divisions.

(8) Similarly, the diffuse water attenuation coefficients k_L and k_F are assumed to remain constant with horizontal surface location and also to be independent of the chlorophyll a concentration n_c.

To obtain a precise value of n_c by use of Equation 1, estimates of σ_c, k_L and k_F must be obtained, generally, by making in situ measurements at a reference sampling station on the water surface being surveyed, on the assumption that these reference values are representative of all possible sampling points on the water surface. However, the laboratory technique for estimating in vivo values for σ_c for a given sample is not easily implemented, requiring specialized equipment and trained personnel. Rather this measurement should be made with an in situ fluorometer so that the various environmental factors mentioned in Section 2, which are known to influence σ_c, remain unchanged. With a view to avoiding this requirement for making in situ measurements, the present airborne experiments are aimed at obtaining a relative measure of surface water chlorophyll a concentration based on the assumption that n_c is directly proportional to the measured airborne data represented by the factor $(P_F/P_L)H^2$, which is the term in the first set of square brackets in Equation 1. All other parameters, although unknown, are assumed to remain constant, including σ_c, k_L and k_F. The success of this technique for monitoring surface water chlorophyll a will then be gauged by rating the degree of covariation obtained between values of $(P_F/P_L)H^2$ and the extracted chlorophyll a determinations made on corresponding surface water ground truth samples.

SECTION 4

INSTRUMENTATION

The laser fluorosensor consists of a laser transmitter and telescope receiver, which are mounted in a lightweight aluminum box in a non-coaxial configuration, as shown schematically in Figure 3. A borne operations are conducted from a Bell UH 1D/H (Huey) helicopter, with the system mounted in a central location over a clear hole cut between two stringers just forward of the transmission housing.

The system operates in a fixed downward-looking mode, which at typical aircraft ground speeds of 20 m/sec and a laser repetition rate of 1 pulse per second (pps) gives a ground footpring spacing of 20 m. At an above-target elevation of 200 m, the laser beam divergence of 6 mrad produces a water surface spot size of 1.2 m diameter. As the ground resolution of the system is essentially set by the (20-m) spacing between laser excitation spots, it would be advantageous to utilize a laser spot diameter similar to this interspot spacing to smooth out the effects of small-scale fluctuations in the concentration of surface water algae. This advantage can be gained by increasing the aircraft height H without increasing the laser beam divergence or the telescope field of view. A limitation to this expedient is set by the $1/H^2$ drop-off in the fluorescence signal with increasing height H. As a result, the sky and solar background signal and noise within the telescope field of view eventually compete with and ultimately dominate the fluorescence signal. In this case the signal-to-background-noise ratio also varies as $1/H^2$. Consequently, doubling the aircraft height produces a fourfold reduction in the signal-to-background-noise ratio (31). Another approach to increasing the laser excitation spot size would be to double the laser beam divergence θ together with the telescope field of view at a given aircraft altitude. In this case the signal-to-background noise varies as $1/\theta$, so that doubling the system field of view halves the signal-to-background-noise ratio (31). However, this approach is much more difficult to implement than that achieved by changing the aircraft height due to the problems involved in continuously and simultaneously adjusting the fields of view for both laser and telescope. A better approach would be to increase the laser repetition rate, thereby increasing the sampling frequency so that the effects of algal patchiness can, if desired, be smoothed out by low-pass filtering the measured chlorophyll a profile.

Adjustment of the position of the surface water laser spot is achieved with the laser beam steering mirror shown in Figure 3, which

119
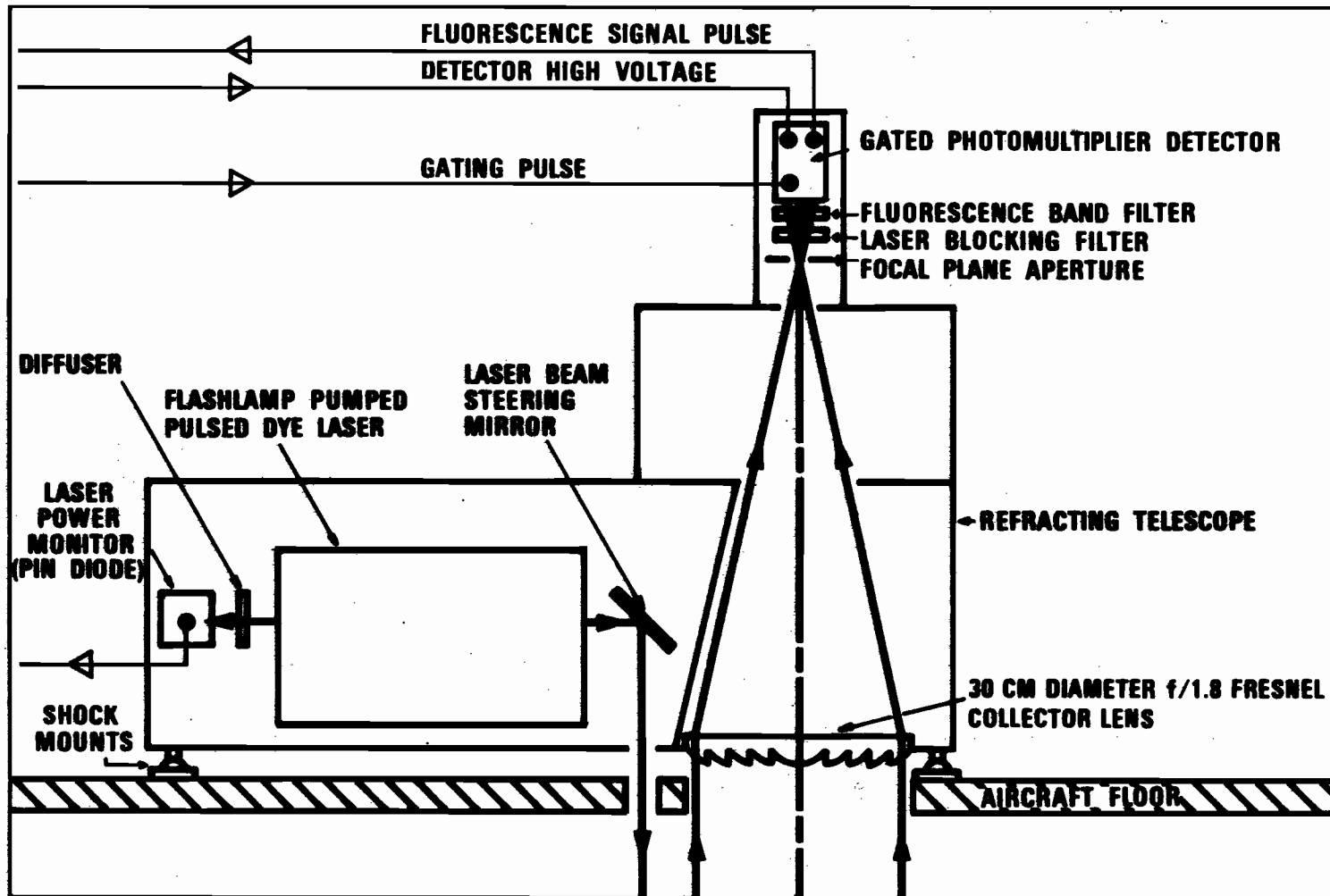
Figure 3. Optical diagram of airborne laser fluorosensor for monitoring surface water fluorescence signal.

positions the laser spot at the center of the telescope field of view. This micrometer adjustment is made during each flight at a prescribed altitude by maximizing the amplitude of the detected surface water chlorophyll a fluorescence signal at a given location.

(a) Laser Transmitter System

Characteristics and typical performance data for the coaxial flashlamp-pumped dye laser (Phase-R DL-1200) are given in Table 1. Performance data for this laser, using a number of dyes in methanolic solution are given in Table 2. With the preferred dye Coumarin 120 used for exciting chlorophyll a fluorescence at 440 nm, the laser emits pulses of 200 kw peak power and 200 nsec FWHM (full width at half maximum) width at a repetition rate of 1 pps. At an energy input of 25 joules per pulse, the laser output declines to the half-power point after 25,000 joule shots/liter. Spectral tuning is achieved using a 60° prism made from Schott SF 10 glass with the FWHM spectral bandwidth of the laser emission varying from about 0.45 nm at 440 nm to 2.1 nm at 639 nm. Laser peak power is monitored by directing a small fraction of the laser output onto a calibrated PIN silicon photodiode via a quartz diffuser plate. The laser signal is also used to provide a signal for triggering the oscilloscope waveform digitizer and photmultiplier gating electronics. Although the laser can operate at up to 10 pps, performance tends to deteriorate rapidly above 1 pps due to the effects of dye degradation and the inability of the flowing dye and cooling water to remove the flash-induced heat buildup prior to the next laser pulse. This latter effect produces refractive index inhomogeneities in the flowing dye which in effect produces a misalignment of the laser cavity. Our measurements indicated that a dye flow rate of at least 5 l/min was required for stable laser performance at a repetition rate of 1 pps. The laser dye and cooling water flow circuits are illustrated schematically in Figure 4. Both dye and cooling water temperatures were maintained at 18°C ± 1°C. Construction materials which do not appear to affect laser performance when exposed to the laser dye solution are stainless steel, glass, quartz, Teflon, Delrin, polyporpylene, polyethylene and silicone rubber. Considerable effort was directed towards achieving a satisfactory dye flow rate through the laser. Magnetically coupled pumps with wetted parts of stainless steel and Teflon are generally satisfactory because of the inert nature of these materials. Unfortunately all high-performance pumps produce both cavitation bubbles and a steady stream of Teflon and stainless steel wear particles, which act as optical scattering centers within the laser cavity, thereby reducing laser output power. These contaminants in turn necessitate the use of an inline filter to trap both bubbles and pump wear products. After much experimentation, a variable-speed magnetically coupled stainless steel and Teflon centrifugal pump (Micropump Model #10-41-316) was chosen, together with a 142-mm-diameter 1μ-pore-size cellulose acetate membrane filter (Millipore Cellotate EA), a pairing that produced a flow rate of 5 l/min at 83 kPa (12psi). The possibility of a flashlamp explosion with subsequent risk of a methanol fire, particularly on board an aircraft, required

TABLE 1. AIRBORNE LASER-FLUOROSENSOR CHARACTERISTICS

LASER TRANSMITTER

Peak power	100 KW - 300 KW
Pulse width (FWHM)	200 nsec - 280 nsec
Pulse energy	40 mj - 70 mj
Beam divergence	6 mrad
Spectral bandwidth	0.45 nm - 2.1 nm
Repetition rate	0.1 pps - 10 pps
Degree of polarization	Linear to within 1 part per 100

TELESCOPE RECEIVER

Refractor	30 cm diam., f/1.8, Acrylic Fresnel
Focal plane aperture	4 mm diam.
Chlorophyll a fluorescence filter	685 nm, 13 nm FWHM, 64% Transmission
Laser blocking filter	Corning 2-64

TABLE 2. LASER DYES EVALUATED FOR USE IN COAXIAL FLASHLAMP-PUMPED DYE LASER EMPLOYED IN AIRBORNE LASER FLUOROSENSOR

Laser dye [A]	Molecular Weight	Molecular Concentration (M) [B]	Peak Wavelength (nm)	Tuning Range (nm)	Peak Power (KW) [C]	Spectral Bandwidth FWHM (nm)	Pulsewidth FWHM (nsec)	Dye Lifetime Joule-Shots/l
Coumarin 120 (EOC)	175.19	5×10^{-4}	452	432-468	200	0.45	200	25,000
Coumarin 339 (EOC)	215.25	2×10^{-4}	482	440-492	210	0.93	240	20,000
Coumarin 311 (EOC)	203.24	2×10^{-4}	485	442-492	255	0.80	225	50,000
Coumarin 314 (EOC)	313.35	1×10^{-4}	520	485-541	300	1.25	250	50,000 +
Coumarin 522F (EXC)	283.25	2×10^{-4}	534	502-572	240	0.97	250	50,000 +
Rhodamine 110 (EOC)	366.80	5×10^{-5}	570	545-590	220	2.00	280	100,000 +
RhodamineB Perchlorate (EOC)	543.02	5×10^{-5}	639	595-655	270	2.10	275	250,000

A) EOC: Eastman Organic Chemicals, Rochester, NY; EXC: Exciton Chemical Company, Dayton, OH.
B) Solvent: Spectral grade methanol.
C) Phase-R DL 1200 Laser: Input energy-25 Joules; Dye temperature-65°F; Dye flow rate- 5 l/min; Repetition rate-1 pulse/sec.
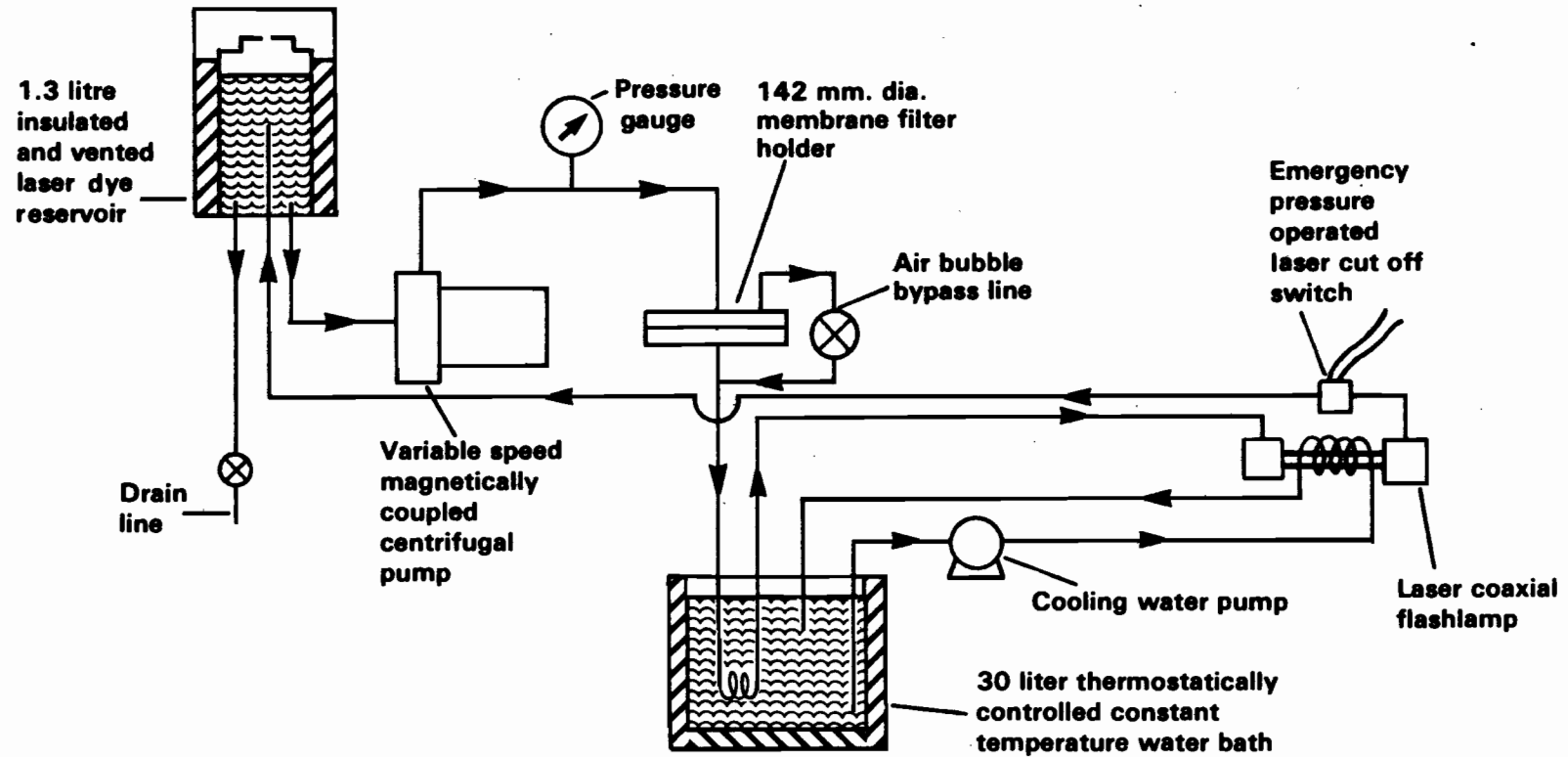
Figure 4. Dye and water cooling flow diagram for coaxial flashlamp-pumped dye laser employed in airborne laser fluorosensor.

careful consideration. A pressure-operated laser cut-off switch was installed downstream of the flashlamp, as shown in Figure 4. The switch was arranged to cut off electrical power to both the dye pump and the laser power supply on loss of dye pressure due to rupture of the flashlamp. An inert nitrogen atmosphere is maintained in the laser cavity during laser operation. Halon fire extinguishers are also made available for use against a possible methanol fire. With a view to avoiding a flashlamp explosion due to increasing lamp resistance with age, a 1000-ohm high voltage resistor was placed in parallel with the flashlamp. As the value of the lamp resistance increases to that of the resistor, a point is reached at which increased current flow through the resistor will cause the resistor to fail in preference to the lamp (32). This expedient not only avoids a flashlamp explosion and fire risk but also acts as a convenient indicator of flashlamp lifetime.

(b) Optical Receiver System

The optical part of the receiver system, consisting of a Fresnel lens, a focal plane aperture, a series of optical filters and a gated photomultiplier, is shown schematically in Figure 3, with characteristics listed in Table 1. The principal advantages of a lightweight acrylic lens (30 cm diameter, f/1.8) are the low cost and minimum requirement for a support structure because of its negligible weight. Its principal disadvantage, other than those due to scattering losses from the grooves, originates from its low f/number refractive nature. Lenses of this type produce large blur circles or circles of least confusion due to the effects of spherical aberration. For a plano-convex acrylic lens of refractive index $\mu = 1.49$ and focal length of 30 cm, the calculated diameter for the circle of least confusion for a point source at infinity is 6 mm (33), whereas the calculated size of the image of a laser spot produced by a 6-mrad laser beam at 200 m is 2-mm diameter. Clearly, if the full fluorescence return signal is to be detected, an aperture of at least 6 mm diameter should be employed rather than the theoretical 2 mm value. However, this increase in aperture produces a 9-fold increase in the solar background signal level that reaches the detector. This change in turn reduces the signal-to-noise ratio by a factor of three (31). In this situation a compromise focal plane aperture of 4 mm diameter was found to be satisfactory. The chlorophyll a fluorescence band at 685 nm is spectrally isolated with a 5-cm square interference filter centered at 685 nm with a 13 nm width (FWHM) and 64% peak transmission. Additional laser blocking is provided by a longwave pass filter with a cutoff at 640 nm (Corning 2-64). Neutral density attenuation filters are employed to ensure that the detected signal does not exceed the photomultiplier linearity limit. The fluorescence detector is a 5-cm diameter, 12-stage, red-sensitive (S-20 response) end-on photomultiplier tube (RCA C31000A). The linearity limit of the detector output is enhanced by using a capacitatively decoupled linear dynode chain as shown in Figure 5. Saturation of the detector, caused by continuous exposure to the backscattered sky and solar background radiation, is avoided by gating on the supply to dynodes 4, 6 and 8 for the duration of each

125
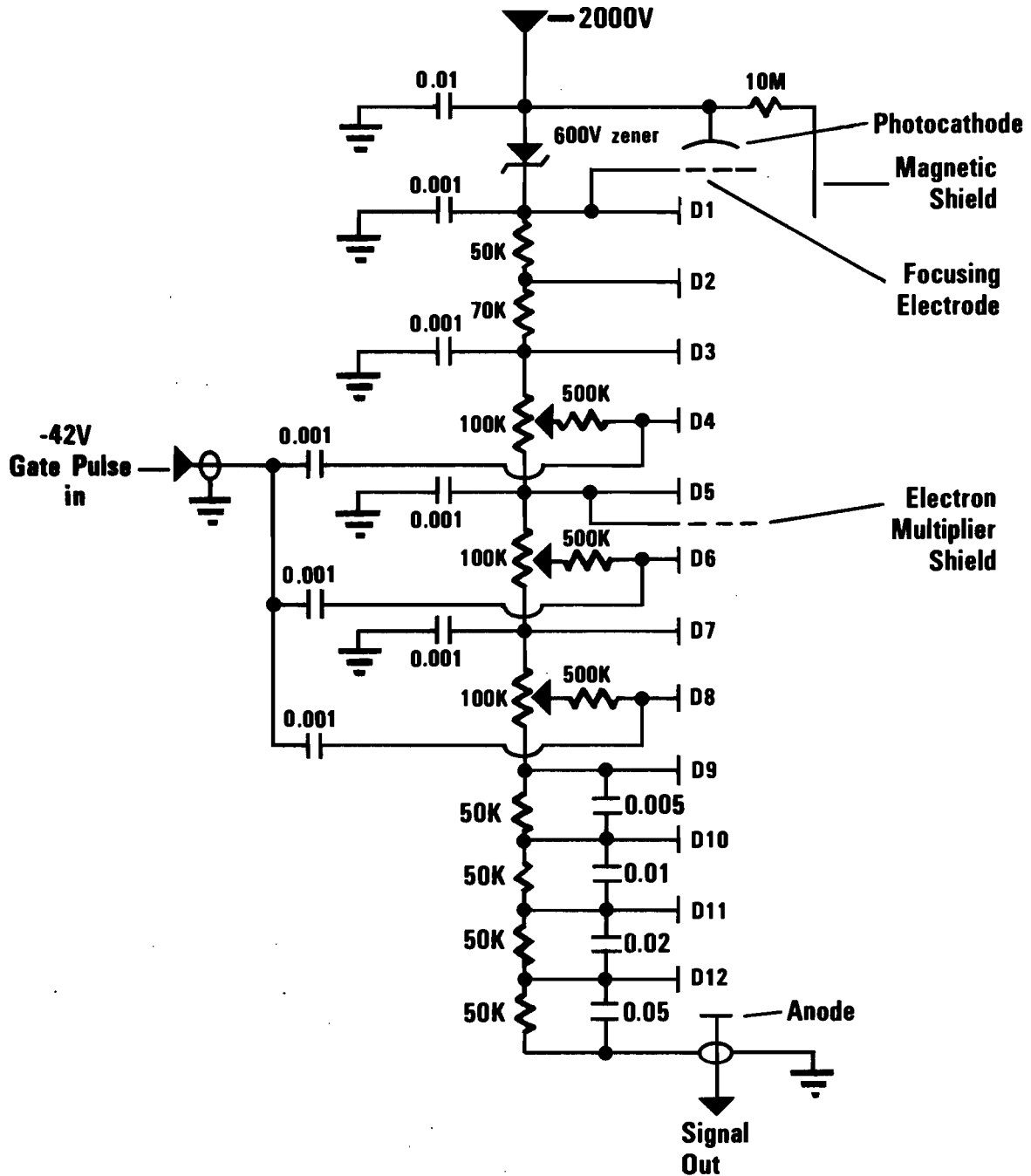
Figure 5. Gate and voltage divider circuit diagram for RCA C31000A photomultiplier.

126

fluorescence return signal. A 42-volt pulse applied as shown in Figure 5 provides an on/off ratio of about 1000:1. Under these conditions with a gate width of 3 μsec, the tube remains linear to 1 volt as measured across a 50-ohm load. In addition, gating the detector also provides a measurement of the steady (DC) background current at the instant the fluorescence pulse is measured. A determination can then be made to ensure that the detector has remained in the linear operating region during the measurement of the fluorescence pulse.

(c) Electronic Monitoring and Recording System

The circuit for the detector gating, monitoring and recording electronic system is shown in Figure 6. Events are initiated by the laser power pulse, which triggers a monitoring oscilloscope (Tektronix R7844). The oscilloscope time base gate output is then used to trigger a pulse generator which in turn initiates formation of a delayed detector gate pulse. The delay period for the detector gate pulse is adjusted so that the detector is activated several hundred nanoseconds before the arrival of the backscattered fluorescence signal. This series of events is conveniently illustrated by the oscillogram shown in Figure 7. In this case, for a height of 309 m (1103 ft), the detector was gated on 1.1 μsec after lasing. Also shown are the laser power pulse and the chlorophyll a fluorescence return from the surface water algae, which is superimposed on the steady 3-μsec background signal. This background signal, consisting of both sky and solar backscatter and sky surface specular reflection components, does not constitute a serious noise source for the present laser-fluorosensor system. However, the same cannot be said of the effects of solar glitter, viz., the direct specular surface reflection of the solar disc seen by the detector. In this case, the solar glitter background signal not only contributes significantly to the overall signal noise level but often drives the detector into a region of non-linearity or saturation. In the light of these observations it was found advisable to avoid making flights over rough surface water at times of high sun angle, when solar glitter can be seen by a downward-looking sensor. The most favorable time was generally in the early morning hours, when the sun angle is low and the water surface is calm. The overall signal waveform, such as that shown in Figure 7, is also digitized into 512 channels, each 10 nsec wide with 8-bit resolution over a 5.12-μsec period using a fast waveform digitizer (Biomation 8100). This digital data is then dumped from an internal buffer memory through an interface bus onto magnetic tape using a 9-track digital tape recorder (Kennedy 9800). The effective bandwidth of both digital and analog electronics is approximately 8 MHz, dictated principally by the 50-ohm low-pass filters used to reduce the amplitude of photon and electromagnetic interference (EMI) noise. These filters are conveniently made from lossy 50 ohm cable whose low-pass cutoff frequency is dependent on the cable length*. These filters are relatively cheap and easy to install

---

*Manufactured by CAPCON, Inc., NY, NY 10001.
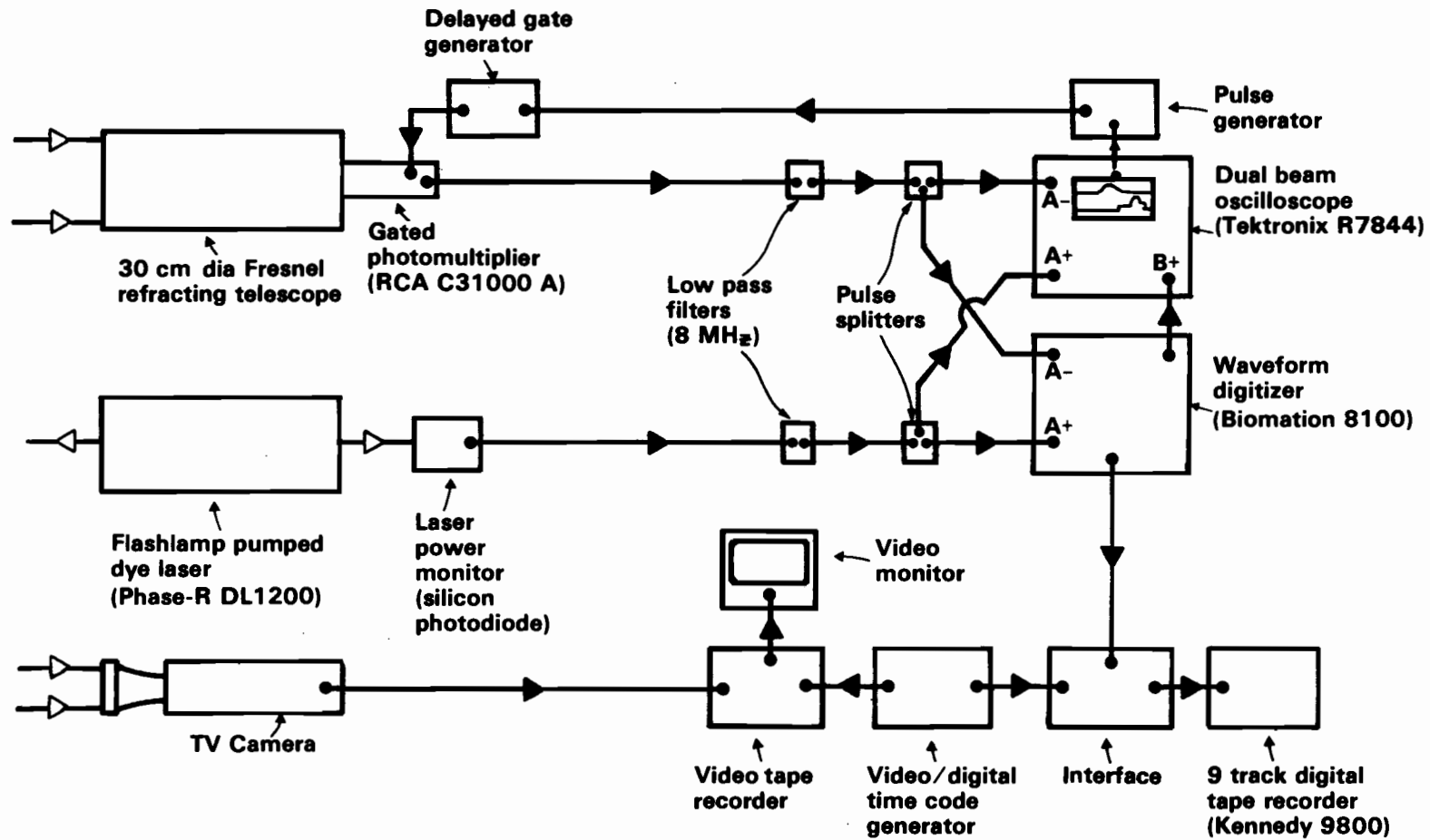
Figure 6. Schematic of airborne laser fluorosensor for measuring chlorophyll a fluorescence showing detection, monitoring and recording systems.

LASER PULSE
AT 440nm

DETECTOR ON

CHLOROPHYLL a
FLUORESCENCE
AT 685nm

100mV   500V

MEASURE OF SURFACE
WATER CHLOROPHYLL a
CONCENTRATION (EXTRACTED
CHLOROPHYLL a = 10.5 μg/l)

MEASURE OF
LASER POWER

MEASURE OF
SOLAR
BACKSCATTERED
RADIATION

200V   20μS   500nS

ALTITUDE = τC/2

= 309m
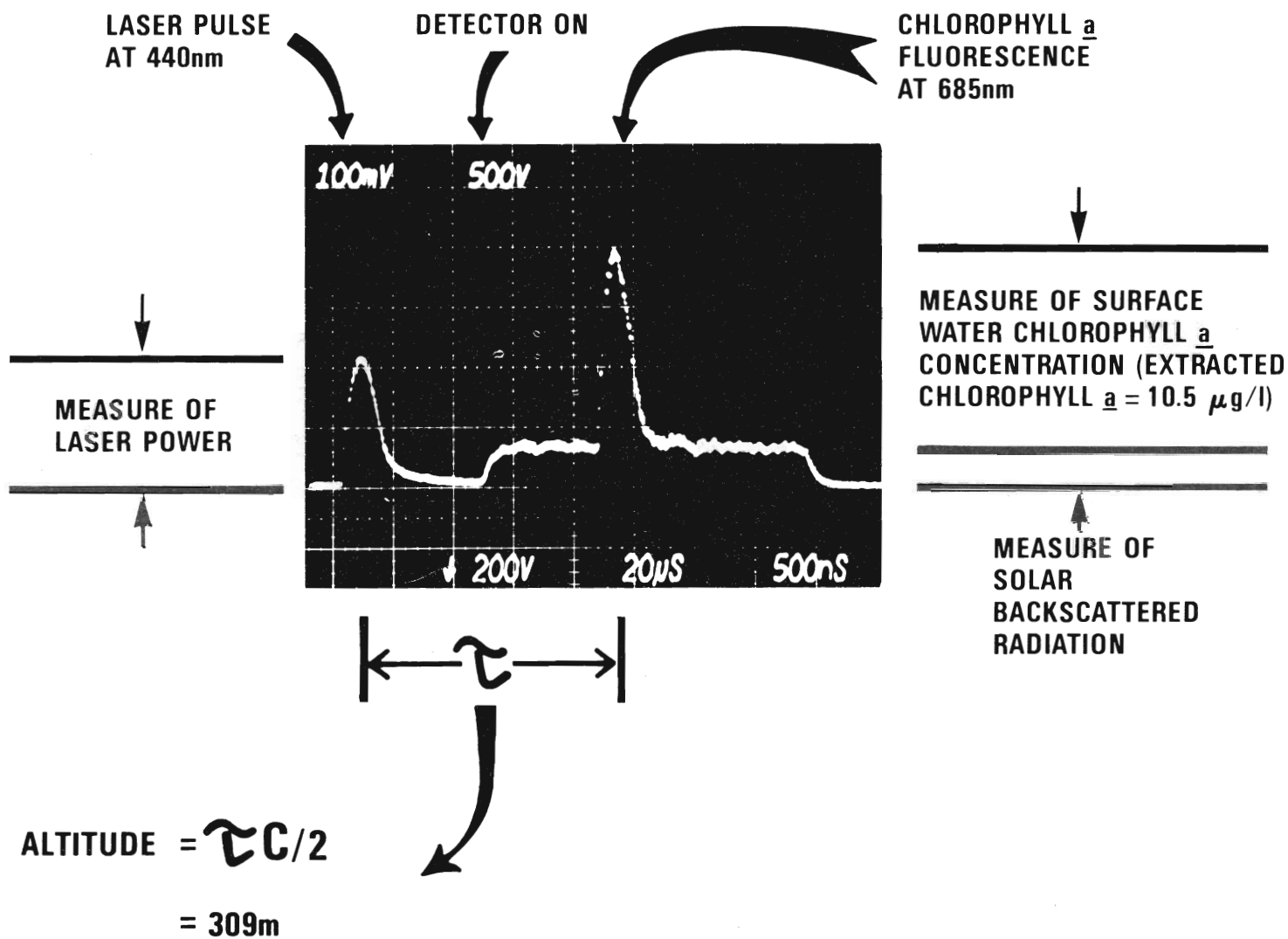
Figure 7. Oscillogram showing sequence of airborne laser-fluorosensor signals obtained over buoy #12 on October 4, 1976, for a measured chlorophyll a concentration of 10.5 µg/l.

with suitable (BNC) connectors and transmit signals free of ringing or line reflections.

Navigation, fluorescence target evaluation and track recovery were facilitated using a TV camera with a wide angle lens mounted directly to the laser fluorosensor module and boresighted with the laser beam. The helicopter flight path over a chosen water surface target can then be viewed directly on a video monitor and the same video image recorded on a video cassette. In order to use this video recording to assist with interpretation of the laser fluorosensor data, a video digital time-code generator was used to index each digital laser fluorosensor record and each video frame with a time signal to the nearest 1/100 sec. An approximate ground location for each laser-fluorosensor record can then be established.

Despite considerable effort expended on the digital recording equipment, satisfactory operation of this part of the system was not achieved for several reasons. The high ambient daytime temperatures encountered in the southern Nevada area often produce temperatures inside the helicopter in excess of 120°F. This heat buildup invariably induces component failure, particularly in the digital electronic equipment. This problem has been temporarily solved by scheduling the test flights during the early hours of the morning when ambient temperatures are some 30°F to 40°F cooler than at midday. However, this expedient will not be acceptable when, of necessity, flights must be made at specific times of the day with a view to monitoring diurnal changes in the distribution of surface water algae. With these requirements in mind, it is planned to provide a dedicated cooling system for the digital rack-mounted instrumentation. Problems that were somewhat more difficult to eradicate concern the influence of vibrations and electronic noise on the performance of the digital recording system. Low-frequency vibrations in the region of 3Hz to 7Hz induced by the helicopter rotor blade were found to affect the precision alignment of the read and write heads of the digital tape recorder in relation to the tape transport assembly. This problem was eliminated by the addition of a stiffening member to the tape-drive support frame. Vibrations may also reduce the integrity of the many mechanical circuit connections in the digital equipment as exist with printed circuit-board connector pins, wire-wrapped circuits and push-fitted integrated-circuit chips. Although successful isolation from low-frequency vibrations in the region below 7Hz is difficult with available aircraft-rated shock mount components, efforts are being made to improve the performance of the shock isolation rack mounting system used to hold the digital recording system. Finally, both the digital recording system and the monitoring oscilloscope have demonstrated a sensitivity to noise in the form of radio frequency interference (RFI) and EMI, particularly in the enclosed aircraft environment. Efforts are being made to improve the shielding of these components from external noise sources through the use of improved RFI screening, elimination of potential ground loops and additional filtering of the aircraft power supply. Due to the aforementioned problems with the digital equipment,

130

it was not always possible to produce digital recordings of the airborne laser fluorosensor data. Consequently, oscillograms obtained at each sampling buoy location were used as the prime data source for comparison with the corresponding chlorophyll a ground truth data.

SECTION 5

AIRBORNE MEASUREMENTS

(a) Field Operations

Airborne testing and evaluation of the laser fluorosensor were
made over the Las Vegas Bay region of Lake Mead; a nautical chart of
this area is shown in Figure 8. This bay is an ideal test site for a
number of reasons. Firstly, it is located approximately 10 minutes
flying time from McCarran (Las Vegas International) Airport. Secondly,
this region has been extensively surveyed over a number of years by the
Department of Biological Sciences, University of Nevada, Las Vegas
(UNLV), because of the concern regarding the influence of nutrients on
the population level of algae (34). High concentrations of nutrients
and other pollutants enter the western end of Las Vegas Bay from Las
Vegas Wash, which is essentially an open stream carrying both partially
treated and untreated sewage water from the City of Las Vegas. At cer-
tain times of the year this pollution has been observed to support algal
communities to the extent that chlorophyll a values will vary from 0.5 µg/l
to 50 µg/l over a distance of 10 km. Finally, ground truth support for
these airborne measurements was conveniently provided through the facili-
ties and personnel of the Department of Biological Sciences at UNLV. A
series of sampling-station marker buoys positioned by the Department
and the National Park Service is shown in Figure 8. This string of
buoys, easily seen from a height of 200 m, was flown as three separate
straight-flight lines. The lengths of these lines from buoys 1 to 7,
7 to 11', and 11' to 12 are respectively 4452 m, 3544 m, and 1607 m.
Not surprisingly, the highest chlorophyll a concentrations generally
occurred in the region of buoy 12, which lies closest to the point where
Las Vegas Wash enters Las Vegas Bay, whereas the lowest concentrations
generally occurred at buoy 1. Lower chlorophyll a levels are encountered
further out in the center of Lake Mead in the direction of Sentinel Island.

Airborne laser-fluorosensor measurements were made over the three
flight lines defined by buoys 1 to 7, 7 to 11' and 11' to 12 con-
current with collection of samples close to the buoys. Surface water
grab samples were obtained at three different locations on the circumfer-
ence of an approximately 25-m diameter circle around each sampling
station in order to minimize the chances of collecting significant
amounts of periphyton, which might break away from the sampling station
buoy surface. These three samples were then mixed in order to minimize
the effects of patchiness in the distribution of surface water algae.
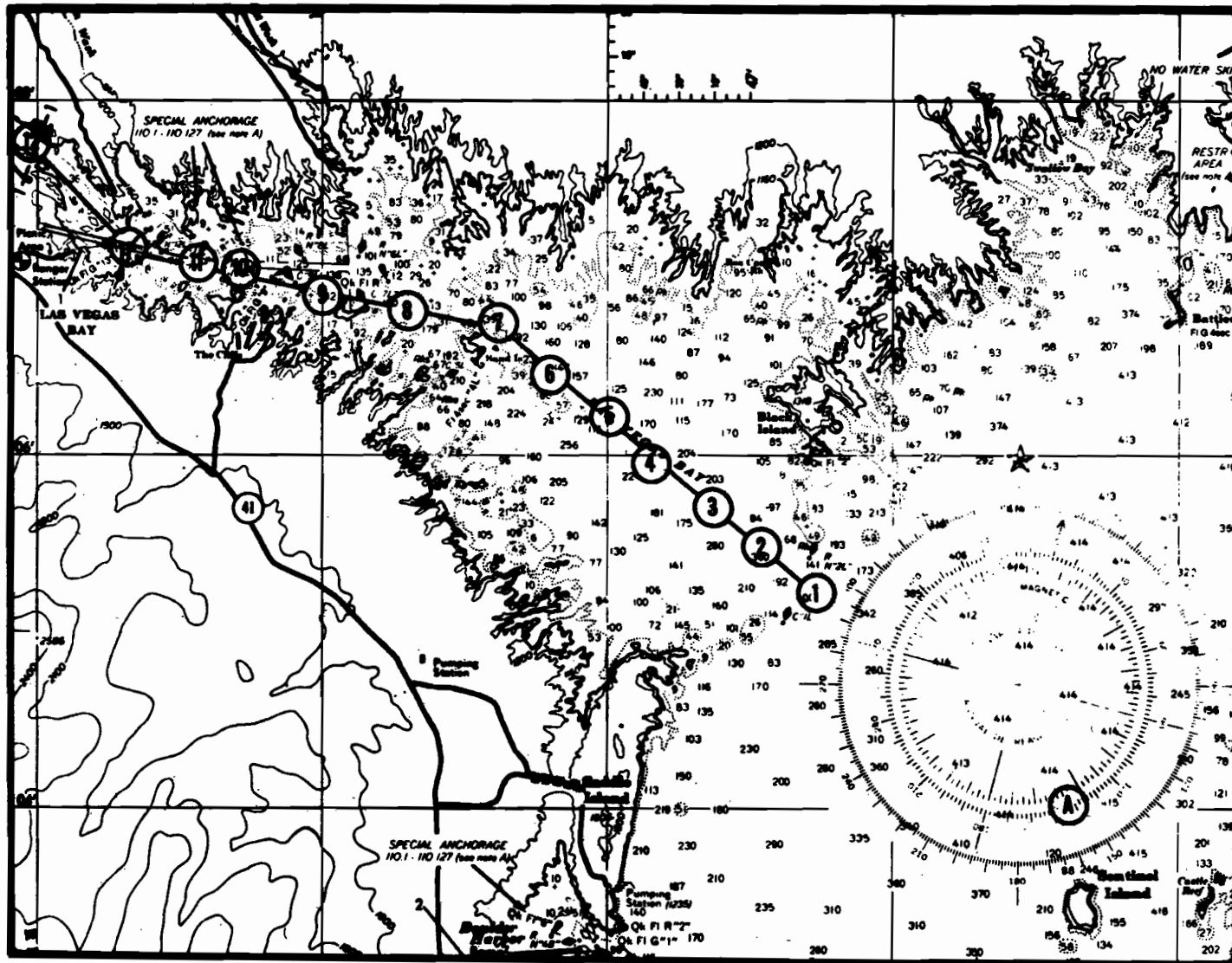
Figure 8. Nautical chart of Las Vegas Bay region of Lake Mead, Nevada, showing location of marker buoy sampling stations.

When exciting chlorophyll a in the Soret absorption band region, the wavelength of the laser transmitter was tuned to lie close to 440 nm. Excitation at 440 nm avoids exciting phaeophytin a, a degradation product of chlorophyll a that has an excitation peak close to 420 nm but whose fluorescence cross section is approximately 10 times less than that of chlorophyll a at 440 nm when using excitation bandwidths smaller than 5 nm (35, 36).

(b) Analysis of Airborne Laser-Fluorosensor Data

As indicated earlier, the airborne data could be collected either continuously in digital format on magnetic tape or in the form of oscilloscope photographic records taken at each buoy site as exemplified by the oscillogram in Figure 7. Flights over desert terrain essentially devoid of vegetation, located immediately adjacent to Lake Mead, produced no signal at 685 nm other than from the solar background, indicating that backscattered laser radiation was not leaking through either the chlorophyll a fluorescence band interference filter or the short wavelength cutoff color glass filter used to block the laser backscatter. However, a small fraction of the pulsed signal at 685 nm comes from the fluorescence of dissolved organic matter in the water rather than from chlorophyll a. This fact is illustrated by the fluorescence spectra shown in Figure 9, obtained in the laboratory from a Lake Mead water sample with a corrected-spectra spectrofluorometer (Perkin Elmer MPF4). The first spectrum in Figure 9 obtained from an untreated subsample shows the characteristic in vivo chlorophyll a fluorescence emission band at 685 nm for a measured extractable chlorophyll a level of 8.4 µg/l. The small spikes visible on this emission band are due to the movement of discrete algal particles across the instrument field of view. The second spectrum was obtained on a similar sample after passage through a 0.3µ membrane filter used to remove the algae. The residual fluorescence background is due to the presence of dissolved organic matter in the sample and illustrates the fact that, at least for Lake Mead waters, this is an insignificant source of error to the present measurement at 685 nm. However for conditions of low chlorophyll a concentration in the presence of a high dissolved organic content, account will have to be taken of this background signal at 685 nm.

As there are no immediate plans to calibrate the airborne laser-fluorosensor data directly in units of chlorophyll a concentration, the effects of varying laser intensity and aircraft altitude on the chlorophyll a fluorescence signal were eliminated by normalizing the fluorescence signal to arbitrary reference values of laser power and aircraft altitude. The elevation H of the helicopter over the water surface target was measured from each record to an accuracy on the order of ± 3 meters. This value was then used to normalize the amplitude of the fluorescence signal to a reference altitude of 200 m using the $1/H^2$ dependence of the fluorescence signal with range. Over the period of a specific airborne mission involving about 1000 laser-fluorosensor sampling sites, the laser output power generally falls to a value equal to 30% of its original value due to degradation of the Coumarin 120
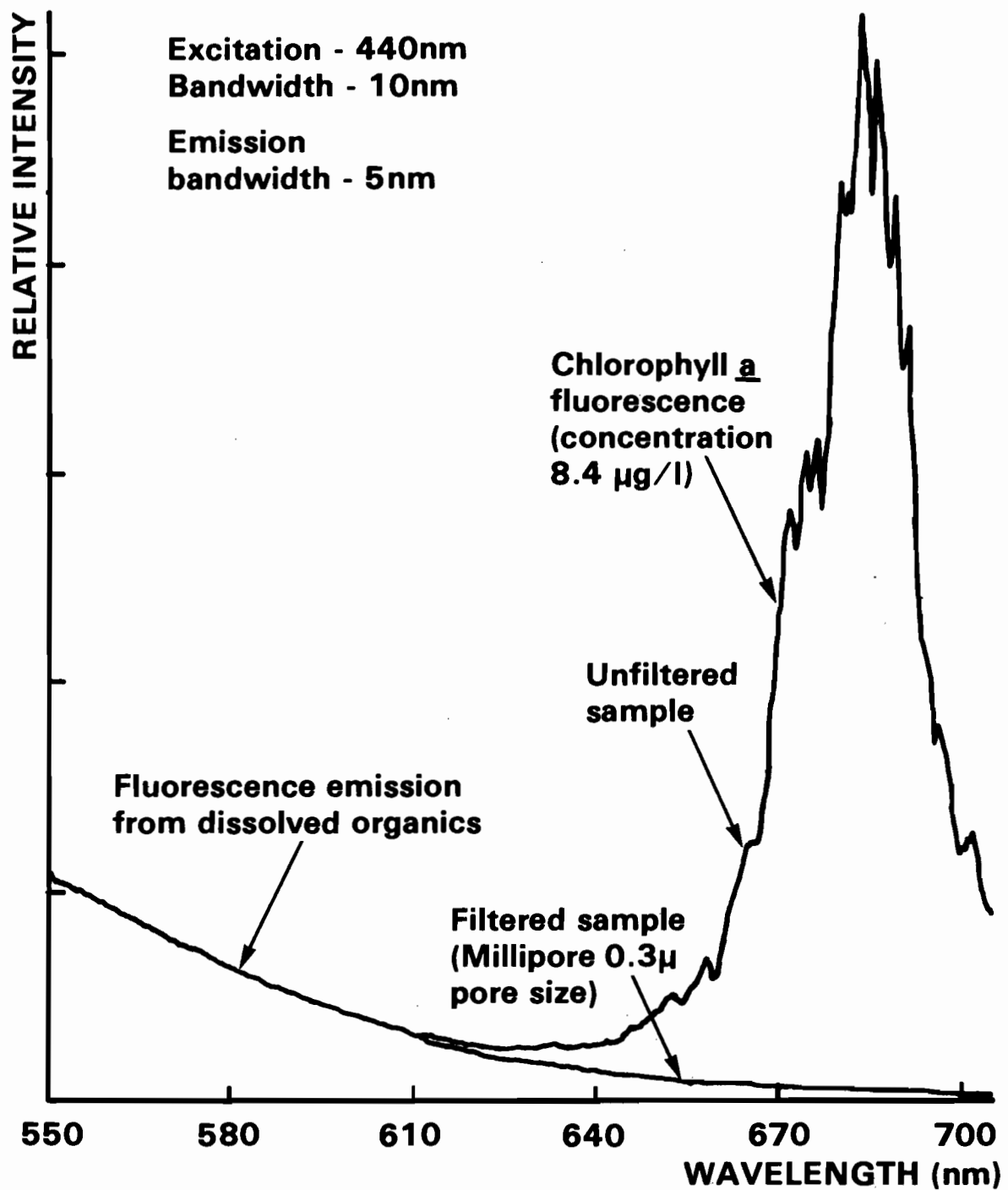
Figure 9. Corrected fluorescence emission spectra of filtered and unfiltered Lake Mead surface water sample, excited at 440 nm, August 16, 1977.

135

laser dye. The laser peak power signal was therefore used to normalize the fluorescence signal to an arbitrary 1-volt laser power signal, assuming a direct linear dependence of fluorescence emission power on laser power. In addition, correction factors for the effects of electronic and optical attenuators were made when necessary. Except for certain pulse-integration and profile-smoothing procedures applied to the analysis of the digital data, interpretation of both analog (oscillographic) and digital data was essentially identical. This involves determination of the amplitude of the measured laser power and fluorescence signal above the solar background together with a value for the time between the laser and the fluorescence pulses. In the case of the digital data, a 5-point least-squares parabolic curve smoothing procedure (37) was applied sequentially to the data for each of the 512 channels using the data from the two channels on either side to provide the smoothing curve. This process is then applied to the next data point and so on. This procedure effectively eliminates the short-term random contributions from digitization, photon and electronic noise while leaving the long-time constant components of the record unchanged. The elapsed time between laser and fluorescence pulses, which is used to calculate the aircraft altitude after correction for photomultiplier transit time, was determined by calculating the position of the centroids for the laser and fluorescence pulses.

(c) Analysis of Ground Truth Water Samples

Determinations of chlorophyll a concentration for the surface water samples were obtained with either the spectroscopic approach of Strickland and Parsons (38) or the fluorometric approach of Holm-Hansen, Lorenzen, Holmes and Strickland (39). The procedure employed for extracting the chlorophyll a from the algae was the same for both methods. This involves collecting the algae on a glass fibre filter paper (Whatman GF/C) pretreated with magnesium carbonate and grinding the filter paper in a prescribed volume of 90% acetone, which is then allowed to sit for three hours, during which the chlorophyll a is extracted into solution from the algae. The centrifuged supernatant solution containing the chlorophyll a is then used undiluted for the spectrophotometric determination. For the fluorometric determination the supernatant solution is further diluted in 90% acetone over the range from 25:1 to 100:1 to ensure that self-absorption of the fluorescence emission does not occur. Spectrophotometric determinations were made using a Coleman Model 620 Junior II Spectrophotometer. Fluorometric determinations were made using a Turner Model 111 filter fluorometer with a standard door, a blue continuous emission lamp and a Hamamatsu R-136 red sensitive photomultiplier detector. For high chlorophyll a concentrations, a Corning 5-58 excitation filter was employed whereas for low concentrations a Corning 5-60 excitation filter was used. A Corning 2-64 short-wavelength cutoff filter was used to isolate the chlorophyll a emission band at 685 nm. For the analysis of the samples for flight #12, a UV blocking filter (Corning 3-73) was employed to reduce the influence of the 404.7 nm mercury line in exciting fluorescence in the pheophytin a fraction (35, 36), while at

the same time passing the continuous blue and discrete 435.8 nm mercury line radiation used for exciting fluorescence in the chlorophyll a fraction. Both spectroscopic and fluorometric determinations were repeated on five subsamples obtained from each grab sample and the means for these groups of subsamples determined for comparison with the corresponding airborne data. Calibration of the fluorometer for each filter door combination was made periodically against a chromatographically pure chlorophyll a standard*.

An indication of the relative concentration of sample particulates (both algae and suspended sediment) was obtained using a 90° scattering nephelometer (Hach Model 2100A).

(d) Comparison Between Airborne and Ground Truth Data

Airborne laser-fluorosensor data for flights #4 and #8, obtained using a laser excitation wavelength of 440 nm and taken about 1 month apart, are shown in Figures 10 and 11 respectively, together with the corresponding chlorophyll a ground truth data obtained by the spectroscopic method of Strickland & Parsons (38).

Elevation above the water surface was about 200 m for both flights. Since absolute calibration of the airborne fluorescence data in terms of chlorophyll a concentration was not provided, it was found convenient to normalize each airborne data set to the corresponding chlorophyll a ground truth data set by minimizing the sum of the squares of the differences between the corresponding airborne and ground truth values (least squares procedure).

Changes in the 10 km long surface water profiles, for both the airborne and ground truth measurements for flight #4, shown in Figure 10, appear to be in general agreement. Comparison between the airborne and ground truth data for this flight gave a linear correlation coefficient of 0.95. The data for flight #8 made over the same path on a later date exhibit a somewhat lower correlation coefficient of 0.77. It is apparent that some of the large point-to-point fluctuations present in the ground truth profile for this flight are also present in the airborne fluorescence profile, though in a somewhat attenuated form. Similar but smaller fluctuations were also present in the fluorometrically determined chlorophyll a data for flight #8, which, when compared to the laser fluorosensor data, gave a correlation coefficient of 0.85. Linear correlations between airborne and ground truth data for these and other flights are presented in Table 3 with the values lying in the range from 0.41 to 0.95. For a sample size of 12 or larger, with $r \geq 0.57$, correlations are significant at the 5% level whereas with $r \geq 0.70$, they are significant at the 1% level. It is interesting to note that the correlation (r=0.41) for the data of flight #12 obtained using a laser fluorosensor excitation wavelength of 622 nm is not

---

*Pure chlorophyll a extract was obtained from Sigma Chemical Co., St. Louis, Mo.
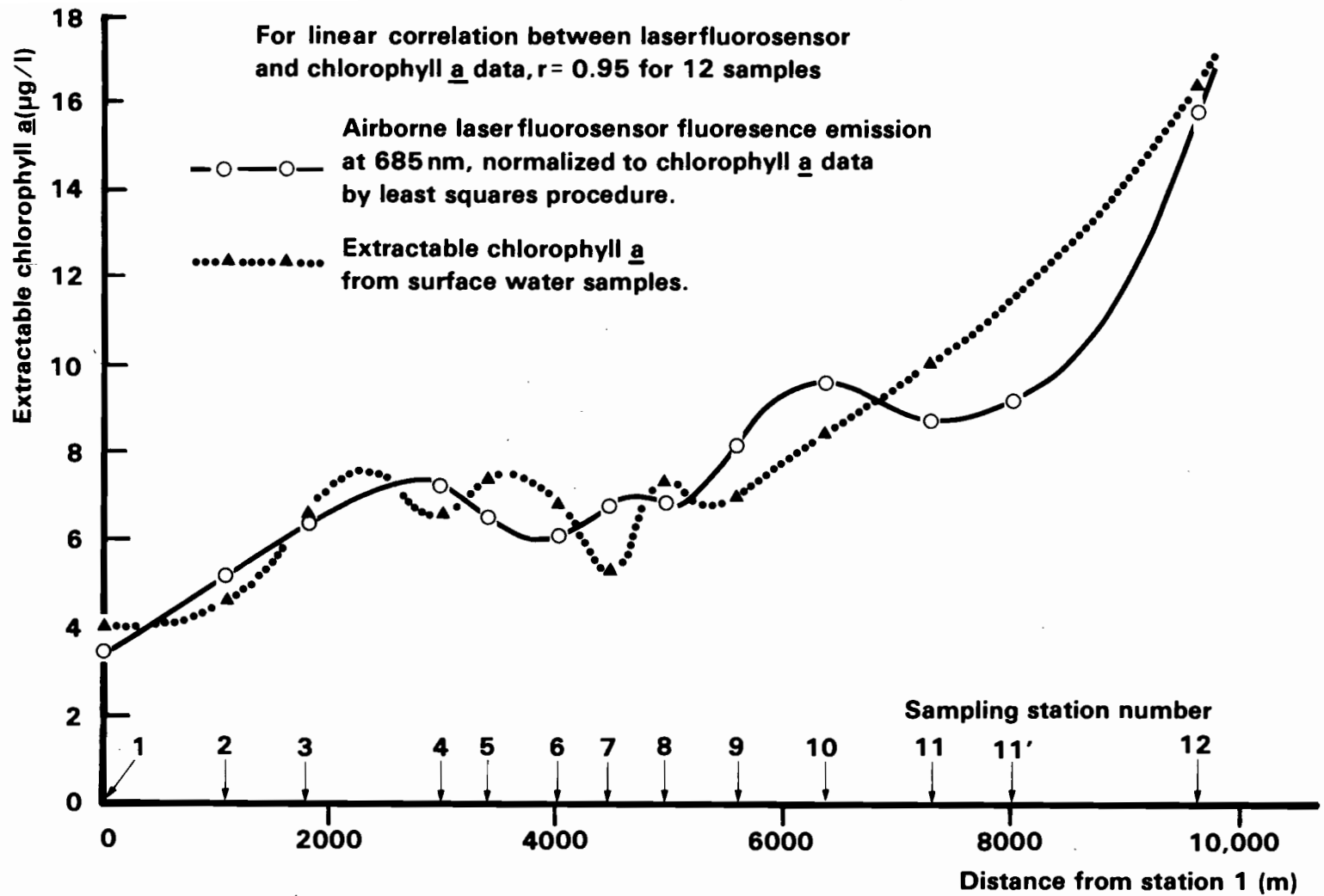
Figure 10. Variation of surface water chlorophyll a and laser-fluorosensor signal with distance for surface water transect of Las Vegas Bay in Lake Mead, Nevada, Flight #4, October 15, 1976.
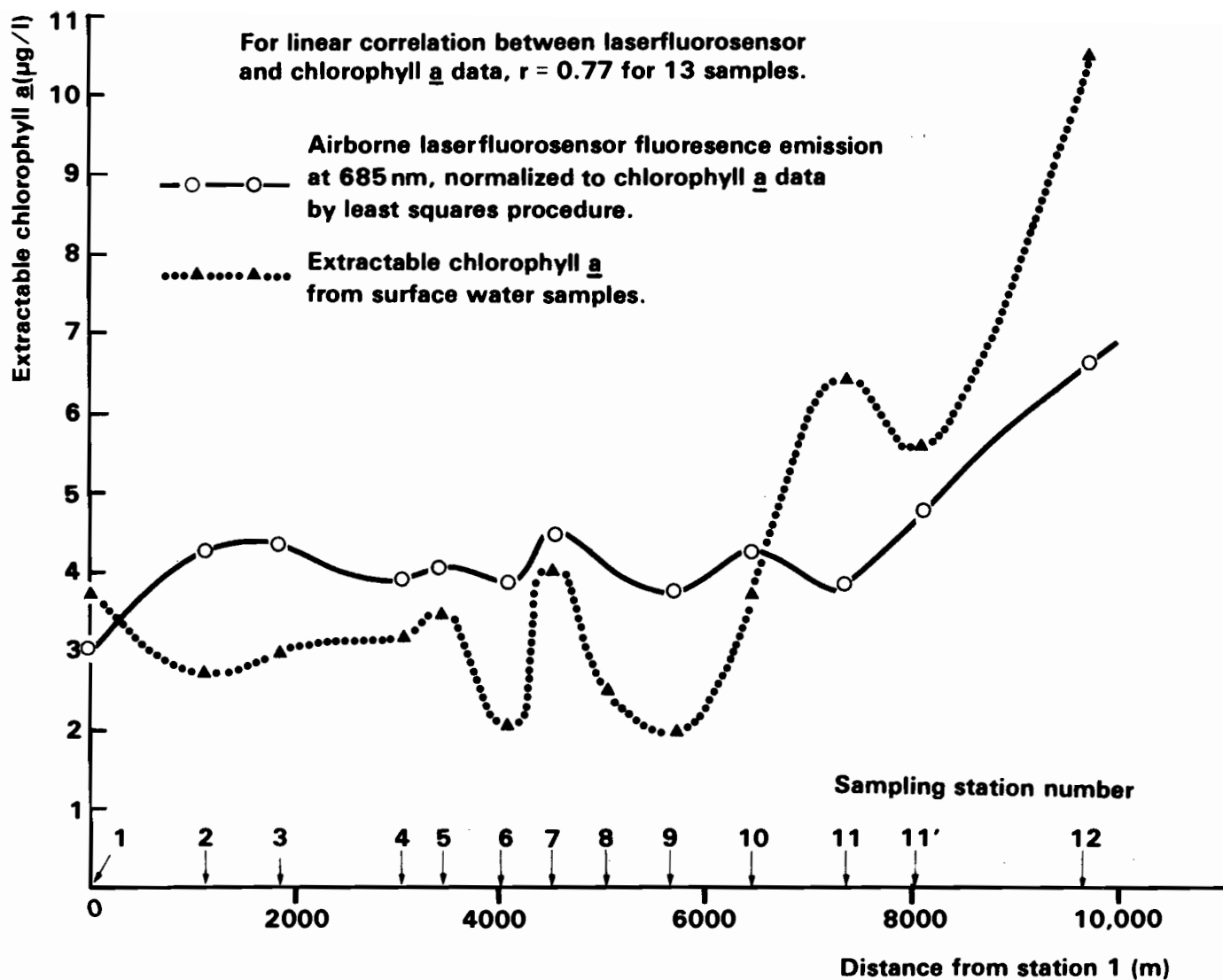
Figure 11. Variation of surface water chlorophyll a and laser-fluorosensor signal with distance for surface water transect of Las Vegas Bay in Lake Mead, Nevada. Flight #8, November 19, 1976.

139

TABLE 3. CORRELATION COEFFICIENTS FOR CORRECTED LASER-FLUOROSENSOR SIGNAL VERSUS TURBIDITY AND CHLOROPHYLL a DATA

Flight Number	Date	Turbidity (NTU)	A Ca (Spectro.) (µg/l)	B Ca (Fluoro.) (µg/l)	C Sample Size	Laserfluorosensor Excitation Wavelength (nm)
3	10/04/76	0.801	---	0.815	12	440
4	10/15/76	0.846	0.953	0.751	12	440
5	11/04/76	0.841	0.870	---	13	440
8	11/19/76	0.708	0.770	0.846	13	440
12	08/16/77	---	---	0.408	13	622

A) Spectrophotometric determination of chlorophyll a using method of Strickland and Parsons (38).

B) Fluorometric determination of chlorophyll a using method of Holm-Hansen et al. (39).

C) Each chlorophyll a laserfluorosensor sample is an average of three measurements.

significant at the 10% level. One of the reasons for using this excitation wavelength was to investigate the correlation between the airborne data and the biomass for specific algal color groups, and in particular for blue-green algae. Further discussion on the data for this flight is deferred to Section 7f. Also shown in Table 3 are the correlation coefficients relating the laser fluorosensor data to that for water turbidity obtained using a 90° scattering nephelometer. It is significant that, in all cases, these coefficients are only slightly less than those for the correlation between the laser fluorosensor data and that for the spectroscopically determined chlorophyll a. This suggests, at least from an optical viewpoint, that the particulate matter in surface waters of Las Vegas Bay consists principally of algae rather than of suspended sediment.

An estimate of the sensitivity limit for the laser fluorosensor in its present form can be gauged from fluorescence pulse data provided by the oscillogram in Figure 7. Assuming that for daytime operation, system sensitivity is limited by the backscattered sky solar background radiation existing within the chlorophyll a fluorescence band, a peak Signal to RMS Background Noise Ratio (SBNR) can be calculated using

$$SBNR = V_P/v_{RMS},$$

where Vp is the steady peak detector voltage of the fluorescence pulse above the steady background level and v_{RMS} is the RMS noise voltage of the background signal. Based on the fact that shot or photoelectron noise is white noise with an instantaneous Gaussian probability distribution, a statistical criterion can be adopted whereby the peak to peak fluctuations of the background lie within a total spread of 5 standard deviations for 99% of the time. Because one standard deviation is defined as the RMS noise voltage v_{RMS}, we can write the equality

$$v_{PP} = 5\ v_{RMS},$$

where vpp is the peak to peak spread in the noise envelope for 99% of the time. The expression for the peak signal to RMS background noise ratio then becomes

$$SBNR = 5\ V_P/v_{PP}.$$

As depicted in Figure 7, Vp = 0.64 volts for a chlorophyll a concentration of 10.5 μg/l and vpp = 0.04 volts; it follows that for a minimum acceptable SBNR of 3, the system can monitor chlorophyll a levels down to 0.4 μg/l. This sensitivity limit is subject to a number of qualifiers. First, these measurements were made under clear skies with the sun near the zenith. With a water albedo on the order of 0.05, the noise due to the solar backscatter (but not surface glitter), was at the high end of the anticipated range. However, albedo values in the range from 0.2 to 0.3, due to high concentrations of suspended sediment, would substantially increase this background noise. Second, it is

141

assumed that the contribution to the laser-induced fluorescence signal at 685 nm due to dissolved organics is negligible. For the surface waters of Lake Mead, the amplitude of the fluorescence signal at 685 nm due to dissolved organics has an equivalent chlorophyll a value of about 0.1 μg/1. For water conditions where this is not the case, an estimate of this background signal must be obtained by making an additional laser-fluorosensor spectral measurement, say in the region of 650 nm. Third, the present sensitivity limit corresponds to water conditions for which the optical transmission is dominated by algal particles. For conditions where suspended sediment is the principal factor limiting transmission, system sensitivity will be reduced in relation to the values indicated above. This situation can be expected to exist for suspended sediment concentrations greater than 50 mg/1.

A number of expedients can be employed to improve system sensitivity. Increasing the laser energy or peak power will directly increase V_p, whereas reducing the laser beam divergence, so that the receiver collects a smaller solar background signal will reduce v_{pp}. The background noise signal v_{pp} can also be reduced to near zero by flying at dawn or dusk or during nighttime in contrast to the present experiments, which were flown close to midday under clear skies but in the absence of significant solar glitter. In this situation, system sensitivity is limited by "in-signal" photoelectron noise. In any case, to achieve a system sensitivity limit down to a chlorophyll a concentration of 0.1 μg/1, with a signal-to-noise ratio of 10 should represent no major technical problems. This sensitivity level, in effect, requires a 13-1/3-fold increase in the overall SBNR over the performance of the present system. With a larger laser flashlamp and increased laser input energy, a doubling in the laser output power and energy can be achieved with a corresponding 2-fold increase in the SBNR (31). Similarly a 1.77-fold enhancement in the SBNR can be achieved by in- creasing the FWHM-bandwidth of the optical filter at 685 nm from its present value of 13 nm to 23 nm, so as to be in close correspondence with the width of the chlorophyll a band. Further, by utilizing a telescope with a reflecting element rather than a refracting element, the circle of least confusion (the blur circle) caused by spherical aberration can be reduced from the present 6-mm-diameter to a size much smaller than the 2-mm-diameter image of the surface water laser spot. A 2-mm-diameter focal plane stop could then be used rather than the present 4-mm-diameter stop, thereby reducing the magnitude of the background signal and noise without affecting the magnitude of the chlorophyll a fluorescence signal. This measure produces an additional 2-fold enhancement in the SBNR (31). Finally, by halving the elevation of the airborne platform over the water surface target, the chlorophyll a fluorescence signal would be enhanced by a factor of 4 based on the $1/H^2$ dependence of the fluorescence signal on altitude; this expedient does not affect the magnitude of the background signal for an extended homogeneous target. This procedure in turn produces a 4-fold increase in the SBNR (31). With implementation of all of the aforementioned system modifications, the SBNR would be increased overall by a factor 27 times the present value, thereby realizing a SBNR of 20 at a

chlorophyll a level of 0.1 μg/1 under the environmental conditions of the present measurements.

It should be noted that reducing the aircraft height also reduces the laser spot size, thereby increasing the sensitivity of the laser-fluorosensor signal to small-scale variations in the concentration of surface water algae. As indicated in Section 4, this can be accommodated for by increasing the laser repetition rate.

(e) Factors Influencing the Relationship Between Airborne and Ground Truth Data

Several explanations exist for the less-than-perfect covariation between the laser-fluorosensor signal and the corresponding surface water chlorophyll a determinations. Factors influencing these correlations are either random or systematic in origin and are discussed separately.

Random errors compounded by a small sample size of 12 or 13 will clearly reduce the degree of correlation. Differences are known to exist between the locations at which the grab samples were obtained and those at which the airborne measurements were made for any one sampling station. Uncertainties on the order of 50 m combined with significant patchiness in the surface water algae distribution can be expected to degrade any such correlation. With a view to minimizing this source of error, samples were collected at three different locations on the circumference of an approximately 25-m-diameter circle around each sampling station buoy and then mixed prior to analysis. At the present time, it is not clear what residual error is present due to differences between the airborne and ground truth sampling locations. Direct grab sampling from the helicopter would eliminate this problem although the helicopter rotor down-wash might induce considerable horizontal mixing and water movement at the sampling site. Random errors are also incurred in the measurement of the extractable chlorophyll a. The established method for extracting chlorophyll a from algae in water samples (40) by filter grinding and extraction in 90% acetone is known to be both inefficient and subject to considerable variability due to the production of chlorophyll a degradation products (41, 42). For a total of five determinations made on each grab sample, coefficients of variation ($s/\bar{x}$) of up to ±50% have been observed for chlorophyll a levels of 1 μg/1. More efficient and reproducible methods for extracting chlorophyll a from algae are presently under investigation and will be reported elsewhere.

Systematic errors are best discussed in terms of the laser fluorosensor equation (Equation 1) for remote monitoring of in vivo chlorophyll a. The environmental factors within the fourth set of square brackets in Equation 1 are considered to be the primary source of systematic error encountered with the laser fluorosensor technique. Specifically, the discussion centers on the validity of the assumptions that the fluorescence cross section σ_c and the water diffuse

143

attenuation coefficients k_L and k_F remain constant for all surface water locations.

As discussed in the Review, σ_c is dependent on a number of factors including temperature, nutrient and pollutant-induced stress and solar radiation intensity levels, as well as on the intensity, wavelength and duration of the excitation source. More significant is the dependence of σ_c on the type and relative concentration of the various algal color groups present in the water surface at any one time and place. In reality, all of the photopigments will contribute to the fluorescence emission at 685 nm. Their individual contributions will depend on the nature of the excitation spectrum for the different algal color groups present, their concentration and the excitation wavelength employed. Under these circumstances, it is clear that the concept of a single unique overall value of σ_c is invalid, a fact that possibly provides, at least in part, an explanation for the variation in the correlation coefficients obtained between the airborne and ground truth data on different occasions, as shown in Table 3. Ideally, the actual value of σ_c for every airborne sample site should be determined by making laboratory fluorometric measurements on grab samples with the appropriate excitation wavelength. By measuring n_c, k_L, k_F, P_L and P_F, and also knowing all the other system and environmental factors, a representative value of σ_c can be established for a given water sample through use of Equation 1, regardless of the photosynthetic pigments contributing to the fluorescence emission at 685 nm. The impracticality of such an approach for a remote sensing application is obvious. An alternative and more attractive approach entails finding an excitation wavelength for which the individual fluorescence cross sections for the different algal color groups are all equal or at least of similar order of magnitude. As mentioned in Section 2, published data (15, 16, 25) suggest the use of wavelengths in the 600-nm to 620-nm region. However more recent measurements made on algal monocultures representative of the different color groups (21) indicate that the fluorescence excitation cross section at 618 nm for a blue-green algal monoculture (anacystis marinus) was, on the average, about 5 times larger than the values for the other color groups. Unfortunately, as mentioned in Section 5 (d), the present airborne measurements, made by using an excitation wavelength of 622 nm, were not successful (the laser fluorosensor and chlorophyll a ground truth data were poorly correlated, with r=0.41). However, as will be discussed in more detail in Section 5 (f), the reason for this poor correlation is related primarily to faulty ground truth chlorophyll a determinations rather than to an inherent weakness in the laser fluorosensor method. A final decision on the choice of an optimum excitation wavelength must therefore await further tests of the airborne laser fluorosensor. At that time it will then be possible to pass judgement on the validity of the concept of using a single unique overall value of σ_c for characterizing the fluorescence of in vivo chlorophyll a at a given excitation wavelength.

Inspection of Equation 1 shows that changes in the surface water

values for k_L and k_F, the diffuse attenuation coefficient at the laser and fluorescence wavelengths respectively, directly influence the laser-fluorosensor determination of n_c, regardless of whether a relative or absolute value is required. The assumption was made that changes in concentration of particulate and dissolved matter were sufficiently small over the extent of a given water surface that k_L and k_F could be considered to be constant. This premise in turn requires the assumption that optical effects caused by algal scattering and absorption contribute a negligible percentage to the total values for k_F and k_L. However, situations exist where the related beam attenuation coefficient α_λ is highly correlated with either extracted chlorophyll a or in vivo chlorophyll a fluorescence.

Kiefer and Austin (28) obtained linear correlation coefficients of 0.95 for variation of the beam attenuation coefficient α_λ versus chlorophyll a fluorescence and of 0.95 for α_λ versus n_c, the concentration of extracted chlorophyll a. These measurements were made in a marine environment for chlorophyll a values ranging from $1\mu g/l$ to $6\mu g/l$. The least-squares best-fit-line for the latter correlation is given by

$$\alpha_\lambda = 0.99 + 0.2\ n_c, \tag{2}$$

where the α_λ values have been corrected for the component of attenuation due to optically pure seawater at wavelength λ. Similar measurements by Baker and Baker (29), made in fresh water environment, realized a correlation coefficient of 0.83 for uncorrected α_λ values versus extracted chlorophyll a levels up to 100 µg/l. The least-squares best-fit line for this data set is

$$\alpha_\lambda = 3.57 + 0.11\ n_c. \tag{3}$$

From these measurements, it would appear that for extracted chlorophyll a levels at least greater than $1\mu g/l$, a linear relationship exists between extracted chlorophyll a with a slope factor lying in the range from $0.1m^{-1}/\mu g/l$ to $0.2m^{-1}\mu g/l$. For surface water samples containing high and variable concentrations of non-algal matter in addition to that for the chlorophyll-related pigments, this relationship can be expected to break down due to the unpredictable contribution to the overall attenuation coefficient from this non-algal matter. This effect is further exacerbated by the fact that algal population growth can become arrested or even reversed by the restrictions put on photosynthetic activity by the reduction in available solar radiation caused by high concentrations of suspended sediment.

Confirmation of a relationship between n_c and α_λ for the surface waters of Las Vegas Bay was obtained by making a concurrent measurement of in vivo chlorophyll a fluorescence and the beam attenuation coefficient at 610 nm. An in situ measurement of the beam attenuation coefficient was obtained using a 1-meter path length transmissometer (Martek Model XMS). This device, which measures beam transmittance T

with a collimated and filtered light source, provides values of α_λ from the expression

$$T = \exp\left(-\alpha_\lambda x\right), \qquad\qquad (4)$$

where x (= 1 m) is the optical path length of the beam. The trans-missometer was rigidly mounted to the bow of the survey launch at a depth of about 1 meter and, as such, provided a continuous chart-recorded profile of the surface water optical transmission. The present measurements were made at a wavelength of 610 nm with a filter with a half-height bandwidth of 32 nm, so that this transmission measurement is a close approximation for k_F, the diffuse attenuation coefficient for the chlorophyll a fluorescence emission wavelength at 685 nm. The concurrent in vivo chlorophyll a fluorescence profile was made using a filter fluorometer (Turner Model 111) as described in Section 5 (c), except that a high volume flow-through sample cell was used in place of the standard cuvette. The entry port for the flow-through sample tube was located directly adjacent to.the optical path of the transmissometer with a sample pump located downstream of the fluorometer in order to avoid damage or contamination of the sample by either cavitation bubbles or pump lubricant. The continuous in vivo fluorescence and optical transmission profiles obtained for the region in Las Vegas Bay between stations 9 and 12 are shown in Figure 12. The in vivo fluorescence data were calibrated in terms of equivalent extracted chlorophyll a through use of the single chlorophyll a determination performed on a sample obtained at station 11, as indi-cated by the single reference point in the chlorophyll a profile.

The discrete α values, plotted for equal intervals of time, were calculated directly from the corresponding 1-meter path length transmission profile data using Equation 4. The variations in the attenuation coefficient data are in almost complete correspondence with those for the chlorophyll a fluorescence data, after corrections are made for the approximately 6-second time delay in the fluorometric data. This delay represents the finite time needed to pump a sample from the location of the submerged transmissometer to the deck location of the fluorometer. The same discrete attenuation coefficient values are also shown in Figure 13 plotted against the corresponding in vivo chlorophyll a values obtained from the calibrated profile in Figure 12; a linear correlation coefficient of 0.96 was obtained from this group of 25 data points. Extrapolating the curve to a zero fluorescence value suggests a background attenuation coefficient value of about $1.7m^{-1}$, due principally to dissolved and non-algal particulate matter. The tendency of the data to deviate from a linear relationship at high chlorophyll a fluorescence levels may be due possibly to self-absorption of the fluorescence radiation within the 19-mm-diameter sample cell or to an unrelated increase in the concentration of dissolved or non-algal particulate matter, which occurs in the region of high chlorophyll a concentration around sample station 12.

To gauge the effect of the relationship between α_λ and n_c on the
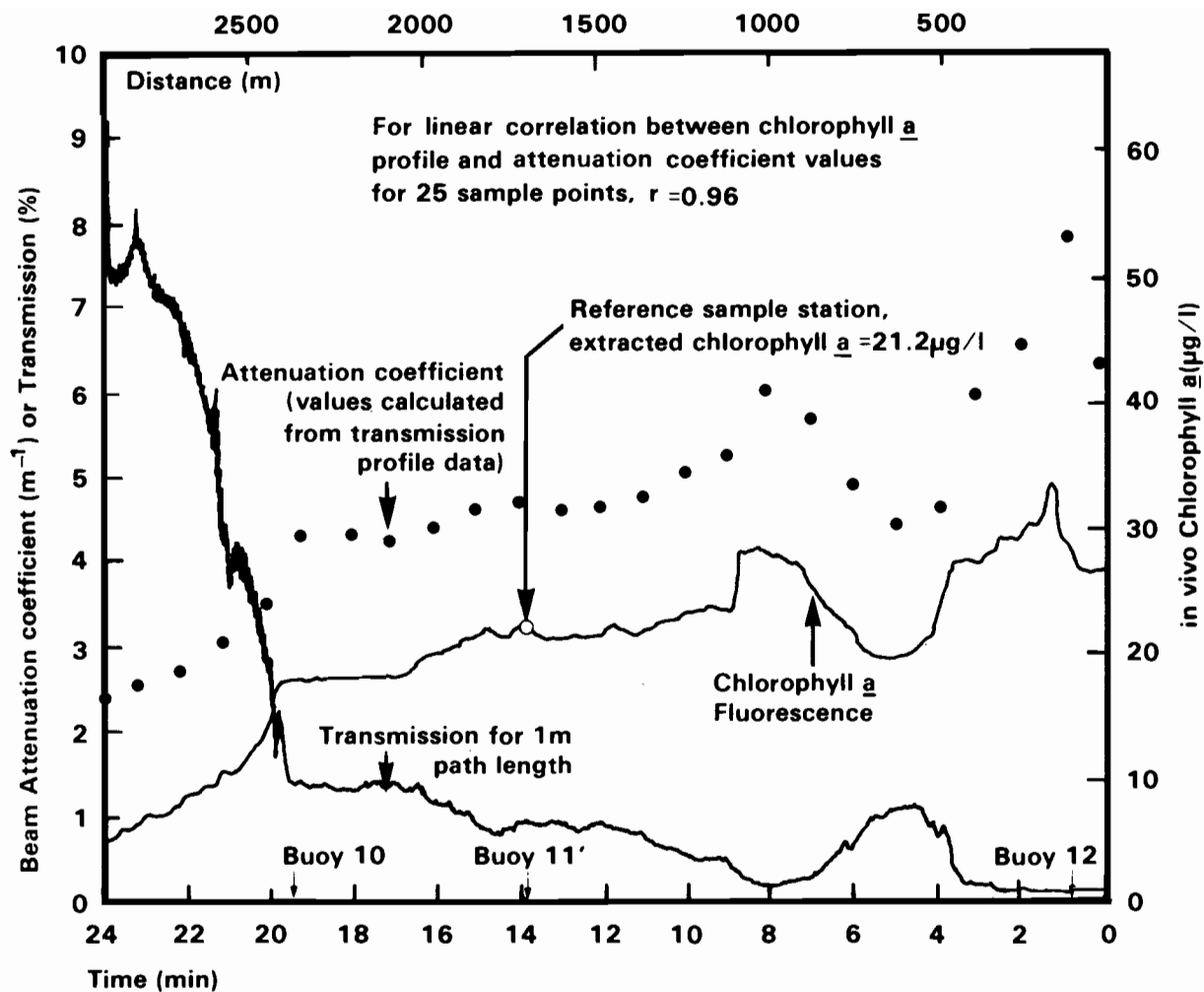
Figure 12. In vivo chlorophyll a fluorescence and water transmission profiles obtained from surface water transect of Las Vegas Bay in Lake Mead, Nevada, June 8, 1977. Also shown are beam attenuation coefficient values calculated for 25 points in the transmission profile. Transmission data measured at 610 nm.

147
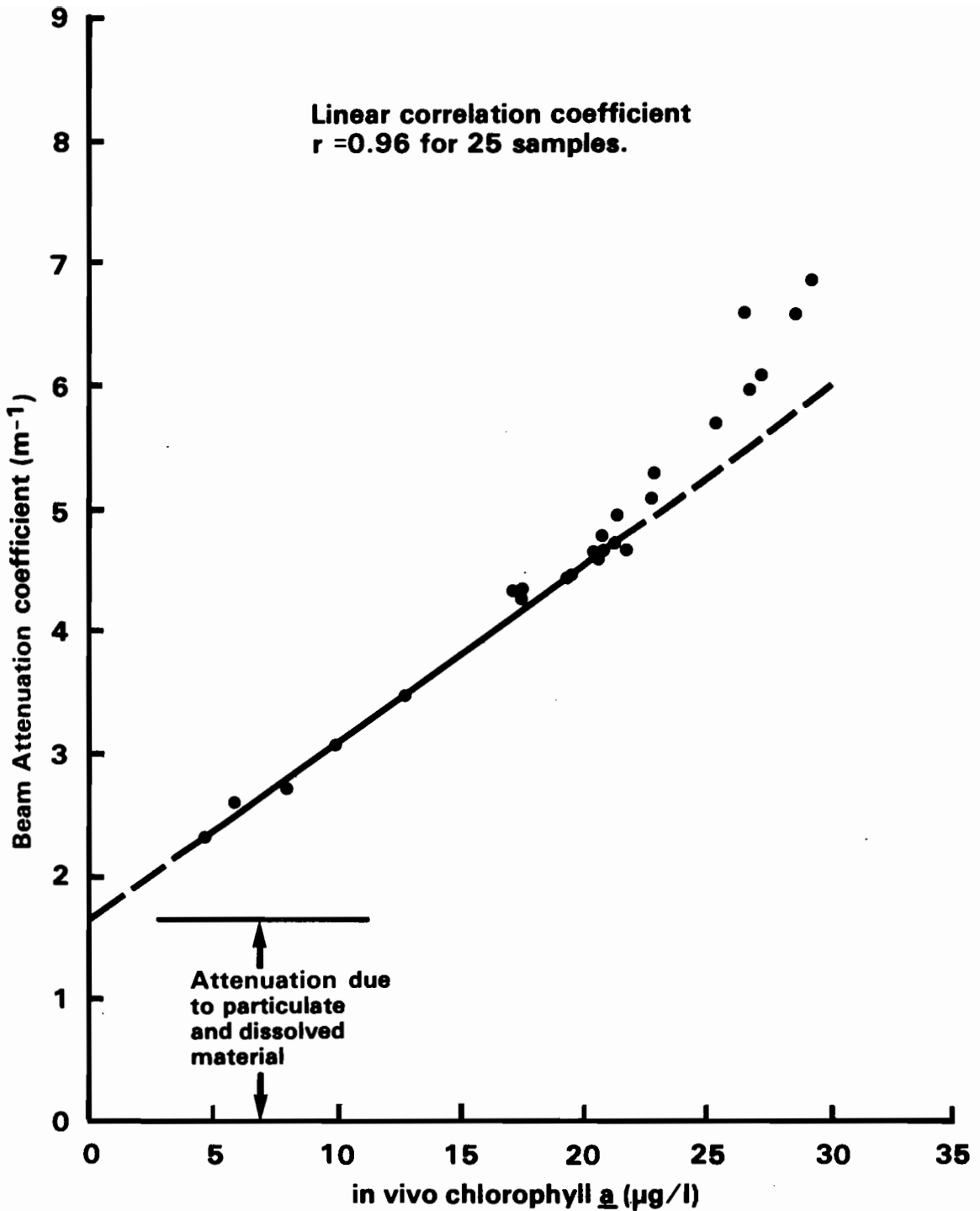
Figure 13. Variation of beam attenuation coefficient with in vivo
chlorophyll a fluorescence for surface water transect of
Las Vegas Bay in Lake Mead, Nevada, June 8, 1977.
Attenuation data measured at 610 nm.

148

performance of the laser fluorosensor, it is necessary to relate the beam attenuation coefficients α_L and α_F to the corresponding diffuse attenuation coefficients k_F and k_L as used in Equation 1. According to Smith & Tyler (27), a_λ and k_λ can be written in terms of their constituent components, such that

$$\alpha_\lambda = \alpha_\lambda + b_{f,\lambda} + b_{b,\lambda} \tag{5}$$

and
$$k_\lambda = Da_\lambda + b_{b,\lambda} , \tag{6}$$

where a_λ is the absorption coefficient due to dissolved, particulate and viable algal matter, and $b_{f,\lambda}$ and $b_{b,\lambda}$ are the forward and backward scatter attenuation coefficients respectively, resulting from all particulate matter. Note that the expression for the diffuse attenuation coefficient contains no forward scatter loss term because irradiance measurements monitor both forward scattered and unscattered radiation that has not been absorbed. A further complication in the process of relating α_λ to k_λ stems from the fact that k_λ is not a simple spectral property of a given water sample but is dependent on the radiance distribution. As a first approximation, this effect is accounted for by the factor D in Equation 6. The lower bound for D exists for the case of a collimated illumination source for which D = 1 whereas the upper bound exists for the case of a totally diffuse source for which D = 2 (27). Fortunately, these two extremes correspond exactly to the laser excitation (D=1) and the fluorescence emission (D=2) configurations that occur during the operation of the airborne laser fluorosensor. The effective doubling of the influence of absorption on k_λ in the case of the diffuse source is due to the increased path length experienced by individual photons that are multiply scattered on their way to a given vertical penetration depth.

The expression for k_λ and α_λ can be further broken down into the contributions for pure water (denoted by subscript w), chlorophyll-related pigments (denoted by subscript c) and all other dissolved and particulate non-chlorophyllous substances (denoted by subscript N), such that

$$\alpha_\lambda = a_{w,\lambda} + a_{c,\lambda} + a_{N,\lambda} + b_{f,c,\lambda} + b_{f,N,\lambda} \tag{7}$$
$$+ b_{b,c,\lambda} + b_{b,N,\lambda}$$

and
$$k_\lambda = Da_{w,\lambda} + Da_{c,\lambda} + Da_{N,\lambda} + b_{b,c,\lambda} \tag{8}$$
$$+ b_{b,N,\lambda} ,$$

where the molecular (Rayleigh) scattering contributions from pure water are considered to be negligible and have been omitted.

Finally a linear expression can be given for α_λ in terms of n_c as typified by the data given in Figure 13, such that

$$\alpha_\lambda = A_\lambda + B_\lambda n_c , \tag{9}$$

where A_λ and B_λ are presumed to be constant for a given locality and wavelength λ. For the laser excitation case where D=1, Equations 7, 8 and 9 can be solved to give k_L in terms of measurable parameters A_L and B_L and the scattering coefficients $b_{f,c,L}$ and $b_{f,N,L}$, where

$$k_L = B_L n_c + A_L - b_{f,c,L} - b_{f,N,L}. \tag{10}$$

Similarly for the fluorescence emission case with D = 2, Equations 7, 8 and 9 provide a similar expression for k_F such that

$$k_F = B_F n_c + A_F - b_{f,c,F} - b_{f,N,F.} \\ + a_{w,F} + a_{c,F} + a_{N,F}. \tag{11}$$

Substituting the expressions for k_L and k_F, given by equations 10 and 11 respectively, into Equation 1, we have

$$n_c = \left[\frac{P_F H^2}{P_L} \right] \left[\frac{4\pi \Delta_F}{T^n Tr^n rec} \right] \left[\frac{\mu_w^2 \exp\{H(\beta_L + \beta_F)\}}{(1-R_w)^2} \right] \left[\frac{1}{\sigma_c} \right] \left[X_c + X_N \right]. \tag{12}$$

X_c, which represents the optical loss terms due to the chlorophyll pigments, is given by

$$X_c = n_c (B_L + B_F) + a_{c,F} - (b_{f,c,L} + b_{f,c,F}). \tag{13}$$

Although the terms $b_{f,c,L}$ and $b_{f,c,F}$ within the expression for X_c are not given explicitly in terms of n_c, it is reasonable to assume a linear dependence such that X_c will also vary as n_c. X_N, which represents all other optical loss terms, is given by

$$X_N = A_L + A_F + a_{N,F} + a_{w,F} - (b_{b,N,L} + b_{f,N,F}). \tag{14}$$

From this expression, it is clear that we no longer have a simple relationship in which P_F varies linearly as n_c, but rather one in which the additional factor X_c is also dependent on n_c. To monitor relative changes in n_c, it now becomes necessary to obtain exact values for all of the other terms in addition to $(P_F/P_L)H^2$, in particular for the chlorophyll a fluorescence cross section σ_c, and the various chlorophyll and non-chlorophyll optical loss terms represented by X_c and X_N respectively. The determination of values for all of these unknown parameters at each surface water sampling point is clearly not feasible, particularly from a remote sensing viewpoint. Two limiting cases of Equation 12 are of interest. First, when absorption and scattering losses from non-algal sources are dominant, such that $X_N/X_c \gg 1$, the term X_c can be omitted so that the attenuation coefficients are no longer dependent on n_c. A situation then exists in which n_c varies as

$(P_F/P_L)H^2$; this is the situation which was assumed to exist in the derivation of Equation 1 by Browell (20). A different situation exists however when scattering losses arise principally from the presence of algae such that $X_C/X_N \ll 1$. In this case, n_C can be eliminated from both sides of Equation 12 and the laser fluorosensor measurement represented by the term $(P_F/P_L)H^2$ remains constant for all values of n_C. Put in physical terms, the lower the concentration of algae or equivalent extractable chlorophyll a, the larger the penetration depth of the laser beam. In turn, this situation means that the laser beam can ultimately intercept the same total algae count it would have encountered in high algae count situations. As a consequence, the received chlorophyll a fluorescence power will remain constant, independent of changes in n_C. In reality, the truth will lie somewhere in between these two extremes depending upon whether optical losses are dominated by algal or non-algal matter.

Because a direct airborne measurement of the absolute values for k_L and k_F is not possible within the framework of the present program, an alternative approach must be considered. A possible means for monitoring changes in k_λ and, in particular, its dependence on n_C can be provided by obtaining a relative indication of laser beam penetration through the surface water layer by concurrently monitoring the water Raman emission signal. As the Raman emission is a property of the water alone, the intensity of the observed signal will depend only on k_λ and hence only indirectly on n_C. Changes in the water Raman emission signal can therefore be used to provide information on changes in k_λ. A more extensive discussion of this method will be presented in Section 6.

On the basis of the foregoing discussion, the relative contributions of variations in σ_C, k_L and k_F to the degradation of the correlation between the airborne and ground truth data are not clear. With implementation of the Raman technique for correcting for changes in k_L and k_F, it should be possible to isolate the residual uncertainty due to σ_C. The effects of variability in σ_C on the correlation between the airborne and ground truth data can then be minimized by finding an excitation wavelength for which the fluorescence cross sections for the different algal color groups are more nearly equal.

(f) Remote Monitoring of Blue-Green Algae

In fresh waters, blue-green algae (cyanophyta) are the only algal divison that contains the photopigment c-phycocyanin. Radiation absorbed by this pigment, which has an excitation peak close to 622 nm, is transferred internally into the chlorophyll a photosynthetic system. The small fraction of this radiation that leaks out as chlorophyll a fluorescence at 685 nm is employed as an indicator of the relative concentration of blue-green algae present in a given surface water sample. This approach assumes that the fluorescence cross section for all possible mixtures of all species of blue-green algae present at a specific location at a given time remains constant with a value at

least 10-fold larger than that for the combined effect of all other color groups.

An airborne experiment was conducted employing laser excitation at 622 nm rather than at 440 nm, with the purpose of selectively exciting fluorescence in the blue-green algae. Variations in the biomass for each algal division, extractable chlorophyll a, and the laser fluorescence signal as measured over the established Las Vegas Bay flight line, are shown in Figure 14. A further comparison of these data is presented in Table 4 in the form of a matrix of linear correlation coefficients relating biomass from each algal division to either extractable chlorophyll a or the laser fluorsensor signal. Biomass determinations were made by collecting the algae from a given sample volume onto a Millipore HA 0.45µ membrane filter. Enumeration for all species present in significant numbers was made with a microscope at either 400X power or 1000X power. At the latter magnification, the filters were soaked in a refractive index-matching fluid to aid in the identification process. Algal counts were made for 10 Whipple fields for each filter and a volume established for each algal species. From these data, biomass in mg/l was calculated for each algal division or color group assuming a constant algal density of 1. Finally, for each sample, an estimate of total algal biomass was obtained by summing the contributions from each algal division.

An examination of Figure 14 shows that the laser fluorosensor signal progressively increases toward station 12 in contrast to the blue-green algal biomass determination, which shows a slight downward trend. The correlation coefficient for covariation between these parameters was -0.48, which is significant at the 10% level. Although no straightforward explanation exists for an apparent inverse dependence of this kind, a number of interfering effects might be responsible. The laser fluorosensor signal appears to follow more closely the trends in the total biomass determination for which the correlation coefficient has a value of +0.82, significant at the 1% level. This observation suggests that excitation radiation at 622 nm is being absorbed directly by the chlorophyll a present in all algae as well as by c-phycocyanin common only to blue-green algae. This conclusion is supported by data presented by Mumola, Jarrett and Brown (16). They show that, although the excitation spectra for blue-green algae peaks close to 618 nm, its absolute value given in terms of its fluorescence cross section differs only slightly from the values for the other algal color groups at 618 nm. In this respect it is interesting to note that more recent measurements made by this same group (21) indicate that the fluorescence cross section for a single blue-green algal species (anacystis marinus) was, on the average, 5 times larger than values obtained from monocultures representing the other three (red, golden brown and green) algal color groups. Assuming that the different algal color groups have similar fluorescence cross sections at 622 nm, it is not difficult to see how the summed effect of all other algal color groups will be sufficient to degrade any possible correspondence between the laser-induced fluorescence intensity and the concentration of blue-green algae even though the blue-greens were the dominant type over much of the flight
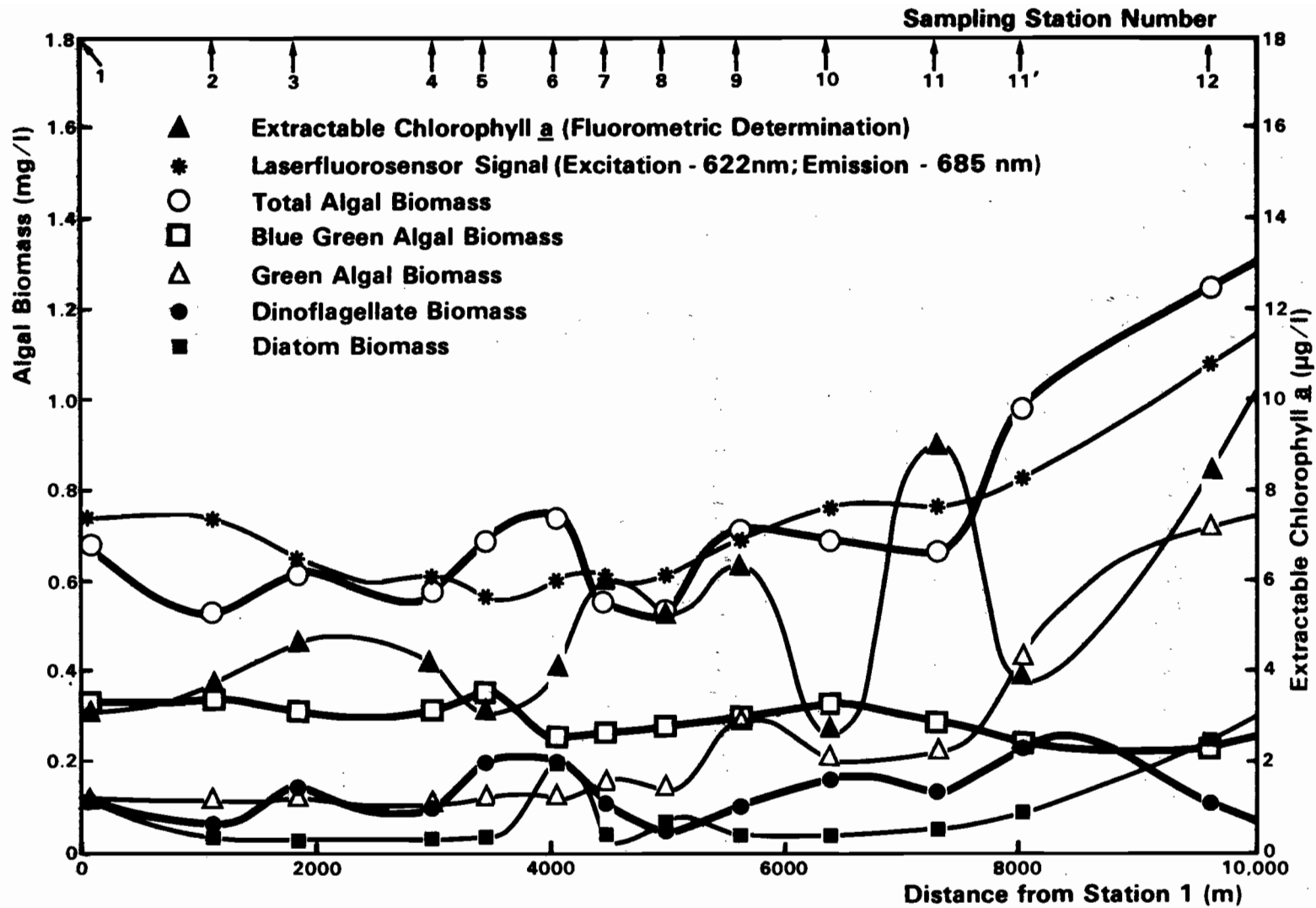
Figure 14. Variation of laser-fluorosensor signal, extractable chlorophyll a, total biomass and algal color group biomass with distance for surface transect of Las Vegas Bay in Lake Mead, Nevada. Flight #12, August 16, 1977.

153

TABLE 4. CORRELATION COEFFICIENT MATRIX FOR ALGAL BIOMASS OBTAINED BY
ENUMERATION VERSUS LASER FLUOROSENSOR SIGNAL AND EXTRACTED
CHLOROPHYLL a FOR A GROUP OF 13 SAMPLES

Biomass by Algal Division (mg/l) \ Chlorophyll a Indicator	Airborne Laserfluorosensor Signal [A]	Extracted Chlorophyll a [B,C]
Cyanophyta - Blue Greens (BG)	-0.48	0.57
Chlorophyta - Greens (G)	0.88	0.51
Bacillariophyta - Diatoms (Dia)	0.54	0.23
Pyrrophyta - Dinoflagellates (Dino)	-0.08	0.36
BG + G	0.90	0.43
BG + G + Dia	0.89	0.42
BG + G + Dino	0.81	0.29
Total Count	0.82	0.31

A) Chlorophyll a fluorescence emission at 685 nm excited at 622 nm.

B) Fluorometric determination of extracted chlorophyll a using method of Holm-Hansen et al. (39).

C) Correlation between chlorophyll a and laserfluorosensor signal gave coefficient of 0.408.

line (see Figure 14). Remote monitoring of blue-green algae is further complicated by the fact that during non-bloom conditions, blue-greens are known to congregate below the surface layer. In other studies performed on Lake Mead (43), it has been noted that the concentration of blue-green algae tends to reach a maximum at depths below the 1-m surface layer. As the attenuation coefficients for the surface water along the flight line change from values less than 1 m^{-1} to values close to $10m^{-1}$ between sampling situations 1 and 12, it is possible that the presence of blue-green algae is being progressively screened from the laser fluorosensor by increasing concentrations of the inter-vening material in the surface layer, in particular algae from other color groups. This explanation assumes that the depth at which the blue-green algae congregate remains a constant regardless of ambient conditions. In reality, however, this situation will be complicated by the tendency of the algae to adjust their depth according to the avail-able light level compounded with the effects of other environmental factors, such as water temperature and availability of nutrients and dissolved oxygen.

It is interesting to note that extractable chlorophyll a exhibited a poor correlation with both total biomass (r = 0.31) and the laser fluorosensor signal (r = 0.41). The first result is somewhat surprising, as both the algae counts and the chlorophyll a extractions were performed on subsamples of the same grab sample material. More disturbing is the fact that chlorophyll a determinations are employed principally as a substitute or indicator for total algal biomass. In the light of these correlations between the laser fluorosensor signal and total algal biomass (r = 0.82), it is suggested that errors in the chlorophyll a determinations are the principal source of this dis-crepancy. As discussed in Section 5 (e), the established procedure for extracting chlorophyll a from algae is both inefficient and unreliable in terms of reproducibility. The large deviations in the extractable chlorophyll a profile in Figure 14 are considered to be due primarily to this problem. Improved methods for extracting chlorophyll a from algae are presently under investigation and will be reported elsewhere. In contrast to the spectrophotometric approach of Strickland and Parsons (38), the fluorometric method of Holm-Hansen et al. (39), used to make the determinations for this flight, does not correct for the fluorescence contributions from the chlorophyll b or carotenoid pigments. It is therefore planned to employ the spectrophotometric technique for es-tablishing extractable chlorophyll a values in all future ground truth surveys. Because of this uncertainty in the accuracy of the chlorophyll a determinations for this flight and its effect on the correlation between the airborne and ground truth data, it has not been possible to establish the efficacy of using the 622-nm excitation wavelength for monitoring chlorophyll a in vivo. Future tests will therefore be conducted at a number of excitation wavelengths, in particular at 622 nm and 470 nm. The latter wavelength, although not responding to the pigments specific to red and blue-green algae, should provide a better chlorophyll a fluorescence response to the chlorophyll b and carotene pigments present in most algae than the original 440-nm excitation wavelength.

SECTION 6

AIRBORNE MEASUREMENTS OF THE INFLUENCE OF THE ATTENUATION COEFFICIENTS

(a) Theoretical Considerations

A relative measure of the variation in the diffuse attenuation coefficient k_λ for surface waters and consequently its dependence on n_c, can be obtained by monitoring the {OH} stretch water Raman emission at wavelength R excited at laser wavelength L, concurrently with the measurement of chlorophyll $\underline{a}$ fluorescence emission at wavelength F. The wavelength of the Raman emission is determined by the excitation wavelength and the Raman frequency shift. For example, with laser excitation at 440 nm and a fixed {OH} stretch water Raman frequency shift of 3418 cm^{-1}, the Raman emission occurs at 518 nm. The intensity of the backscattered Raman emission signal will depend on the values of k_L and k_R and not on n_w, the concentration of water, which remains essentially constant. A laser fluorosensor equation for the detected Raman emission power P_R can be written in a form analogous to the expression for the fluorescence power P_F obtained from Equation 1 such that

$$P_R = \left(\frac{P_L}{H^2}\right) \; \frac{n_w \, \sigma_w \, d_R}{(k_R + k_L)} \quad , \tag{15}$$

where σ_w is the Raman emission cross section for the {OH} stretch vibrational mode of liquid water. σ_w is weakly dependent on temperature (44) and salinity (45) and exhibits a $1/\lambda^4$ dependence on the excitation wavelength, but, for a fixed laser-wavelength and over a limited temperature range (5°C to 25°C) in freshwaters, it is assumed to remain constant. d_R is dependent on the known system and environmental factors and is given by the expression

$$d_R = \left[\frac{T^\eta Tr^\eta Rec}{4\pi\Delta R}\right]\left[\frac{(1-R_w)^2}{\mu_w^2 \, \exp\{H(\beta_L + \beta_R)\}}\right], \tag{16}$$

where Δ_R is that fraction of the Raman band seen by the detector and β_R is the atmospheric attenuation coefficient at the Raman wavelength. All other terms are as defined for Equation 1. For clear atmospheric conditions over paths on the order of 300 m, the term $\exp\{H(\beta_L + \beta_R)\}$ is assumed to have a value that remains close to unity, so that d_R is essentially a constant.

156

A similar expression for the received fluorescence power is obtained by rearranging Equation 1 such that

$$P_F = \left(\frac{P_L}{H^2}\right) \frac{n_c \, \sigma_c \, d_F}{(k_F + k_L)} \quad , \tag{17}$$

where

$$d_F = \left[\frac{T^\eta T_r^\eta Rec}{4\pi\Delta F}\right] \left[\frac{(1-R_W)^2}{\mu_W^2 \, \exp\{H(\beta_L + \beta_F)\}}\right], \tag{18}$$

and is considered to be constant for the same reasons as given for d_R. An expression can now be written for the ratio (P_F/P_R) using Equations 15 and 17, so that

$$\left(\frac{P_F}{P_R}\right) = \frac{n_c \, \sigma_c \, d_F}{n_w \, \sigma_w \, d_R} \left(\frac{k_R + k_L}{k_F + k_L}\right) . \tag{19}$$

As n_w, σ_w, σ_c, d_R and d_F are all considered to be constant, a new expression can be written for P_F/P_R in which

$$\left(\frac{P_F}{P_R}\right) = n_c \, \delta \left(\frac{k_L + k_R}{k_L + k_F}\right) \quad , \tag{20}$$

where $\delta = \left(\dfrac{d_F \, \sigma_c}{d_R \, n_w \, \sigma_w}\right)$ is a constant.

The ratio (P_F/P_R) is now seen to be dependent on n_c and the ratio $(k_L + k_R)/(k_L + k_F)$ but is independent of the laser power P_L and aircraft altitude H. However, care must still be taken to minimize H and maximize P_L to ensure a good signal-to-background-noise ratio in the measurement of (P_F/P_R). The question now arises as to the dependence of the ratio $(k_L + k_R)/(k_L + k_F)$ on changes in algae concentration and other dissolved and particulate matter in the surface waters. As changes in both n_c and the concentration of the other substances will induce changes in all the k_λ values simultaneously with the exact magnitude of the change depending on the specific wavelength, it is suggested that this ratio will exhibit only a weak dependence on n_c or on the concentration of non-chlorophyllous materials. Consequently, if $(k_L + k_R)/(k_L + k_F)$ is assumed to be constant, then (P_F/P_R) will vary simply as n_c.

A significant advantage of this approach to monitoring the degree of penetration of the laser radiation into the surface water is that it

1571

is independent of the theoretical model employed to describe the attenuation coefficients k or α used in the laser-fluorosensor equation. In reality, the Raman radiation will be subject to the same physical constraints as the fluorescence radiation except for the effects due to the difference in wavelength. Clearly it would be advantageous to employ an excitation wavelength which shifts the water Raman emission band closer to the chlorophyll a fluorescence emission band at 685 nm.

It is therefore proposed to modify the airborne laser fluorosensor described in Section (4) so that the water Raman signal can be detected, monitored and recorded concurrently with the fluorescence signal, P_F, which will still be corrected for variations in P_L and H. The ratio (P_F/P_R) will then be correlated with chlorophyll a ground truth data. An improved correlation between (P_F/P_R) and the chlorophyll a ground truth data, rather than with P_F alone, will justify the assumption that the ratio $(k_L + k_R)/(k_L + k_F)$ remains essentially constant.

(b) Laboratory Measurement of Fluorescence to Raman Ratio for Lake
      Water Samples

Before adding a Raman emission detection channel to the existing laser fluorosensor, it was considered expedient to conduct a laboratory experiment to simulate the airborne measurement of the ratio (P_F/P_R) and in particular to ensure that P_R, the Raman emission power, could be measured with the same degree of sensitivity as the chlorophyll a fluorescence power, P_F. Liquid water consists of two spectroscopically distinct forms in thermal equilibrium. These polymeric monomeric types influence the {OH} molecular band strength and ultimately the intensity, spectral shape and polarization state of the {OH} stretch Raman emission (45). In particular, the spectral characteristics of the Raman emission are highly dependent on the state of polarization of the excitation radiation, the scattering configuration used to view the emission and the polarization state of the detection system (46). The airborne laser fluorosensor, of necessity, operates in a downward-looking mode which constitutes a 180° scattering angle with a plane-polarized laser source. Consequently, because of the dependence of the Raman band depolarization ratio on the scattering configuration, the state of polarization of the laser output, and the polarization sensitivity of the detection system, it is essential that the laboratory measurements simulate the airborne measurement as closely as possible. A plane-polarized laser was therefore employed as the excitation source, and the Raman radiation was viewed in the 0° scattering configuration. The 0° scattering configuration, which is spectroscopically equivalent to a 180° format, was found to be more convenient to implement in a laboratory experiment. Finally, precautions were taken to ensure that the polarization sensitivity of the grating monochromator did not introduce errors into the measurement of the (P_F/P_R) ratio. This step was accomplished by depolarizing both the fluorescence and Raman emission prior to transmission through the monochromator. This procedure was found to be necessary because spectral discrimination in the airborne system is performed with interference filters at normal incidence, which are not sensitive to the

state of polarization of the incident radiation.

An optical schematic of this laboratory-mounted system is shown in Figure 15. A nitrogen laser pumped dye laser (AVCO Model 3000A), operating at 440 nm and, at a repetition rate of 500 Hz, was used to irradiate the lake water samples. This laser output has a pulse width of approximately 5 nsec with a spectral bandwidth of about 0.2 nm and is linearly polarized to within 1 part per 1000. The stability of the laser output power was monitored with use of a beam splitter to deflect a small percentage of the beam onto a PIN silicon phtodiode via a quartz diffuser. The fluorescence and Raman emissions from the 2 cm pathlength cell were collected and focused onto the entrance slit of an f/6.8 scanning monochromator. A compensated quartz wedge depolarizer was used to depolarize the fluorescence and particularly the Raman emission with a view to avoiding introduction of polarization artefacts into the (P_F/P_R) ratio by the polarization sensitive grating mono-chromator.

Due to use of the 180° scattering configuration, care had to be taken to ensure that laser radiation did not reach the detector. In addition to the spectral discrimination provided by the single mono-chromator, a short wavelength cutoff glass filter (Hoya Y46) was employed to block wavelengths shorter than 460 nm. Further laser blocking was achieved by placing a small piece of black tape in front of the filter on the laser beam axis as shown in Figure 15. A fast, high-gain, red sensitive photomultiplier (Hamamatsu R928), located close to the monochromator exit slit, was used to detect the fluorescence and Raman signals. Fluorescence and Raman bands of interest were obtained by scanning the monochromator over the spectral region of interest while monitoring the peak value of the emission pulse detected by the photomultiplier. The amplitude of this pulse was measured using a sampling oscilloscope (Philips PM 3400) operating in the non-scanning mode. The calibrated DC output signal from the oscilloscope sample and hold circuit, a measure of the peak amplitude of the detected pulse, was low-pass filtered to reduce photon noise effects and then plotted out directly as a function of wavelength using a strip chart recorder. The monochromator slit width and scanning rate, the low-pass filter cutoff frequency, and the chart recorder speed were all adjusted so as to ensure that the narrowest spectral feature could be faithfully resolved. The {OH} stretch water Raman band which is located at 518 nm when excited at 440 nm has an established FWHM bandwidth of 11.5 nm at this wavelength and consequently is an ideal source for this purpose.

The spectra for two Las Vegas Bay surface water samples collected on 8/16/77 and 3/31/78 are shown in Figures 16 and 17 respectively. The respective chlorophyll a levels were 8.4 µg/1 and 3.4 µg/1. It is clear, even from these rather noisy spectra, that, for the chlorophyll a range of interest (about 0.1 µg/1 to 50 µg/1), the Raman band will provide a large and measurable signal for the airborne laser fluoro-sensor in relation to the chlorophyll a signal level as represented
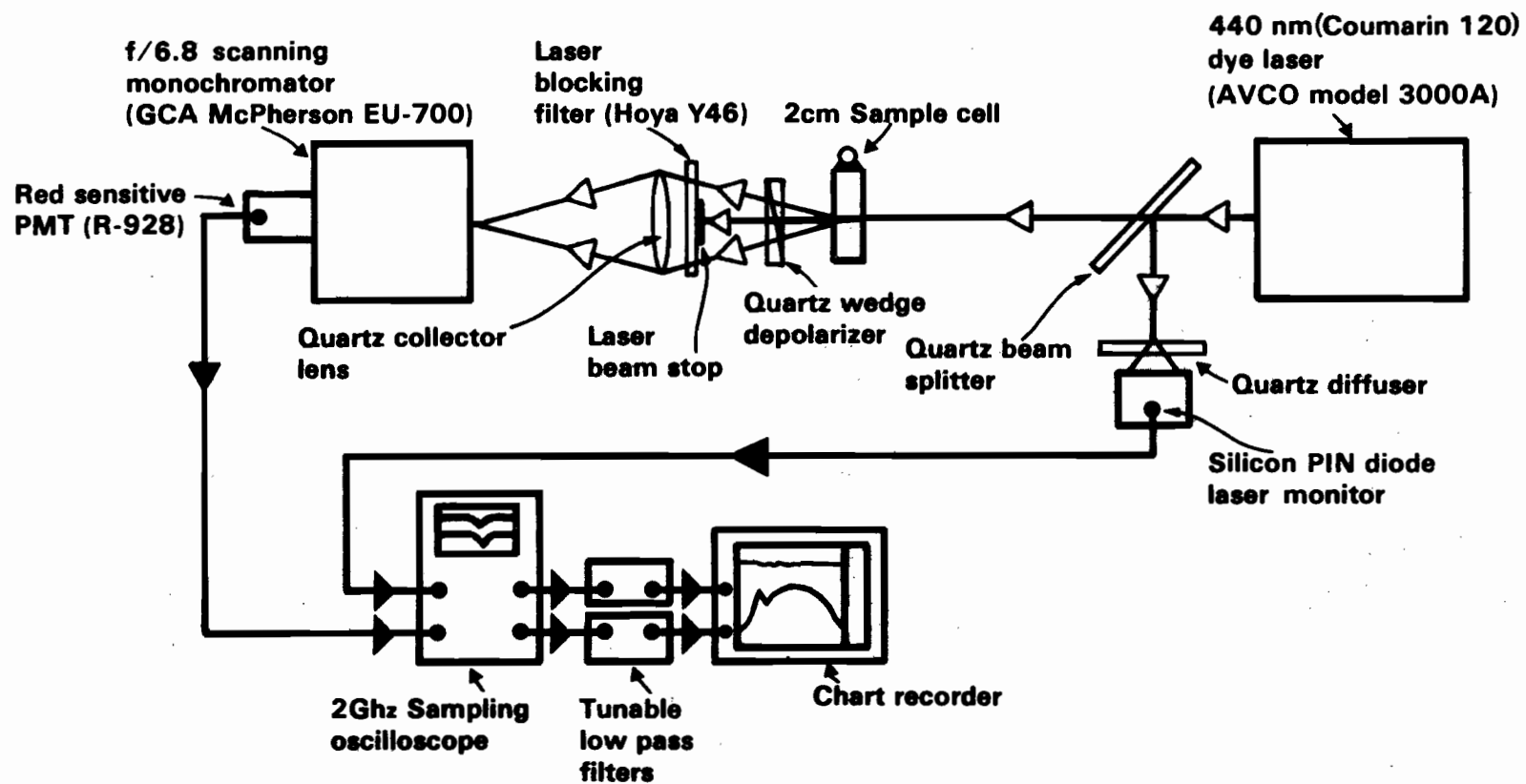
Figure 15. Laboratory simulation of airborne laser fluorosensor for monitoring chlorophyll a fluorescence and water Raman signals.

by the fluorescence pulse shown in Figure 7 for a chlorophyll _a_ level of 10.5 μg/1.

Two points are worthy of note with regard to these spectra. First they are uncorrected for the varying spectral sensitivity of the grating monochromator and the photomultiplier. Both components have lower sensitivities in the red region at 685 nm than in the blue region at 518 nm. The blue-to-red sensitivity ratio for the R928 photomultiplier is on the order 1.71 to 1, whereas that for the grating monochromator is approximately 1.25 to 1, giving a total ratio of 2.14 to 1. However, as the C31000A photomultiplier used in the airborne laser fluorosensor has a blue-to-red sensitivity ratio of approximately 2.75 to 1, it is clear that the airborne measurement of the water Raman signal will be further enhanced in relation to the chlorophyll _a_ fluorescence signal. The second point concerns the fluorescence background due to dissolved organics, indicated in Figures 16 and 17 by broken curves. This background signal, which has a fluorescence emission maximum in the region of 430 nm, constitutes only a small fraction of the total signal at 685 nm for Lake Mead surface water and, as such, its influence on the chlorophyll _a_ fluorescence measurement can be neglected. In addition this background fluorescence signal has been shown to remain fairly constant over the extent of Lake Mead at any one time (47). The present plan is therefore to use the total emission intensity at the Raman band wavelength as a reference signal rather than just the peak intensity of the Raman band. This expedient is acceptable provided that the concentration of dissolved organics for a given water surface remains constant in both the horizontal and vertical dimensions at any one time as the background fluorescence signal at this wavelength will be attenuated equally with the Raman signal. This assumption will be unacceptable for situations where the concentration of surface-water dissolved organics varies considerably over short horizontal distances at any one time. A more advanced laser fluorosensor would therefore have to separate the water Raman band from the background fluorescence. This goal could be achieved by monitoring the background fluorescence intensity on either side of the Raman band in addition to the total peak intensity at the Raman band wavelength. By simple interpolation, the peak intensity of the Raman band can then be determined.

(c) Modifications to Laser Fluorosensor needed to Measure the Fluorescence-to-Raman Ratio

The proposed modifications to the airborne laser fluorosensor system are shown schematically in Figure 18.

The transmitter-receiver unit is identical to the existing laser fluorosensor shown in Figure 3 except for the addition of the Raman band photomultiplier detector (RCA 31000A), which is gated in the same manner and at the same time as the fluorescence detector. The Raman signal is separated from the fluorescence signal by means of a neutral (50/50) beam splitter. The modified electronic detection, monitoring and recording system is shown schematically in Figure 19.
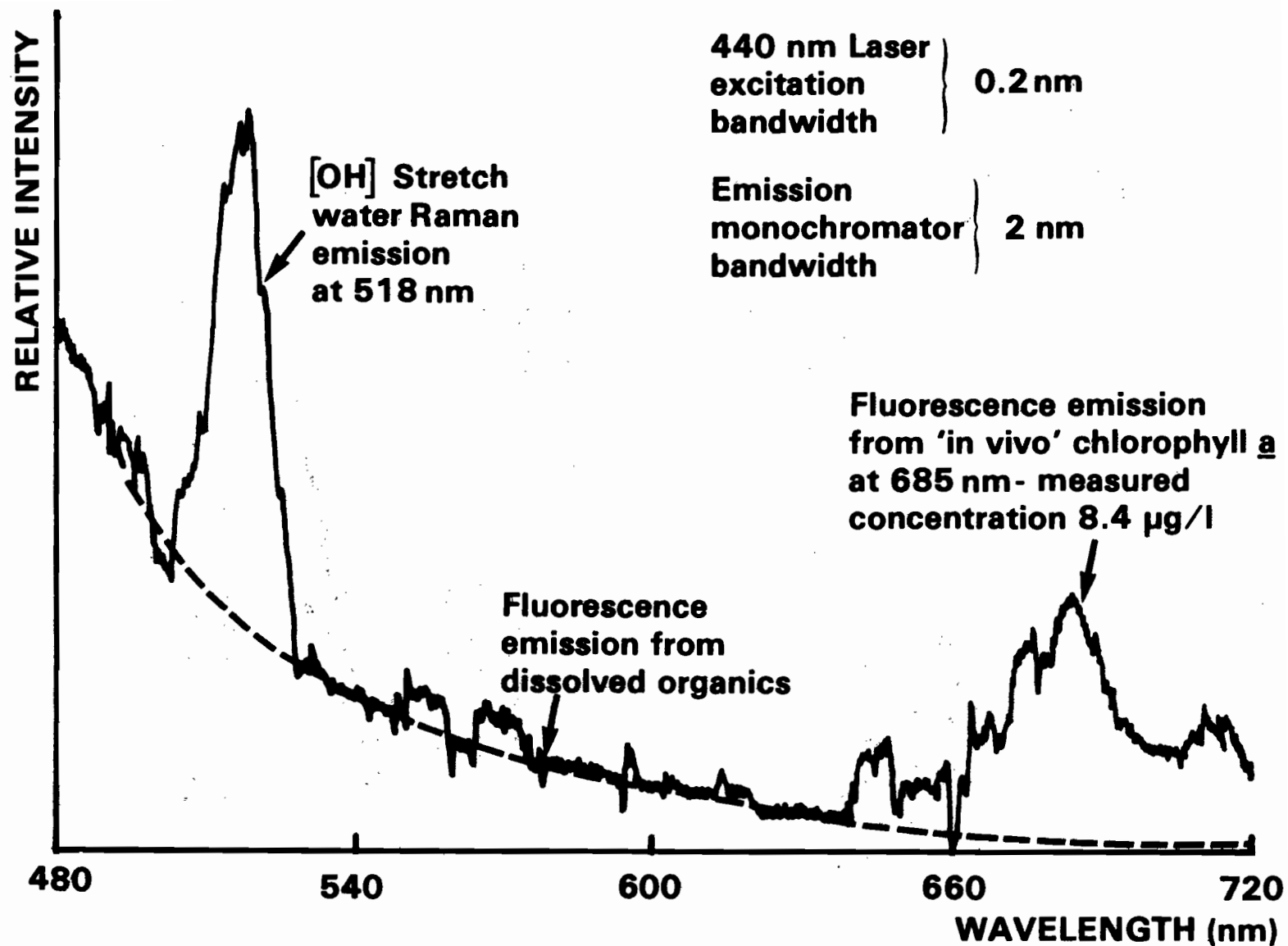
Figure 16. Uncorrected fluorescence and Raman emission spectra of Lake Mead surface water sample, excited at 440 nm, August 16, 1977.
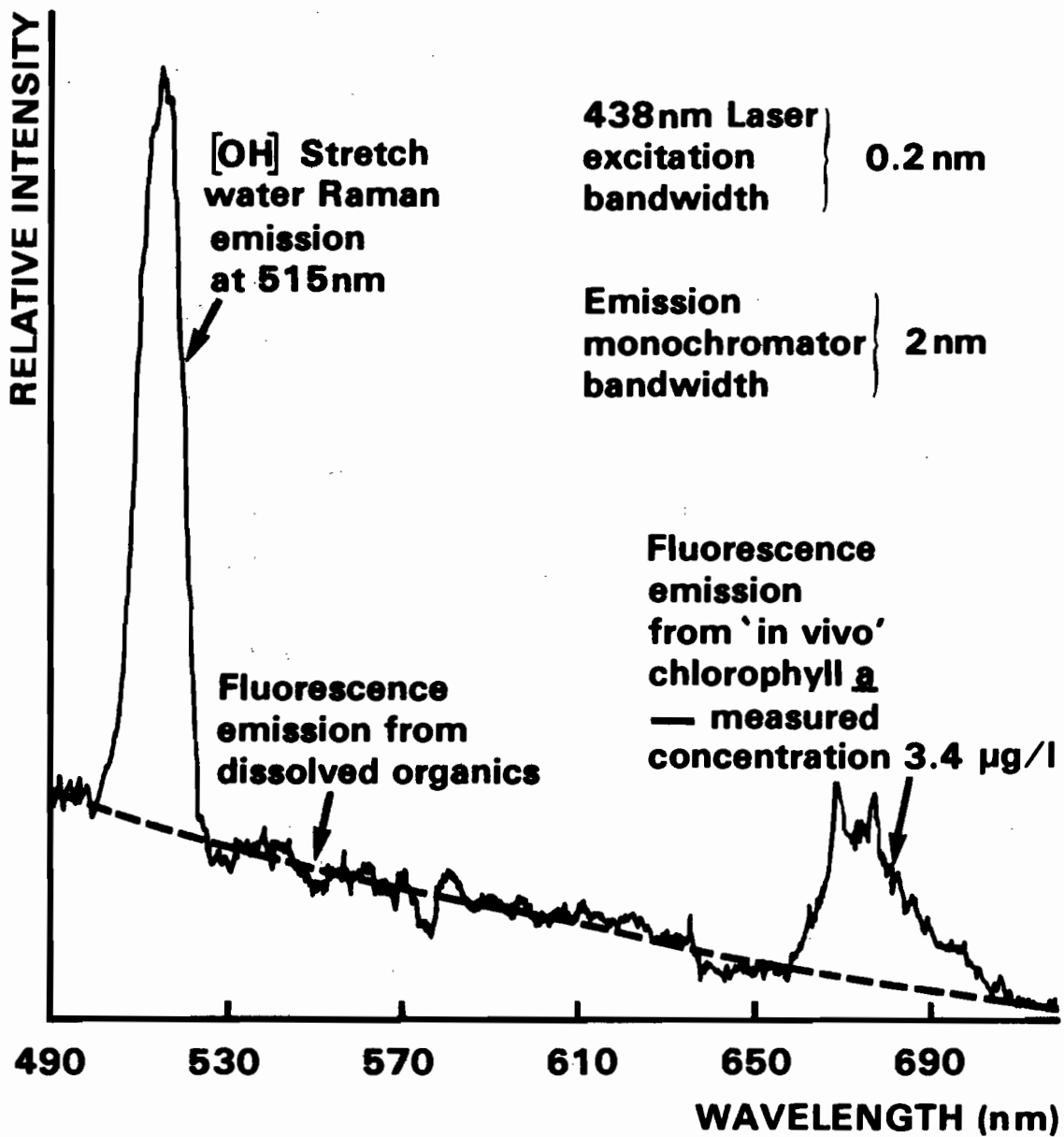
Figure 17. Uncorrected fluorescence and Raman emission spectra of Lake Mead surface water sample, excited at 438 nm, March 31, 1978.
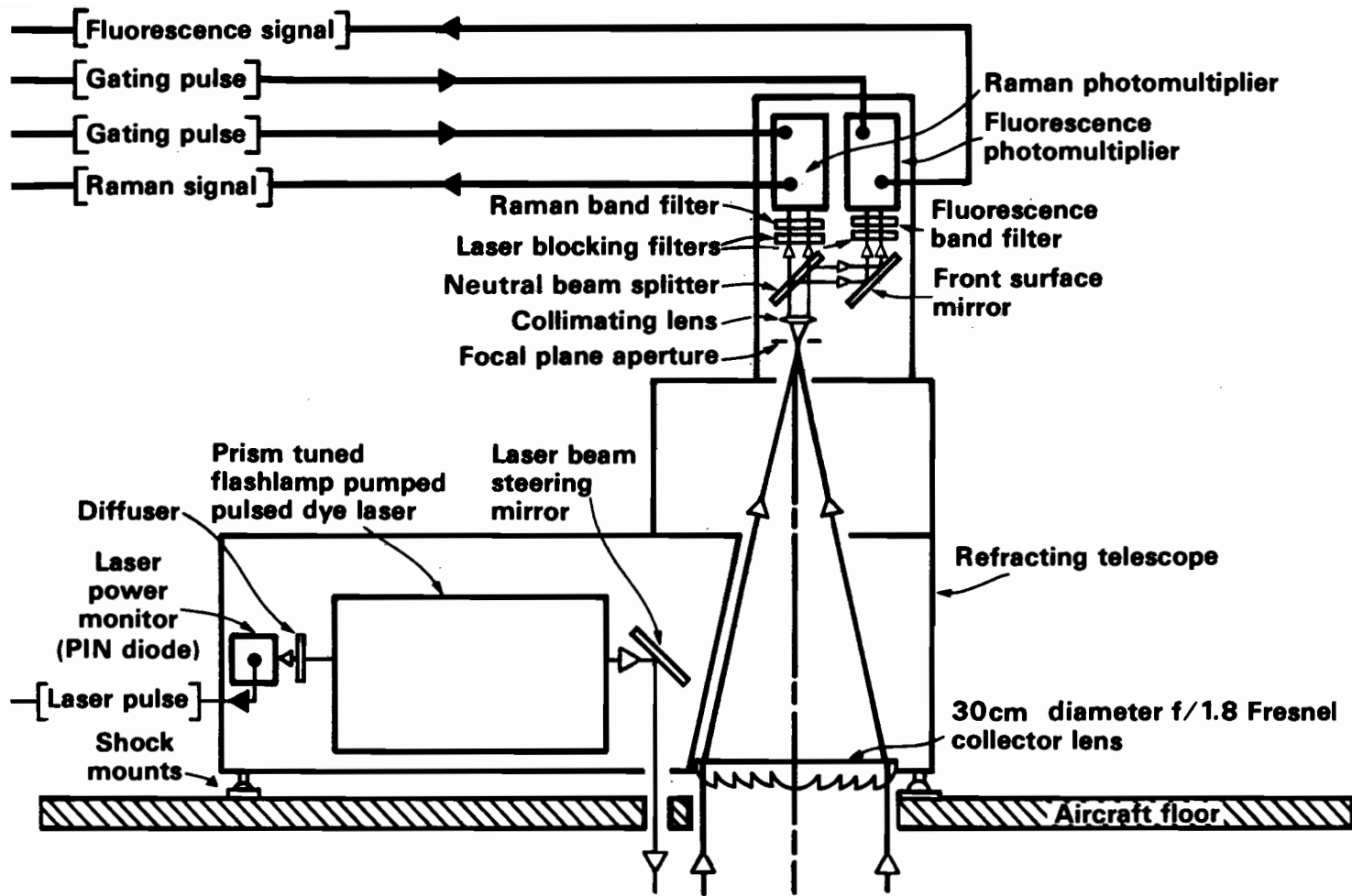
Figure 18. Optical diagram of airborne laser fluorosensor for monitoring chlorophyll a fluorescence and water Raman signals.
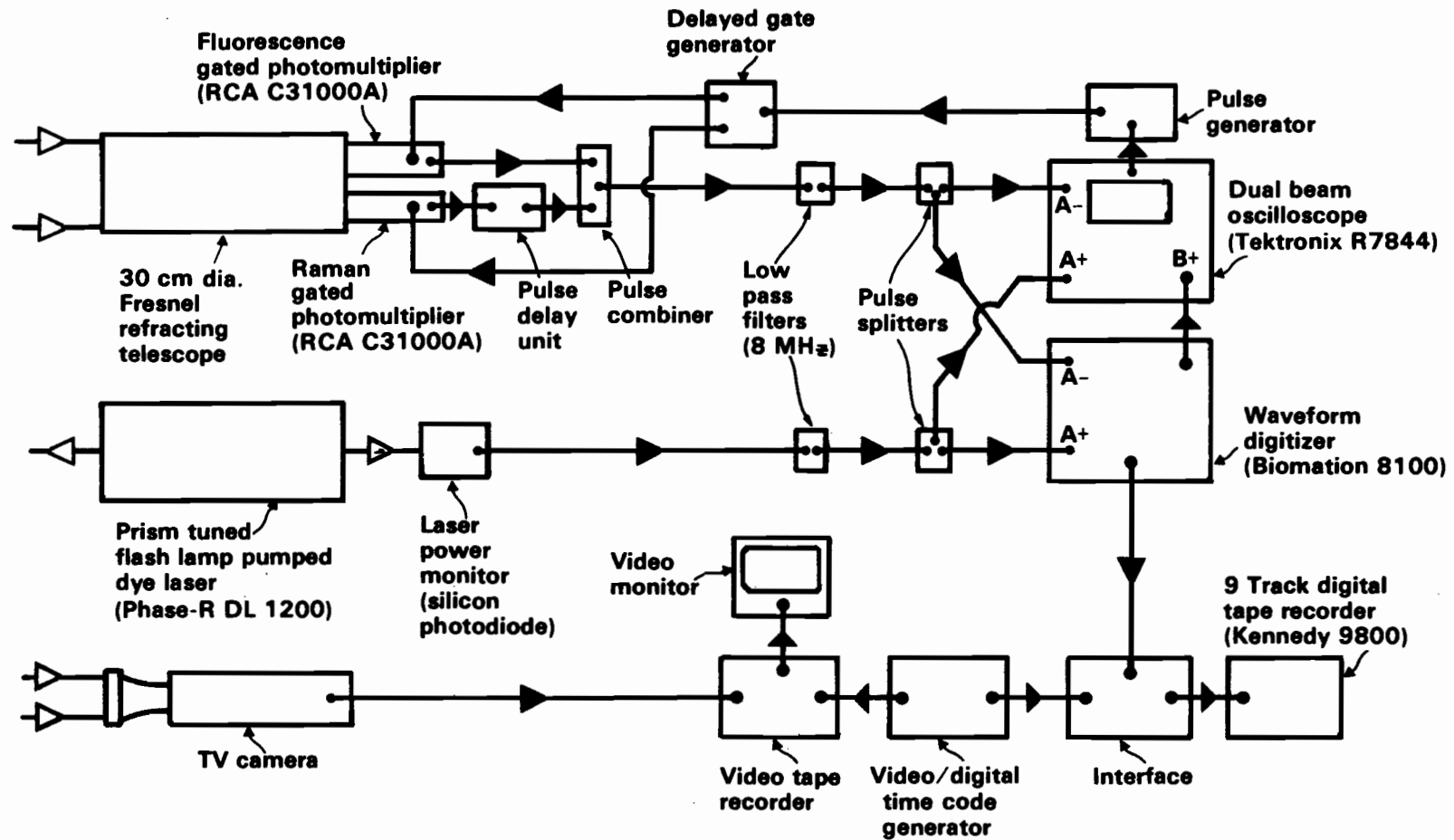
Figure 19. Schematic of airborne laser fluorosensor for measuring chlorophyll <u>a</u> fluorescence and water Raman emission showing detection, monitoring and recording systems.

This system is essentially identical to the original one shown in Figure 6 but with the addition of a 50-ohm delay line needed to delay the Raman signal in relation to the fluorescence signal. This delay allows the fluorescence and delayed Raman pulses to be combined and recorded sequentially on a single waveform digitizer input channel. By employing this approach, loss of analog input bandwidth in the digitizer (Biomation 8100) is avoided. The anticipated waveform is shown schematically in Figure 20, where the fixed delay period between the fluorescence and Raman pulses will have a value of 3 μsec.
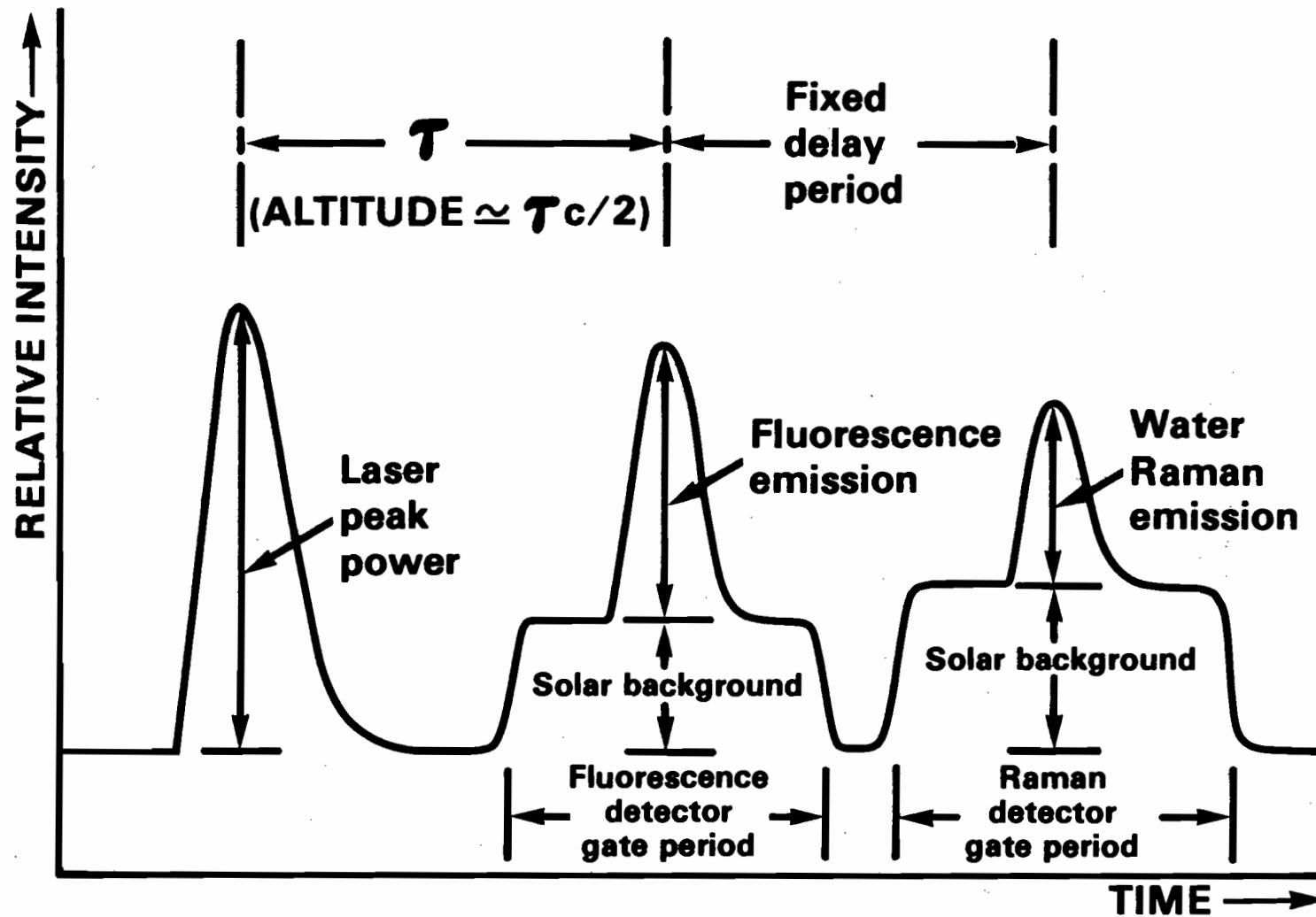
Figure 20. Variation of laser, fluorescence and Raman laser-fluorosensor signals as a function of time.

SECTION 7

CONCLUSIONS

The laser fluorosensor described in this report has been used to produce flight-line profiles of relative surface water chlorophyll a concentrations that vary over a range from $2\mu g/l$ to $20\mu g/l$ at operating elevations from 200 m to 400 m. In its present form the laser fluorosensor is estimated to be capable of monitoring chlorophyll a concentrations down to $0.4\mu g/l$ with a minimum signal-to-RMS background noise ratio of 3. With the implementation of measures to increase the fluorescence signal and reduce the background noise, it will be possible to monitor chlorophyll a concentrations down to $0.1\mu g/l$ with a minimum signal-to-RMS background noise ratio of 20 under the same environmental conditions encountered in the present measurements.

Presently, the degree of correlation between the airborne chlorophyll a fluorescence profiles and those for the corresponding ground truth chlorophyll a data is somewhat less than ideal, with linear correlation coefficients lying in the range between 0.77 and 0.95. Several reasons exist for this discrepancy between the airborne and ground truth data. Firstly, chlorophyll a determinations made according to presently accepted standards are both inefficient and of low reproducibility, whereas it is estimated that the airborne measurements, although prone to systematic errors, are reproducible to better than $\pm$ 5%. It is therefore suggested that investigations be conducted with the purpose of improving both the efficiency and accuracy of the method used for making chlorophyll a determinations at least to the point where the error is comparable to that for the airborne data. Secondly, the airborne chlorophyll a fluorescence signal is known to be dependent on changes in the surface water diffuse attenuation co-efficients in addition to the chlorophyll a concentration. It is therefore proposed to obtain a relative indication of this variation by concurrently monitoring the water Raman emission signal. Theoretical and experimental considerations indicate that this approach is feasible. Modifications to the airborne laser-fluorosensor needed for measuring this Raman signal are straightforward and can be readily implemented with a minimum of modification to the present system. Finally, the dependence of σ_c on the relative concentrations of the different algal color groups present in a given sample can be minimized by choosing a laser excitation wavelength at which the fluoroscence cross section for the different algal color groups are more nearly equal. It is therefore proposed to conduct a series of evaluating different excitation wavelengths for monitoring in vivo chlorophyll a.

Attempts to monitor changes in the concentration of blue-green algae by selectively exciting c-phycocyanin, a chlorophyll a-coupled photopigment unique to this freshwater algal division, were not successful. It is likely that the reason for this failure is the relatively low fluorescence cross section for this pigment in relation to that for chlorophyll a itself. It is possible that monitoring specific algal groups can be better accomplished by employing the multiwavelength excitation approach.

A fully-developed airborne laser fluorosensor will be able to produce contour maps of surface water chlorophyll a fluorescence. Due to the problems encountered in determining absolute values for the chlorophyll a fluorescence cross section and the diffuse water attenuation coefficients, it is not possible to produce a calibrated surface water chlorophyll a concentration map with airborne data alone. Rather this map must be calibrated in units of chlorophyll a concentration by the provision of ground truth chlorophyll a determinations obtained at one or two selected reference sites.

Future airborne laser fluorosensors for making routine surveys of surface water chlorophyll a will require a number of additional features not available with the present system:

(a) Rapid installation in a variety of different aircraft will require a system considerably smaller than the present package that can be quickly and easily installed and either palletized or constructed of a number of discrete modular units suitable for rapid transportation and integration in the field.

(b) Provisions must be made for navigation data accurate to within a few meters in order that the airborne data can be reproduced in the form of a surface water map showing isopleths of constant chlorophyll a fluorescence. This can be accomplished by using an airborne range-positioning system which employs a microwave transmitter to interrogate two portable ground-based transponder units.

(c) A degree of real-time capability should be built into future laser fluorosensors for use as a quality control feature. A contour map of surface water chlorophyll a could then be produced and continuously updated on a CRT display for evaluation by the system operator. Current microprocessor technology is ideally suited to this application.

(d) Finally, the optical receiver for the laser fluorosensor will contain two extra spectral detector channels, in addition to those for the water Raman and chlorophyll a fluorescence signals. These additional detectors will monitor spectral intervals close to the water Raman and chlorophyll a fluorescence bands, thereby providing estimates of the background fluorescence due to dissolved organics at these two bands.

169

REFERENCES

1. Johnson, R. W. Quantitative Mapping of Chlorophyll a Distributions in Coastal Zones by Remote Sensing. Presented at 43rd Annual Meeting of American Society of Photogrammetry, Washington, D.C. February 27 - March 5, 1977.

2. Arvesen, J.C., E.C. Weaver and J.P. Millard. Rapid Assessment of Water Pollution by Airborne Measurement of Chlorophyll Content. Presented at Joint Conference on Sensing of Environmental Pollutants, Palo Alto, California, November 8-10, 1971, AIAA Paper #71-1097.

3. McNeil, W.R., K.P.B. Thompson and J. Jerome. The Application of Remote Spectral Measurements to Water Quality Monitoring. Canadian Remote Sensing Journal 2, 48-58, 1976.

4. Witte, W.G. Evaluation of the Dual Differential Radiometer for Remote Sensing of Sediment and Chlorphyll in Turbid Waters. Proceedings of Fourth Annual Remote Sensing of Earth Resources Conference, Tullahoma, Tennessee, March 24-26, 1975.

5. Johnson. R. W. Application of Aircraft Multispectral Scanners to Quantitative Analyses and Mapping of Water Quality Parameters in the James River, Virginia. Presented at XIX Meeting of COSPAR - Latest Results of Earth Survey. Philadelphia, Pa., June 1976. Published in COSPAR Space Research Vol. XVII, Pergamon Press, Oxford 1977.

6. Bowker, D.E. and W.G. Witte. The Use of LANDSAT for Monitoring Water Parameters in the Coastal Zone. Proceedings of AIAA 1977 Joint Conference on Satellite Applications of Marine Operations, New Orleans, La., November 15 - 18, 1977.

7. Neville, R.A., and J.F.R. Gower. Passive Remote Sensing of Phytoplankton via Chlorophyll a Fluorescence. J. Geophys. Res. 82, 3487-3493, 1977.

8. Stoertz, G.E., W.R. Hemphill and D.A. Markle. Airborne Fluorometer Applicable to Marine and Estuarine Studies. Marine Technology Society Journal, 3, 11-26, 1969.

9. McFarlane, C., and R.D. Watson. The Detection and Mapping of Oil on a Marshy Area by a Remote Luminescent Sensor. Proceedings of API 1977 Oil Spill Conference. March 8-10, 1977. New Orleans, La. pp 197-201.

10. Hemphill, W.R., R.D. Watson, R.C. Bigelow and T.D. Hessen, Measurement of Luminescence of Geochemically Stressed Trees and Other Materials. Proceedings of First Annual William T. Pecora Memorial Symposium, October 1975, Sioux Falls, South Dakota, pp 93-112.

11. Kim, H.H. and G.D. Hickman. An Airborne Laser Fluorosensor for the Detection of Oil on Water. Proceedings of the Symposium on the Use of Lasers for Hydrographic Studies, NASA Wallops Island, Virginia, September 12, 1973, NASA Special Publication, SP375, Washington, D.C. 1975.

12. O'Neil, R.A., A.R. Davis, H.G. Gross and J. Kruus. A Remote Sensing Laser Fluorometer. Am. Soc. Test. Mater., Special Technical Publication #573, pp 424-436, 1975.

13. Bristow, M.P.F., Airborne Monitoring of Surface Water Pollutants by Fluorescence Spectroscopy. Remote Sensing of Environment $\underline{7}$, 105-127, 1978.

14. Fantasia, J.F. and H.C. Ingrao. Development of an Experimental Airborne Laser Remote Sensing System for the Detection and Classification of Oil Spills. Proceedings of the 9th International Symposium on Remote Sensing of the Environment, Environmental Research Institute of Michigan, April 15-19, 1974, pp 1711-1745.

15. Kim H.H. New Algae Mapping Technique by the Use of Airborne Laser-fluorosensor. Appl. Opt. $\underline{12}$, 1454-1459, 1973.

16. Mumola, P.B., O. Jarrett and C.A. Brown. Multiwavelength Laser Induced Fluorescence of Algae in-vivo: A New Remote Sensing Technique. Proceedings of Second Joint Conference on Sensing of Environmental Pollutants, Washington, D.C., December 10-12, 1973.

17. Hickman, G.D. and R.B. Moore. Laser Induced Fluorescence in Rhodamine B and Algae. Proceedings of the 13th Conference on Great Lakes Research, Buffalo, New York, March 31 - April 3, 1970. pp 1-14.

18. Mumola, P.B. and H.H. Kim. Remote Sensing of Marine Plankton by Dye Laser Induced Fluorescence. Proceedings of IEEE Conference on Engineering in the Ocean Environment, Newport, Rhode Island, September 13-15, 1972, pp 204-207.

19. Loftus, M.E. and H.H. Seliger. Some Limitations of the In Vivo Fluorescence Technique. Chesapeake Science 16, 79-92, 1975.

20. Browell, E.V. Analysis of Laser Fluorosensor Systems for Remote Algae Detection and Quantification, NASA Tech Note TN D-8447, June 1977.

21. Brown, C.A., F.H. Farmer, O. Jarrett and W.L. Staton. Laboratory Studies of In Vivo Fluorescence of Phytoplankton. Proceedings of Fourth Joint Conference on Sensing of Environmental Pollutants, New Orleans, La. November 6-11, 1977, pp 782-788.

22. Blasco, D. Variations of the Ratio in vivo - Fluorescence/α - Chlorophyll and its Applications to Oceanography. Effect of Limiting Different Nutrients, of Night and Day and Dependence on the Species Under Investigation. NASA Technical Translation TTF - 16,317, 1975 from original Spanish document published in Investigacion Pesquera 37, 533-556, 1973.

23. Tunzi, M.G., M.Y. Chu and R.C. Bain. In Vivo Fluorescence, Extracted Fluorescence and Chlorophyll Concentrations in Algal Mass Measurements. Water Research 8, 623-635, 1974.

24. Anon., Chlorophyll and Pheophytin. Technical Note 10-577 - C & P, 1977, Turner Designs, Mountain View, California.

25. Friedman, E.J. and G.D. Hickman. Laser Induced Fluorescence in Algae. A New Technique for Remote Detection. NASA Contractor Report CR-62090, 1972.

26. Lorenzen, C.J. A Method for the Continuous Measurement of in vivo Chlorophyll Concentration. Deep Sea Research 13, 223-227, 1966.

27. Smith, R.C. and J.E. Tyler. Transmission of Solar Radiation into Natural Waters. Photochemical and Photobiological Reviews. 1, 117-155, 1976. Ed by K.C. Smith, Plenum Press, New York.

28. Kiefer, D.A. and R.W. Austin. The Effect of Varying Phytoplankton Concentration on Submarine Light Transmission in the Gulf of California. Limnol. Oceanogr. 19, 55-64, 1974.

29. Baker A.L. and K.K. Baker. Estimation of Planktonic Wind Drift by Transmissometry. Limnol. Oceanogr. 21, 447-452, 1976.

30. Campillo, A.J., V.H. Kollman and S.L. Shapiro. Intensity Dependence of Fluorescence Lifetime of in vivo Chorophyll excited by a Picosecond Light Pulse. Science, 193, #4249, July 16, 227-229, 1976.

31. Bristow, M.P.F. and N. deVilliers. On the Relative Merits of Using Either C.W. Helium - Cadimum or Pulsed Nitrogen Lasers as the Fluorescence Excitation Source in Airborne Laser Fluorosensing Systems. Technical Note 73-6. November 1973, Canada Centre for Remote Sensing, Department of Energy, Mines and Resources, Ottawa, Canada.

32. Grant, W.B. and J.G. Hawley, Prevention of Fire Damage due to Exploding Dye Laser Flashlamps. Appl. Opt. 14, 1257-1258, 1975.

33. Riede, M.J., The Single Thin Lens as an Objective for IR Imaging Systems. Electro-Optical Systems Design, 6, #11, 58-65, 1974.

34. Deacon, J.E. Lake Mead Monitoring Program. Final Report. Dept. of Biological Sciences, University of Nevada, Las Vegas, September 1977.

35. Loftus, M.E., D.V. Subba Rao and H.H. Seliger. Growth and Dissipation of Phytoplankton in Chesapeake Bay. I. Response to a Large Pulse of Rainfall. Chesapeake Science, 13, 282-299, 1972.

36. Baudouin, M.F. and P. Scoppa. Fluorometric Determination of Chlorophyll a in the Presence of Pheopigments: Effect of the Half - Value width of the Excitation Source. Marine Biol. 10, 66-69 (1971).

37. Scheid, F. Chapter 21 in 'Numerical Analysis', Schaums Outline Series, Schaum, New York, 1968.

38. Strickland, J.D.H. and T.R. Parsons. A Practical Handbook of Seawater Analysis. Second Edition, Part IV, Section 3.1, Spectrophotometric Determination of Chlorophylls and Total Carotenoids. Fisheries Research Board of Canada, 1972.

39. Holm-Hansen, O., C.J. Lorenzen, R.W. Holmes and J.D.H. Strickland. Fluorometric Determination of Chlorophyll. J. Cons. perm. int. Explor. Mer. 30, 3-15, 1965.

40. Standard Methods for the Examination of Water and Wastewater, 14th Edition, American Public Health Association, 1975.

41. Shoaf, W.T. and B.W. Lium. Improved Extraction of Chlorophyll a and b from Algae Using Dimethyl Sulfoxide. Limnol. Oceanogr. 21, 926-928, 1976.

42. Marker, A.F.H. The Use of Acetone and Methanol in the Estimation of Chlorophyll in the Presence of Phaeophytin. Freshwat. Biol. 2, 361-385, 1972.

43. Deacon, J.E. and R.W. Tew. Inter-relationships between Chemical, Physical and Biological Conditions of the Waters of Las Vegas Bay of Lake Mead. Final Report, Dept. of Biological Sciences, University of Nevada, Las Vegas, 1972.

44. Walrafen, G.E. Raman Spectral Studies of the Effects of Temperature on Water Structure, J. Chem. Phys. 47, 114-126, 1967.

45. Chang, C.H. and L.A. Young. Seawater Temperature Measurement from Raman Spectra. AVCO Research Note 960, AVCO Everett Research Laboratory Inc., Everett, Mass. January, 1974.

46. Gilson, T.R. and P.J. Hendra. Laser Raman Spectroscopy. Wiley-Inter-science, New York. 1970.

47. Bristow, M. and D. Nielsen. The Application of Fluorescence Spectroscopy to Remote Monitoring of Total Organics in Surface Waters. To be published.

A LASER FLUOROSENSING STUDY -- SUPPLEMENTARY NOTES

Hongsuk H. Kim
Charles R. McClain
James T. McLean
Frederick Vonbun, Jr.*
NASA/Goddard Space Flight Center
Greenbelt, Maryland 20771

*Zoology Department, University of Maryland
College Park, Maryland

This paper describes laboratory and theoretical studies which add important supplementary data to the existing knowledge of the fluorometric properties of ocean phytoplankton.

In order to detect ocean phytoplankton with an airborne lidar system, there is a strong need for accurately determining the fluorescence efficiency in absolute quantum yield terms. The particular yield measured using an integration sphere has an average value of 0.0063 units of 685 nm emission per unit of 488 nm radiation absorbed. The extinction properties of a 488 nm laser beam were also measured using a special absorption chamber. The observed absorption coefficient was 0.26 m^{-1} for 1 μgs/ℓ in-vivo concentration of ocean phytoplankton. Based on these measured parameter values and radiation transfer equation, the expected return signal intensity was determined as a function of the chlorophyll concentration in sea water, and the effects of laser beam penetration was evaluated. The implications of the distortion in return signal with vertical penetration of the laser beam is also discussed.

1. INTRODUCTION

The study of chlorophyll pigment has become of great interest in recent years. Especially remote measurements of the plant pigment have become significant in research dealing with oceanology, marine biology and coastal water ecology. This is because remote sensing of chlorophyll levels can be used as a direct measure of ocean phytoplankton populations and the information of the phytoplankton distribution in the sea serves as an indicator of the nutrients available in the sea.

Presently both passive and active remote sensing approaches are being developed to appreciate the influence of chlorophyll pigments on the coloration of aquatic and oceanic water. Among the two, passive ocean

colorimetric technique is better known method. In this technology, multispectral color scanner is used to detect the extent of sunlight absorption in the blue region of the spectrum by the photosynthetic pigments. The other less-known method deals with chlorophyll pigment measurements by induced fluorometric method. Originally, the fluorometric technique was developed for use in the laboratory to determine chlorophyll concentrations in acetone extracts (Yentsch and Menzel, 1963). Currently a continuous-flow fluorometer which actually records in-vivo concentrations in the field is widely used (Strickland, 1968; Lorenzen, 1966). A novel variant of this fluorometric device which utilizes a laser beam as the excitation source was demonstrated from a fishing pier and airborne platform to show that chlorophyll concentration can be detected remotely and its distribution in large areas can be rapidly mapped (Kim, 1973).

In recent years, a number of investigators have used airborne laser fluorosensor for remote sensing of water resources (Barringer et al. 1977; Bristow, 1978; Brown et al. 1977). Continuing efforts with this technique are aimed at proving the soundness and practicality of the airborne active sensor as an advanced scientific tool for oceanic studies.

This report presents laboratory and theoretical studies which are considered to be supplementary to the existing knowledge of the active sensor. Authors have felt that indeed there is a strong need for understanding the effects of laser beam penetration of surface layer and the fluorescence efficiency in absolute quantum yield terms.

The study results described herein are aimed at elucidating these effects and the following sections discuss the laser fluorosensing equation and the absorptional parameters which influence the return signal intensity. The particular yields were attained using an integration sphere and the absorption coefficients were derived from laser beam extinction determinations using a special absorption chamber.

2. LIDAR EQUATION

In order to discuss laser-induced fluorescence, a basic lidar equation that can be used with this new class of remote sensor has to be established.

In Figure 1, an airborne (or satellite-borne) laser fluorosensor is illuminating the ocean surface at nadir. The laser beam, $I^{\circ}_{\lambda_1}$, experiences attenuation from both the atmosphere and the hydrosphere. We wish to estimate the power returned to the instrument at the fluorescence wavelength (I_{λ_2}). The atmosphere is assumed to have attenuation coefficient (k_{λ_1}) that is independent of the vertical coordinate. The air-sea interface is assumed to be smooth.
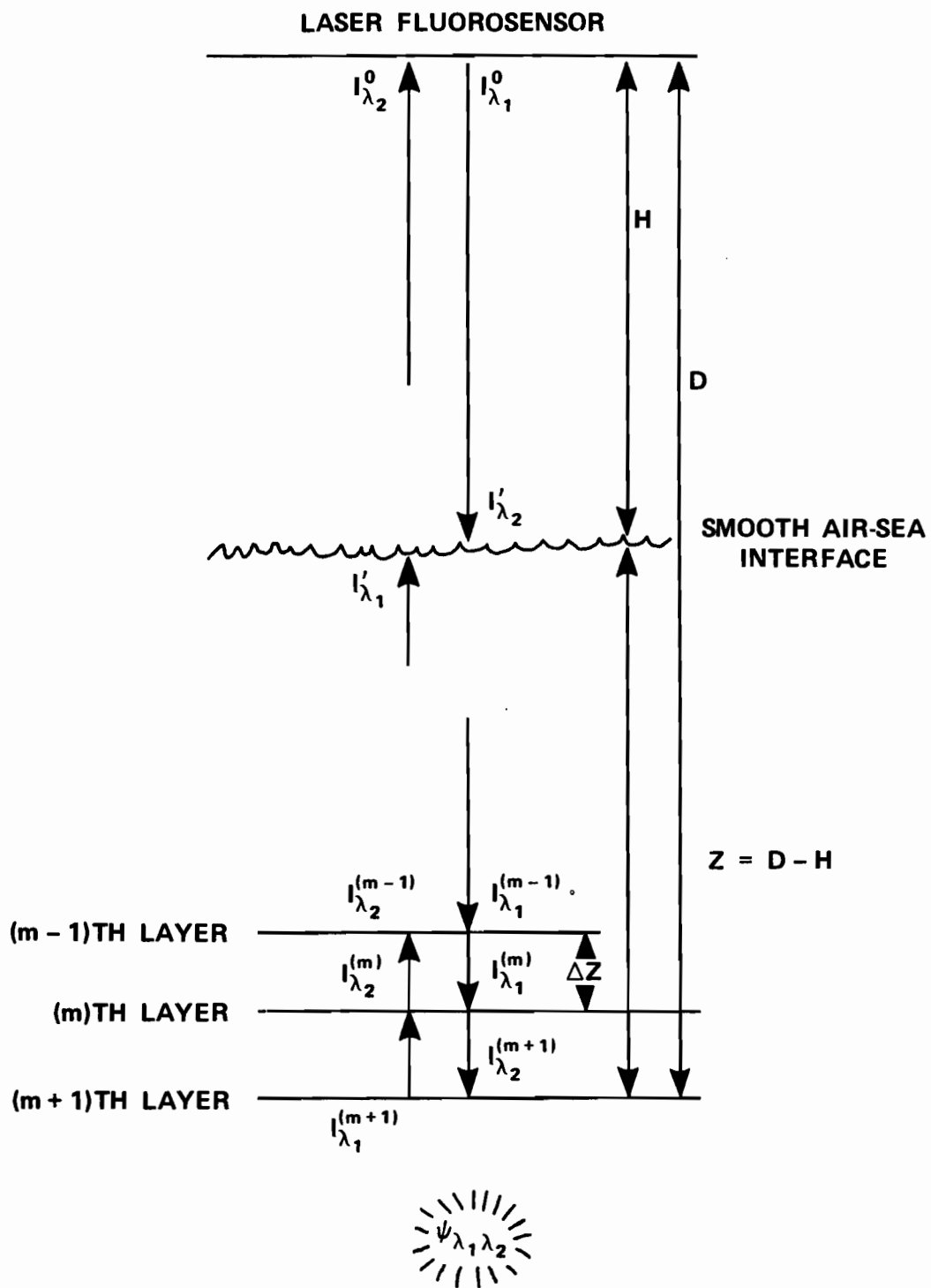
Figure 1. Geometry considered in calculating lidar returns.

Then, after propagating through the atmosphere and the interface, the incident intensity is

$$I'_{\lambda_1} = I^o_{\lambda_1}(1-\rho)e^{-k_{\lambda_1}H} \, ,$$

where the terms are defined in Table 1. The downward laser flux undergoes absorption and scattering processes and the resulting intensity is

$$I_{\lambda_1}(z) = I'_{\lambda_1}e^{-\int_H^Z \alpha_{\lambda_1}(z)dz} \, , \tag{1}$$

where the extinction coefficient is not held to be constant due to variations in the fluids composition with depth. The extinction coefficient, α_{λ_1}, can be defined as

$$\alpha_{\lambda_1} = a_{w_{\lambda_1}} + [n]a_{ch_{\lambda_1}} + S_{w_{\lambda_1}} + S_{p_{\lambda_1}} \, . \tag{2}$$

Since fluorescence results from absorption, the energy lost via absorption must be determined. If the energy loss due to the scattering caused by the presence of particles in the water and water itself is

$$I_{s_{\lambda_1}}(z) = I'_{\lambda_1}e^{-\int_H^Z S_{\lambda_1}(z)dz} \, , \tag{3}$$

where, $S_{\lambda_1} = S_{w_{\lambda_1}} + S_{p_{\lambda_1}} = S(p+w)_{\lambda_1}$, is the total scattering coefficient, then the loss due to the absorption is

$$I_{a_{\lambda_1}}(z) = I_{\lambda_1}(z) - I_{s_{\lambda_1}}(z)$$

$$= I'_{\lambda_1}\left[e^{-\int_H^Z \alpha_{\lambda_1}(z)dz} - e^{-\int_H^Z S_{\lambda_1}(z)dz}\right] \, . \tag{4}$$

The conversion efficiency, $\psi_{\lambda_1\lambda_2}$, is defined as the fraction of energy absorbed at wavelength λ_1 that is converted to the fluorescence radiation λ_2

$$\psi_{\lambda_1\lambda_2} = \frac{I_{\lambda_2}(z)}{I_{a_{\lambda_1}}(z)} \, . \tag{5}$$

In order to produce a value for the total fluorescent radiation intensity reaching to the surface I'_{λ_2}, the fraction of I'_{λ_1} absorbed, the conversion

178

Table I.

Symbols Used in Analytical Equations

$I^o_{\lambda_1}$	Initial intensity transmitted at wavelength λ_1.
I'_{λ_1}	Incident intensity at fluid interface at wavelength λ_2.
$I^{ref}_{\lambda_1}$	Intensity of reference signal reflected at interface.
$I_{\lambda_1}(z)$	Intensity of radiation at λ_1.
$I^o_{\lambda_2}$	Returned fluorescence radiation at λ_2 at receiver.
I'_{λ_2}	Total upwelled fluorescence radiation reaching the interface.
$I_{\lambda_2}(z)$	Intensity of radiation at λ_2.
$\delta I_{\lambda_1}(z)$	Energy at λ_1 lost by absorption, $\delta I_{a_{\lambda_1}}$, and by scattering, $\delta I_{s_{\lambda_1}}$.
δI_{λ_2}	Energy emitted at wavelength, λ_2
$\Psi_{\lambda_1\lambda_2}$	Fluorescence conversion efficiency or quantum yield at λ_1 excitation and λ_2 emission.
ρ	Reflectivity of the surface $= (n-1/n+1)^2$ where n = refractive index of water.
$k_{\lambda_1}, k_{\lambda_2}$	Extinction coefficients of atmosphere for λ_1 and λ_2 respectively.
$\alpha_{\lambda_1}, \alpha_{\lambda_2}$	Extinction coefficients of fluid for λ_1 and λ_2 respectively.
$a_{w_{\lambda_1}},$ $[n]a_{ch_{\lambda_1}}$	Absorption coefficients at λ_1 for water and chlorophyll where [n] is the chlorophyll concentration.
$S_{w_{\lambda_1}}, S_{\rho_{\lambda_1}}$	Scattering coefficients at λ_1 for water and chlorophyll where S_p depends on particulate concentration.

179

efficiency, $\psi_{\lambda_1\lambda_2}$, and the extinction effects at λ_2 during its upward transit must be incorporated at each location in the vertical.

Analytical expressions for these quantum absorptional and emission processes are given in the following.

From Figure 1, the downward fluxes at $(m-1)$, (m) and $(m+1)$th layers with Δz thickness are:

$$I_{\lambda_1}^{(m-1)} = I_{\lambda_1}' e^{-(m-1)(\alpha_{\lambda_1})(\Delta z)}$$

$$I_{\lambda_1}^{(m)} = I_{\lambda_1}' e^{-(m)(\Delta z)(\alpha_{\lambda_1})} \tag{6}$$

$$I_{\lambda_1}^{(m+1)} = I_{\lambda_1}' e^{-(m+1)(\alpha_{\lambda_1})(\Delta z)} .$$

The induced fluorescence emanating from the mth layer is, from the relations (5) and (6)

$$I_{\lambda_2}^{(m)} = [I_{\lambda_1}^{(m-1)} - I_{\lambda_1}^{(m)}] \psi_{\lambda_1\lambda_2}$$

$$= I_{\lambda_1}' e^{-(m-1)\alpha_{\lambda_1}\Delta z}(1 - e^{-\alpha_{\lambda_1}\Delta z}) \psi_{\lambda_1\lambda_2} . \tag{7}$$

The fluorescence from the mth layer which reaches to the surface is

$$I_{\lambda_2}^{(m)'} = I_{\lambda_1}' \psi_{\lambda_1\lambda_2}(1 - e^{-\alpha_{\lambda_1}\Delta z}) e^{-(m-1)\alpha_{\lambda_1}\Delta z} \cdot e^{-m\alpha_{\lambda_2}\Delta z} \tag{8}$$

and the total fluorescent radiation, I_{λ_2}, at the surface is in the sum of the series

$$\sum_{m=1}^{\infty} I_{\lambda_2}^{(m)'} = \sum_{m=1}^{\infty} \{I_{\lambda_1}' \psi_{\lambda_1\lambda_2}[(1 - e^{-\alpha_{\lambda_1}\Delta z}) e^{-(m-1)\alpha_{\lambda_1}\Delta z} \cdot e^{-m\alpha_{\lambda_2}\Delta z}]\}$$

$$= I_{\lambda_1}' \psi_{\lambda_1\lambda_2} \cdot \left[\frac{1-c^{-\alpha_{\lambda_1}\Delta z}}{e^{-\alpha_{\lambda_1}\Delta z}}\right] \int_0^{\infty} e^{-m(\alpha_{\lambda_1}+\alpha_2)\Delta z} dm$$

and

$$I'_{\lambda_2} = \frac{I'_{\lambda_1}\psi_{\lambda_1\lambda_2}}{(\alpha_{\lambda_1}+\alpha_{\lambda_2})\Delta z} \left[\frac{\text{absorbed}}{\text{transmitted}}\right] \quad , \tag{9}$$

where $(\alpha_{\lambda_1}+\alpha_{\lambda_2})\Delta z$ is the sum of the optical depths at λ_1 and λ_2.

We have assumed a uniform distribution of chlorophyll and other particulates in deriving the equation (9). Of course, natural ecosystems do have a more complicated structure as discussed in Wimpenny (1966) and Kitchen (1977). Also, the attenuation loss at λ_1 is largely assumed as the absorptional rather than scattering (see Section 4 of this article for the arguments).

In order to obtain $I_{\lambda_2}^0$, the I'_{λ_2} is modified by another surface reflection, the area of the receiver, A, and a z^{-2} dependence. As a special case, if we assume that the altitude of the sensor is much greater than the depth of light penetration in the ocean H>>D-H.

$$I_{\lambda_2}^0 = \frac{I_{\lambda_1}\psi_{\lambda_1\lambda_2}(1-\rho)^2 e^{-(K_{\lambda_1}+K_{\lambda_2})H} \cdot A}{4\pi H^2 (\alpha_{\lambda_1}+\alpha_{\lambda_2})\Delta z} \left[\frac{1-e^{-\alpha_{\lambda_1}\Delta z}}{e^{-\alpha_{\lambda_1}\Delta z}}\right] \quad . \tag{10}$$

Often it is best to monitor a small fraction of the incident radiation to provide a reference signal for each pulse. This is to minimize the sources of noise or uncertainty in a lidar system. The reference signal at λ_1 due to the sea-air interface reflection is

$$I_{\lambda_1}^{\text{ref}} = I_{\lambda_1}^0 \rho\frac{Ae^{-2K_{\lambda_1}H}}{2\pi H^2} \quad . \tag{11}$$

The ratio of $I_{\lambda_2}^0$ and $I_{\lambda_1}^{\text{ref}}$ is

$$\frac{I_{\lambda_2}^0}{I_{\lambda_1}^{\text{ref}}} = \psi_{\lambda_1\lambda_2} \frac{(1-\rho)^2}{\rho} \frac{e^{H(K_{\lambda_1}-K_{\lambda_2})}}{(\alpha_{\lambda_1}+\alpha_{\lambda_2})\Delta z} \left[\frac{1-e^{-\alpha_{\lambda_1}\Delta z}}{e^{-\alpha_{\lambda_1}\Delta z}}\right] \quad . \tag{12}$$

It is to note that the atmosphere transmission properties $e^{H(K_{\lambda_1}-K_{\lambda_2})}$ can be factored out for wavelengths λ_1 and λ_2. This assumption should be valid in most of visible region except in the vicinity of 0.6 μ where an ozone absorption band of moderate strength (optical depth $\approx$ 0.03) may influence the value of return signal ratio. The expression (12) is a convenient form which states that if a prior knowledge of $\psi_{\lambda_1\lambda_2}$ is determined, the observed values are of a function of the absorption coefficients and the chlorophyll density [n] contributes to fluctuation of the absorptional properties of the ocean.

181

3. FLUORESCENCE YIELD MEASUREMENTS

The $\psi_{\lambda_1 \lambda_2}$ term in the equation (5) is an important conversion efficiency for chlorophyll determination by fluorometric method. The measurement of this parameter for chlorophyll pigment was first reported by Latimer, et al. in 1956. An integration sphere (or Ulbricht sphere) was used in their experiment. However, their measurements were taken from algae cells suspended in culture media and the reported fluorescence yield of 2.7% was based on the sum of total fluorescence yield outside of the excitation wavelength, 430 nm, in the visible region. Unfortunately this knowledge does not contribute to our 685 nm fluorosensing technique. Therefore, laboratory measurements of 685 nm emission band from in-vivo phytoplankton chlorophyll were conducted. Salient features of our laboratory measurement consist of a 50 cm diameter integration sphere and an Argon ion laser illumination source at 488 nm as shown in Figure 2. A 4 cm diameter bulbous quartz cell holds an aliquot of sea water containing in-vivo phytoplankton cells at the center of the sphere. The conversion efficiency of 488 nm to 685 nm radiance from equation (5) is

$$\psi(488 \text{ nm}, 685 \text{ nm}) = \frac{I_{(688 \text{ nm emitted})}}{I_{(488 \text{ nm absorbed})}} .$$

$I_{(685 \text{ nm emitted})}$ is the fluorescence intensity measured at position D with a 685 nm interference filter ($\Delta\lambda$ = 5 nm) in the Figure 2 (see Table 2). In order to measure the fraction of 488 nm absorbed by the algae sample, the fraction of 488 nm radiation transmitted and reflected with and without algae portions in the quartz cell were compared. According to Rabideau et al. (1946),

$$I_{(\lambda_1 \text{ absorbed})} = I_{(\lambda_1 \text{ incident})}[1 - (R+T)] ,$$

where (R+T) represents the fractions of incident radiation which were reflected and transmitted. Laboratory measurements of $I_{(488 \text{ nm absorbed})}$ were done by placing a 488 nm filter at C position. The differences of the photo-current outputs between the tapwater and chlorophyll-a containing sea water sample is equivalent to the portion of radiation absorbed by the chlorophyll-a in the quartz cell. Data shown in Table 3 are actual photocurrent readouts and the Figure 3 lines are the plot of Table 3 for distilled water (A) and sea water samples (B) taken on April 6, 1978.

The $\psi_{\lambda_1 \lambda_2}$ measurements were repeated with several Chesapeake Bay water samples which were collected during the period of October 1977 to April 1978 as shown in Table 4.

In-vitro analyses of chlorophyll-a and Phaetophytin concentrations were performed by Maryland State Natural Resources Laboratory in Annapolis,

SEA WATER

A

B

C

D
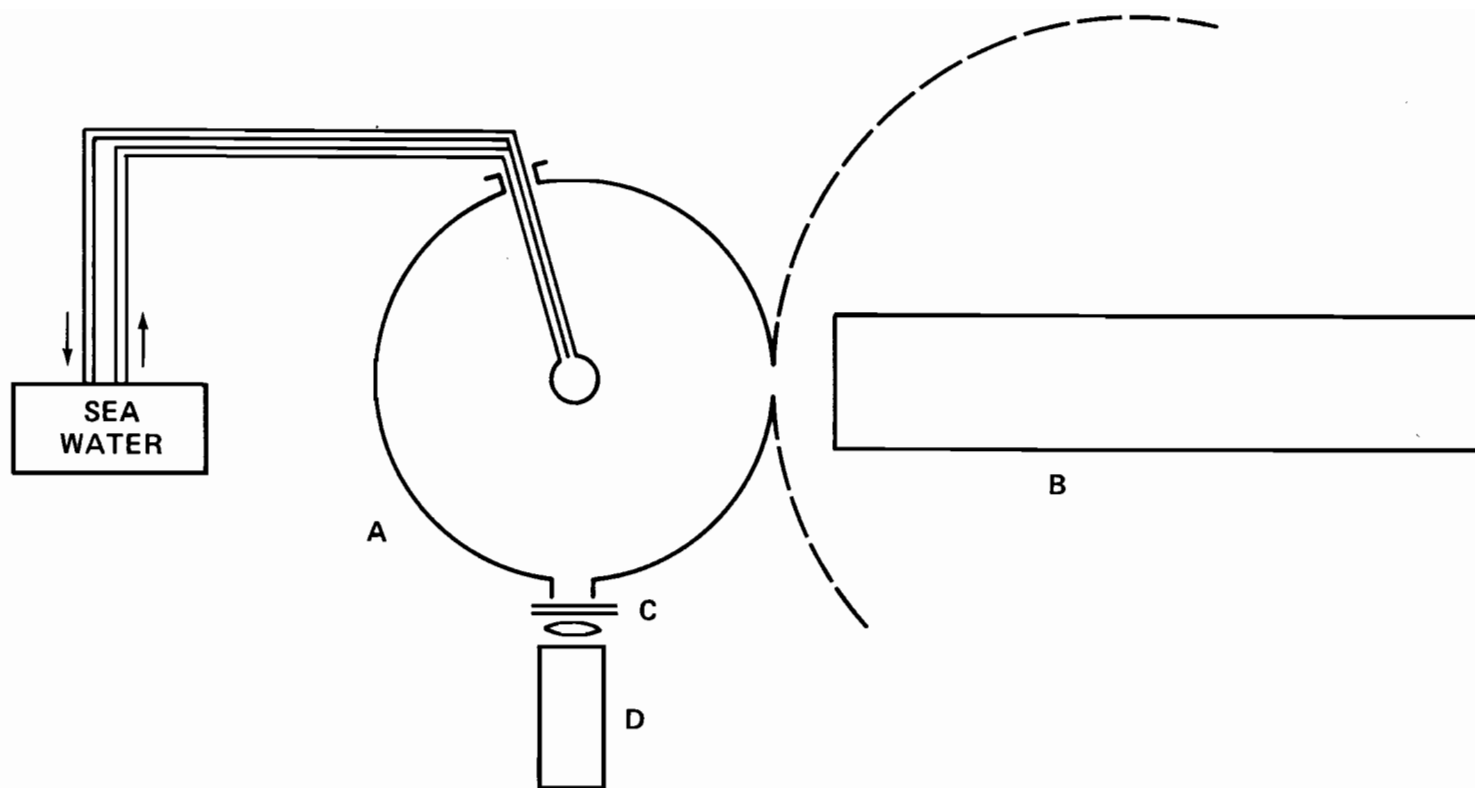
Figure 2. Fluorescence yield measurement setup: A, 40 cm integration sphere, B, illuminating light source, C, narrow band filter (488 nm or 685 nm) and D, photomultiplier tube.

Table II.

Measured Fluorescence Intensities at 685 nm for Clean Water and Sea Water

I (inc–488 nm) INCIDENT LASER POWER (mW)	I (EMISSION 0.685 nm) (AMP X 10^8)	
	CLEAN WATER	SEA WATER
80	1.0	—
100	1.2	1.79
120	1.3	—
150	—	2.3
200	1.82	2.95
220	1.95	3.3
270	2.28	3.8
300	2.4	—
360	—	4.8
370	2.93	5.0

Table III.

488 nm Intensity Readings Out of the Integration Sphere After
Reflection and Transmission Processes

INCIDENT LASER POWER (mW)	I (R + T) SIGNAL (AMP X 10^8)	
	CLEAN WATER	SEA WATER
60	1.4	1.3
100	—	2.1
105	2.4	—
110	2.5	2.4
135	3.1	—
160	3.61	3.25
180	4.0	3.6
190	4.1	3.8
195	—	3.9
200	4.5	—
220	5.0	—
240	5.4	4.9
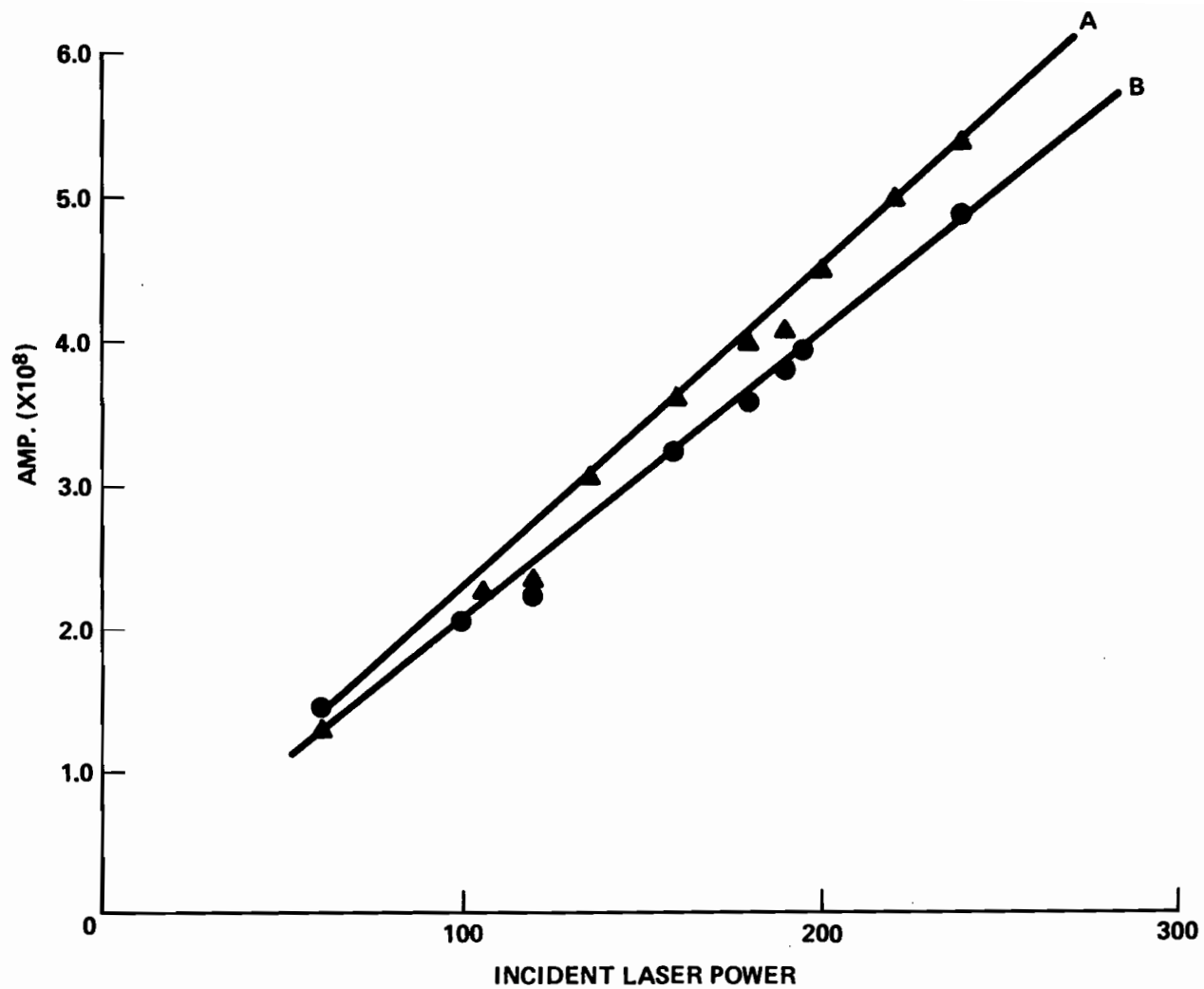
Figure 3. Reflected and transmitted 488 nm radiation intensity curves for clean water (A) and sea water (B). The fraction of the radiation absorbed by phytoplankton chlorophyll can be obtained from (A)–(B).

Table IV.

Fluorescence Yield Summary

DATE	CHLOROPHYLL-A CONC. IN (μgs/ℓ)	ψ(MEASURED)
OCT. 4 77	12.0	2.0×10^{-3}
OCT. 20 77	10.4	1.2×10^{-2}
OCT. 25 .77	4.5	9.5×10^{-3}
NOV. 1ST. 77	12.0	3.5×10^{-3}
NOV. 11TH. 77	6.0	3.6×10^{-3}
APRIL 6 78	14.0	7.8×10^{-3}
APRIL 12 78	12.0	9.2×10^{-3}

$$\psi(AVG) = 6.8 \times 10^{-3}$$
$$STD. DEV = 3.76 \times 10^{-3}$$

Table V.

A Summary of Absorption Coefficient Measurements

Date	Chlorophyll-A μgs/ℓ	Phaeophytin μgs/ℓ	Measured Absorption Coefficients	
			at 488 nm (m^{-1})	at 632 nm (m^{-1})
JULY 27, 1978	40.2	19.5	0.30	0.22
AUG 2, 1978	33.0	20.5	0.27	0.23
AUG 9, 1978	30.5	—	0.29	0.21
AUG 11, 1978	39.9	20.1	0.23	0.17
AVG.	—	—	0.274	0.208

Maryland. The average $\psi_{\lambda_1 \lambda_2}$ value, 6.8 x 10^{-3} units per unit of 488 nm
radiation absorbed includes a standard deviation on the order of
3.7 x 10^{-3}. The figure is smaller than estimated yields on the order of
a few percent reported by C.S. French (1960) and Latimer, but it is to
be noted that our measurement is based on 5 nm bandwidth at 685 nm which
is to be used for laser fluorosensing applications.

4. ABSORPTION MEASUREMENTS

An airborne laser fluorosensor detects trace amounts of fluorescent
material in the sensor field-of-view. In phytoplankton measurements,
the sensor system will read the total upwelled chlorophyll signal which
reaches the surface from subsurface layers of water body. In order to
assess the influences of the vertical element, we must determine the
absorption coefficients of downward laser beam and upward fluorescent
radiation returning to the surface. A definition of the extinction prop-
erties of laser beam is given in equation (2). However, in-situ measure-
ment of chlorophyll pigment absorption coefficient, a_{ch}, is not simple.
This is because the standard transmissometer (α-meter) is essentially a
small angle diffusion device which accounts for the loss due to the
scattering of light as well as the absorption loss. Therefore a proced-
ure was developed in the laboratory in order to circumvent the complex
problems associated with scattering losses that obscure true in-vivo
absorption measurements of phytoplankton in sea water. As shown in
Figure 4, a broad beam absorption chamber was fabricated. The dimensions
of the laboratory chamber are 91.44 cm (3 feet) in length and 40 cm in
diameter. This relatively large diameter of the chamber is an important
feature which was designed to capture all the forward scattering lobe of
the incident beam. A check of forward scattering of the incident beam
at the receiving end window with 40 μgs/ℓ chlorophyll and 22 μgs/ℓ
phaeophytin is shown in Figure 5. A collecting lens, D, with 15 cm
diameter was required to capture all the forward scattering and focus
the light onto the photomultiplier tube at position E in Figure 4. It
takes a minimum of 230 liters (60 gallons) of sea water to run a test.
A circulation pump, shown in laboratory overview Figure 6, was used to
keep a good mixing of sea water with fresh water dilution. An Argon ion
laser at 488 nm and a He-Neon laser at 632 nm were used as light sources.
The transmittances were recorded for several dilutions of original sea
water with fresh water. The resultant laboratory measurements are shown
in Figure 7. The absorption coefficient was derived from an extrapola-
tion of the curve which extends from the original full strength sea water
to infinite dilution.

This method permits an accurate measurement of true chlorophyll
absorptivity in-vivo as the radiation loss due to the scattering, $S_{(W+P)}$,
has been largely negated as long as one does not create the conditions
of multiple scattering within the chamber. In other words, under certain
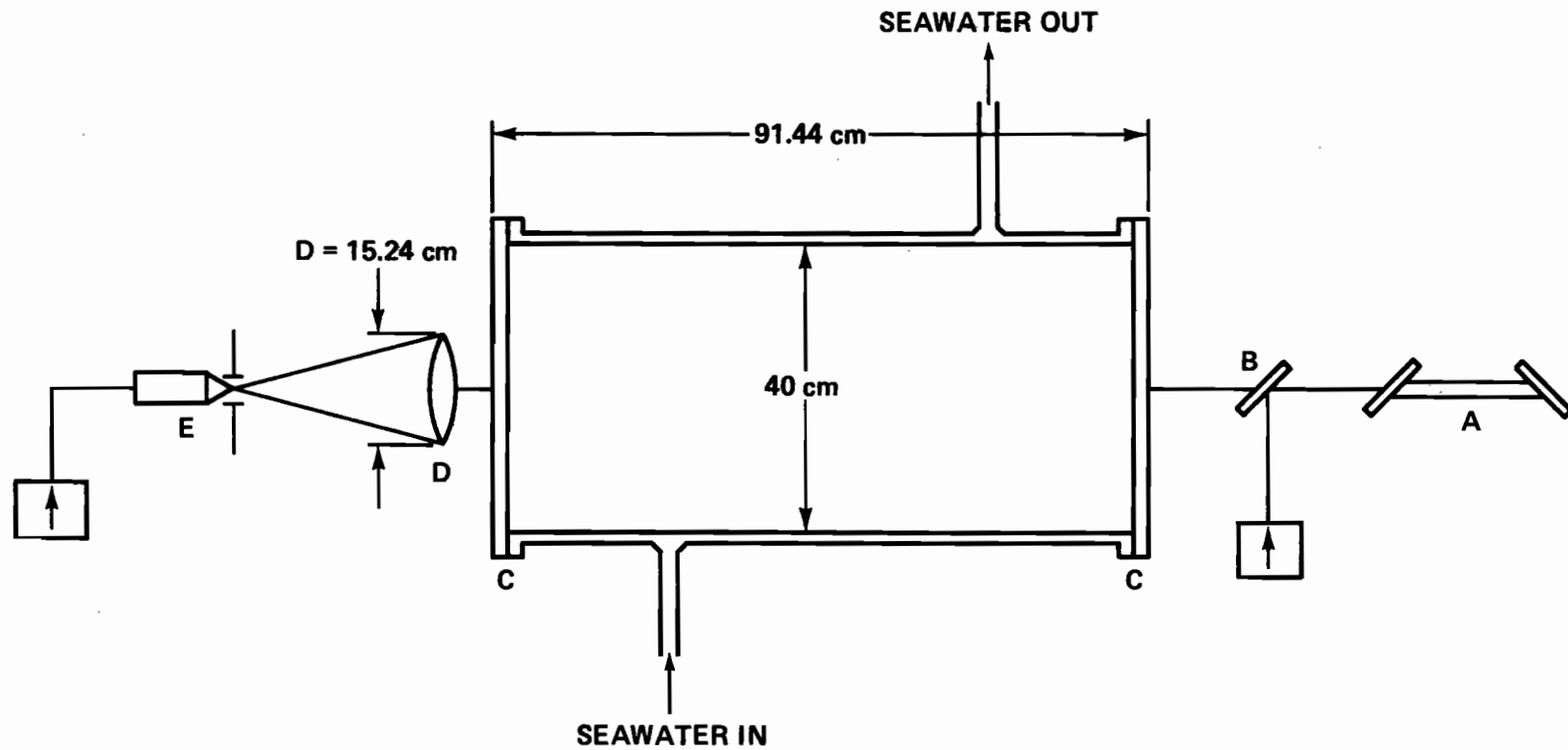
Figure 4. Arrangement of apparatus used for measuring laser beam attenuation: A. laser light source, B. beam splitter, C. plexi-glas windows, D. collecting lens, and E. PM tube.
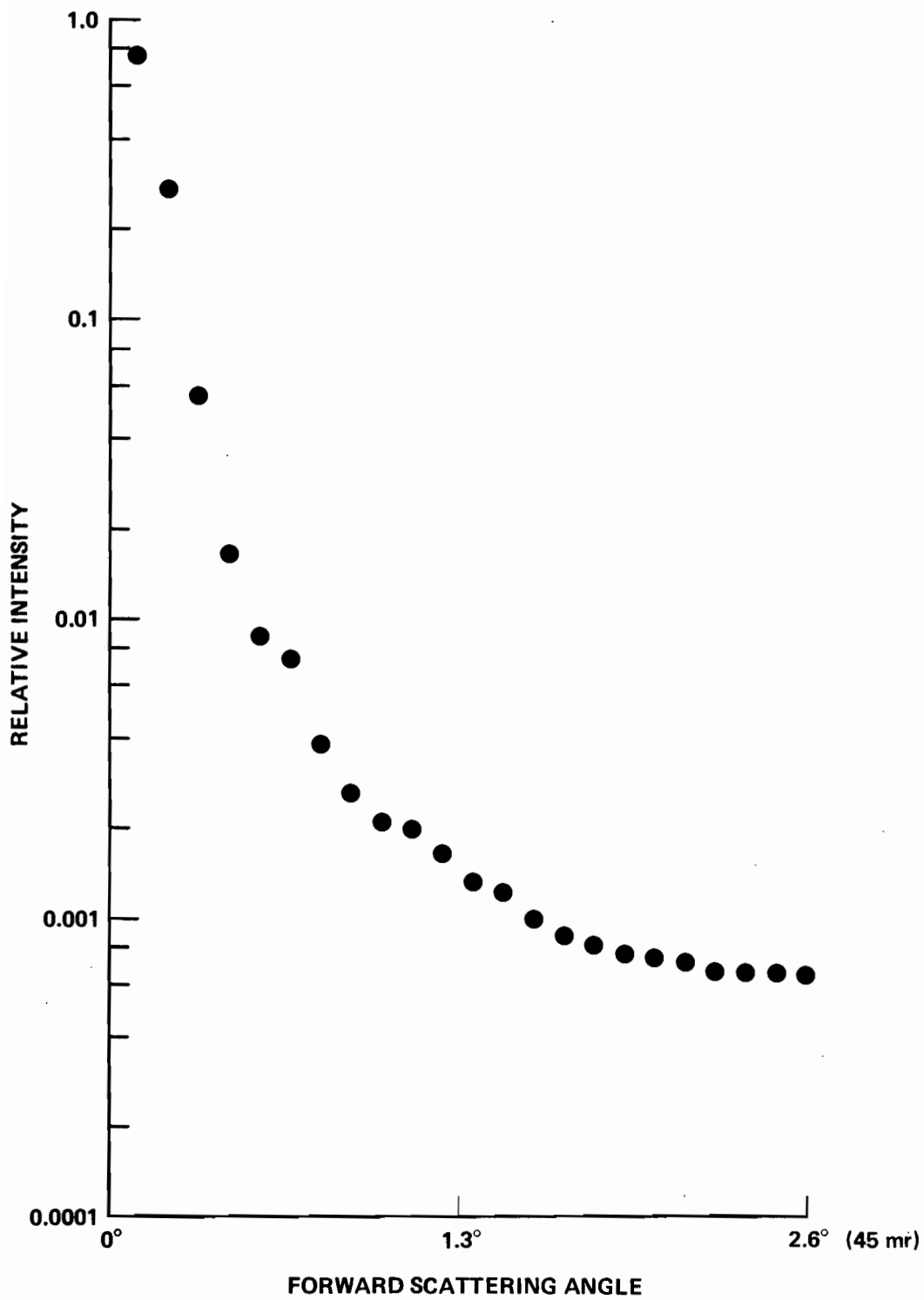
Figure 5. Angular power distribution of forward scattering of laser beam.
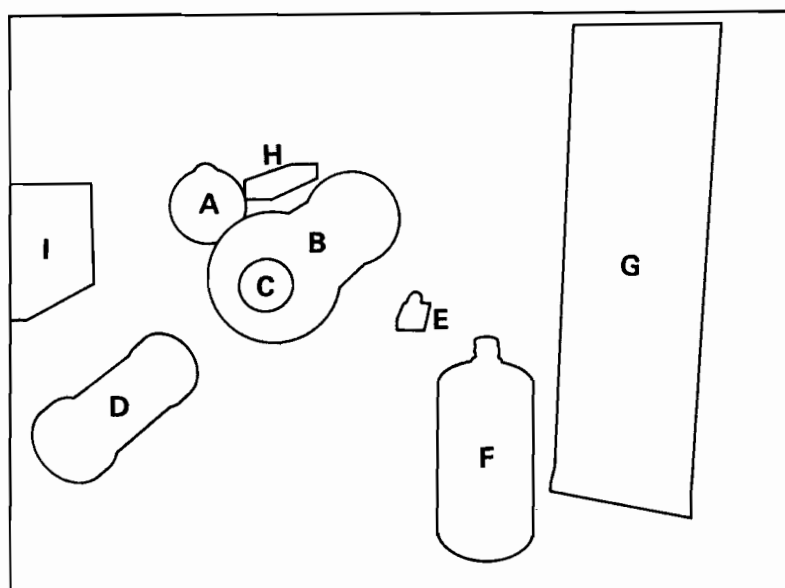
Figure 6. Laboratory setup for laser fluorosensing studies: A. inte-
gration sphere, B. absorption chamber, C. collecting lens,
D. PM tube, E. circulation pump, F. seawater reservoir,
G. electronics, H. Argon ion laser and I. monochromator.
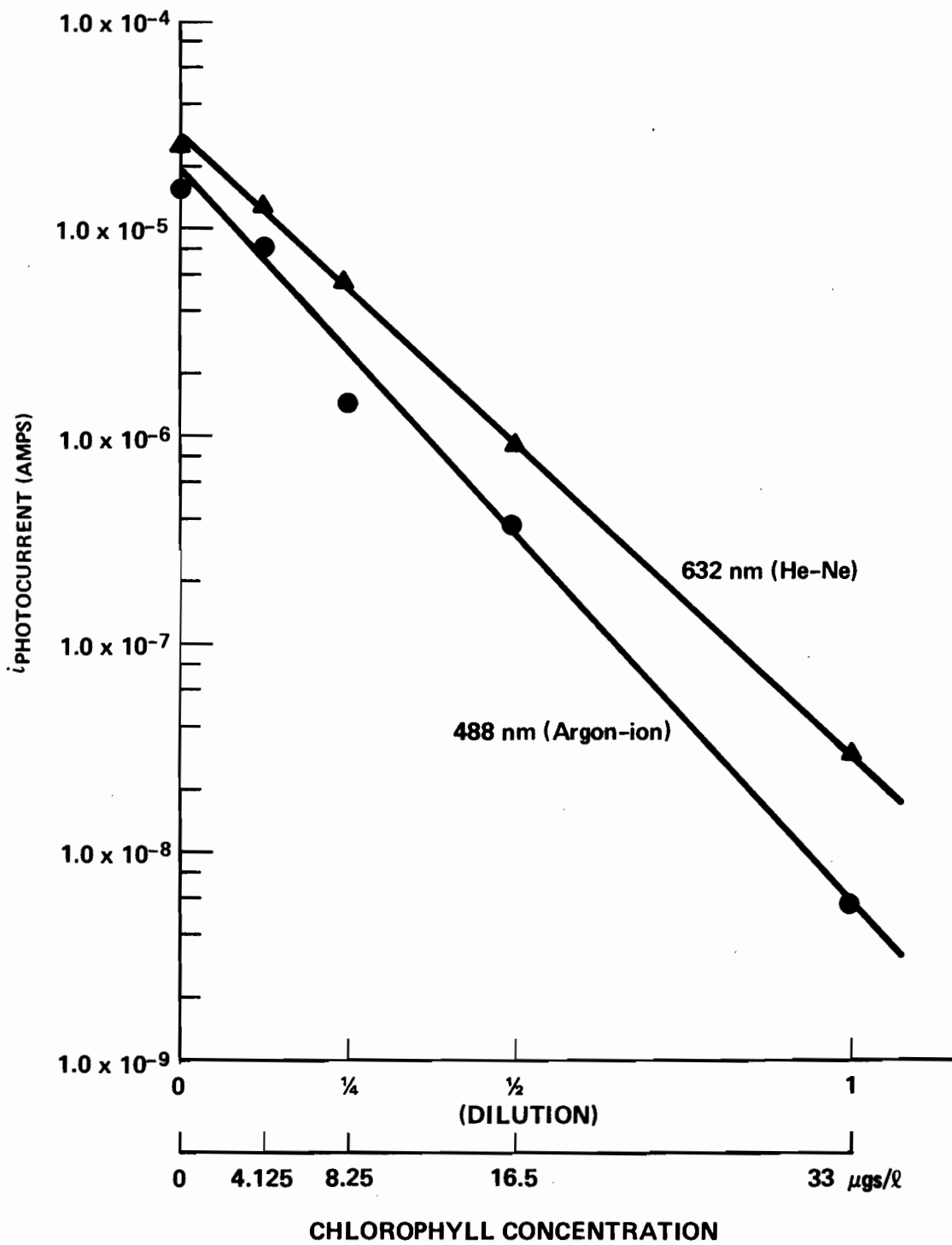
Figure 7. Absorptional losses at 488 nm (A) and 632 nm (B) due to the chlorophyll-a in the seawater samples.

conditions, this broad beam measurement provides the scattered light within the 10° cone as if it were unscattered and subject only to absorption as the incident beam travels the length of the chamber. These conditions are true in most lidar applications since lidar systems have a sufficiently large field-of-view to contain the illuminated target area and immediately adjacent areas. Smooth curve fitting shown in Figure 7 results underscores the validity of our assumption. Table 5 shows the average values of absorption coefficients for 488 nm and 632 nm. These in-vivo measurement values of 0.274 m^{-1} and 0.208 m^{-1} do seem higher than Yentsch's values (1963), but can be compared with Shibata's in situ measurement in 1957. Literature survey shows that the absorption coefficients due to the presence of phytoplankton are less definitive. The most generally used coefficients are attributed to Yentsch's measurement. However, his extinction spectra were taken via a particular laboratory sample processing technique and one might raise the question of whether it is valid to directly apply to the models of true ocean conditions.

The absorption coefficients, a_w, of clean sea water for 488 nm, 632 nm, and 685 nm were taken from the values given in Duntley's article (1962).

5. PENETRATION DEPTH OF LASER FLUOROSENSOR

We can now evaluate the performance of an airborne fluorosensor by substituting the $\psi_{\lambda_1\lambda_2} = 6.8 \times 10^{-3}$, and $a_{ch} = 0.274$ m^{-1} per µgs/ℓ at 488 m, into the expressions (2) and (8). Intensity of 685 nm radiation which leaves the surface per watt of 488 nm incident laser power at the illuminating surface is tabulated as the function of chlorophyll concentrations in Figure 8. In Table 6, the intensities of 685 nm contributing the total upwelling fluorescent signal from each 1 meter thick layer are given. Water absorption coefficients 0.00375 m^{-1} and 0.48 m^{-1} were used for 488 nm and 685 nm respectively (Duntley, 1962). The absorption coefficient of phytoplankton at 685 nm is extremely difficult parameter to measure and since a_w at 685 nm is already large, the a_{ch} at 685 nm contribution was neglected in Table 6 computation. Table 6 indicates that the relationship between the laser penetration depth and chlorophyll concentration is roughly in a hyperbolic function. An exponential decay is to be expected. However, as shown in the following Figure 8, a careful numerical analysis shows that a plot of the total sums of all the $I^{\downarrow}_{\lambda_2}$ radiances which reach to the surface vs. the chlorophyll concentrations in sea water is not linear as we have expected. This perturbation in the return signal power is caused by relatively large water attenuation coefficient at 685 nm which influences the fluorescent radiation of deep layers reaching the surface. It is interesting to see that our single laser beam penetration model matches the vertical variation of organic matter as illustrated by photosynthesis curve which is light dependent as presented by Sverdrup in 1953.
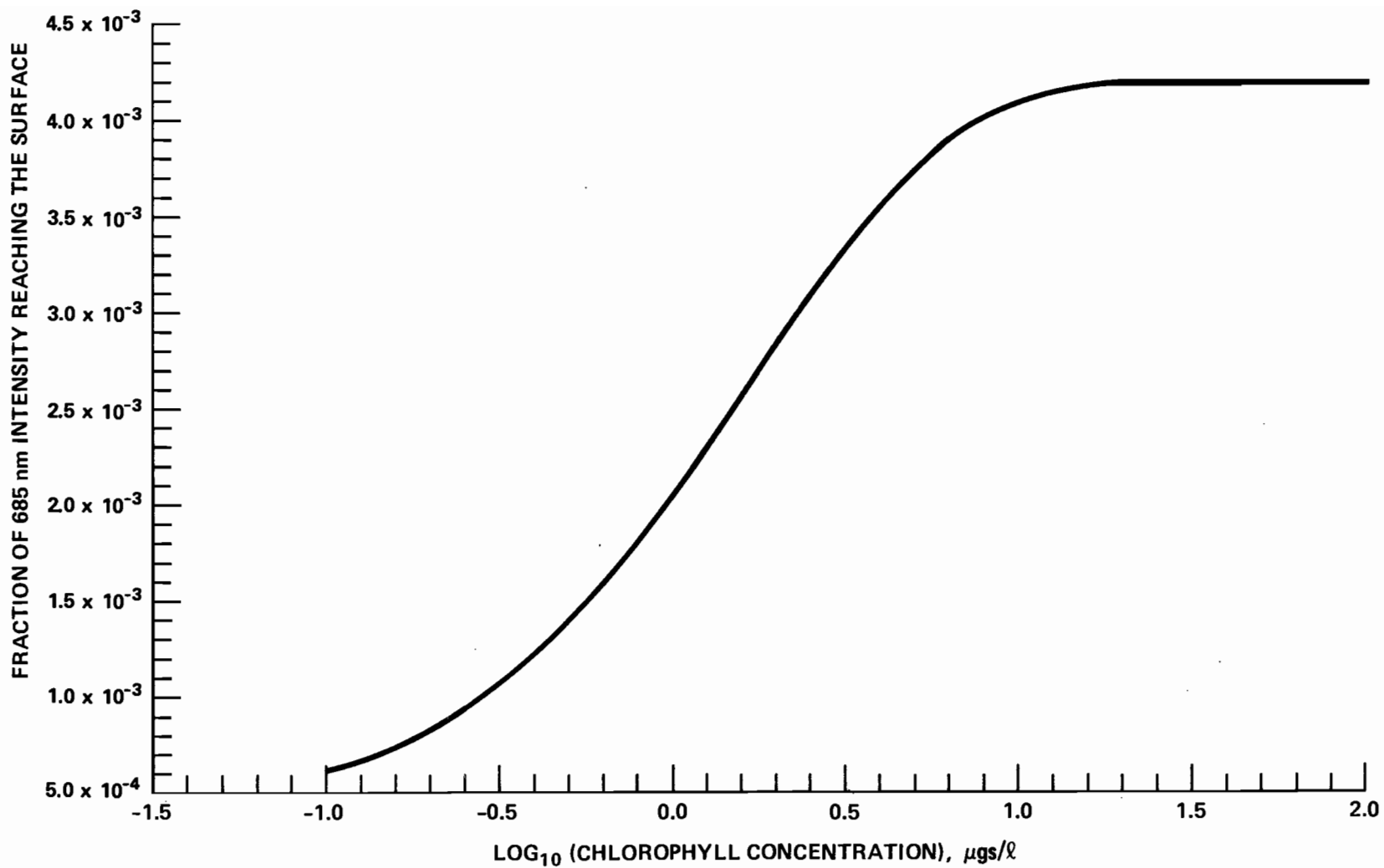
192

Figure 8. The number of units of 685 nm radiation reaching the surface per unit of incident 488 nm radiation vs chlorophyll–a concentrations from 0.1 to 30 µgs/ℓ.

Table VI.

Units of 685 nm Fluorescence Reaching to the Sea Surface from Each Subsurface Layer

Depth (m) / μgs/ℓ	CHLOROPHYLL-A CONCENTRATION								
	0.1	0.5	1.0	2.0	3.0	5.0	10.0	20.0	30.0
1	2.57×10^{-4}	6.67×10^{-4}	1.12×10^{-3}	1.86×10^{-3}	2.42×10^{-3}	3.17×10^{-3}	3.94×10^{-3}	4.19×10^{-3}	4.20×10^{-3}
2	1.49×10^{-4}	3.47×10^{-4}	5.08×10^{-4}	6.42×10^{-4}	6.35×10^{-4}	4.81×10^{-4}	1.52×10^{-4}	1.04×10^{-5}	6.76×10^{-7}
3	8.68×10^{-5}	1.81×10^{-4}	2.31×10^{-4}	2.22×10^{-4}	1.67×10^{-4}	7.31×10^{-5}	5.86×10^{-6}	2.60×10^{-8}	1.0×10^{-10}
4	5.04×10^{-5}	9.41×10^{-5}	1.05×10^{-4}	7.65×10^{-5}	4.38×10^{-5}	1.11×10^{-5}	2.26×10^{-7}	1.0×10^{-10}	—
5	2.93×10^{-5}	4.90×10^{-5}	4.76×10^{-5}	2.64×10^{-5}	1.15×10^{-5}	1.68×10^{-6}	8.70×10^{-9}	—	
6	1.70×10^{-5}	2.55×10^{-5}	2.16×10^{-5}	9.18×10^{-6}	3.02×10^{-6}	2.55×10^{-7}	3.0×10^{-10}	—	
7	9.89×10^{-6}	1.33×10^{-5}	9.81×10^{-6}	3.14×10^{-6}	7.92×10^{-7}	3.87×10^{-8}	—		
8	5.74×10^{-6}	6.92×10^{-6}	4.45×10^{-6}	1.09×10^{-6}	2.08×10^{-7}	5.9×10^{-9}			
9	3.33×10^{-6}	3.60×10^{-6}	2.02×10^{-6}	3.75×10^{-7}	5.45×10^{-8}	9.0×10^{-10}			
10	1.94×10^{-6}	1.87×10^{-6}	9.18×10^{-7}	1.29×10^{-7}	1.43×10^{-8}	1.0×10^{-10}			
12	6.54×10^{-7}	5.08×10^{-7}	1.89×10^{-7}	1.54×10^{-8}	1.0×10^{-9}	—			
15	1.28×10^{-7}	7.18×10^{-8}	1.77×10^{-8}	6.0×10^{-10}	1.78×10^{-11}				
20	8.5×10^{-9}	2.7×10^{-9}	3.0×10^{-10}	3.1×10^{-12}	—				
30	3.71×10^{-11}	4.0×10^{-12}	1.2×10^{-13}	—					
Total	6.1×10^{-4}	1.4×10^{-3}	2.1×10^{-3}	2.8×10^{-3}	3.3×10^{-3}	3.7×10^{-3}	4.1×10^{-3}	4.2×10^{-3}	4.2×10^{-3}

6. DISCUSSIONS

Further useful extension of this work is that an ocean algae detection experiment may be feasible from a spacecraft platform (i.e., space shuttle-borne laser facility). Simulations using the lidar equation (8) and our measured parameter values predict that the return signal will be clearly large enough for detection with single laser firing of 100 joule pulsed system even in daylight. The following system characteristics were used in the simulated calculations.

H.	Platform Altitude	300 km
J.	Laser energy	100j/pulse in 0.5-0.6 μ region
τ	Laser pulse duration	1 μs
	Beam divergence	0.1 mr
A_{rec}	Receiver area	1 m diameter
$A_{(fov)}$	Receiver FOV	0.2 mr
Δλ	Filter bandwidth	5 nm at 685 nm center wavelength
ψ	Fluorescence conversion efficiency at sea surface	0.004/0.1 μg/1 chlorophyll (from Table 6)

For daylight operation, the background equivalent noise P_b is estimated by the following expression:

$$P_b = \frac{(S)(Albedo)(Ac)(\xi)(\Delta\lambda)(A\ fov)(\tau)}{2\pi H^2(\frac{hc}{\lambda})} \quad ,$$

where

S = 1500 mW/M^2 - nm at 685 nm

Albedo = 0.1

ξ = Optical system efficiency 0.1

τ = 1 μs sampling time .

The computation shows approximately 5×10^4 photon/μs will impinge on the receiver due to background. From the expression (2), we have obtained 4.9×10^5 photon return signal from 0.1 μgs/ℓ area illumination with 100j pulse. The estimated percent of error for such a system is:

195

$$(\%)E = \sqrt{\frac{P_b}{P_s + P_b}} \times 100$$

which puts the signal-to-noise ratio in the vicinity of 200. During the next decade, the NASA space shuttle will use lidar system to probe atmospheric and meteorological parameters. For this purpose a lidar facility is under construction. Among many potential applications of the lidar facility, algae fluorosensing appears to be one of the more tangible experiments to be tested from the platform because of its high sensitivity and simplicity of its working mechanism as our S/N study indicates.

In conclusion, the work described in this paper predicts that a minimum of 0.0006 units of 685 nm fluorescence signal will upwell to the sea surface as a unit of 488 nm radiation illuminates the ocean surface area with 0.1 µgs/ℓ chlorophyll concentration. This conversion efficiency will increase to 0.0042 as the chlorophyll density increases to 20 µgs/ℓ. The results of this calibration study are much higher than the performance of a prototype lidar unit which was tested in earlier days (Kim,1973). In order to confirm the lidar efficiency that has been predicted in this article, further investigations involving in-situ measurements of phyto-plankton concentration will be necessary. Especially the relationship between the remote sensed data and nature must be well understood. In any event, the study clearly indicates that laser induced algae fluoro-sensing is a powerful remote sensing method which can be extended to a space altitude.

The authors are regretful that the measurements of fluorescence quantum yields and absorption properties of phytoplankton chlorophyll have not been expanded to include the entire visible spectrum in order to gain knowledge on the excitation wavelength dependency. To do this task in a satisfactory manner, it would have been truly a time-consuming major proposition.

7. ACKNOWLEDGEMENTS

8. REFERENCES

Barringer, A., J.H. Davies, and R. Dick (1977). *4th Joint Conference on Sensing of Environmental Pollutants,* New Orleans, November 6-11.

Bristow, M. P. F. (1978). Airborne monitoring of surface water pollutants by fluorescence spectroscopy. *Remote Sensing of Environment,* vol. 7, Elsevier, New York, pp. 105-107.

Brown, C. A., F. H. Farmer, O. Jarrett, Jr., and W. L. Station (1977). Laboratory studies of in-vivo fluorescence of phytoplankton, *4th Joint Conference on Sensing of Environmental Pollutants,* New Orleans, November 6-11, 1977.

Duntley, S. Q. (1962). Light in the sea, *JOSA* 55: 216.

French, C. S. (1960). In *Encyclopedia of Plant Physiology,* Springer Verlag, Berlin, p. 231.

Kitchen, J. C. (1977). Particle size distributions and the vertical distribution of suspended matter in the upwelling region off Oregon, Oregon State University School of Oceanography Ref. 77-10, p. 118.

Kim, H. H. (1973). New algae mapping technique by the use of an airborne laser fluorosensor, *Applied Optics* 12: 1454-58.

Latimer, P., T. T. Bannister and E. Rabinowitch (1957). The absolute quantum yields of fluorescence of photosynthetically active pigments, in *Research in Photosynthesis,* Interscience, pp. 107-112.

Lorenzen, C. J. (1966). A method for the continuous measurement of in-vivo chlorophyll concentration, *Deep Sea Research* 13: 223-227.

Rabideau, G. S., C. S. French and A. S. Holt (1946). The absorption and reflection spectra of leaves, chloroplast suspensions, and chloroplast fragments as measured in an Ulbricht sphere, *Am. J. Botany* 33: 769-777.

Shibata, K. (1958). Spectrophotometry of intact biological materials, absolute and relative measurements of their transmission, reflection and absorption spectra, *J. Biochem.* 45(5): 599-623.

Strickland, J. D. H. (1968). Continuous measurement of in-vivo chlorophyll; a precautionary note, *Deep Sea Research* 15: 225-227.

Wimpenny, R. S. (1968). The plankton of the sea, Am. Elsevier, New York, pp. 130-131.

Yentsch, C. S. and D. W Menzel (1963). A method for the determination of phytoplankton chlorophyll and phaeophytin by fluorescence, *Deep Sea Research* 10: 221-231.

List Of Participants

Gary A. Borstad

Seakem Oceanography
9817 West Saanich Road
Sidney, B.C.   V8L 3S1

Mike Bristow

EPA
P.O. Box 15027
Las Vegas, Nevada   89114

Otis B. Brown

RSMAS/MPO
University of Miami
4600 Rickenbacker Causeway
Miami, Florida   33149

Joseph R. Buckley

Seakem Oceanography Ltd.
9817 West Saanich Road
Sidney, B.C.   V8L 3S1

K.L. Denman

Institue of Ocean Studies
P.O. Box 6000
Sidney, B.C.   V8L 3S1

Pierre Y. Deschamps

Laboratoire d'Optique Atmospherique
Université de Lille
B.P. 36
59650 Villeneuve d'Asq, France

Roland Doerffer

Institue Hydrobiologie U. Fischereiwissenschaft
Universitat Hamburg
Palmaille 55
2 Hamburg 50, W. Germany

Hans Dolezalek

Code 462
Office of Naval Research
Arlington, Virginia   22217

H.R. Gordon

NOAA/PMEL
3711 15th Avenue, N.E.
Seattle Washington   98105

Jim Gower   Institute of Ocean Sciences, Patricia Bay
                                 P.O. Box 6000
                                 Sidney, B.C.   V8L 3B2

John Guagliardo   U.S. Naval Ocean R & D Activity
                                 National Space Tech. Labs.
                                 NSTL Station, MS   39529

Gary C. Guenther   NOAA/NOS
                                 EDL, C61
                                 Rockville, Maryland   20952

Joseph Hirschberg   Department of Physics
                                 University of Miami
                                 Coral Gables, Florida   33124

Frank E. Hoge   NASA
                                 Wallops Flight Center
                                 Building E-106
                                 Wallops Island, Virginia   23337

Clarence A. Jensen   Ball Aerospace Systems Division
                                 P.O. Box 1062
                                 Boulder, Colorado   80306

Hongsuk H. Kim   NASA-Goddard
                                 Code 941
                                 Greenbelt, Maryland   20721

Donald A. Leonard   Computer Genetics Corporation
                                 18 Lakeside Office Park
                                 Wakefield, Massachusetts   01880

Condon McDonough   Avco-Everett Research Lab
                                 2385 Revere Beach Parkway
                                 Everett, Massachusetts   02149

André Y. Morel   Lab. Physique & Chimie Marines
                                 (Univ. P. & M. Curie, Paris)
                                 BP8 F 06230 Villefranche sur ner, France

R. O'Neil   Canada Centre For Remote Sensing
                                 2464 Sheffield Road
                                 Ottawa, Ontario   K1A 0Y7

Bertil Ostrom   National Board Of Fisheries
                                 Laboratory Of Marine Research
                                 FACK
                                 40310 Goteborg, Sweden

Dave Rayner

Division of Biological Sciences
National Research Council Of Canada
100 Sussex Drive
Ottawa, Ontario   K1A OR6

John Ryan

Canada Centre For Remote Sensing
2464 Sheffield Road
Ottawa, Ontario   K1A OY7

Ron Schwiesow

ERL/NOAA/WPL
R45x3
Boulder, Colorado   80302

Boris Sturm

JRC Ispra
Cas. Post. No. 1
121020 Ispra (Italy)

H.H. Zwick

Canada Centre For Remote Sensing
2464 Sheffield Road
Ottawa, Ontario   K1A OY7